NMR studies of thermally-treated Zeolite Y

Peter G Clarke

NMR STUDIES OF THERMALLY–TREATED ZEOLITE Y

Peter G. Clarke (Department of Chemistry, University of Durham)
Submission for the degree of Doctor of Philosophy, 1991

ABSTRACT

The effect of thermal treatments on the lattice of Zeolite Y and on intracrystalline non–lattice material is investigated by solid–state magic–angle–spinning NMR. ^{29}Si and ^{27}Al NMR show that large amounts of both silicon and aluminium are dislodged from the lattice by calcination and steaming treatments. Non–lattice material is readily observed by ^{29}Si CP/MAS; the presence of such material may also be deduced from the single–pulse spectra by means of spectral deconvolution techniques. Non–lattice aluminium atoms occur in tetrahedral and octahedral coordination; a technique is proposed for measuring the ratio of Al in these two environments. Leaching with aqueous $(NH_4)_2EDTA$ removes non–lattice Al but also attacks lattice Si and may re–insert some Al into the lattice.

A reliable technique has been developed for acquisition of ^{1}H MAS–NMR spectra of totally dehydrated samples of Zeolite HY. Exceptionally well–resolved signals have been observed for silanol groups and Brönsted–acidic protons. Particular attention has focused on a broad signal at 2.3 ppm attributed to OH groups on non–lattice Al atoms, whose intensity depends on the degree of polymerization of the non–lattice alumina. The degree of polymerization rises on prolonged heating under vacuum. If the sample is kept dry for several months, the AlOH concentration rises at the expense of other hydroxylated species present, suggesting a slow reversal of the polymerization process. The highly–condensed material is also capable of reacting with injected water.

Cation–containing Zeolite Y behaves quite differently from HY on dehydration. NaY requires severe heating under vacuum to achieve dryness; however, the product is free from non–lattice material. NH_4Y releases its intracrystalline water readily but, on decomposition of NH_4^+ at around $300^{o}C$, a new broad signal emerges close to 4 ppm; this is tentatively assigned to NH_3 trapped in small lattice cages.

NMR STUDIES OF THERMALLY-TREATED ZEOLITE Y

by

PETER G. CLARKE BA

A Thesis submitted in partial fulfilment of the requirements for the degree of Doctor of Philosophy of the University of Durham

Department of Chemistry
University of Durham
1991

MEMORANDUM

The research presented in this thesis has been carried out the the Department of Chemistry, University of Durham, between October 1988 and September 1991. It is the original work of the author unless stated otherwise. None of this work has been submitted for any other degree, except for the section so indicated in Chapter 3.

ACKNOWLEDGEMENTS

My thanks are extended to my supervisors, Prof. R.K. Harris (University of Durham) and Dr. E.G. Smith and Dr. K. Gosling (Unilever Research Port Sunlight Laboratory) for a great deal of useful advice and helpful suggestions. The assistance of the following is also gratefully acknowledged: from Durham, Dr. D.C. Apperley, Ms. N.A. Davies, Mr. B.J. Say and Dr. A.M. Kenwright; from Port Sunlight, Mr. J.W. Rockliffe, Mr. L.P. Hughes, Ms. C.M. Black and Mrs. J.M. Jones. The financial support of the Science and Engineering Research Council and Unilever Research is acknowledged.

I would particularly like to thank my landlords, Bryan and Sue Gordon (who elected me their son's Godfather), and all the members of Emmanuel Church, Durham, for a covering of love and support that cannot be measured. And I thank my God, too, for his faithful fatherhood.

CONTENTS

ABBREVIATIONS

The following abbreviations appear in the text of this thesis:

AAS	Atomic Absorption Spectrometry
acac	Acetylacetone [$CH_3COCH_2COCH_3$] or its anion
AQ	Acquisition time [of FID]
CP	Cross–Polarization
CP/MAS	Cross–Polarization with magic–angle spinning
CRAMP	Combined Rotation And Multiple Pulse
CRAMPS	CRAMP Spectroscopy
CT	Contact time [for CP/MAS]
EDTA	Ethylenediaminetetraacetic acid [$((HO_2CCH_2)_2NCH_2)_2$] or its anion
EFG	Electric field gradient
HWHH	Half width at half–height [of NMR signals]
FID	Free Induction Decay
FWHH	Full width at half–height [of NMR signals]
MAS	Magic–angle spinning
NLA	Non–lattice alumina
NNN	Next–nearest neighbour
NT	Number of transients or averages
NMR	Nuclear Magnetic Resonance [Spectroscopy]
o.d.	outside diameter
PA	Pulse nutation angle
ppm	parts per million
Q^n	Si site attached to n –OSi groups
RD	Recycle delay [in pulse sequences]
RF	Radio Frequency
RH	Relative Humidity
RMM	Relative molar mass
RO	Rotation rate for magic–angle spinning
S/N	Signal–to–noise [ratio]
SCP	Selective Cross–Polarization
SP	Single–pulse
ssb	spinning sideband
T–site	Tetrahedrally coordinated lattice site
TMS	Tetramethylsilane
TMS Salt	Sodium (3–trimethylsilyl)propanesulphonate [$Me_3Si(CH_2)_3SO_2Na$]
TPD	Temperature–Programmed Desorption
UCS	Unit cell size
WRAC	Wideline Relaxation And Cryogenics [spectrometer system]
XRD	X–Ray Diffraction
XRF	X–Ray Fluorescence

CHAPTER 1: INTRODUCTION

1A: THIS WORK

Solid–state NMR is already well–established as a technique of considerable importance in the study of zeolites. The research described in the following Chapters employs NMR to investigate the effect on zeolites of certain widely–used treatments, particularly hydrothermal ones. A range of established and novel multinuclear measurements is presented to demonstrate that solid–state NMR is capable of revealing extensive information concerning changes in the lattice and in any amorphous material present. In addition, a thorough drying technique has been developed and evaluated, permitting the elucidation of subtle changes to the hydroxyl groups in dehydrated samples. Such detailed information cannot be obtained by any other technique, with the possible exception of infra–red spectroscopy.

The research work was carried out during the period October 1988 – September 1991, predominantly in the Department of Chemistry at the University of Durham. The project's academic supervisor was Prof. R.K. Harris. Extensive collaborative links were established with Unilever Research, who sponsored the project under the SERC's CASE scheme. The industrial supervisors were Dr. E.G. Smith and Dr. K. Gosling of Unilever Research Port Sunlight Laboratory, where some of the practical work and spectroscopy were carried out.

Preliminary results were presented in the form of a poster at the 13th Annual Meeting of the British Zeolite Association at Chislehurst, Kent, in July 1990, and as a lecture at the North–East Graduate Symposium in March 1991 and in a colloquium at ICI Chemicals & Polymers Ltd, Runcorn, in April 1991.

1B: INTRODUCTION TO ZEOLITES

Zeolites comprise a substantial family of inorganic crystalline materials composed of three–dimensional networks of TO_4 tetrahedra, where T is most commonly Si or Al. There are also many related substances containing other tetrahedrally coordinated atoms such as B, Ge, Ga, P and Fe. One of the most important and distinctive features of these materials is that they crystallize in such a way as to leave large, regular cages and channels within the lattice which can be accessed from outside by other substances, subject to size constraints.

The zeolite under consideration in this work is Zeolite Y, which occurs naturally as faujasite and is also manufactured on a large scale by crystallization from alkaline silicate and aluminate solutions, with a typical lattice Si/Al ratio of around 2.5. Its structure is shown in outline in Figure 1.1. Each vertex in the Figure is occupied by either Si or Al; the bridging oxygen atoms are not shown. The structure is composed of cages made of four– and six–membered rings of

Figure 1.1: Outline of the structure of Zeolite Y, showing small and large cages and channels.

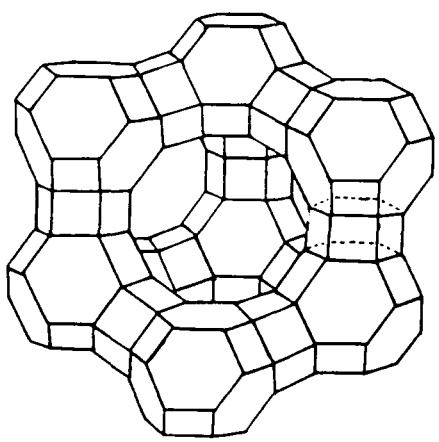

vertex–sharing TO_4 tetrahedra (seven of these cages are shown in Figure 1.1); these are known as *sodalite*, *β–* or *small cages.* The small cages in turn are linked together by oxygen bridges to form large cages with interconnecting channels circumscribed by six–membered rings; the large cages are sometimes known as *α–* or *supercages.* The structure as a whole has cubic symmetry (a hexagonal polymorph is also known) and each T–atom site is crystallographically equivalent.

Since the structure is notionally composed of SiO_2 and AlO_2^-, there is one net negative charge on the lattice per Al present. This charge is balanced by cations such as Na^+ or NH_4^+, which can readily be exchanged in aqueous solution. Heating the NH_4^+ form of Zeolite Y drives off NH_3, leaving H^+ as the charge–balancing species; the resulting material is then known as HY. The H^+ is associated with lattice Al to form a site with strong Brönsted acidity which may be shown thus:

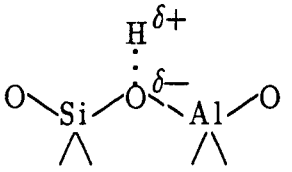

In addition to the charge–balancing cations, the cages and channels may also contain amorphous non–lattice material. This is created by the displacement of atoms, especially Al, from the lattice during certain treatments (further details are given in Chapter 4). The non–lattice material, which is ill–defined and poorly understood, is composed primarily of Al, O, H and sometimes Si and is widely believed to exhibit Lewis–acidic character. The Brönsted and Lewis acid character of a given sample may readily be probed by a range of techniques (see Chapter 5); for example, infra–red studies of adsorbed pyridine clearly show the type of site to which it is attached.

The Brönsted and Lewis acidity of Zeolite Y is of the utmost industrial importance for its application in gas–oil cracking catalysts. In addition, the

confinement of the channel and cage system imposes size and shape selectivity on the reactions occurring at the internal active sites. Some of the work reported in the following Chapters of this thesis is concerned with investigating the changes to the lattice and to non–lattice material which result from hydrothermal (steam) treatments, which are used to simulate the effect of prolonged service in a catalytic reactor system.

1C: THE THESIS

This thesis can be considered to fall into two main sections: techniques (Chapters 2 and 3) and results (Chapters 4 – 7). Chapter 2 covers the necessary theoretical and technical aspects of solid–state NMR and outlines the basis of its application to zeolites. Chapter 3 discusses all the other practical details, including a description of the drying procedure and non–NMR techniques employed as well as a discussion of some computer software written for use in this project.

Chapter 4 describes the results of studies into the effects of thermal and chemical treatments on the zeolite lattice, preceded by a review of previously reported work in this area. Chapters 5 – 7 are concerned with ^{1}H NMR studies of intracrystalline water and dried samples: water and the drying process are discussed in Chapter 5, the behaviour of non–lattice material in dried samples in Chapter 6, and the effects of drying samples containing cations in Chapter 7. Finally, Chapter 8 summarizes the principal conclusions from the work described. Appendices A and B provide lists of the samples and drying treatments employed.

CHAPTER 2: NMR THEORY AND PRACTICE

2A: NMR THEORY

Nearly all the NMR techniques employed in the present work are already well understood both in terms of theory and of experimental procedure. Accordingly, this section contains only a brief consideration of the theory applied; rigorous treatments may be found in standard texts.[1,25]

1. Basis of NMR; The Rotating Frame

The nuclei of a great many isotopes have quantum–mechanical spin, defined by a fixed ground–state quantum number I, which can take any positive half–integral value. The basis of the phenomenon of Nuclear Magnetic Resonance is the occurrence of different possible orientations of the spin vector of any nucleus with non–zero spin; these are defined by an azimuthal quantum number m_I, which can take the values $-I$, $-I+1$, ..., $+I$. When the nucleus is placed in a static magnetic field of flux density B_0, the degeneracy of the energy levels arising from these $2I+1$ possible orientations is lifted (a phenomenon referred to as *Zeeman splitting*) so that (a) the Boltzmann populations of the energy levels become unequal and (b) transitions become possible between them. In order to maximize the population difference, and hence the intensity of the transitions, the strongest available static magnetic field B_0 is employed, typically in the range $1.4 - 14.1$ Tesla. This puts the transition frequency (or *Larmor frequency*) of the ^{1}H nucleus in the range $60 - 600$ MHz, which is in the radiofrequency region of the electromagnetic spectrum. The Larmor frequency is given approximately by $\nu_L = \gamma B_0$ where γ is the gyromagnetic ratio of the nucleus.

When analyzing the behaviour of the nuclear spins of a particular isotope (say ^1H) during an NMR experiment, it is usual to consider the net, or bulk, magnetization – that is, the sum of all the nuclear spin vectors (which have associated magnetic moments). At equilibrium, the bulk magnetization lies parallel to the static magnetic field B_0, along what is usually taken as the z–axis in three–dimensional coordinate space. On application of a radiofrequency pulse of intensity B_1 in a plane perpendicular to this, the bulk magnetization is induced to precess about B_1. Visualized in a frame of reference rotating about the z–axis at the Larmor frequency, the bulk magnetization tips towards the x–y plane, eventually passing through it as the magnetization vector rotates about the axis in which B_1 is applied (see Figure 2.1) – a motion described as *nutation*. Any component of the bulk magnetization that lies in the x–y plane when the B_1 pulse is shut off is detected by the RF signal it induces in the receiver coil. The spin system is now able to relax to its equilibrium state in a process known as Free Induction Decay (FID). The detected FID signal contains characteristic frequencies for all the ^1H nuclei present. These vary slightly (over a range rarely

Figure 2.1: Nutation of bulk magnetization (M) about y–axis in rotating frame resulting from the application of a RF field (B_1) along the x–axis. In this case, the RF field is switched off after M has nutated through an angle $\alpha = \pi/2$; had the field been applied for longer, M would have continued to precess about the x–axis towards the $-z$ direction. (Derived from Ref. 2b)

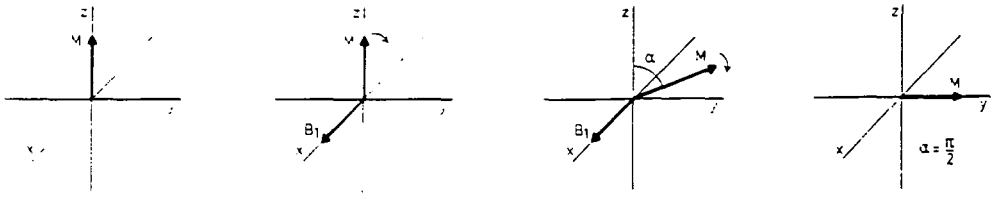

exceeding 10 kHz) due to the different actual magnetic field strengths at the places where the nuclei are located. The differences arise from

(a) varying electron density ('shielding') around the nucleus, which is linked with the atom's chemical environment; this generates the phenomenon of *chemical shift*; and

(b) interactions between two or more nuclear spins, giving rise to small variations in field at the nuclei in question; this generates the phenomenon of *spin–spin coupling.* Two distinct coupling mechanisms exist: direct through–space magnetic interactions (known as *dipolar coupling*) and indirect (*J–coupling*) mediated *via* the magnetic dipoles of bonding electrons.

Chemical shift and spin–spin coupling are readily detectable and are extremely important sources of information about the environment of the nucleus.

2. Relaxation

There are two important relaxation processes to consider in NMR. The first is *spin–lattice relaxation*: an excited nucleus senses a magnetic field fluctuating at its Larmor frequency due to motion in its surroundings (the 'lattice' – whether literally crystalline or not), and exchanges energy with the lattice, relaxing to a lower energy level. Averaged over the whole sample, this process decays exponentially with time, characterized by the *spin–lattice relaxation time* T_1. T_1 is a useful measure of the relative mobility of the nucleus and its surroundings: the more high–frequency motion present, the shorter the observed T_1. Generally speaking, each magnetically inequivalent nucleus has a different T_1.

The second significant relaxation mechanism is *transverse* or *spin–spin relaxation*, in which two nuclei (usually of the same isotope) exchange spin states

in a quantum flip–flop process known as *spin diffusion.* The effect of this is the smearing–out of magnetization among coupled spins of a given isotope, so that the component of the bulk magnetization in the x–y plane gradually disappears. The rate at which this component is lost, and hence also the rate of disappearance of the NMR signal, is characterized by the *spin–spin relaxation time* T_2. If spin diffusion is slow compared with the rate of spin–lattice relaxation, as is generally the case in liquids, T_2 will be dominated by the latter process and so $T_2 = T_1$. In solids, however, spin diffusion is generally fast due to the intense unaveraged coupling between spins, and so T_2 is often much shorter than T_1. In solids, T_2 is a measure of the strength of coupling between spins, which is controlled by several factors, most importantly the physical separation between nuclei and their mobility (highly mobile nuclei, *e.g.* chemically exchanging ones, are not strongly coupled to anything on average).

The T_1 and T_2 relaxation times of a sample can readily be measured using techniques known as inversion–recovery and CPMG, respectively, which are discussed in many standard texts.[2]

3. Line–Broadening Influences

The discussion so far has considered each nucleus to resonate at a single frequency, dependent on its gyromagnetic ratio, its shielding environment, and its coupling to other nuclei. The spectra that result from an NMR experiment on an ensemble of spins, however, contain signals that are significant, and possibly very substantial, in frequency width. Of the several possible origins of line broadening, four of the most important are considered below, together with methods for minimizing their effect on the spectrum.

1. Shielding anisotropy. The shielding effect of a cloud of electrons around a

nucleus, as already stated, alters the actual magnetic field strength at that nucleus, and hence affects its resonance frequency. However, the magnitude of the effect is also controlled by the orientation of the molecule relative to B_0. In a solid, where the molecules are in fixed alignments, many different orientations are present; the result is a spread of resonance frequencies being observed. In a liquid, the rapid tumbling of molecules has the effect of averaging out this spread, and so just a single frequency is actually measured: the spectral line is narrow. This tumbling effect can be effectively simulated in solids by aligning the sample container along an axis subtending an angle 54.7° (the 'magic angle') to B_0 and spinning it rapidly about this axis – a technique known as *magic–angle spinning* (MAS). A typical MAS rate is 3 kHz, but special applications may demand up to 14 kHz.

2. Spin–Spin Coupling. As already mentioned, spins which are strongly coupled affect the field strength felt by each of them, since they themselves have magnetic moments. Any given nucleus senses the presence of all other magnetic nuclei in the vicinity, which will influence it to a greater or lesser extent depending on the distance between them (and on other factors, such as their relative orientations and the strength and nature of the bonds, for *J*–coupling). Thus, as with shielding anisotropy, a range of different resonance frequencies arises.

There are two distinct types of coupling to consider: homonuclear (between nuclei of the same isotope) and heteronuclear (between different isotopes). Heteronuclear *decoupling* is quite easily achieved in solids and liquids by irradiating one nucleus continuously at the same time as performing the normal pulsed NMR experiment on the other. The continuous irradiation causes rapid transitions which result in a complete time–averaging of the coupling effect to zero. The irradiation has to be intense in solids and so is described as

high–power decoupling.

Homonuclear decoupling is more difficult. In solutions, the only observed coupling tends to be intramolecular *J*–coupling (since tumbling averages away dipolar couplings) and the small number of well–defined homonuclear couplings that remain show up clearly as splittings in the spectra which are of importance as an analytical tool. In solids, however, such a range of dipolar couplings exists that the signals of abundant nuclei (such as ^{1}H) are often broadened beyond all recognition. Homonuclear decoupling techniques in solids rely on averaging out the couplings by making the *bulk magnetization* tumble, just as it would if the molecules were in rapid motion. (Fast MAS could achieve the same effect, but many samples would require unattainably high rotation rates.) Special and elegant multiple pulse sequences are applied during acquisition of the FID to bring this tumbling about. When combined with MAS, the technique is known as *C*ombined *R*otation *A*nd *M*ultiple *P*ulse *S*pectroscopy (CRAMPS).[3]

3. Chemical Shift Dispersion. This is more a chemical than a magnetic effect. If the nuclei giving rise to a particular signal are not in chemically identical environments, they will probably differ somewhat in chemical shift. If the range of environments is continuous (as for a glass or otherwise amorphous solid), the result will be a broadening of the observed signal. In this project, this phenomenon is of significance in the interpretation of many ^{29}Si and ^{1}H NMR spectra.

4. Quadrupolar Nuclei. Any nucleus which has a spin I greater than $\frac{1}{2}$ has an electric quadrupole moment. Such a quadrupolar nucleus differs from others in that its quadrupole moment interacts with any gradient in the surrounding

electric field, resulting in a quadrupolar splitting of the energy levels supplementary to the Zeeman splitting created by B_0. The practical effect of this is a change in the observed transition frequency. The perturbation is dependent on the angle θ between the electric field gradient (EFG) axis and B_0, and on which of the $2I+1$ possible transitions is being considered; in solutions the quadrupolar effect is substantially (but often not totally) averaged out by molecular tumbling, but in powdered solids all possible values of θ are present, resulting in a broad and characteristic line shape. In principle MAS could narrow this, but sufficiently high spin rates can seldom be achieved. Various other techniques are available, however, such as spinning about an axis at another angle to B_0, or about two axes simultaneously.

In the present work, involving the quadrupolar nucleus ^{27}Al ($I = \frac{5}{2}$), the situation is actually simpler than the preceding discussion implies.[4] Firstly, unless the quadrupolar interaction is very small (*i.e.* the nucleus is in a highly symmetric environment), all the transitions other than the central $m_I = \frac{1}{2} \leftrightarrow -\frac{1}{2}$ are unobservable, because they occur at frequencies outside the excitation bandwidth of the RF pulse used. The remaining central transition is also unaffected by the quadrupolar interaction to first order, because the energies of the $m_I = \frac{1}{2}$ and $m_I = -\frac{1}{2}$ states change equally. This means that there is also (again to first order) no dependence of the transition frequency on θ, and so the band is narrow by the standards of most other quadrupolar signals. Second–order effects produce a broadening and a shift in the position of the band; neither of these effects is as great as the chemical shift difference between Al in tetrahedral and octahedral environments in zeolites, however, as discussed in Section C.

4. Spin–Locking and Cross–Polarization

Once magnetization has been developed in the x–y plane of the rotating frame of reference, it normally undergoes spin–spin relaxation to return to the equilibrium state, with no net magnetization component in the x–y plane. It is possible to prevent this from happening by applying a RF field B_1 aligned along the same axis as the magnetization, a procedure known as *spin–locking.* During spin–locking, the bulk magnetization decays, dispersing its magnetization to the lattice, at a rate (often exponential) characterized by the *rotating frame spin–lattice relaxation time* $T_{1\rho}$. As the spins are controlled only by B_1 and not by B_0 during spin–locking, their effective Larmor frequency becomes equal to γB_1, and it is lattice motion at this frequency which stimulates $T_{1\rho}$ relaxation. The relevant frequency is of the order of tens of kilohertz.

Spin–locking creates the possibility of flip–flop transfer of magnetization between dissimilar nuclei, *e.g.* ^{1}H and ^{29}Si. In order to achieve this, the ^{1}H magnetization is flipped into the x–y plane and then both nuclei are spin–locked simultaneously with different B_1 fields so that their effective Larmor frequencies are equal. This can be expressed as

$$\gamma_H \, B_{1,H} = \gamma_{Si} \, B_{1,Si}$$

which is the *Hartmann–Hahn matching condition.* The overall effect is transfer of magnetization from the previously excited nucleus (here ^{1}H) to the other nucleus (^{29}Si), a very important procedure known as *Cross–Polarization* (CP).[5] The transferred magnetization can then be observed in the usual way. The pulse sequence for CP is shown in Figure 2.2.

The CP experiment, which is usually performed with magic angle spinning (CP/MAS), differs in several important respects from single pulse (SP) spectroscopy:

1. The resulting signal intensity may be greater than that obtained from

Figure 2.2: The Cross–Polarization Pulse Sequence

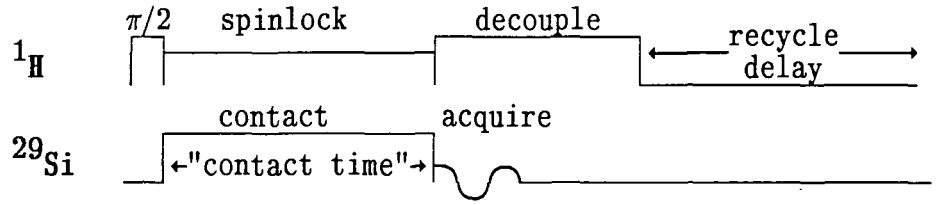

a single pulse experiment, improving the observed signal–to–noise (S/N) ratio. (When all factors are taken into account, however, the overall gain for ^{29}Si CP/MAS of zeolites is often insignificant.),

2. The pulse sequence is dependent on the ^{1}H magnetization being fully relaxed between repetitions, not that of the ^{29}Si. As ^{1}H T_1 values in zeolites are always much shorter than ^{29}Si, recycle times can be much shorter than for SP spectra, resulting in a substantial saving of spectrometer time.

3. The ^{1}H and ^{29}Si spins must be efficiently coupled to permit CP. This basically requires that they be fairly close together and not too mobile.[6] As a result, CP/MAS spectroscopy is selective for strongly coupled spins, which provides another source of information about the system; however, CP/MAS signal intensities are therefore not related to site population alone.

Two useful variants of CP/MAS have been employed in this work:

1. Variable Contact CP/MAS: In this experiment, the spectrum is recorded repeatedly with different durations of the contact time, that is, the period for which both B_1 fields are turned on, during which CP takes place. The results are obtained as a plot of signal intensity *vs.* contact

time for each peak. The plot is described by an equation of the following form:[7]

$$I = \frac{S}{1 - \frac{T_{CP}}{T_{1\rho}}} \left(1 - \exp\left[\frac{\left[\frac{T_{CP}}{T_{1\rho}} - 1\right]\tau}{T_{CP}}\right]\right) \exp\left[\frac{\tau}{T_{1\rho}}\right]$$

where τ is the contact time, S is the maximum intensity of the peak and T_{CP} is the time constant for magnetization transfer, which basically describes the efficiency of CP and hence the coupling relationship between the nuclei. (The formula makes the usually valid assumption that $T_{1\rho}^{^{29}Si}$ is much longer than the contact times used, which are generally in the range 1 – 30 ms.)

2. ^{1}H T_1–selective CP/MAS: This novel experiment involved pre–treatment of the ^{1}H magnetization before CP. Normally a sample was chosen with two signals in the ^{1}H spectrum which differed substantially in T_1. Instead of exciting the ^{1}H spins with a simple $\pi/2$ pulse, the sequence $\pi - \text{delay} - \pi/2$ was used, as in the inversion–recovery experiment. The duration of the delay was selected to be $\ln 2$ times the T_1 value of one of the ^{1}H species present, so that the magnetization of this species just decayed to zero at the moment of the $\pi/2$ pulse. The only remaining magnetization, arising from the other ^{1}H species, was spin–locked and cross–polarized in the usual way. The overall effect was to achieve CP from just one of the two ^{1}H species at a time provided that the species did not exchange energy by spin diffusion or chemical exchange. This amounts to a form of selective cross–polarization (SCP). The resulting ^{29}Si CP/MAS spectra show which ^{1}H spins are most effectively coupled to each ^{29}Si species. The complete pulse sequence for the SCP experiment is shown in Figure 2.3.

Figure 2.3: The SCP Pulse Sequence

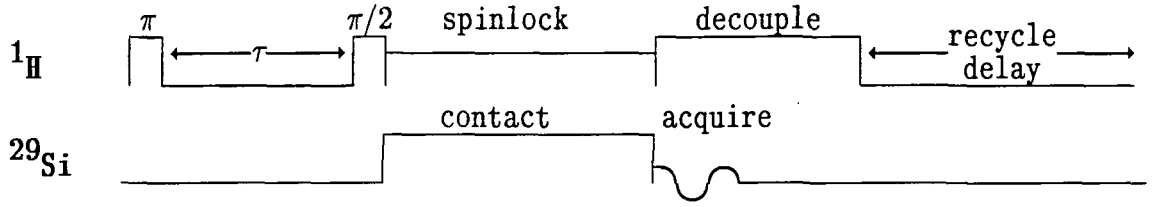

5. Quadrupolar Nuclei: Influence of Environment on NMR Behaviour

It has already been mentioned that, on application of a B_1 field (RF pulse), the bulk magnetization arising from an ensemble of spins nutates around the axis along which B_1 is aligned, circulating at a rate determined only by the intensity of B_1. This is only strictly true for non–quadrupolar ($I = \frac{1}{2}$) nuclei. For quadrupolar nuclei, the situation is much more complex, as follows.

The behaviour of the nuclei can be described in terms of two limiting cases.[8] The first is when the intensity of the B_1 field (as described by the angular nutation frequency ω_{RF}) is much greater than the quadrupole splitting (ω_Q, where $\omega_Q/2\pi = \chi$, the quadrupole coupling constant) – *i.e.* when the nuclear environment is highly symmetrical. Then the intensity, I_1, of the NMR signal of the transition $m_I \leftrightarrow m_I+1$ resulting from a pulse of duration t_p is given by

$$I_1 = \tfrac{1}{2}\xi^2 \sin(\omega_{RF} t_p)$$

where $\xi^2 = I(I+1) - m_I(m_I+1)$. If all transitions are observed the total intensity measured is the sum of the contributions from each transition. In the case of the ^{27}Al nucleus, this is 35/9 times the intensity of the central transition ($\frac{1}{2} \leftrightarrow -\frac{1}{2}$). In zeolites, however, only the central transition is usually excited, and so this correction need not be taken into consideration.

The second case is when ω_Q greatly exceeds ω_{RF}. Then the intensity I_2

of the signal is

$$I_2 = \tfrac{1}{2}\xi \sin(\xi\omega_{RF}t_p).$$

The important property of this result is that it reduces to the first case when the term in the brackets is so small that the approximation $\sin\alpha \simeq \alpha$ becomes valid. For this to occur, $\omega_{RF}t_p$ needs to be small, preferably $\pi/20$ or less. This then effectively removes the ω_Q dependence of the NMR intensity, since the two limiting cases become virtually equal ($I_1 \simeq I_2$).

Thus, in order to obtain quantitatively comparable ^{27}Al NMR intensities from sites differing in ω_Q, it is necessary to use a small flip angle. This approach has been widely adopted in the present work; a flip angle of $3\pi/40$ was employed for many samples.

2B: NMR EQUIPMENT USED

The majority of the NMR spectroscopy for this work was performed with a Bruker CXP–200 instrument in the Department of Chemistry, University of Durham. Other spectrometers were used for certain supplementary experiments: Bruker CXP–300 at Unilever Research Port Sunlight Laboratory; Varian VXR–300 at the University of Durham Industrial Research Laboratories; and a custom–built 60 MHz FT instrument, referred to hereafter as 'the WRAC',[9] in the Department of Chemistry, University of Durham. These instruments are all dedicated to solid–state spectroscopy.

1. CXP–200

Most of the spectroscopy carried out on this instrument employed a Bruker broadband double–resonance probe. The probe is equipped with a

double–bearing magic–angle spinning facility, driven by dried compressed air. This system uses a 7 mm o.d. zirconia rotor with a Kel–F cap, and is capable of spinning up to at least 4.5 kHz, with a typical stability of ±5 Hz.

The angle of the spinner axis was adjusted to the magic angle using the ^{79}Br resonance of KBr. The FID was inspected and the angle adjusted to maximize the intensity of the rotational echoes (spikes). The conditions used were as follows: operating frequency = 50.143502 MHz; carrier offset = 0 Hz; dwell time = 4 μs; acquisition time = 16 ms; recycle delay = 5 s; pulse angle = $\pi/2$; number of averages = 1; rotation rate = 850 Hz; receiver attenuation = 28 dB; no ^{1}H–decoupling.

For **^{1}H spectroscopy**, the decoupler channel of the probe is used. The primary reference is tetramethylsilane (0 ppm), with a sample of silicone rubber (0.06 ppm) used as a secondary reference. The Larmor frequency of TMS is 200.130000 MHz ± 4 Hz (the deviation is taken into account when calculating chemical shifts); this frequency is checked by observing the FID signal to be 'on resonance' (*i.e.* not oscillating) when the carrier frequency of 200.130000 MHz is subtracted. No field–frequency lock is employed, as the spectrometer remains indefinitely stable to within a few hertz. The silicone rubber sample is used for shimming, for which a full width at half height (FWHH) of $16-20$ Hz is routinely achieved. It is also used for adjustment of the B_1 field strength, which is typically set to 62.5 kHz (*i.e.* $\pi/2$ pulse duration of 4 μs). The proton probe and rotor background signal is negligibly weak.

For **^{29}Si spectroscopy**, the primary reference is again TMS, with silicone rubber (–22.7 ppm) serving as a secondary reference, and for adjustment of the B_1 field strength to 62.5 kHz. The operating frequency is 39.760206 MHz, checked as before by setting the signal from TMS on resonance. High–power ^{1}H decoupling (at a power level equivalent to 62.5 kHz) is often employed. Once

again, the background signal is negligible. When cross–polarization is used, the ^1H amplifier is driven by a Wavetek 5155A synthesizer, with a modified Bruker decoupler unit used for modulation. The Hartmann–Hahn match is set using a silica abrasive material known as GASIL–200 provided by Mr J.W. Rockliffe of Unilever Research Port Sunlight Laboratory. This is a hydrated amorphous silica, containing very small amounts of trace metals, with a surface area of 700 m^2g^{-1} and a particle size of ~4 μm, and was supplied by Crosfield Catalysts, Warrington. The tuning–up procedure used is as follows. First the ^1H amplifier

Figure 2.4: ^{29}Si CP/MAS spectrum of GASIL–200
NT=16 RO=1207 RD=500ms CT=10ms

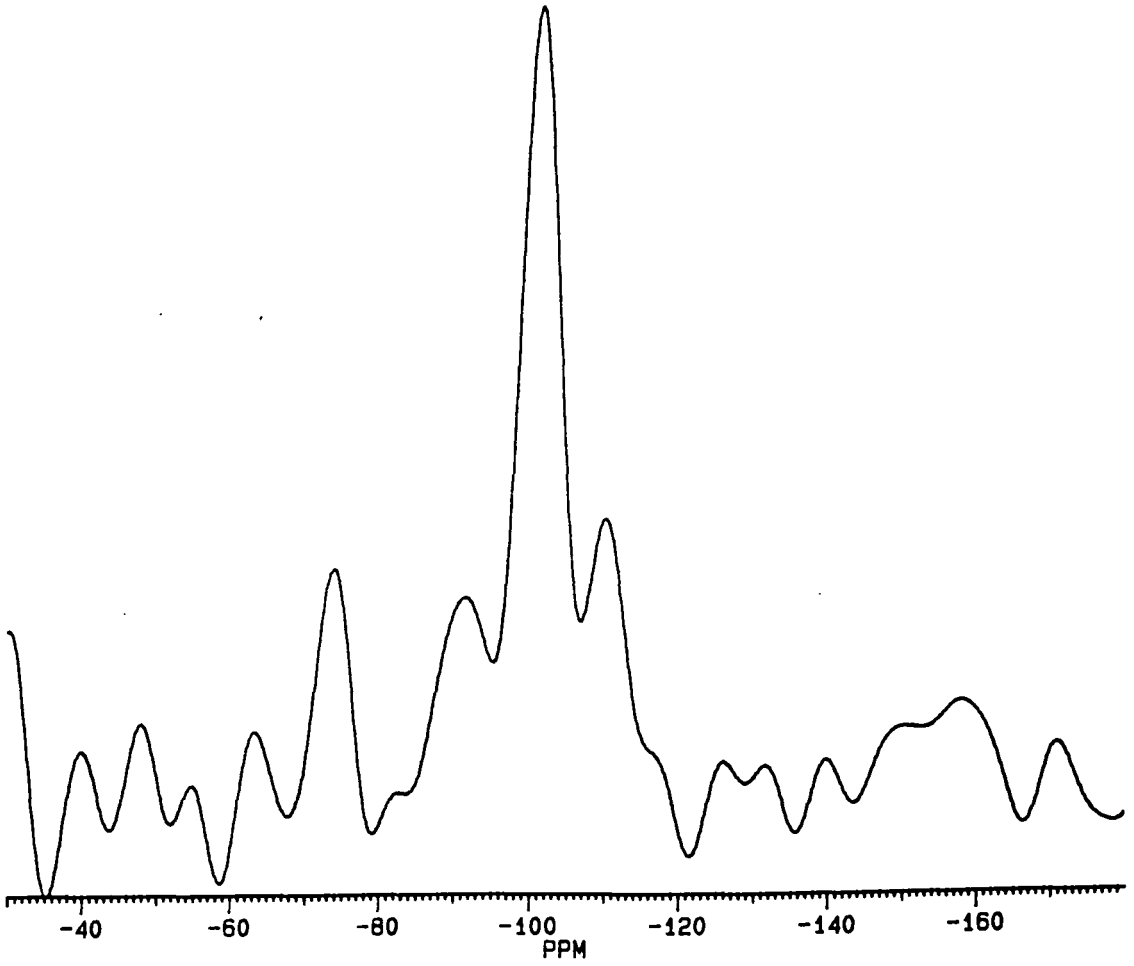

is set to give a $B_1(^1H)$ field strength of 62.5 kHz, using the silicone rubber sample as described above. Then CP is attempted with the GASIL–200 sample using the following conditions: pulse duration = 4 μs, contact time = 10 ms, recycle delay = 250 ms, dwell time = 25 μs, acquisition time = 2.5 ms, number of averages = 16, carrier offset = –2 kHz. When the $B_1(^{29}Si)$ field strength has been adjusted to optimize the Hartmann–Hahn match, a cluster of three peaks is clearly visible (with a typical signal–to–noise ratio of 15) at –91.6, –101.3 and –109.6 ppm, in the approximate intensity ratio 1:3:1 (see Figure 2.4).

For **^{27}Al spectroscopy**, the reference used is a dilute aqueous solution of $AlBr_3$ (0 ppm). This sample is also used for adjustment of the B_1 field strength to 62.5 kHz. The operating frequency is 52.147630 MHz, checked by setting the signal from the primary reference sample, 1M $AlCl_3$ (aq), on resonance. High–power proton decoupling is usually employed. The background signal is again negligible.

A small amount of ^{13}C NMR has also been carried out. The primary reference is TMS, with adamantane used as a secondary reference (38.5 and 29.5 ppm) and for adjustment of the B_1 field strength and Hartmann–Hahn match. The operating frequency is 50.322695 MHz, checked with TMS as before.

The confidence in quoted chemical shifts is generally around 0.1 ppm, although caution must be exercised where broad lines are concerned, since it can be difficult to pinpoint the exact centre of the band, especially if the spectrum is noisy.

2. CXP–300

This spectrometer, which is located at Unilever Research Port Sunlight Laboratory, uses the same probe type, MAS system and rotors as the CXP–200 at Durham. Experimental procedures are identical with the following exceptions.

The ^{1}H operating frequency is 300.13 MHz. The power level used for ^{1}H and ^{29}Si SP and CP/MAS is 50 kHz ($\pi/2$ pulse length = 5 μs). The sample used to tune for CP is the cubic octamer $(Si(OSiMe_3))_8$, often referred to as Q_8M_8, supplied by Bruker Spectrospin Ltd. The following settings are used: operating frequency = 59.621 MHz; carrier offset = 1 kHz; number of transients = 8; recycle delay = 20 s; contact time = 10 ms; acquisition time = 100 ms. There is no ^{29}Si background signal. The ^{1}H background has been subtracted from all appropriate spectra in this thesis.

3. VXR–300

The **^{1}H spectroscopy** carried out on the VXR–300 employed a Doty broadband probe and 7 mm sapphire or zirconia rotors with Kel–F or Vespel end–caps. Dry air was used as a drive gas (for this and all nuclei on the VXR). Tetramethylsilane was used as a reference and for tuning up; the B_1 field strength was typically 62.5 kHz ($\pi/2$ pulse = 4 μs). The probe has a background signal at 1.4 ppm (FWHH 160 Hz).

For **^{29}Si spectroscopy**, the Doty 7 mm probe was used. Sodium 3–(trimethylsilyl)–1–propanesulphonate ('TMS Salt') was used as a secondary reference (1.8 ppm), for tuning up (B_1 = 62.5 kHz) and for setting the Hartmann–Hahn match for CP. Chemical shifts were reproducible on different days to within ±0.2 ppm. The probe gave no background signal.

For **^{27}Al spectroscopy**, a Varian PLE probe with 7 mm plastic rotor was mainly used. The reference and tuneup sample was a molar aqueous solution of $AlCl_3$. The B_1 field strength was normally set to 41.7 kHz with a $\pi/6$ (2 μs) pulse being employed. The probe gave no background signal. Occasionally a Doty fast–spinning probe with 5 mm Si_3N_4 rotors was used. This probe has a substantial background signal, which was subtracted from the spectra before

plotting. ^{27}Al CP/MAS was performed on the PLE probe. The Hartmann–Hahn match was set using $NH_4Al(SO_4)_2$ with a recycle delay of 1 s, a 500 μs contact time, a 20 ms acquisition time and four averages.

4. The WRAC

This is a 60 MHz (for ^1H) FT instrument without sample spinning; it was used primarily in this work for measuring ^1H relaxation times. The secondary reference and tuneup sample used is liquid butane–1,4–diol in a 7 mm NMR tube. The field strength is typically set to about 140 kHz ($\pi/2$ pulse duration = 1.8 μs) for T_1 and T_2 measurements, and to 20 kHz ($\pi/2$ pulse duration = 12.5 μs) for $T_{1\rho}$ measurements. Normally just the first point of the FID is recorded (corresponding to the instantaneous magnetization around 8 μs after the end of the pulse) for each cycle of the pulse program used for relaxation time measurements; these points are gathered together to form a magnetization *vs.* delay time relaxation profile, which can generally be deconvoluted into separate (often exponential) decaying components using home–written software.

2C: APPLICATION OF SOLID–STATE NMR TO ZEOLITES

NMR is now well established as an important and informative technique for the study of zeolites. In conjunction with other spectroscopies such as infra–red and X–Ray Diffraction (XRD), and with physical techniques such as Temperature Programmed Desorption and Elemental Analysis, it provides key information enabling the characterization of zeolite samples. Its principal advantages over other techniques are its non–invasiveness (ensuring that the

sample is in the desired form during the measurement) and its sensitivity to small, localized changes. Under appropriate conditions, it is also possible to use NMR for quantitative analysis.

The spectra shown in this thesis were obtained by Fourier Transformation of the acquired FID truncated beyond the point at which the signal content of the data was judged by inspection to have decayed to a negligible level; no line–broadening or resolution–enhancement was employed. Baseline roll was removed by subtraction of a manually–generated polynomial curve from the spectrum, or (rarely) by left–shifting of the FID. The following sections describe typical operating conditions for each nucleus studied and discuss the existing knowledge concerning the interpretation of the results obtained.

1. ^{29}Si NMR

Operating Conditions. The usual manner of acquiring ^{29}Si NMR spectra of zeolites is by means of a single pulse experiment with or without high–power ^{1}H decoupling. Normally, in order to ensure that the signal intensities observed are quantitatively accurate, it is necessary to leave a delay of at least five times the longest ^{29}Si T_1 relaxation time present after each pulse–acquire sequence. In practice, this is effectively prohibited on account of the spectrometer time that would be required since the observed ^{29}Si T_1 values can be very long (>100 s).[10] Also, the T_1 values of a given sample are found to be (i) quite similar to each other,[22] and (ii) dramatically reduced by small amounts of adsorbates and impurities, especially paramagnetic species such as O_2[24] and Fe^{3+}. Accordingly, it is generally considered acceptable to use a recycle delay of $10 - 20$ s and still have reasonable confidence that the relative intensities of signals in a given spectrum are representative of the populations of different silicon sites within a reasonable error margin. A recycle delay of 20 s has been employed for most of the present work. Some workers have employed Ernst's procedure[23] of applying pulses of an angle less than $\pi/2$ with a recycle delay shorter than $5T_1$ in order to maximize the signal intensity acquired in a given time; this practice has however

not been used here on account of the variability of the ^{29}Si T_1 values in the materials studied.

Other typical operating conditions are as follows: number of averages = 2000–10000; MAS rate = 2–3 kHz; spectral width = 20 kHz; pulse angle = $\pi/2$; carrier offset = –2 kHz (the signals occur at around –4 kHz relative to TMS, but the carrier was usually set a little away from this point to avoid the appearance of artifacts in the region of interest); acquisition time = 5 ms. High–power ^1H decoupling was generally found to have no observable effect on the spectrum.

Basic Appearance of the Spectrum. In highly crystalline Zeolite Y, all Si sites are crystallographically equivalent. Thus, for a ^{29}Si nucleus in a silicon–rich region of the crystal, only a single chemical shift should arise. This is indeed observed for highly dealuminated samples (see Figure 2.5(a)). However, when the observed nucleus is only a few bonds away from Al atoms isomorphically substituted into the lattice, the Al atoms alter the electronic environment of the ^{29}Si nucleus: they deshield it by withdrawing electron density, on account of the lower electronegativity of Al compared with Si, resulting in an increased chemical shift. Each Al in a nearest–neighbour relationship to a ^{29}Si nucleus increases its chemical shift by about 6–7 ppm. In a zeolite lattice, each tetrahedral atom has four nearest neighbours, bonded to it *via* oxygen bridges. A Si atom with n nearest–neighbour Si and $(4-n)$ nearest–neighbour Al is referred to as being in a Si(4–n Al) or Q^n site. (The Q^n notation is used throughout in the present work.) So, for Zeolite Y, a ^{29}Si nucleus in a Q^4 site typically resonates at about –107.5 ppm, as in Figure 2.5(a), where all ^{29}Si are in Q^4 sites. Q^3 sites are observed at about –101 ppm, Q^2 at –94.5 ppm and so on.[11] Figure 2.5(b) shows the spectrum of an aluminium–rich sample of Zeolite Y in which all five possible

Figure 2.5: ^{29}Si SP MAS spectra
(a) Steamed Zeolite Y, showing single Q^4 peak NT=8000 RD=20s RO=1221
(b) NaY as synthesized, with Q^0–Q^4 sites NT=2000 RD=10s RO=3094

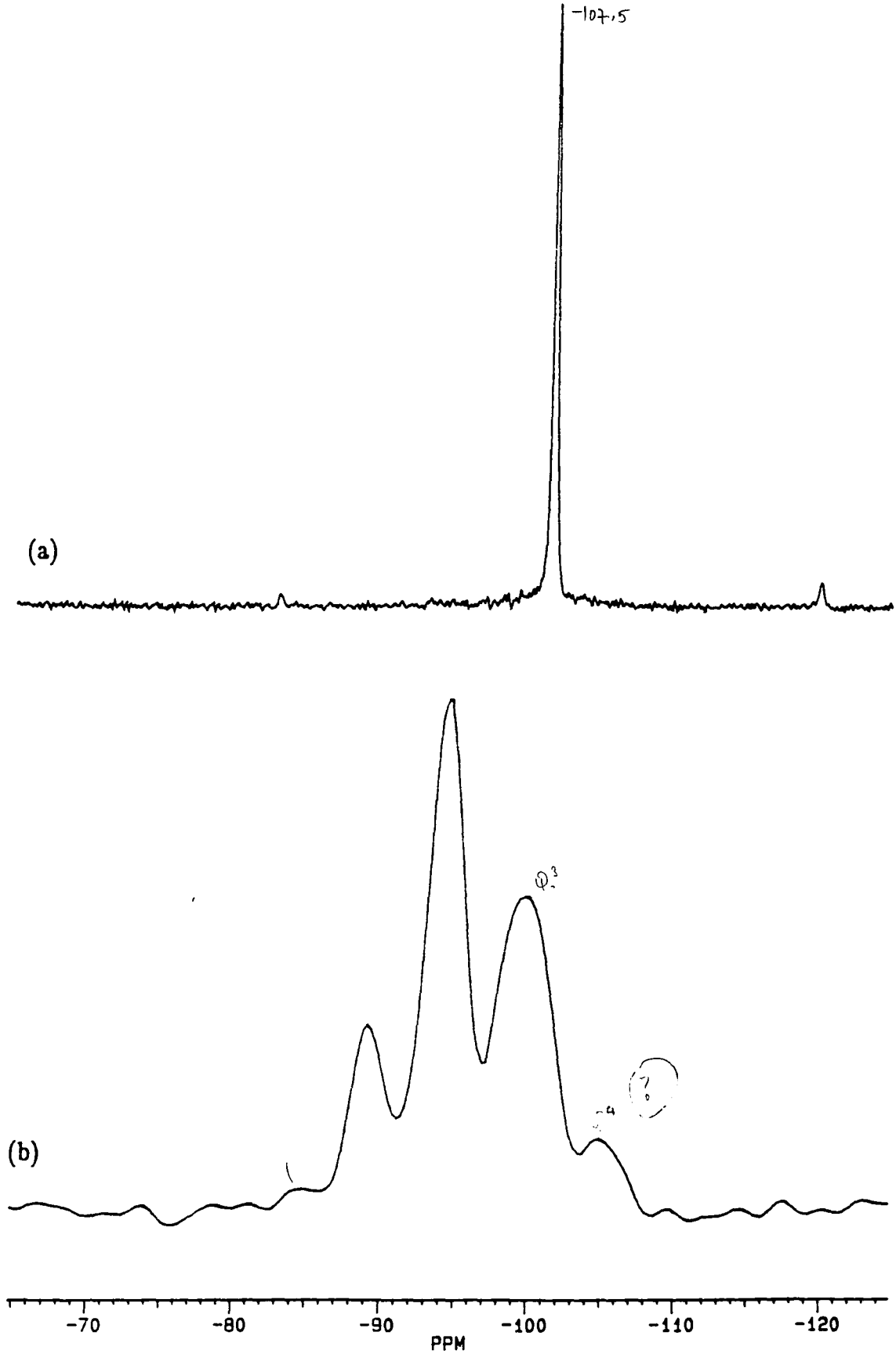

sites are observed, with different populations.

Estimation of Lattice Si/Al Ratios. Using a spectrum such as that shown in Figure 2.5(b), it is possible to calculate the ratio of lattice tetrahedral sites (T–sites) occupied by Si to those occupied by Al. The following assumptions are made:

(i) The lattice structure is as described earlier (perfectly crystalline, with each T–site crystallographically equivalent and occupied by Si or Al); this is generally an acceptable approximation, although there are some complications: see Chapter 4 for a detailed discussion.

(ii) There are no Al atoms on adjacent T–sites, i.e. no Al–O–Al linkages. This is known as *Loewenstein's Rule*[12] which is always obeyed for Zeolite Y.

The analysis runs as follows. Each ^{29}Si in a Q^n site detected by ^{29}Si NMR shows the presence of $4-n$ Al atoms. The intensity of the signal from a Q^n site is directly proportional to the population of that site. So, if I_n is the intensity of the Q^n signal (in appropriate units), the number of Al atoms detected is given by $0I_4 + 1I_3 + 2I_2 + 3I_1 + 4I_0$, which can be written as $\sum_{m=0}^{4}(4-m)I_m$. However, by this analysis, each Al is counted four times (as Loewenstein's Rule requires it to be bonded to four Si atoms). Therefore, the ratio of Si to Al in the lattice is given by the total Si content divided by $\frac{1}{4}\sum_{m=0}^{4}(4-m)I_m$, i.e.[13]

$$\mathrm{Si/Al} = \frac{4\sum_{m=0}^{4} I_m}{\sum_{m=0}^{4}(4-m)I_m}$$

From this, the number of Al atoms per unit cell (x) can be found: as there are 192 T–sites per unit cell, the Si/Al ratio is $(192-x)/x$; this rearranges to give

$$x = 192 \,/\, (1 + \text{Si/Al ratio})$$

In practice, it is not sufficiently accurate to use integration to find the I_n values from the spectrum, since the peaks always overlap; nor is it adequate simply to use peak heights, since the linewidths of the Q^n signals vary. The normal method employed is spectral deconvolution by computer, as described in Chapter 3.

Influences on Linewidths. In addition to the chemical shift effects already discussed, there is another feature of ^{29}Si single–pulse spectra of zeolites worthy of consideration: the linewidths of the observed signals. Most of the normal sources of line broadening can be considered negligible in this case: the ^{29}Si nucleus is rare, and so homonuclear dipolar couplings are weak; high–power decoupling is applied to remove the broadening effect of heteronuclear coupling to ^{1}H; MAS averages out the effects of shielding anisotropy. ^{29}Si–^{27}Al coupling can further be ruled out on the grounds that a change to higher B_0 field strength results in no significant improvement in spectral resolution.

It is now widely believed that the linewidth of ^{29}Si signals in zeolites arises from chemical shift dispersion caused by the fact that a given Q^n site may have a wide range of possible Al occupancies in the next–nearest–neighbour (NNN) lattice position.[14] For example, a Q^4 site has four nearest neighbours, each with three other neighbours, resulting in twelve NNN sites for the central Q^4 site. Any number of these may be occupied by Al, subject to the constraints of Loewenstein's Rule. The NNN Al occupancy influences the chemical shift of the central site, either by shielding effects or by subtle variations in the bond angles around the site, which have been shown to be important in controlling ^{29}Si chemical shifts.[15] In a thorough study of chemical shifts obtained and published by a number of workers over a period of several years, Newsam[16]

conclusively demonstrated the existence of a significant shielding effect, extrapolating to a difference in chemical shift of some 5 ppm between a Q^4 site with nine NNN Si atoms and in one with nine NNN Al atoms. There was also shown to be a good correlation between the possible number of NNN Al for a given Q^n site (limited by Loewenstein's Rule) and the gradient of a plot of ^{29}Si chemical shift *vs.* Al content, indicating that the NNN shielding effect is indeed a factor of importance. The correlation with the number of NNN sites physically close to the central site was much poorer, indicating that the shielding is transmitted through bond connectivity, and not through space as originally proposed by Klinowski *et al.*[17] Newsam's study did not discriminate explicitly between direct shielding and bond–angle effects, although it was pointed out that bond angles may well change with NNN Al occupancy, resulting in the observed shift being a hybrid of the two effects. In some systems, such as the Si, Ga analogue of Zeolite Y, the bond angle changes are much more pronounced, and the NNN occupancy is found to have a much stronger influence on the ^{29}Si chemical shift.[18]

It is clear, then, that NNN occupancy has a significant effect on ^{29}Si chemical shifts. In a zeolite with a range of NNN occupancies for each Q^n site, this will result in splitting, or, more likely, inhomogeneous line broadening. Confirmation of this is found in the observation that very narrow signals are obtained from high–quality minerals, which have highly ordered structures (i.e. a low scatter of NNN occupancy), from Zeolite A, which has strict Si, Al alternation on lattice sites, and from highly siliceous zeolites, like that in Figure 2.5(a).

Newsam[16] has pointed out that the observed *chemical shift* of a given Q^n signal should be directly correlated with the lattice Si/Al ratio. An estimate of this quantity made by deduction from this relationship is likely to be more

trustworthy than one made by the conventional approach of measuring the *intensities* of the Q^n peaks for samples with Si/Al > 10, since the peaks for $n \lesssim 3$ become very weak.

In the light of this discussion, it seems that most of the line broadening in ^{29}Si single pulse NMR spectra of Zeolite Y arises from chemical shift dispersion due to next nearest neighbour effects. This implies that ^{1}H–^{29}Si heteronuclear dipolar coupling, if present, is not very strong, since heteronuclear decoupling is observed to have no effect on the spectra.

Appearance of SiOH Groups. So far this discussion of ^{29}Si NMR spectra of zeolites has considered only perfect crystals, that is, those with a Si or Al atom at every T–site in the lattice. Zeolite samples which have not undergone any treatment other than ion–exchange since synthesis are usually of high crystallinity, with very few T–sites unoccupied. However, once a sample has been subjected to thermal treatment, a certain amount of degradation of the lattice takes place, initially by loss of individual T atoms and later by collapse of small zones of the crystal to form cavities known as *mesopores.* (These processes are discussed further in Chapter 4.)

It is generally considered that the unsatisfied coordination sites of the T atoms surrounding a newly–formed lattice vacancy are filled by the formation of OH groups. As the T atom lost from the lattice is much more often an Al than a Si, the new linkages are likely to be SiOH groups. It is widely held, on the basis of evidence from silica gel, that the OH group on a lattice Si has a similar ^{29}Si NMR appearance to the lost Al, and so the formation of a 'nest' of four SiOH groups concomitant with the loss of one lattice Al has almost no net effect on the ^{29}Si single pulse NMR spectrum. This is indeed observed to be true in some cases, but very far from true in others; a detailed study of this subject has been

carried out and is described in Chapter 4.

Appearance of Amorphous Silica. In addition to the silicon present in the zeolite lattice, it is possible for some silicon to exist in the pores of the crystal, presumably as some form of amorphous silica. (Evidence for this is discussed in the first part of Chapter 4.) This material can be detected by ^{29}Si NMR as a broad band underlying the relatively narrow Q^0–Q^4 signals from lattice silicon, or as a shoulder on the low–frequency side of the Q^4 peak (at around –110 to –113 ppm). Spectral deconvolution may permit estimation of the amount of silicon present in a non–lattice environment. X–Ray Diffraction measurements can also provide an indication of the total amount of non–crystalline material present; to ascertain how much of this is alumina, the non–lattice alumina content of the sample can be estimated by ^{27}Al NMR under suitable conditions.

Cross–Polarization NMR. In addition to the single–pulse NMR techniques already described, it is possible to employ the cross–polarization experiment described in Section A. The intensities of the signals resulting from a ^{29}Si CP/MAS NMR experiment are determined not only by the populations of the sites (as in single–pulse NMR) but also by the strength of the time–average dipolar coupling between ^{1}H and the ^{29}Si in question. In zeolites, the most significant influences on the magnitude of this coupling are as follows: firstly, the distance between ^{29}Si and the nearest ^{1}H nucleus; and secondly, the isotropic mobility of the latter on the relevant time scale (typically a few milliseconds). Any ^{29}Si nucleus which is close to a relatively static, or anisotropically mobile, ^{1}H nucleus is likely to show a strong signal in the CP spectrum.

This inherent additional information content of CP spectra is one of the main advantages of the technique for zeolite systems. Another major benefit is

that the recycle delay required to avoid signal saturation is controlled by the T_1 relaxation time of the ^{1}H nuclei, not that of the ^{29}Si, as discussed in Section A. As the ^{1}H T_1 times in zeolites are rarely in excess of 400 ms, ^{29}Si CP/MAS spectra can be acquired with a recycle delay as low as 2 s, representing a substantial saving in spectrometer time when compared with the normal single–pulse value of $10 - 20$ s. Other typical operating conditions used are as follows: number of averages, $4000 - 90000$; MAS rate = $1.2 - 2$ kHz; spectral width = 20 kHz; B_1 field strength = 62.5 kHz ($\pi/2$ pulse duration = 4 μs), both for the excitation pulse and for spin–locking; contact time = $1 - 20$ ms (10 ms is usual); acquisition time = 5 ms.

2. ^{27}Al NMR

Nearly all the ^{27}Al NMR spectroscopy in this project was carried out using the single pulse technique, with or without high–power ^{1}H decoupling. As discussed in Section A, it is necessary to use a small pulse flip–angle with quadrupolar nuclei to achieve quantitatively accurate signal intensities.[19] Typical conditions employed were as follows: B_1 field strength = 62.5 kHz; pulse duration = 600 ns (corresponding to a $3\pi/40$ nutation angle); number of averages = 2000–10000; recycle delay = 100 ms (the ^{27}Al T_1 values in these samples are extremely short[20]); operating frequency = 52.147630 MHz; carrier offset = 0 Hz; spectral width = 50 kHz; acquisition time = 2 ms; MAS rate = 4.5 kHz.

Figure 2.6 shows ^{27}Al spectra of Zeolite Y samples during various treatments as follows: (a) NaY as synthesized; (b) HY after calcination (mild steam treatment); (c) HY after severe steam treatment. It can be seen that the original NaY sample shows a single relatively narrow peak at around 50 ppm, which is assigned to four–coordinate ^{27}Al in the lattice. After calcination,

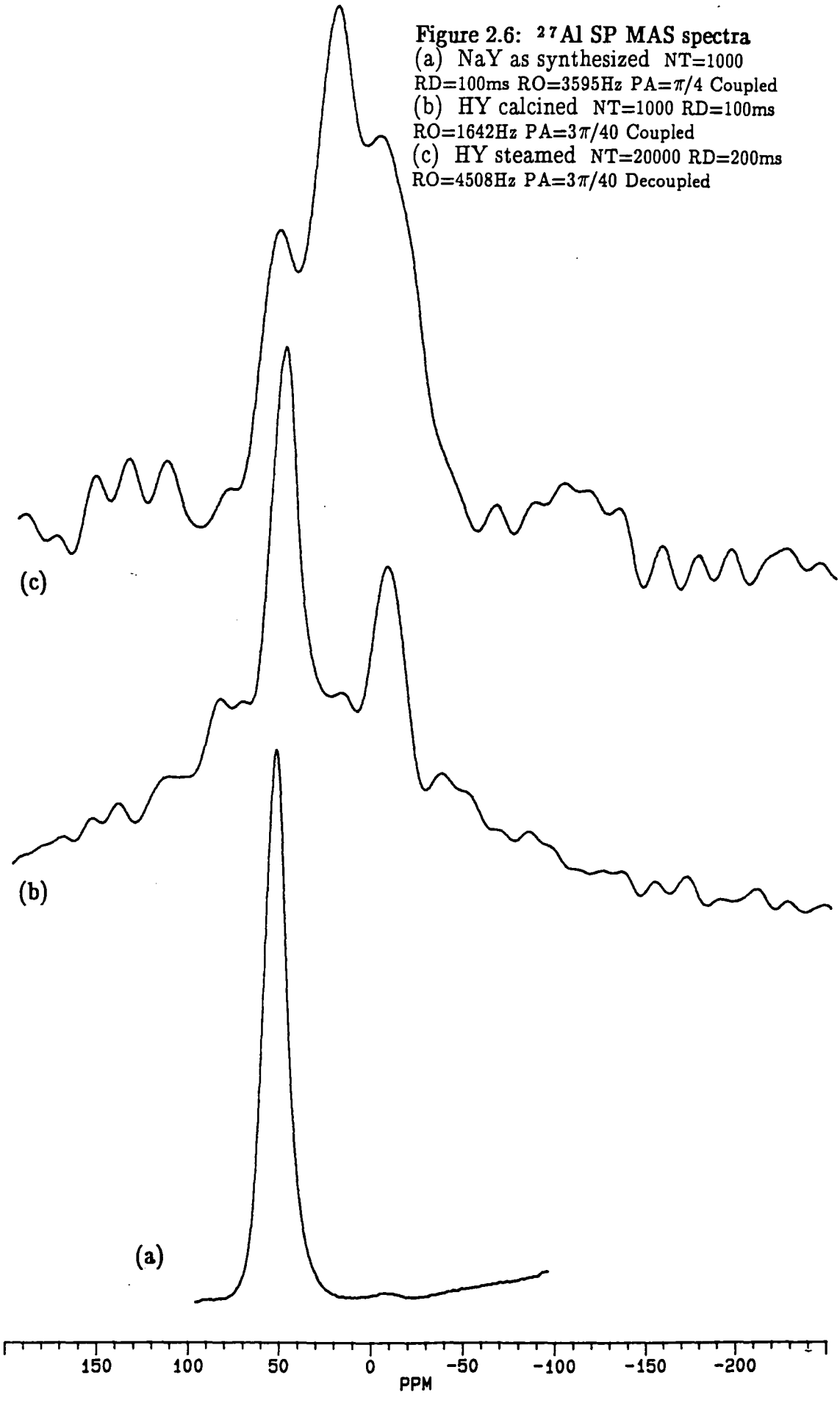

Figure 2.6: ^{27}Al SP MAS spectra
(a) NaY as synthesized NT=1000 RD=100ms RO=3595Hz PA=π/4 Coupled
(b) HY calcined NT=1000 RD=100ms RO=1642Hz PA=3π/40 Coupled
(c) HY steamed NT=20000 RD=200ms RO=4508Hz PA=3π/40 Decoupled

another peak appears at 0 ppm which is generally considered to arise from six–coordinate ^{27}Al existing as some form of alumina or oxyhydroxide in the crystal cavities; this is referred to as *non–lattice alumina* or NLA. This peak becomes much stronger and the whole spectrum broadens on severe steaming, showing a general loss of symmetry in the nuclear environment as the sample crystallinity decreases. The occurrence and nature of zeolitic Al is considered in greater detail in Chapter 4.

Quantification of Al Species Present. Provided that the nutation angle of the pulse used to excite the ^{27}Al nuclei is small enough, the quantitative régime ($I_1=I_2$) described in Section A pertains, and so the intensities of the signals from the lattice and non–lattice aluminium can in principle be used as an indication of their relative populations, provided that the signals can be acceptably deconvoluted. This procedure has been employed in the present work, as will be described later. It is important, however, to recognize the limitations of this approach:

(i) The software available permitted only simple (mainly Gaussian) line shapes to be used in simulating the spectra (using clusters of several such curves to represent a single spectral peak where necessary). Accordingly, the fitting must be regarded as somewhat approximate. In the case of spectra like that shown in Figure 2.6(c), it is believed that complex quadrupolar line shapes are present, heavily overlapping with each other (see Chapter 4 for a discussion); the simple Gaussian deconvolution process is invalid when this occurs. Furthermore, many ^{27}Al signals from zeolites have spinning sidebands, which are also broad and tend to overlap with other signals, as a result of the limited MAS rate available. In some cases an attempt has been made to take these into account

explicitly.

(ii) As zeolitic ^{27}Al signals are broad, a significant fraction of the FID occurs during the first 50 μs or so. Throughout this period, the spectrometer is 'blind', the RF receiver having been 'dazzled' by the large burst of energy pumped into the probe. (This interval is referred to as the instrumental *dead time*). Observed signal intensities are proportional to the amount of magnetization left at the *end* of this time, and so the relative magnitudes of signals differing significantly in relaxation rate will become distorted in the final spectrum. In the case of the present work, this effect is unlikely to be a major problem, since the signals in any given spectrum tend to be comparable in width, and no attempt has been made to fit very broad signals (for which the effect would be most significant).

3. ^{1}H NMR

As with ^{29}Si and ^{27}Al NMR, the ^{1}H spectroscopy carried out in this project employed predominantly the single–pulse technique. The basic operating conditions used were as follows: operating frequency = 200.130000 MHz; carrier offset = 0 Hz; spectral width = 10 kHz; MAS rate = 3 kHz; pulse angle = $\pi/2$. Other conditions depended substantially on whether the sample was wet or dry. Typical values used were as follows:

Parameter	Wet	Dry
Receiver Attenuation/dB	20–30	0–15
Acquisition time/ms	10	50
Number of averages	16	100
Recycle delay/s	1	3–5

The assignments of the most commonly occurring features of ^{1}H NMR spectra of Zeolite Y are now fairly well established (the evidence is discussed in

Figure 2.7: ^{1}H SP MAS spectra
(a) Hydrated NH_4Y, showing NH_4^+ and water peaks
NT=32 RD=2s RO=1600Hz
(b) Typical dried HY sample – see Chapter 5 for discussion
NT=48 RD=5s RO=3000

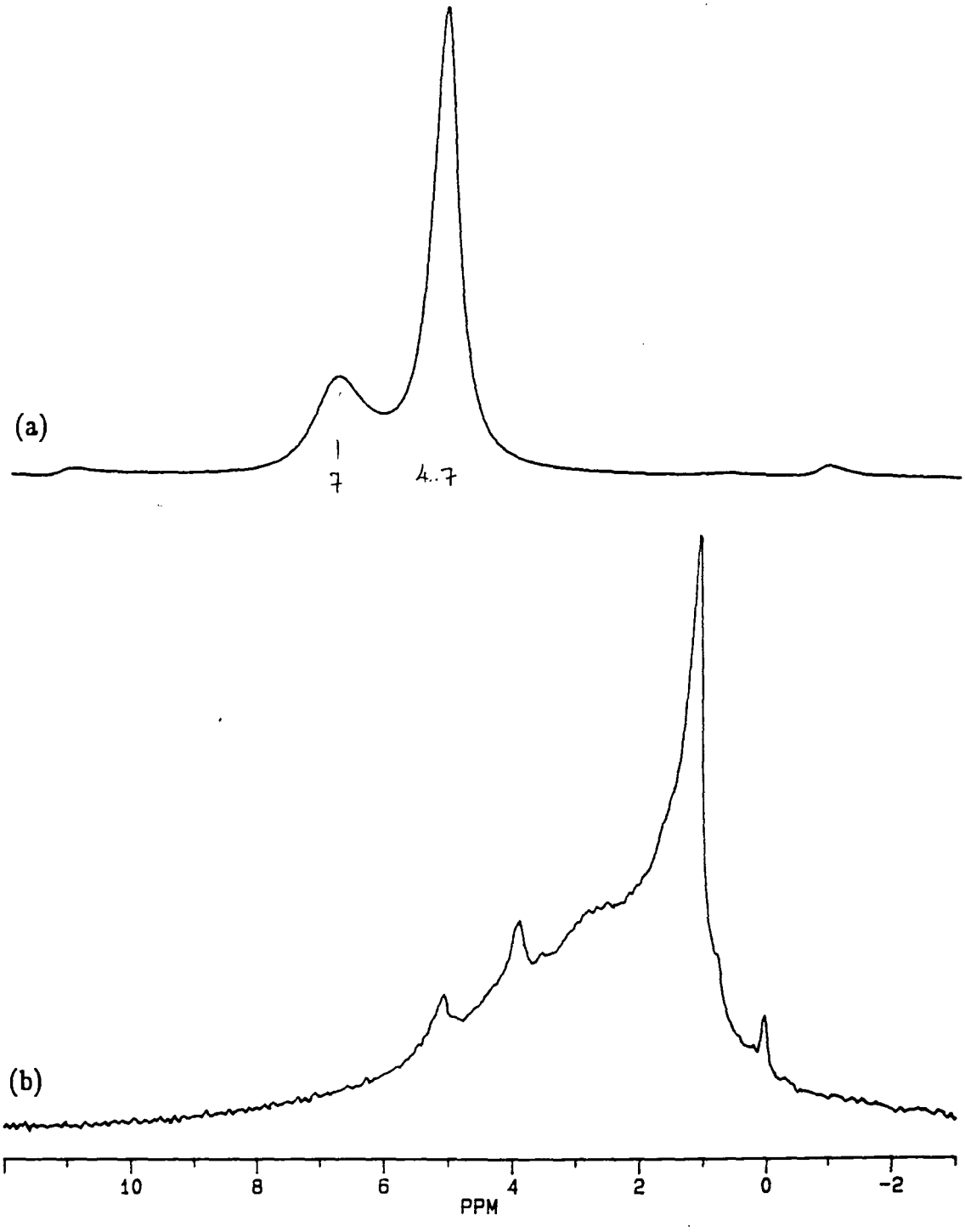

Chapter 5). Figure 2.7 shows two typical spectra: (a) NH_4Y untreated, under atmospheric conditions; (b) HY dried by heating to 400°C under vacuum and kept in an airtight capsule (see Chapter 3 for details of this). The NH_4Y spectrum shows two major features: NH_4^+ ions at 7.0 ppm and adsorbed water at 4.7 ppm. The water peak always occurs in Zeolite Y samples exposed to the atmosphere, and is usually sufficiently intense to mask most other signals. The dried sample, however, shows no peak due to free water, but instead the following signals: 5.2 and 4.0 ppm arising from ^1H on Brönsted sites ($SiO\diagdown^{H}_{Al}$), 2.3 ppm (broad) thought to be due to H_2O adsorbed on, or –OH groups bonded to, NLA; and one or more narrow peaks in the range 0.8 – 1.6 ppm attributed to SiOH. Figure 2.8 shows the typical positions of frequently–occurring signals in the ^1H MAS spectra of Y–type zeolites.

Relaxation Time Measurements. ^1H NMR relaxation times have been measured in a large number of samples and are quoted extensively in Chapters 4 – 7. Spin–lattice (T_1) relaxation times were measured by the inversion–recovery

Figure 2.8: Schematic illustration of the typical positions of signals in the ^1H MAS NMR spectra of hydrated and dehydrated Zeolite HY

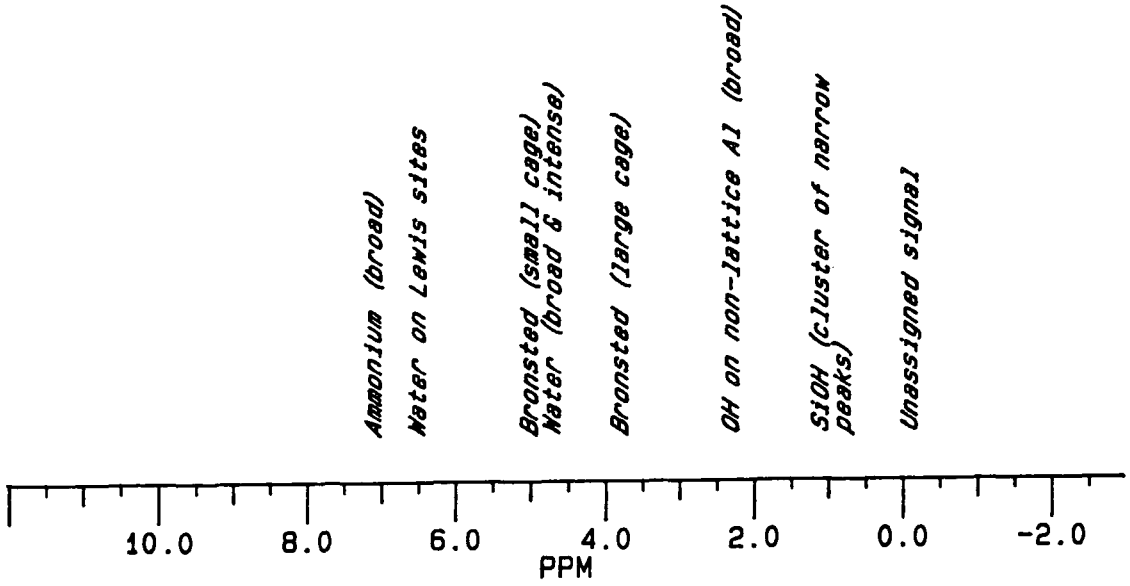

method. For experiments performed on the CXP–200 spectrometer, the conditions used were substantially the same as for single–pulse spectrometry. The inter–pulse recovery times used generally ranged from 1 ms to 100 ms for wet samples or up to $0.5 - 1$ s for dry samples. On the WRAC spectrometer, $100 - 500$ averages were used with similar recovery times to the CXP.

The magnitude of T_1 of a given nucleus is known to pass through a minimum as the rate of motion of components of the system decreases (for a discussion, see Ref. 1, page 87). Most motions in the liquid state occur on the 'fast' side of the minimum; therefore, the T_1 values of more mobile components are longer (further from the minimum). The opposite situation pertains in most solids, including the systems under consideration in this work. Thus, longer T_1 values are generally associated with *slower* motion (*e.g.* due to decreased concentration or stronger binding of adsorbates) in the discussions in later Chapters.

Rotating–frame spin–lattice ($T_{1\rho}$) relaxation time measurements were made on the CXP–200 and WRAC instruments, using spin–locking times up to 30 ms. The spin–locking field strength used on the CXP–200 was 62.5 kHz, and on the WRAC 20 kHz.

Transverse (T_2) relaxation times were measured using the CPMG pulse sequence on the CXP–200 and WRAC systems, typically employing 100 echoes spaced at $50 - 500$ μs intervals.

Relaxation times are typically quoted to lie within confidence limits of $5 - 10\%$. The principal sources of experimental variability are temperature and spectrometer instability (which are of greater significance in long multiple–pulse sequences such as CPMG) and poor signal–to–noise ratio. In particular, deconvolution of relaxation data into several superimposed components (performed extensively in the present work) can only be undertaken with

confidence if the data set is large and the signal–to–noise ratio high, so that the shape of the empirical relaxation curve is well–defined. A detailed investigation of the sources and magnitudes of errors in measured relaxation times was not considered necessary in the context of this work, since the results have been interpreted almost entirely qualitatively (*i.e.* as an aid to spectral assignment) rather than quantitatively, *e.g.* for assessing mobilities of species present.

Multiple–Pulse Homonuclear Decoupling Procedures. CRAMPS was used to confirm that homonuclear dipolar couplings were generally weak in the samples studied.[21] The MREV–8 and BR–24 sequences were employed, all experiments being performed on the CXP–200 instrument.

REFERENCES

1. R K Harris, *Nuclear Magnetic Resonance Spectroscopy*, Longman, Essex, 1986.
2. (a) Ref. 1, p. 81; (b) A E Derome, *Modern NMR Techniques for Chemistry Research*, Pergamon Press, Oxford, 1987, p. 91.
3. P Jackson, R K Harris, *Magn. Reson. Chem.* **26**, 1003 (1988); D P Burum, W–K Rhim, *J. Phys. Chem.* **71**, 944 (1979).
4. C A Fyfe, *Solid–State NMR for Chemists*, CFC Press, Guelph, Ontario, Canada, 1983, pp. 126, 534.
5. A Pines, M G Gibby, J S Waugh, *J. Chem. Phys.* **59**, 569 (1973).
6. D Schulze, H Ernst, D Fenzke, W Meiler, H Pfeifer, *J. Phys. Chem.* **94**, 3499 (1990).
7. M Mehring, *High–Resolution NMR Spectroscopy in Solids*, Springer–Verlag, Berlin, 1976, p. 138.
8. P P Man, J Klinowski, A Trokiner, H Zanni, P Papon, *Chem. Phys. Lett.* **151**, 143 (1988).
9. R K Harris, A M Kenwright, A Royston, B J Say, *Meas. Sci. Technol.* **1**, 1304 (1990).
10. R Challoner, R K Harris, K J Packer, M J Taylor, *Zeolites* **10**, 539–45 (1990).

11. E Lippmaa, M Mägi, A Samoson, M Tarmak, G Engelhardt, *J. Am. Chem. Soc.* **103**, 4992 (1981).

12. W Loewenstein, *Am. Mineral.* **39**, 92 (1954).

13. G Engelhardt, U Lohse, E Lippmaa, M Tarmak, M Mägi, *Z. Anorg. Allg. Chem.* **482**, 49 (1981).

14. C A Fyfe, G C Gobbi, G J Kennedy, C T de Schutter, W J Murphy, R S Ozubko, D A Slack, *Chem. Lett.* 1984, 163.

15. S Ramdas, J Klinowski, *Nature* **308**, 521 (1984); A–R Grimmer, R Radeglia, *Chem. Phys. Lett.* **106**, 262 (1984); J M Thomas, J Klinowski, S Ramdas, B K Hunter, D T B Tennakoon, *Chem. Phys. Lett.* **102**, 158 (1983); L V C Rees, *Nature* **303**, 204 (1983).

16. J M Newsam, *J. Phys. Chem.* **89**, 2002 (1985).

17. J Klinowski, S Ramdas, J M Thomas, C A Fyfe, J S Hartman, *J. Chem. Soc., Faraday Trans. 2* **78**, 1025 (1982).

18. X Liu, J Klinowski, J M Thomas, *Chem. Phys. Lett.* **127**, 563 (1986).

19. P P Man, J Klinowski, *J. Chem. Soc., Chem. Commun.* 1988, 1291.

20. J Haase, H Pfeifer, W Oehme, J Klinowski, *Chem. Phys. Lett.* **150**, 189 (1988).

21. S Dec, C E Bronnimann, R A Wind, G E Maciel, *J. Magn. Reson.* **82**, 454 (1989).

22. J Klinowski, T A Carpenter, J M Thomas, *J. Chem. Soc., Chem. Commun.* 1986, 956.

23. R R Ernst, W A Anderson, *Rev. Sci. Instrum.* **37**, 93 (1966).

24. D J Cookson, B E Smith, *J. Magn. Reson.* **63**, 217 (1985).

25. G E Maciel, *Science* **226**, 282 (1984); K J Packer, in *The Multinuclear Approach to NMR Spectroscopy* (J B Lambert & F G Riddell, eds.), 111 (1983); B C Gerstein, *Anal. Chem.* **55**, 781A (1983).

CHAPTER 3: PRACTICAL METHODS

This Chapter includes a description of all the practical techniques employed in the research discussed in Chapters 4–7, except those directly involving NMR. The basic technique used for removing all sorbates, primarily water, from Zeolite Y samples is covered in detail in Section A. Other thermal treatments used for modification of the lattice are discussed in Section B, while Section C described the chemical treatments employed, including chemical dealumination and cation–exchange. The analytical techniques used other than NMR are covered in Section D, and the Chapter closes with a discussion of the computer software written by the author for spectral deconvolution.

3A: DRYING TECHNIQUE

1. Outline

^{1}H NMR was identified as a key technique in the present work for the investigation of the fine structure of the zeolite lattice, in particular the catalytically active acid sites and the non–lattice material, on account of its sensitivity, high information content and directness. However, the ^{1}H NMR characteristics of zeolites under ambient conditions are almost always strongly dominated by the intracrystalline water sorbed on the samples, as most zeolites, including those discussed in this thesis, are strongly hydrophilic. It is necessary, therefore, to employ a technique for removal of sorbed water when study of the ^{1}H chemically associated with the zeolite lattice is required. In addition, many industrially important processes catalyzed by zeolites are conducted under anhydrous conditions, and so the state of the lattice during these processes will be better simulated for NMR study by preparing dried samples.

Quite severe conditions are required to remove the intracrystalline water from most forms of Zeolite Y, as described shortly. The samples prepared in the present study are known generally by the nomenclature *c*Y–*n* where *c* is the predominant cation (H, Na, NH_4 or Ag) and *n* is an experiment number. A full catalogue of all seventy–two of the dried samples investigated is provided in Appendix B.

2. Previously–Published Dehydration Techniques

The drying procedures reported in recently published work always involve the application of high temperature for a number of hours, usually in conjunction with vacuum treatment. One important research group has devised a pair of techniques known as 'deep–bed' (DB) and 'shallow–bed' (SB) treatments.[3] The DB method involves heating 1 g of sample (usually NH_4Y) in a 10 mm diameter tube under atmospheric pressure; the sample is generally packed several centimetres deep. The temperature is raised at a rate of 100^oC per hour to a target level, usually in the range $300 - 600^oC$. After a two–hour hold, the sample is evacuated for twenty hours and sealed. The presence of large quantities of desorbed water vapour during the two–hour period is thought to result in substantial damage to the lattice (see Chapter 4 for further discussion). This method therefore effectively achieves calcination and dehydration in one step. The main disadvantage, however, is its intrinsic ill–definition and lack of reproducibility which has created difficulties in interpreting experimental results on occasions.

In order to obtain dehydrated samples without significant change to the lattice structure, the SB method is employed. This involves heating a sample no more than 3 mm deep to $300 - 600^oC$ under vacuum. The temperature ramp rate is 10^oC per hour. When the target temperature is reached, the sample is

sealed immediately. Generally no lattice damage is observed below 450^{o}C; thereafter, the lattice begins to degrade on account of its high Al content (the calcining stage in the DB treatment reduces the Al content of the lattice). Another 'drying–only' technique employed by the same workers involved heating the sample under vacuum to 400^{o}C for 24 hours and sealing in glass ampoules.[4]

The work for which the DB and SB treatments were employed used ^{1}H NMR as the primary study technique. For infra–red studies, however, such rigorous drying methods do not seem to be required. One group[5] has recently reported a technique for obtaining dried NH_4Y without the use of vacuum: the sample is pressed into a self–supporting wafer and heated *in situ* in the spectrophotometer to 350^{o}C at a rate of 10^{o}C per minute (much faster than the work described above) in a stream of dry N_2. The sample is held at 350^{o}C for 10 minutes and cooled under the same environment.

3. Details of the Technique Employed

A diagram of the apparatus used for dehydration of zeolite samples is shown in Figure 3.1. It consists of a double–manifold vacuum line attached to rotary and diffusion pumps (the diffusion pump, which was charged with hydrocarbon oil, was never used). A trap, installed between the line and the diffusion pump,, was cooled in some experiments with liquid air. The terminations on the vacuum line are of the Young type, push–fitting with rubber O–rings. Greased joints are unsuitable for the present work because of the difficulty of degreasing without sorbing air or solvent onto the sample.

The zeolite itself is placed in a thick–walled Pyrex tube (or silica when temperatures above 400^{o}C are required) of 10 mm outside diameter. The sample is packed by gentle tapping of the tube to a bed depth of about 10 mm. A small plug of glass wool is pushed loosely into the neck of the tube to prevent the

Figure 3.1: Apparatus used for dehydration of zeolites and controlled sorption onto freshly–dried samples

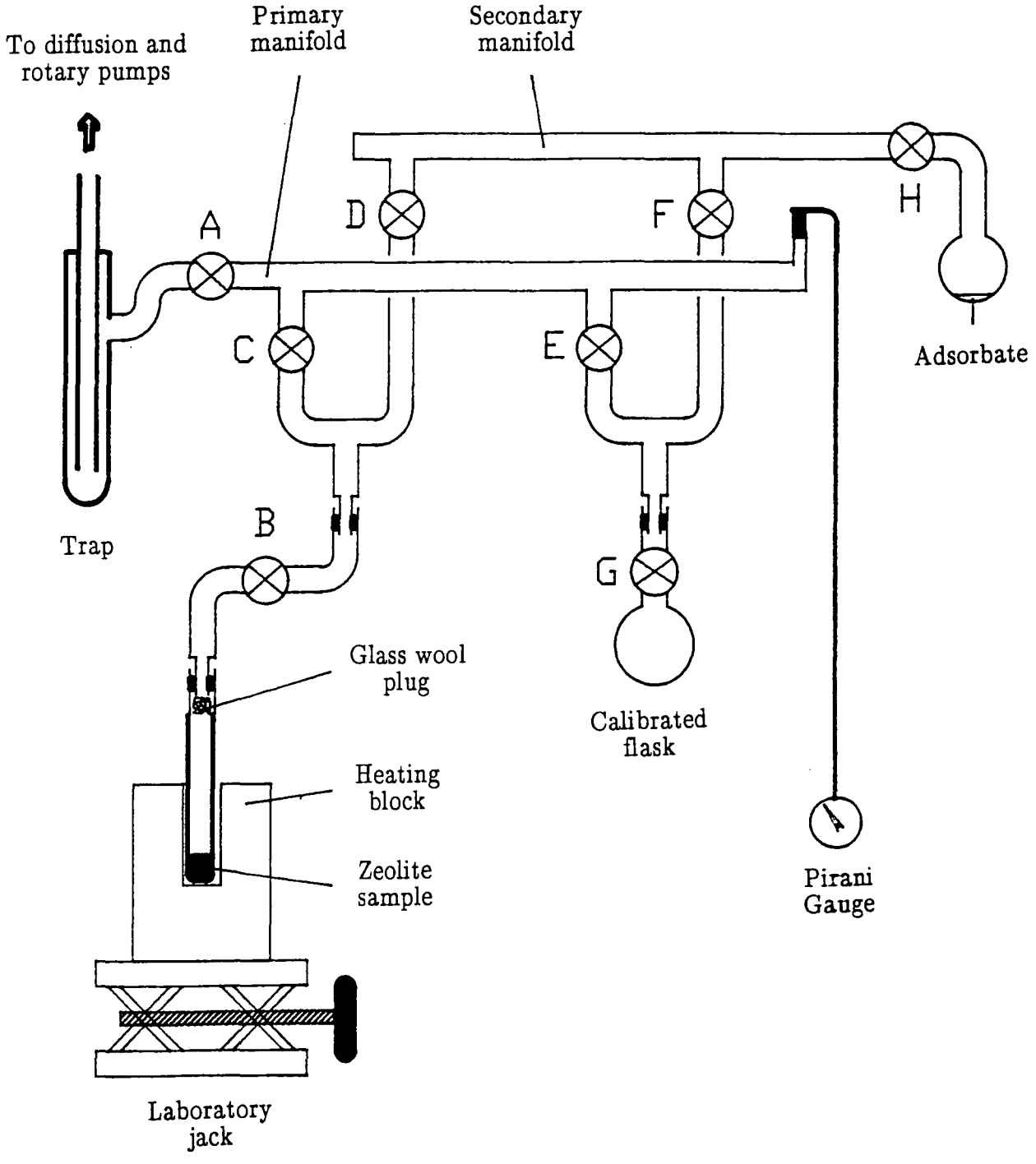

escape of the finely–powdered sample into the vacuum system. The tube is then attached, *via* an S–shaped linkage including a tap, to the Young port on the vacuum line.

The tap in the linkage (designated 'B' in Figure 3.1) is closed initially whilst the upper part of the joint to the vacuum line is evacuated by opening taps A and C. Tap B is then opened slowly to permit gradual removal of the air in the sample tube and desorption of air from the sample; this process takes about twenty minutes. The pressure on the vacuum line should not be allowed to exceed about 0.1 mbar during this process, since rapid desorption is observed to cause sucking of parts of the sample into the upper region of the tube. When the sample is fully evacuated, the system pressure settles at around 0.05 mbar, measured with a Pirani gauge.

The sample tube is embedded in a well–fitting hole in a heavily–insulated aluminium block heated by two mains–powered electric cartridge elements. The heaters are regulated by a Eurotherm programmable controller, which senses the temperature in the block *via* a thermocouple. The Eurotherm unit is set to operate at a heating duty cycle of 60% to prevent overshoot. The heating must initially be carried out slowly, since most of the water desorbs from the sample in the range $40 - 60^{o}C$, when sputtering occurs if the heating rate is too fast. The following programme is satisfactory:

(i) Raise temperature from ambient to $50^{o}C$ at a rate of $1^{o}C$ per minute.

(ii) Hold at $50^{o}C$ for 1 hour.

(iii) Raise temperature to target level at $2^{o}C$ per minute.

(iv) Hold for a specified interval.

(v) Cool naturally or quench (see text).

The target temperature is typically $400^{o}C$; values used in the present study

ranged from 100°C to 500°C (see Appendix B). The hold time at this temperature ranged from nil to 63 hours, with 4 hours being typical for HY.

The cooling step has a number of variants. The tap to the vacuum line may be left open, or closed so that the sample is in a closed environment. The sample tube may be left in the heating block to cool slowly (typically taking 1 hour to fall from 400°C to 250°C and 6 hours to fall from 400°C to room temperature) or removed to 'quench' the sample rapidly; the heating block is supported on a laboratory jack so that it may be lowered away to permit quenching with the sample tube still attached to the vacuum line.

The treatment described above was sometimes observed to result in discolouration of the top part of the sample to a grey, brown or black colour. This occurred particularly often with NaY, which was subjected to more severe treatments than other samples. There was no correlation observed between discolouration and cooling method. The dark colour may arise from the decomposition of any adsorbates present, especially carbonaceous, and has often been observed in other laboratories.

Handling of Dry Samples. Particular diligence is required during the handling of dehydrated materials to avoid adsorption of contaminants. Brief exposure to the ambient atmosphere is sufficient to permit sorption of significant quantities of water, which spoils the appearance of the sample's ^{1}H NMR spectrum.

The handling procedure employed in the present work is as follows. On completion of the cooling step of the dehydration program, taps B, C and D are closed, the heater removed and the sample tube and linkage disconnected together from the vacuum line by pulling apart the Young joint between taps B and C. Then the sample tube, still under vacuum, is transferred to a glovebox containing an atmosphere of dry N_2. The sample is then loaded into a small

cup–shaped capsule made of Kel–F, and inert fluorocarbon plastic. The capsule, which has a tight push–fitting cap, is specially designed to fit snugly into the magic–angle spinning rotor used with the Bruker CXP–200 and CXP–300 NMR spectrometers to permit study of the material at leisure;[1] see Figure 3.2 for an illustration. (It is referred to hereinafter as a *rotor insert* for this reason.) The sample must be packed densely and evenly to enable good spinning to be achieved; a special cylindrical tool is used for this purpose. When properly loaded, the rotor insert can be spun stably at $3-4$ kHz without difficulty and holds $35-50$ mg of dry zeolite.

The rotor insert can be re–used since there is a threaded recess cut into the outer face of the cap, enabling removal of the cap using a suitable screw. If necessary, the cap can be loosened by dipping into liquid nitrogen.

Figure 3.2: Cross–section of Kel–F airtight rotor insert and push–fitting cap. Shallow channels are cut in the outside surface of the insert to assist air flow during insertion into and removal from the rotor. All dimensions are in millimetres. (Derived from Ref. 1)

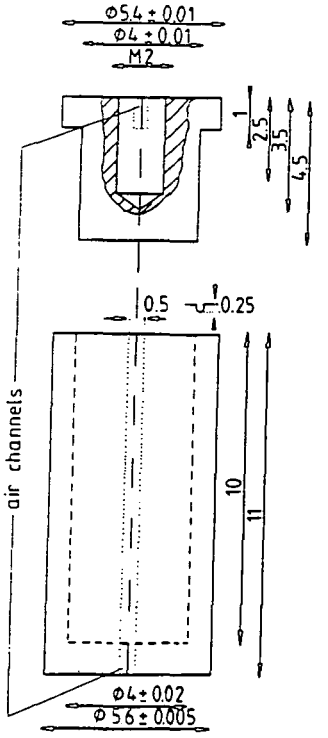

The rotor inserts are particularly well–suited to the study of dry zeolites on two accounts. Firstly, they are very air– and watertight, as discussed in a later section. Secondly, they give no background signal in ^{27}Al and ^{29}Si single–pulse or CP/MAS NMR spectra, and only a weak signal in ^{1}H single–pulse and ^{13}C CP/MAS. The relevant background spectra are shown in Figure 3.3.

One unsolved difficulty encountered which was associated with the use of the glovebox arose from the tendency of the finely–divided, extremely dry zeolite samples to scatter, presumably on account of electrostatic interactions. It was frequently found that significant portions of the sample were lost to aerial dispersion within the glovebox, whilst others clung to items of glassware and even to nickel spatulæ. The use of plastic items of equipment in the box, rather than glass or metal, was found to reduce this effect. Other laboratories employ small quantities of ionizing radiation to reduce the accumulation of static.

4. Tests of Sample Dryness

A number of methods were devised to check that as much water as possible was removed from the zeolite samples. In early experiments it was observed that the vacuum–line pressure was unaffected by closing tap B after 24 hours of heating, indicating that no further desorption was being detected. Other techniques involved the application of ^{1}H NMR. The first of these involved the measurement of the absolute ^{1}H content of the sample by comparison with a reference sample, which could be internal or external. The sample chosen was a fragment of silicone rubber tubing, whose ^{1}H content was estimated to be 6.0% by weight using elemental analysis and 5.6% by weight from solution–state NMR. The latter value was obtained by dissolving a weighed portion of silicone rubber in CF_3CO_2D, adding a known quantity of $MeCO_2Na.3H_2O$ and

Figure 3.3: ^{1}H SP MAS background spectrum from a Kel–F rotor insert
RD=5s NT=256 RO=1507Hz

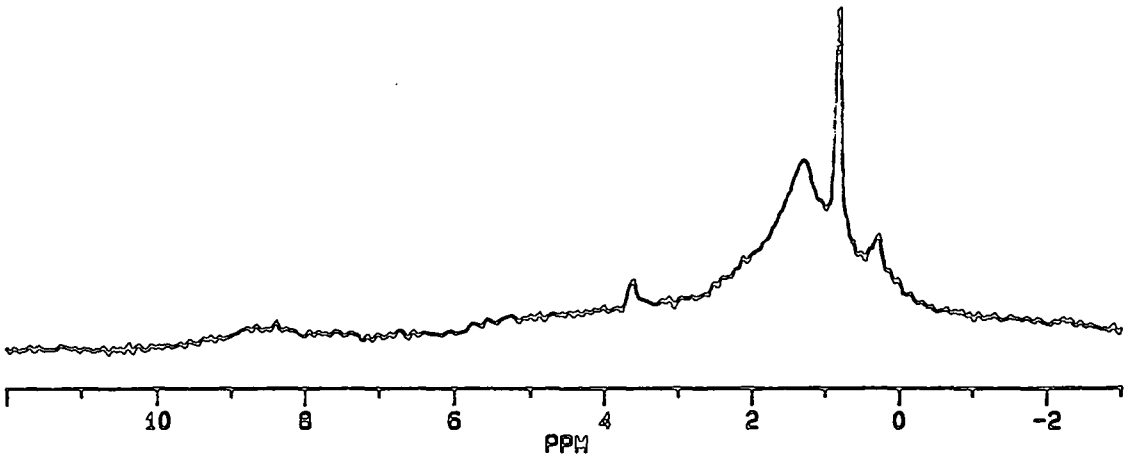

Figure 3.4: ^{1}H SP MAS spectra of HY–4 during aging in rotor insert
(a) Fresh RD=500ms NT=128 RO=4004Hz
(b) 28 days old RD=500ms NT=128 RO=2600Hz
(c) 76 days old RD=1s NT=16 RO=3015Hz

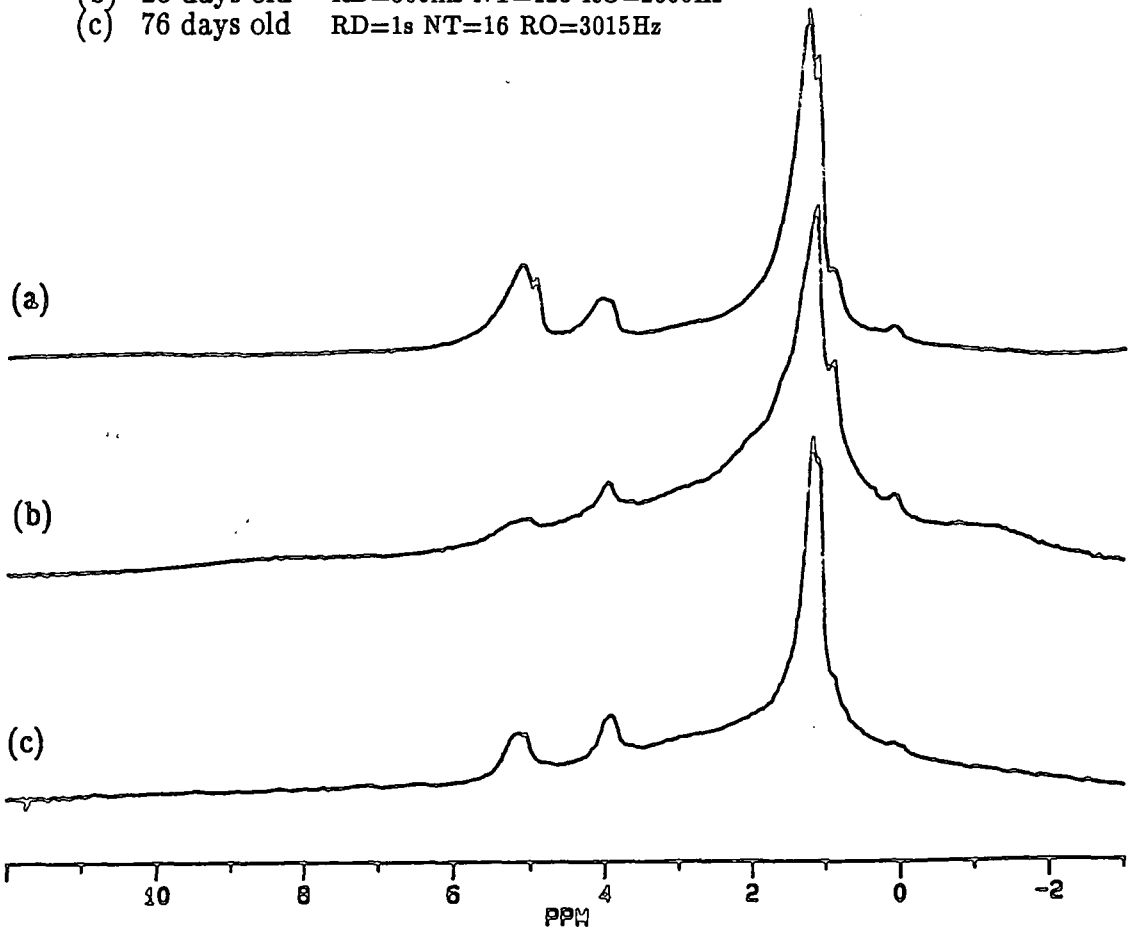

measuring the relative concentrations of ^1H in the rubber and the salt by integrating the ^1H spectrum. The silicone rubber was selected as a reference on account of its stability, inertness and convenient appearance in the ^1H solid–state MAS–NMR spectrum (it gives a very narrow signal close to 0 ppm, which is readily distinguishable and well away from most signals of zeolitic origin). The relative concentrations of ^1H in silicone rubber and in a zeolite sample could be compared by integration either directly, when the rubber was included in the MAS rotor, or indirectly (using the CXP 's 'absolute intensity mode' when used as an external reference. The absolute ^1H content of the zeolite could then be found, given a knowledge of the mass of rubber employed. Generally speaking, wet samples were found to have a ^1H content in excess of 0.3% by weight (often as high as 1%), whereas properly–dried materials always contained less than 0.05%. Detailed figures are given in Chapters 5 and 6.

The other major difference between wet and dry samples observed by ^1H NMR is in the relaxation times of the nuclei. The T_1 times are found to rise by a factor of 10 or more, from around 20 ms to at least 200 ms (at 200 MHz). $T_{1\rho}$ values rise similarly. The T_2 profile changes in a characteristic manner, with the loss of components associated with intracrystalline water (particularly 25 μs). Detailed discussions are reserved for Chapter 5.

5. Sample Longevity in Rotor Inserts

A number of results are presented in Chapters 6 and 7 which show that the total ^1H content of dried samples kept in rotor inserts for a few weeks does not increase, suggesting that the inserts are sufficiently impervious to contaminants from outside to allow confidence in samples studied during this time. Other results (for example, the study of HY–S–10 presented in Chapter 6) indicate that the samples are liable to attack by water invading from outside

after an interval of several months. In general, no precautions were taken to protect the inserts from the ambient atmosphere; for example, they were not kept in the dry glovebox. For safe storage they normally resided in numbered plastic bottles with O–rings in the caps which were kept in the open laboratory.

The ^{1}H MAS–NMR spectrum of dried sample HY–4 (discussed further in Chapter 5) was acquired under similar conditions on three occasions, when the sample was brand–new and after 28 and 76 days of aging in the rotor insert. The three spectra, which appear in Figure 3.4, show that very little attack of water from outside has occurred, if any. There is certainly no sign of the characteristic broad free water peak at 4.7 ppm. Clearly, then, it is reasonable to be confident that the inserts maintain the integrity of the ample for a number of weeks, resisting encroachment of sorbates from outside.

6. Controlled Adsorption Studies

A series of experiments was conducted to investigate the effect of adsorbing a known quantity of a substance such as water on a freshly–prepared sample of dried HY. The apparatus used was the same as that for the drying itself, as shown in Figure 3.1; the experimental method is as follows.

The volume of the flask below tap G is first measured by evacuating it, closing tap G, removing the flask from the vacuum line, weighing, placing the neck under water and opening tap G to admit water into the evacuated space, finally weighing again. (This was repeated five times and the mean value taken as the volume of the flask.)

A small amount of the desired sorbate (*e.g.* distilled water) is placed in the flask beyond tap H. The secondary vacuum line is evacuated by closing B and G and opening A, E and F. Then the water is degassed by freezing with liquid air, evacuating (by opening and closing tap H), and allowing to melt; this

procedure is repeated several times.

The flask on tap G is evacuated again and then charged with a known amount of water vapour by closing A and B, opening F and G and carefully opening H to admit a certain pressure of water vapour into the system, measured by the Pirani gauge. The amount of water in the flask, n_w, can be found from the standard gas formula $pV = n_w RT$, where p is the pressure of water vapour (in excess of the background pressure), V the measured volume of the flask, R the gas constant and T the absolute temperature.

Now the excess water vapour in the vacuum line is pumped away by closing F and H and opening A. When the pressure has dropped, the water can be adsorbed on the zeolite by closing A, C and E and opening G, F, D and B, passing the vapour through the secondary vacuum line. Although the water should adsorb entirely onto the dry zeolite in the space of a few minutes, it was considered prudent in the present work to freeze the sample tube to ensure that all the water condensed there as rapidly as possible, because the vacuum line was not very airtight.

Finally, tap B was closed and the sample removed and packed into a rotor insert in the normal manner. The results of controlled adsorption experiments carried out with water, D_2O and pyridine–d_5 as sorbates are described in Chapters 5 and 6.

7. Controlled Rehydration

In order to obtain zeolite samples with stable hydration levels, it is necessary to equilibrate them for several days in an atmosphere with a regulated humidity. In the present work, this was achieved by placing the samples in a desiccator containing evaporating basins half–filled with a saturated solution of a salt. For full hydration, the salt chosen was $KHSO_4$, which generates a relative

humidity of about 85% at room temperature.[2] Drier conditions were maintained by the use of LiCl or $CaCl_2$, which produce about 15% and 35% respectively. Full details of the results of controlled hydration experiments are given in Chapter 5.

3B: HYDROTHERMAL TREATMENTS

1. Calcination

Three of the samples used in this study were calcined (that is, strongly heated) in the presence of an atmosphere containing steam. (The purpose and effect of this treatment are discussed in detail in Chapter 4.) The treatment was carried out at Unilever Research Port Sunlight Laboratory, using a Carbolite rotary calciner. This consists of a cylindrical silica vessel 30 cm long and 20 cm in diameter, in which 300 g of the starting NH_4Y is placed, occupying up to 20% of the internal volume. Glass tubes 20 cm long and 5 cm in diameter emanate from each end of the cylindrical vessel, which is laid horizontally in a chamber lined with electrically–heated firebricks. The chamber has a heavily–insulated lid which is closed during the calcination. The vessel is rotated at 25 rpm and heated at 32°C per minute to the target temperature of 550°C or 650°C. When the temperature is above 250°C, steam is generated by passing water into the vessel at a rate of 0.5 ml per minute *via* a long 1 mm diameter needle, using a peristaltic pump. The temperature is sensed by a thermocouple immersed in the sample and regulated by a Eurotherm controller. The target temperature is held for 30 minutes, after which natural cooling is carried out by raising the lid of the calciner.

One effect of calcination is to eliminate NH_3 from the sample; the

desorbing gas is collected by passing the effluent over dilute hydrochloric acid and the residue is pumped to the outside atmosphere. The zeolite product is in the HY form. The HY sample discussed in Chapters 5 – 7 was calcined in this way at 650°C. In addition, two portions of the starting NH_4Y discussed in Chapter 4 were calcined at 550°C and 650°C, giving rise to HY–C550 and HY–C650 respectively.

2. Steaming

A much more severe treatment of NH_4Y with steam generates changes in the lattice structure of the material which are thought to resemble those resulting from prolonged service in a fluidized catalytic cracking unit (see Chapter 4 for further discussion).

The steamed sample HY–S used for the studies covered in Chapters 5 and 6 was made from as–synthesized NaY by the following route. The sample was exchanged with NH_4^+ and calcined to give HY; it was then exchanged again with NH_4^+ to reduce the residual sodium content. (This is an important step in the preparation of materials for industrial use, because the presence of Na^+ leads to widespread lattice breakdown during catalytic service.) The sample was then calcined as described in the previous section, and exchanged once more with NH_4^+. It was finally subjected to an atmosphere of 100% steam at 816°C for 5 hours to give HY–S.

Analogous steam treatments were used to prepare the samples HY–C550–S, HY–C650–S and HY–CS–S considered in Chapter 4.

3C: CHEMICAL TREATMENTS

1. Chemical Dealumination

A sample of NH_4Y was dealuminated by treatment with $(NH_4)_2SiF_6$ as follows. 50 g of hydrated NH_4Y was slurried in 280 ml of a 3.5 M solution of ammonium acetate, stirred and heated to 50^oC. 13.9 g $(NH_4)_2SiF_6$ was dissolved in deionized water to make a 0.74 M solution with a volume of 105 ml. The latter solution was added dropwise to the former over a period of 200 minutes by means of a peristaltic pump; the reactant vessel was stirred and maintained continuously at 50^oC. At the end of the addition, the product was immediately filtered on a Buchner funnel to a 10 mm bed depth and promptly washed with 1 ℓ deionized water at 65^oC, then 1 ℓ 1 M ammonium acetate solution at 65^oC, then five 1 ℓ portions of deionized water at 65^oC. Finally the extracrystalline water was removed by drying overnight in an oven at 100^oC. This procedure resulted in the replacement of 28 Al per unit cell with Si. The product, known as NH_4Y–CS, was characterized by a range of techniques including NMR; the results are discussed in Chapter 4.

Caution must be exercised when handling $(NH_4)_2SiF_6$ as it is toxic by inhalation, ingestion and skin contact and extremely irritating to skin and eyes.

2. Extraction of Non–Lattice Alumina with EDTA

Extraction with $(NH_4)_2$EDTA of the steamed sample HY–S was carried out in order to remove the non–lattice alumina as selectively as possible. The diammonium salt of EDTA was chosen on the grounds that

(i) it is sufficiently water–soluble to allow a high concentration to be used, so that a large excess of EDTA can be employed to force the extraction reaction;

(ii) it would not introduce any unwanted Na^+ into the zeolite.

The procedure used is as follows. 11.5 g H_4EDTA is slurried in 30 ml deionized water. 50% NH_3 solution is added until the EDTA had dissolved and the pH reaches a stable value of 7.5. The resulting $(NH_4)_2EDTA$ solution is diluted to 100 ml and 1.0 g of the steamed zeolite is added. The slurry is refluxed for 6 hours, then filtered on a sintered–glass funnel. The zeolite is washed first with five 10 ml portions of deionized water at room temperature, then with five 20 ml portions of 10% NH_4Cl solution at 50–60^oC, and finally with five 20 ml portions of deionized water at 50–60^oC. Extracrystalline water is removed as before by drying in an oven at 100^oC.

The final product is designated HY–S–L; characterization results are presented in Chapter 6.

3. Back–Exchange of HY with Na^+ and Ag^+

A sample of HY was exchanged with Na^+ in the form of aqueous NaCl. The intention was to displace readily exchangeable H^+, observing the effect this had on the ^1H NMR spectrum of the sample. The method used is as follows. 2 g hydrated HY is stirred with 20 ml 1 M NaCl (aq) for 4 hours at room temperature. The slurry was filtered on a hardened filter paper and washed three times with 20 ml portions of deionized water. The extracrystalline water is removed by drying in a warm oven (*c.* 60^oC).

The resulting sample is designated NaY–ex. A similar procedure, using 1 M $AgNO_3$ solution, gave rise to AgY–ex. Studies of these samples are described in Chapter 7.

3D: NON–NMR ANALYTICAL TECHNIQUES

1. X–Ray Diffraction (XRD)

Unit cell size measurements were performed by XRD at Unilever Research Port Sunlight Laboratory using a Philips PW1730 X–Ray generator (Cu Kα X–Ray tube running at 2.2 kW, 50 kV, 36 mA) and a Philips PW1050 goniometer in the standard configuration. The method employed was that described in the Annual Book of ASTM Standards, Volume 05.03 (ASTM, Philadelphia, 1990), standard number D3942.

Crystallinity measurements were obtained by comparing the intensities of certain bands in the diffractogram with those obtained from a standard sample of highly crystalline Zeolite NaY. The ASTM number is D3906.

2. X–Ray Fluorescence (XRF)

This technique provides a measurement of the concentration of a particular element in a sample. It was employed to obtain bulk Si/Al ratio estimates and was carried out at Unilever Research Port Sunlight Laboratory. The sample is vitrified by fusing 2 g sample with 9 g "Spectraflux 100B", a eutectic mixture of lithium metaborate and lithium tetraborate, containing an additional 0.5 g, ammonium nitrate (to ensure preservation of maximum oxidation states) and 0.14 g lithium bromide, to assist wetting of the platinum crucibles in which the glass is cast. The heating is carried out at 1250^{o}C for 12 minutes using a Hertzog HAG12 apparatus. The X–Ray experiment employs a Philips PW1404 wavelength dispersive X–Ray fluorescence Spectrometer, using the top surface of the glass for the analysis.

3. Surface Area Measurements

These were performed according to ASTM standard D3663 using a Sorpty 1750 single–point surface area instrument.

3E: SPECTRAL DECONVOLUTION

In order to facilitate the deconvolution of NMR spectra into component signals with simple band shapes, a computer program known as SpecMan (an abbreviation of Spectral Manipulator) was prepared during the course of this research. The program was developed from one previously created at the University of Oxford under the supervision of Dr. M. J. T. Robinson.[6] SpecMan is written in ISO–Pascal and runs on an Acorn Archimedes 440 microcomputer.

The decision to develop custom–written software instead of employing commercial packages was based on the following factors. Firstly, at the commencement of the project, only a very limited and rather untrustworthy package was accessible to the Author. Secondly, it was not clear at the outset what type of mathematical functions might be required for simulation; in view of this, the software was designed to facilitate the introduction of new types of model for fitting. Thirdly, a number of other features were desired, such as flexible plotting routines and interactive starting–parameter selection.

Extensive use has been made of the deconvolution technique in the present work. It has been found to provide a particularly valuable insight into the underlying signals observed in ^{29}Si single–pulse spectra, providing evidence for the existence of broad bands attributable to non–lattice silica.

1. Outline of SpecMan's Function

Raw data, in the form of an FID, are taken from the spectrometer on which they were acquired, and displayed graphically on the screen. Standard manipulations such as Fourier Transformation and phase–correction may then be performed and the resulting spectrum saved on disk. This spectrum (or the original FID) can be simulated by a curve calculated from the sum of a set of standard line shape functions, such as Gaussian and Lorentzian; the simulation is performed by an iterative fitting routine as described below. Interactive routines are provided to assist the user in the preparation of starting guesses for the parameter values used in the fitting.

Once the iteration is complete, the user may inspect the results of the fit graphically, obtain a listing of the final parameter values and save them on disk for later reference. The original and simulated data may also be plotted; this facility was used to prepare a number of the Figures in this thesis.

Communications and data–format translation software have also been written where necessary to permit the handling of data from any of the NMR spectrometers used.

2. Mathematical Method Used for Optimization of the Simulated Data

The intensity of the simulated spectrum or FID at a given point is defined as a function f of a set of parameters contained in a column vector $\underline{x}$; these parameters are altered to optimize the fit between simulated and experimental data values. The optimization involves the minimization of an error function Z, which is the sum of squares of differences between the values of f and corresponding points in the experimental data. The optimization calculation is performed iteratively until the value of Z falls on successive cycles by less than a given threshold value, typically 0.1%.

The fitting algorithm implemented is a hybrid of the two methods described below. It is popular and widely used, having been previously applied by the Research Group to the fitting of multiexponential curves to relaxation data.

The first method is a multi–variable relative of the common single–variable Newton–Raphson approximation to the solutions of functions. For a function Z of an array of parameters $\boldsymbol{x}$, the Taylor expansion can be expressed as follows:

$$Z(\boldsymbol{x} + \Delta\boldsymbol{x}) = Z(\boldsymbol{x}) + g^{\mathrm{T}}\Delta\boldsymbol{x} + \tfrac{1}{2}\Delta\boldsymbol{x}^{\mathrm{T}}H\Delta\boldsymbol{x} + \ldots \qquad \{1\}$$

where $\Delta\boldsymbol{x}$ is a vector of parameter changes, g is a column vector of first partial derivatives with respect to all parameters, and H is an n x n symmetric matrix of second partial derivatives (known as the *Hessian matrix*). If $\Delta\boldsymbol{x}_{\mathrm{m}}$ is the jump in parameters required to move from the present parameter values $\boldsymbol{x}$ to the values at which Z is minimized, it can be shown from Equation {1} that[8]

$$\Delta\boldsymbol{x}_{\mathrm{m}} = -H^{-1}g \qquad \{2\}$$

provided that the function is quadratic in nature. This is true for many physical functions near the minimum, as high–order terms become less important, but further from the minimum this often proves an unacceptable approximation. In such circumstances, another approach is required; one possibility is the *steepest descent* method. This involves calculation of the parameter–change vector $\Delta\boldsymbol{x}$ by ensuring that it is antiparallel to the vector of first derivatives g at the starting point of each step. Thus, each iterative step is taken in the direction that is most steeply 'downhill'. The parameter change $\Delta\boldsymbol{x}$ can thus be expressed as $\Delta\boldsymbol{x} = -kg$ where g is the vector of first derivatives as before, and k is a scalar controlling the length of the downhill step.

In order to select whichever of the two methods is most appropriate at a given point in the minimization, an arbitrary parameter λ is introduced and

defined as follows:

$$\Delta \boldsymbol{x} = -\tfrac{1}{2}\,(\lambda I + \tfrac{1}{2}H)^{-1}\, g \qquad \{3\}$$

where I is an identity matrix. In this formula, λ has the effect of mixing the two optimization methods: when $\lambda = 0$, the value of $\Delta \boldsymbol{x}$ is the same was that given in Equation {1} for the Newton–Raphson minimization, whilst $\lambda = \infty$ gives the steepest–descent value for $\Delta \boldsymbol{x}$ (with $k = \frac{1}{2}$). Intermediate values can be considered to 'damp' the Newton–Raphson step length by mixing a proportion of steepest–descent character into the optimization.

A number of methods may be used for the selection of λ; the one applied in the present work, proposed by Fletcher,[7] involves the calculation of an efficiency parameter R after each parameter change, which is the ratio of the actual decrease in the error function Z to that predicted by the Newton–Raphson method; the latter can be found by

$$\Delta Z_{\text{predicted}} = -2Z(\boldsymbol{x})\boldsymbol{g}^{\mathrm{T}}\Delta \boldsymbol{x} - \Delta \boldsymbol{x}^{\mathrm{T}}H^{-1}\Delta \boldsymbol{x} \qquad \{4\}$$

A high value for R shows that the function Z is behaving in such a way as to be efficiently optimized by the Newton–Raphson method. Accordingly, if R is above 0.75, the value of λ is halved (or set to 0 if previously 1). Low values of R show that steepest–descent character is more appropriate; therefore, if R is below 0.25, λ is doubled (or set to 1 if previously zero). These adjustments to λ are performed automatically by the computer during the fit, to optimize the rate at which Z falls. In practice it is found that, provided the starting guesses for the parameters contained in $\boldsymbol{x}$ are good and the experimental curve is not too noisy, λ rarely rises above 8 during fitting of spectra.

3. Application of the Deconvolution Procedure

The SpecMan program was used extensively in the present work to obtain quantitative estimates of the intensities of the component signals in ^{1}H,

^{29}Si and ^{27}Al MAS–NMR spectra. The data were always fitted in the frequency domain (that is, spectral rather than FID–fitting) and Gaussian band shapes were generally used. The fit was judged to be acceptable when further iterations resulted in parameter changes of less than 0.01% and the residue trace (experimental minus simulated spectra) showed noise only. Sometimes a small amount of baseline correction was applied before fitting, especially when a large fraction of the spectral width (*e.g.* for some ^{1}H spectra) was to be simulated.

The function used to generate the simulated Gaussian band shape is[9]

$$I_g(\omega) = M \exp\left[\frac{(\omega - F)^2}{-W^2}\right]$$

where $I_g(\omega)$ is the intensity at spectral frequency ω, M is the maximum amplitude of the band, F is the centre frequency and W the half–width at half–height. By means of Simpson's Rule it can be shown that the area of the band is $A_g = k_g MW$ where k_g is found by experiment to have a value of 3.7794. The Lorentzian function employed is

$$I_\ell(\mathrm{w}) = \frac{MW^2}{W^2 + 4(\mathrm{w}-F)^2}; \quad A_\ell = k_\ell MW$$

where $k_\ell = 5.0142$.

Parameter values obtained by simulation can be used to calculate absolute ^{1}H contents as follows. The ^{1}H NMR spectrum is obtained from a standard sample (*e.g.* the silicone rubber described in Section A) with a known mass of ^{1}H equal to m_S. The acquisition conditions NT_S (the number of accumulated transients) and RG_S (the receiver attenuation in decibels) must be known also. Then the resulting signal is fitted and yields an area of A_S, which is calculated from the formulæ above. SpecMan normalizes spectral data prior to simulation, and the normalization constant, known as the *intensity scale factor* (IS_S), must be known: this is shown on the printout obtained from the program.

The experimental sample is treated in the same manner, with acquisition conditions NT_e and RG_e; the band of interest yields an area A_e with an intensity

scale factor IS_e. Then the mass of ^1H represented by the band, m_e, can be calculated as follows:

$$\frac{m_e}{m_s} = \frac{A_e\, NS_s\, IS_e}{A_s\, NS_e\, IS_s} \times 10^{(RG_e - RG_s)/20}$$

If the sample is a dry zeolite HY containing x Al per unit cell (lattice or non–lattice), the concentration of ^1H in the band of interest can be expressed in terms of atoms per unit cell as follows. The molecular formula of the sample is $H_xSi_{192-x}Al_xO_{384}$, provided it can be assumed that the composition of any non–lattice material is the same as that of the lattice. Thus, the molar mass m_m of the unit cell can be calculated as $[11536.090 - 0.094x]$ g (from which it can be seen that, since x has only a very slight influence on the total, an educated guess at its value is sufficient). If the total sample mass is T, the sample contains T/m_m moles of unit cells. The amount of ^1H represented by the band of interest is $m_e/1.0079$; hence, the number of ^1H atoms per unit cell is

$$N_H = \frac{m_e m_m}{1.0079T}.$$

These formulæ have been applied extensively in the present work to generate many of the quantitative results given in Chapters 4 – 7.

REFERENCES

1. L H Merwin, A Sebald, J E Espidel, R K Harris, *J. Magn. Reson.* **84**, 367 (1989).
2. *CRC Handbook of Chemistry & Physics* (64th Edition), CRC Press, Boca Raton, Florida, 1983, p. E42.
3. D Freude, T Fröhlich, M Hunger, H Pfeifer, G Scheler, *Chem. Phys. Lett.* **98**, 263 (1983).
4. M Hunger, D Freude, H Pfeifer, *J. Chem. Soc., Faraday Trans.* **87**, 657 (1991).
5. L M Parker, D M Bibby, G R Burns, *Zeolites* **11**, 293 (1991).
6. P G Clarke, Part II Thesis, University of Oxford, 1988.
7. D W Marquardt, *J. Soc. Indust. & Appl. Math.* **11**, 431 (1963); R Fletcher, *AERE Harwell Tech. Report No. R6799* (1971).
8. P R Adby, M A H Dempster, *Introduction to Optimization Methods*, Chapman & Hall, London, 1974, p. 64.
9. A Abragam, *The Principles of Nuclear Magnetism*, Oxford, 1961, p. 107.

CHAPTER 4: NMR STUDIES OF ZEOLITE Y DURING CALCINATION AND STEAMING

4A: LITERATURE REVIEW

1. Introduction

The usual synthesis of Zeolite Y generates a highly crystalline material containing Na^+ as the charge–balancing cation. The lattice is generally rich in aluminium, typically having a Si/Al ratio of around 2.5 (i.e. 55 out of 192 tetrahedral atoms in the unit cell are Al). To make the zeolite active as an acidic catalyst, it must be converted to the form with H^+ as the cation. This cannot be achieved simply by treatment with aqueous acid because the lattice Al is susceptible to attack by acids; the method generally employed proceeds in two steps as follows. The first involves exchange with NH_4^+ by washing repeatedly with a hot aqueous solution of an ammonium salt such as the nitrate. The second involves heating of the material to liberate NH_3, yielding the H–form of the zeolite. It is generally believed that the first ion–exchange step leaves the lattice in a largely unchanged state, retaining a high degree of crystallinity.[1] Concerning the changes taking place during the second step, and in subsequent treatments, there is much less certainty.

The HY zeolite made in this way is generally too reactive to be useful as a catalyst: the concentration of Brönsted acidic sites is so great that the substrate molecules frequently react several times, often generating involatile, entrapped highly carbonaceous side–products (known generically as *coke*) which rapidly deactivate the catalyst by chemisorbing to active sites and by physically obstructing the crystal channels. Accordingly, the zeolite normally undergoes a pre–treatment to reduce its acid site density. This is achieved by removing a

proportion of the Al atoms present in the lattice. The treatment takes one of two forms. The first is known as *calcination* and involves treatment with an atmosphere of steam at $300 - 600^{o}C$ for about 30 minutes.[6] The second is by means of a chemical agent which isomorphically substitutes Si for Al in the lattice, a process often described as *chemical stabilization* or *ultrastabilization*. Typical reagents used are $SiCl_4$ (vapour) or $(NH_4)_2SiF_6$ (in aqueous solution).[2]

Although it is possible to control either of these treatments to create a wide range of Si/Al ratios, the detailed nature of the final product differs substantially. Calcination generates a material whose lattice Al distribution (and hence acid site density) resembles that of the precursor. However, the Al dislodged from the lattice is deposited in the zeolite channels,[6] reacting with steam to produce various aluminium oxy–hydroxide species which are loosely bound to the lattice. In addition, the sites vacated by Al may be left unoccupied, and so there is a concomitant loss in sample crystallinity. By contrast, chemical stabilization leaves no vacant sites and creates no non–lattice material.[3] However, the outermost regions of the crystallite are most heavily dealuminated[4] due both to constraints imposed on diffusion of the reagent by the zeolite channels and to deposition of silica on the exterior face of the crystallite.[5]

Application of a more severe calcination treatment usually known simply as *steaming* (typically 100% steam atmosphere at $800^{o}C$ for 5 hours) results in displacement of nearly all Al from the lattice to a non–lattice environment and substantial destruction of the lattice, generating cavities known as *mesopores* which have dimensions of the order of 100 Å. These changes are thought to resemble those occurring over a period of months during the regeneration phase of the catalytic cycle used in commercial reactors,[7] in which the coke entrapped in the zeolite is released by burning in a stream of air containing $10 - 20\%$ steam at $650 - 750^{o}C$.[8]

The present study is concerned with the investigation of particular characteristics of Zeolite Y during these processes. Recent reports from the literature are reviewed in the following pages: firstly on the calcination process and the nature and behaviour of the NLA formed; secondly on the ^{27}Al NMR signals arising from NLA; then the lattice defect sites created by calcination will be considered, and finally the widely–reported but little–understood phenomenon of zeolite 'superacidity' and the occurrence of non–lattice silica will be discussed.

2. Calcination and the Formation of Non–Lattice Alumina

As described briefly above, calcination gives rise to a substantial change in the nature of a zeolite sample. By means of X–Ray Diffraction (XRD) it is possible to discern a significant loss in sample crystallinity,[9,10] while sorption studies show a loss in internal surface area,[10] consistent with local collapse of the lattice to form mesopores.[20] The damage to the lattice seems to arise initially from loss of aluminium from tetrahedral sites, being dislodged into a less well–defined non–lattice environment.[3] The loss of lattice aluminium is linked with the diminution in Brönsted acid site concentration (since each Al is associated with one Brönsted site in a H–form zeolite)[11,12,13] and also with the loss of affinity for water which accompanies the polar character of Al–O bonds.[23] The empty sites formed by loss of Al may appear as SiOH clusters to satisfy the valency of the bridging oxygens around the vacancy,[24] while the Al itself forms non–lattice alumina resident in the crystallite channel system (or even outside). The process may be represented schematically as follows:

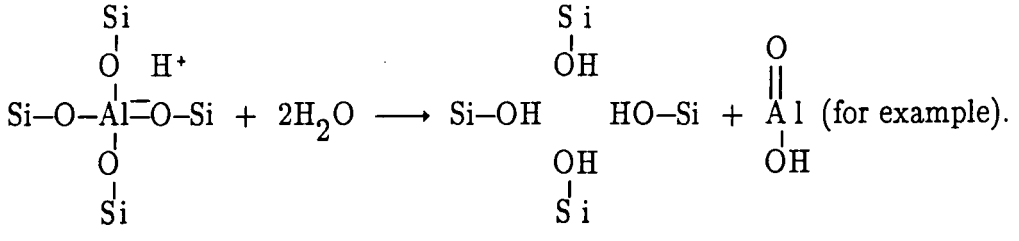

It is widely believed that, although the acid concentration falls smoothly on calcination, the catalytic activity of the zeolite first rises to a peak and then falls as the calcination increases in severity.[34] Several explanations have been advanced for this. One study[14] has ascribed the rise in activity to the increase in sorbate mobility arising from a reduced density of strongly adsorbing acid sites. Most others, however, attribute it to an increase in the acid strength of the remaining sites.[17,18] Often the ^{1}H NMR chemical shift of the Brönsted hydrogens is observed to rise[15] and the IR stretching frequency of the O–H bond falls,[16] as expected for sites of increasing acidity. There are two well–established causes for the increasing acid strength. The first is an increase in the intrinsic acidity of the Brönsted sites as the lattice becomes more silicon–rich, due to the greater electronegativity of silicon relative to aluminium.[18] This is supported by theoretical calculations which suggest that isolated lattice Al gives rise to stronger Brönsted acidity.[19] The second cause is thought to be the appearance of *superacidity*, which is generally believed to arise from a synergistic interaction between a Brönsted site and something else, probably NLA. (Further discussion of superacidity is reserved for Section 5.) The observed fall in activity after very severe calcination (steaming, in the limiting case) is generally attributed to the very low population of acid sites remaining.[27]

The mechanism by which calcination displaces Al from the lattice is poorly understood. Generally the steam used is implicated in hydrolysis of the O–Al bonds.[20] This process seems to be inhibited by the presence of metal cations such as Na^{+} [20,22,88] or lanthanides, with the result that NaY is very difficult to dealuminate by calcination in a controlled manner. There is also some evidence that the Al is only partially removed from the lattice (that is, not all of its four bonds to bridging oxygens are broken) in the absence of water vapour. A recent study by Parker *et al.*[1] has suggested that, under these

conditions, total removal of Al occurs only afterwards when the sample is allowed to rehydrate at low temperature (<100°C). They found that addition of a small amount of water (up to 4 molecules per unit cell) to a sample of HY freshly calcined and kept dry during cooling caused a disappearance of Brönsted OH groups in the IR spectrum and the formation of a small amount of SiOH. These changes reversed on gentle desorption of water. Addition of a larger amount of water caused permanent loss of Brönsted acidity. It is reasonable to assume that the disappearance of the Brönsted signal in the IR spectrum is cause by loss of Brönsted functionality and not by exchange between water and Brönsted protons, since exchange phenomena are rarely visible in the infra–red.

A mechanism that allows for reversible destruction of Brönsted acidity in this manner is likely to involve fission of some, but not all, Al–O lattice linkages, and their replacement with Al–OH groups. A partially–dislodged Al atom (*e.g.* $\begin{matrix}Si{-}O\\Si{-}O\end{matrix}\!>\!Al\!<\!\begin{matrix}OH\\OH\end{matrix}$) will probably generate little Brönsted acidity because it is bonded to fewer electron–withdrawing lattice Si atoms than an Al atom fully attached to the lattice (*i.e.* $Al(OSi)_4$). This view is strongly supported by an *ab initio* quantum–mechanical study of the acidity of Al–OH groups,[80] and by the observation that the Brönsted acid site concentration often decreases more than the lattice Al content on calcination.[28] Any reasonable mechanism for hydrolysis of lattice Al–O bonds must also concur with the observed inhibiting effect of metal cations. The following mechanism is one possibility:

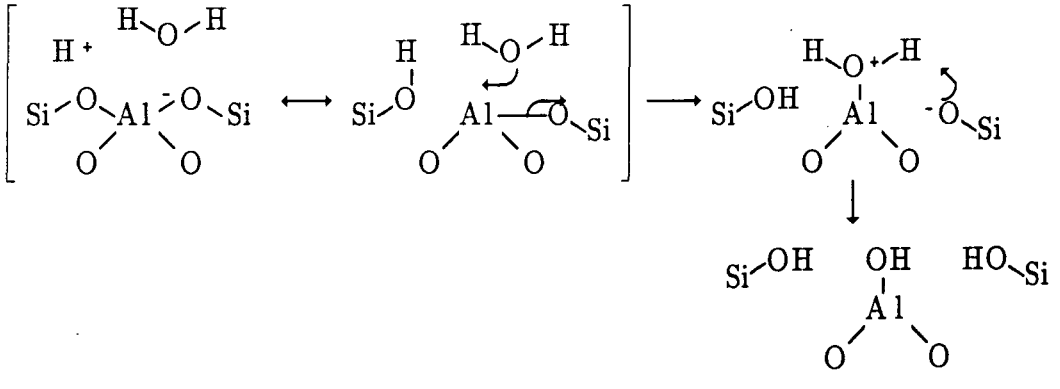

This mechanism involves attack of steam on the Al in the non–zwitterionic resonance form (at the right in the braces above) of the Brönsted site, followed by proton migration from water to the lattice; the net result is the loss of two lattice Al–O linkages and their replacement by two SiOH functionalities[26] and a new –OH group on the Al, which is still partly bonded to the lattice. It is easy to envisage how this process is reversible and also how it could proceed further to achieve complete release of Al from the lattice as an oxyhydroxide species. In addition, it accounts for the inhibiting effect of Na^+, since the Na–form of the Brönsted site would have a much stronger contribution from the zwitterionic resonance structure, which is inactive in the present mechanism. Furthermore, it has been observed[10] that fluoride treatment generates NLA; the mechanism proposed above would allow for the action of fluoride as a Brönsted base in the same manner as steam, with the formation of fluorinated non–lattice aluminium species.

The proposed existence of four–coordinate Al partly bonded to the lattice is supported by a study by Ray[25] in which a broad ^{27}Al NMR signal attributed to non–lattice four–coordinate Al was found to narrow on treatment with water, presumably due to removal of the distortion from pure tetrahedral symmetry around the Al nucleus, as the last lattice Al–O bonds are hydrolyzed.

Nature of Non–Lattice Alumina. Once Al has been fully removed from the lattice, it generally seems to form a polymeric oxyhydroxide species[16,31] which may resemble boehmite[32] (γ–AlOOH). NLA is predominantly six–coordinate,[36] like Al in boehmite, but may include some four–coordinate Al[20,33] (although whether this is simply material that is incompletely cleaved from the lattice is unclear). Early suggestions of three–coordinate NLA have now been largely discounted.[32,34] The degree of polymerization that takes place is highly

dependent on the severity of the treatment[36] and on the post–calcination handling (Chapter 6 is concerned with a study of this); addition of water or acid at room temperature is often sufficient to hydrolyze the oxygen bridges to form much smaller (possibly mononuclear) units.[34,37] Lewis acidity is often attributed to NLA,[24] although the degree of acidity is much less when the material is polymeric;[30,31,36,39] boehmite itself has very little intrinsic Lewis acidity.[32] The NLA often carries terminating OH groups which are visible in the IR spectrum at 3690 cm^{-1} [6,10,29,39] and in the ^{1}H NMR spectrum at 2.6 – 3.6 ppm. The degree of polynucleation can be assessed by measuring the Lewis acidity, OH concentration, or the ^{27}Al NMR linewidth (which is larger in more polymeric structures,[37] due to the greater asymmetry of the environment[35]). The location of NLA seems also to depend on the severity of the calcination; Shannon[32] was able to distinguish NLA in the large cages of Zeolite Y generated by treatment at 300°C from NLA in both large and small cages formed at 500°C. The same study employed an X–Ray technique to show the polymeric species to be composed of edge–sharing chains of AlX_4 octahedra (X: OH, =O, H_2O).

Behaviour of Non–Lattice Alumina. NLA appears to interact significantly with the lattice, although there is disagreement over the nature of the interaction. It is often observed that the Brönsted site concentration drops below the concentration of lattice Al when NLA is present; three possible explanations are available: (i) partially dislodged Al still registers as lattice Al by most measurement methods, but has no Brönsted acidity associated with it, as discussed earlier; (ii) fully dislodged NLA coordinates to Brönsted sites, removing their functionality; (iii) cationic NLA species charge–balance Brönsted sites in the same manner as Na^{+}, again destroying their acidity. In any case, it

is observed that treatment with aqueous acid or with a complexing agent such as EDTA or acac is sufficient to restore the Brönsted concentration to its 'expected' value and, in some cases, to remove the NLA from the crystallite altogether.[16,28] One study[40] found that this leaching–out of NLA increased the concentration of SiOH groups, and attributed this to coordination of NLA to SiOH sites; the observation can however be explained by recourse to the suggestion extended above that calcination may produce half–dislodged aluminium which, on release with acid or water, forms two further SiOH groups in the lattice vacancy.

There is much disagreement over whether NLA is active in catalytic reactions.[41,42] The general consensus seems to be that it enhances reactions involving hydrogen transfer,[44] but may decrease the overall reactivity of the catalyst by physical obstruction of the channels.[43] The catalytic importance of the superacidity it allegedly generates, however, is considerable, as will be discussed in Section 5.

3. ^{27}Al NMR Appearance of Non–Lattice Alumina

There are two principal features of the ^{27}Al NMR spectrum of zeolites which have been widely used to investigate the NLA present. The first is chemical shift. Although ^{27}Al shifts may be distorted by second–order quadrupolar effects, peak positions can broadly be used to determine the coordination number of the ^{27}Al atom. Tetrahedral Al species in zeolites (including lattice Al) occur in the range $50 - 65$ ppm. Octahedral species (always non–lattice) occur close to 0 ppm. Several workers have reported signals around 30 ppm; some assign this to five–coordinate NLA,[46] by deduction from its chemical shift (intermediate between 4– and 6–coordinate NLA); others suggest that it arises from four–[34] or six–coordinate NLA in such an environment that the quadrupolar line shape contains two maxima, one of which

may appear near 30 ppm.[48] There is convincing evidence to support both views, suggesting that either situation may pertain under appropriate conditions. Some workers have identified the occurrence of separate signals (especially well–resolved in the 2D nutation spectrum) for 'distorted framework' Al,[47,49] which may correspond to the partly dislodged Al described earlier.

The other spectral feature valuable in assisting assignment is the linewidth. As discussed in Chapter 2, the linewidth and asymmetry of the nuclear environment are closely linked. Several workers have identified very broad ^{27}Al NMR signals, which are assigned to 'distorted framework' Al[49] or polymeric NLA.[37] (A similar dependence of linewidth on polynuclearity is seen in aluminates in aqueous solution.[35]) One study[37] described the appearance of two octahedral NLA peaks near 0 ppm, one broad and the other narrow; on acid treatment, intensity was transferred from the narrow to the broad peak, presumably due to hydrolysis of the NLA to a mononuclear form.

Many workers have referred to the existence of 'NMR–invisible' aluminium in zeolite samples;[50] this refers to the fact that Al in a very highly distorted environment is usually too broad to observe reliably, since most of the signal decays during the NMR probe's ring–down time. For this reason it is usually impossible to obtain a ^{27}Al NMR spectrum of a dry sample,[51] and samples must be fully hydrated if quantitative signal intensities are required.

4. Lattice Defects and SiOH Groups

It is widely believed that certain preparations and treatments generate zeolitic hydroxyl groups wholly attached to a single lattice silicon atom. These SiOH groups will always be present at the outer surface of the crystal to terminate it, but can also occur in high concentrations inside the crystal.[52] They are generally associated with one of the following features: (i) missing

tetrahedral lattice atoms (commonly Al); (ii) large–scale lattice defects, such as phase boundaries and intergrowths; (iii) occluded non–lattice siliceous material. The present work, and this brief review, are primarily concerned with the first case.

A freshly made, highly crystalline zeolite sample usually has very few lattice defects and a low concentration of SiOH. Many workers have reported, however, that thermal destruction of the organic 'template' molecule often used in the synthesis is sufficient to create SiOH sites.[40,65] Calcination also creates lattice defects containing these groups,[24] as already discussed. Chemical dealumination reagents such as $SiCl_4$ vapour have been reported to generate SiOH.

It is now generally, but not undisputedly, held that SiOH groups often exist in 'nests' of up to four such groups surrounding a single lattice vacancy.[69] Freude *et al.*[56] found that 4.8 SiOH were created per 1 Al lost from the lattice during calcination of Zeolite Y. Yamagishi *et al.*,[53] investigating the reverse process, found that treatment of an SiOH–rich zeolite with $AlCl_3$ vapour resulted in the incorporation of one Al for every four SiOH groups lost. A series of studies by Kraushaar *et al.* involved treatment of SiOH–containing samples with Me_3SiCl, which converts an ≥SiOH group to ≥$SiOSiMe_3$. They found[54] that a high concentration of secondary and tertiary products was obtained in addition to the expected primary products, the former arising presumably from repeated reaction of the –$OSiMe_3$ groups with further suitably–positioned lattice SiOH, releasing methane. The tertiary product was greater in concentration than in a corresponding sample of silica gel, suggesting an especially favourable arrangement of SiOH groups in the zeolite.[55] To refute a claim that the higher–order products arose from multiple reactions on the crystallite surface,[57] the authors treated the silylated zeolite with potassium *tert*–butoxide to cleave

surface silyl ethers. This destroyed nearly all the silylated sites in silica gel, but hardly any in the zeolite, showing the SiOH groups to be interior. However, it has been pointed out that such clustered SiOH groups are likely to undergo H–bonding,[64] which is in disagreement with the observed narrowness of the IR band assigned to these species.[57,62]

Characterization of SiOH Groups. There is disagreement over the ^{29}Si NMR chemical shift at which lattice SiOH groups appear. In view of the stronger Si–O–H bonding in a SiOH group (which is non–acidic) compared with a $Si–O\diagdown^{H}_{Al}$ Brönsted species, it is reasonable to suggest that the former could be selectively observed by using cross–polarization with a short contact time. Ray *et al.*[62] applied this technique to deduce that $(SiO)_3Si–OH$ appears at –101 ppm, the same position as that normally assigned to $(SiO)_3Si–OAl$.[61] Other workers, however,[67] using the same technique, have suggested that $(SiO)_3Si–OH$ resonates at –103 ppm. Engelhardt *et al.*[63] suggested that this peak arises from SiOH on non–lattice silica, but Woolery *et al.*[62] found no peaks due to $–Si(OH)_3$ which would be expected to occur in non–lattice silica; this and other evidence led them to deduce that the observed –103 ppm peak arose from a lattice moiety. Another study[61] suggests that $(SiO)_3Si–OH$ groups contribute to the intensity of a peak at –107 ppm, which is normally assigned to $(SiO)_4Si$. It was also proposed that $(SiO)_2Si\langle^{OH}_{OAl}$ groups (with the Al in the lattice or partly dislodged) appeared at –100 ppm.

Other techniques are also capable of detecting the presence of SiOH. The ^{1}H NMR signal occurs at 1.4 – 2.2 ppm and is usually quite narrow. It has been suggested that the more densely clustered the hydroxyl groups, the higher their chemical shift and linewidth, on account of the mutual H–bonding present.[40] Maciel has conducted an elegant study of dipolar coupling between

^{1}H nuclei in nearby SiOH groups in silica gel,[68] although the narrowness of the signals from SiOH in zeolites suggests that this effect is not so important in more crystalline systems, probably on account of the lower SiOH concentration in the latter. Other workers have shown that there is little coupling between ^{1}H in SiOH groups and Al.[56,69] An infra–red band at 3724 cm^{-1} has been assigned to SiOH.[17,71,74] Finally, the concentration of SiOH in a given sample seems to be linked to the crystallinity[17,70,71] (as measured by XRD and Transmission Electron Microscopy). SiOH nests affect the unit cell size measured by XRD: they occupy less space than the lattice Al they replace but more than a lattice Si.[73]

Chemical Nature of SiOH Groups. Isolated zeolitic SiOH groups appear to exhibit very little Brönsted acidic character, as suggested by their low resonance frequency in the ^{1}H NMR spectrum; they are found not to protonate bases such as pyridine. It is suggested, however, that hydrogen–bonding between adjacent pairs of SiOH permits a small degree of Brönsted acid and cation–exchange[52,62] behaviour. There is very little evidence that they are active in catalysis. On heating above 200^{o}C, adjacent pairs of SiOH groups may condense, forming a new Si–O–Si linkage and releasing water.[40,53,56,69] A sample which has been 'annealed' in this way may have a lower affinity for water and a greater affinity for non–polar sorbates, presumably due to the loss of polar character and H–bonding capacity inside the crystallite.[26] A lattice which is rich in SiOH is also found to be less stable to thermal degradation.[73]

Healing and Re–Insertion into Vacancies. It is now well–known that Si can be inserted into SiOH–surrounded vacancies by treatment with a tetravalent Si compound such as $SiCl_4$, SiH_4 or Me_3SiCl. Al can be inserted by treatment with

$AlCl_3$ vapour,[24] even after the SiOH sites have been condensed.[53] Treatment with H_3PO_4 has also been observed to cause loss of SiOH groups, whether by insertion of P into the lattice or by H_3PO_4 encouraging the condensation process by removing water.[75]

Some workers have suggested that steam treatment causes migration of Si from one region of the crystal to another in order to heal SiOH–surrounded defects.[76] A mechanism has been proposed for this process.[77]

5. Superacidity

There has been much discussion in recent years concerning the possible existence of a mechanism by which very strong Brönsted acidity may be generated in a zeolite.[28] This 'superacidity' was first proposed to explain the substantial increase in catalytic reactivity towards hydrocarbons[27,81] (especially in alkyl–transfer reactions such as $2PhMe \longrightarrow C_6H_6 + C_6H_4Me_2$[42]) exhibited by some samples after calcination. The superacid sites are said to be capable of protonating linear alkanes,[83] in a manner reminiscent of magic acid. The site gives rise to an IR OH–stretching band at 3610 cm^{-1},[6,29,85] located between the two resonances attributed to Brönsted sites, at 3640 and 3540 cm^{-1};[15,71,78] this is strange, perhaps, since a highly acidic –OH group might be expected to appear at a lower wave number. Furthermore, there is little evidence for strongly acidic H *per se* in the ^1H NMR spectrum. Superacid sites are selectively poisoned by Na^+ addition in the presence of ordinary Brönsted sites. Sorption studies show that they bind pyridine up to 400^{0}C, demonstrating their very strong acidity[6] (150–180 kJ mol^{-1} [32]).

It is widely believed that superacidity arises from the interaction of Lewis acidic and lattice Brönsted sites.[34,79] Both Brönsted acidity and NLA[10,24,42] appear to be necessary for its formation. Not all NLA participates

in the development of superacidity,[31] perhaps because of clustering or polymerization. Nor is every Brönsted site involved;[87] Na^+–poisoning studies[85] have suggested that the ratio of superacid site to lattice Al concentration is only $10-20\%$. Some workers have suggested that the lattice Al involved has to be isolated, i.e. in a siliceous environment.[84,85] Others postulated the involvement of partially dislodged lattice Al.[82] The mechanism of interaction seems to be withdrawal of electron density from the Brönsted acidic H by the Lewis acidic species,[86] which has been suggested to be AlO^+,[86] $AlOH^{2+}$,[85] or $[Al<^{O}_{O}>Al]^{2+}$.[79,85]

6. Non–Lattice Silica

As mentioned in Chapter 2, the ^{29}Si NMR spectrum of many zeolite samples suggests the presence of amorphous siliceous material[60] (silica or silica–alumina) by a broad underlying hump centred on approximately –100 ppm and by a narrower peak, on the low–frequency edge of the normal lattice Q^4 signal, at –110 ppm. It is believed that non–lattice silicon–containing species may be formed during calcination, in addition to NLA,[67] although it may represent less than 5% of the total amount of non–lattice material.[9] It can also arise from chemical stabilization treatments after acid leaching.[60] Similar ^{29}Si NMR peaks have been observed in silica and in silicate glasses.[89] Lewis acidity has been attributed to non–lattice silica–alumina, and is strongest when the material is silicon–rich.[17]

4B: NMR STUDIES OF ZEOLITE Y DURING DEALUMINATION TREATMENTS

1. Samples and Treatments

The methods used to prepare the samples in this study are described fully in Chapter 3; the samples are listed in Appendix A, and outlined briefly here for convenience.

All samples were derived from a common precursor NH_4Y, known as NH_4Y[1], with a low residual Na^+ content. This was calcined at two different temperatures, 550°C and 650°C, to produce two HY samples known as HY–C550 and HY–C650. Portions of these were steamed at 816°C for 5 hours to produce HY–C550–S and HY–C650–S. The precursor NH_4Y[1] was also chemically dealuminated with $(NH_4)_2SiF_6$ to produce NH_4Y–CS, part of which was steamed (under the same conditions as above) giving rise to HY–CS–S. The samples emerged from these treatments in a partially hydrated form. Full hydration was carried out in some cases by allowing the sample to equilibrate for

Table 4.1: Analytical Results for All Samples Obtained by Techniques Other Than NMR (Cryst = Crystallinity)

Sample	Cryst /% (XRD)	Surf Area/ m^2g^{-1}	Si/Al Ratio ±0.2 (XRF)	(UCS ±0.01) /Å	Al/u.c. ±1 (UCS)	Si/Al Ratio (UCS)
NH_4Y	80	802	2.5	24.62	38	4.1±0.1
HY–C550	75	728	2.5	24.45	21.5	7.9±0.4
HY–C650	75	686	2.9	24.39	15	11.8±0.9
HY–C550–S	66	577	–	24.23	0	∞
HY–C650–S	67	539	–	24.26	2	95±48
NH_4Y–CS	85	804	4.6	24.51	27	6.1±0.3
HY–CS–S	55	534	–	24.20	0	∞

three days or longer in an atmosphere of 85% relative humidity.

Table 4.1 gives the results from non–NMR analyses of all these samples. Table 4.2 lists all Figures showing NMR spectra for easy reference.

Table 4.2: Figures Containing NMR Spectra

Fig.	Nucleus	Contents
4.1	^{29}Si	(a) NH_4Y SP + deconvolution (b) NH_4Y–C550 SP + deconvolution (c) NH_4Y–C650 SP + deconvolution
4.2	^{29}Si	(a) NH_4Y CP/MAS (b) HY–C550 CP/MAS (c) HY–C650 CP/MAS
4.3	^{27}Al	(a) NH_4Y (b) HY–C550 with ^{1}H decoupling (c) HY–C550 coupled (d) HY–C550 hydrated, decoupled (e) HY–C650 hydrated, decoupled (f) HY–C650 hydrated, coupled
4.4	^{29}Si	(a) HY–C550–S SP + deconvolution (b) HY–C650–S SP + deconvolution
4.5	^{27}Al	(a) HY–C550–S (b) HY–C550–S fully hydrated (c) HY–C650–S
4.6	^{1}H	HY–C550–S: (a) as made; (b) hydrated; (c) dried
4.7	^{29}Si	(a) HY–C550–S CP/MAS (b) HY–C650–S CP/MAS
4.8	^{29}Si	NH_4Y–CS SP + deconvolution
4.9	^{27}Al	NH_4Y–CS: (a) decoupled; (b) coupled
4.10	^{29}Si	NH_4Y–CS CP/MAS
4.11	^{29}Si	HY–CS–S: (a) SP + deconvolution; (b) CP/MAS
4.12	^{27}Al	HY–CS–S decoupled

2. Starting Material and Calcination Treatment

Figure 4.1 shows the ^{29}Si single–pulse spectra of NH_4Y[1], HY–C550 and HY–C650. The NH_4Y[1] sample contains a greater population of ^{29}Si in aluminium–rich sites (low Q^n), showing that lattice Al is lost during calcination, as expected. Deconvolution of the spectra (also shown in Figure 4.1) enables calculation of the lattice Si/Al ratio, giving results as follows: NH_4Y[1], 4.01; HY–C550, 10.01; HY–C650, 31.68 (although this value must be treated with caution: it is generally accepted that ^{29}Si NMR estimates for samples with Si/Al ratios above 10 are not reliable). It may be noted that these values are not always in agreement with those found from other techniques; further discussion on this topic is reserved for Section C. Traces (b) and (c) also contain an extra small peak at about –111 ppm, which is discussed later. Spectrum (c) requires the use of two superimposed Gaussian line shapes to simulate the Q^4 band acceptably well; this arises from the distribution of Si environments resulting from differing next–nearest neighbour occupancy, as discussed in Chapter 2.

The ^{29}Si CP/MAS spectra are shown in Figure 4.2. The CP spectrum for NH_4Y[1] resembles the corresponding single–pulse spectrum, but those for the calcined samples differ substantially from theirs. The relatively intense Q^3, Q^2 and (in HY–C650) Q^1 and possibly even Q^0 peaks may arise from three sources: (i) remaining Si(4–n Al) lattice sites; (ii) lattice $Si(OH)_n$ species resulting from loss of lattice Al; (iii) non–lattice silicon–containing material. The first of these possibilities can be entertained only if an intense interaction between ^{1}H–containing NLA and remaining lattice Brönsted sites is invoked, since the presence of NLA is the only major difference between the calcined and uncalcined samples which could give rise to such a marked difference in CP NMR appearance of such Brönsted sites.

Possibilities (ii) and (iii) are both plausible, and would be difficult to

Figure 4.1: ^{29}Si SP spectra with decoupling and Gaussian deconvolution
(a) NH_4Y PA=$\pi/2$ NT=4100 RO=1160Hz RD=20s
(b) HY–C550 PA=$\pi/2$ NT=3590 RO=1830Hz RD=20s
(c) HY–C650 PA=$\pi/2$ NT=3760 RO=2000Hz RD=15s

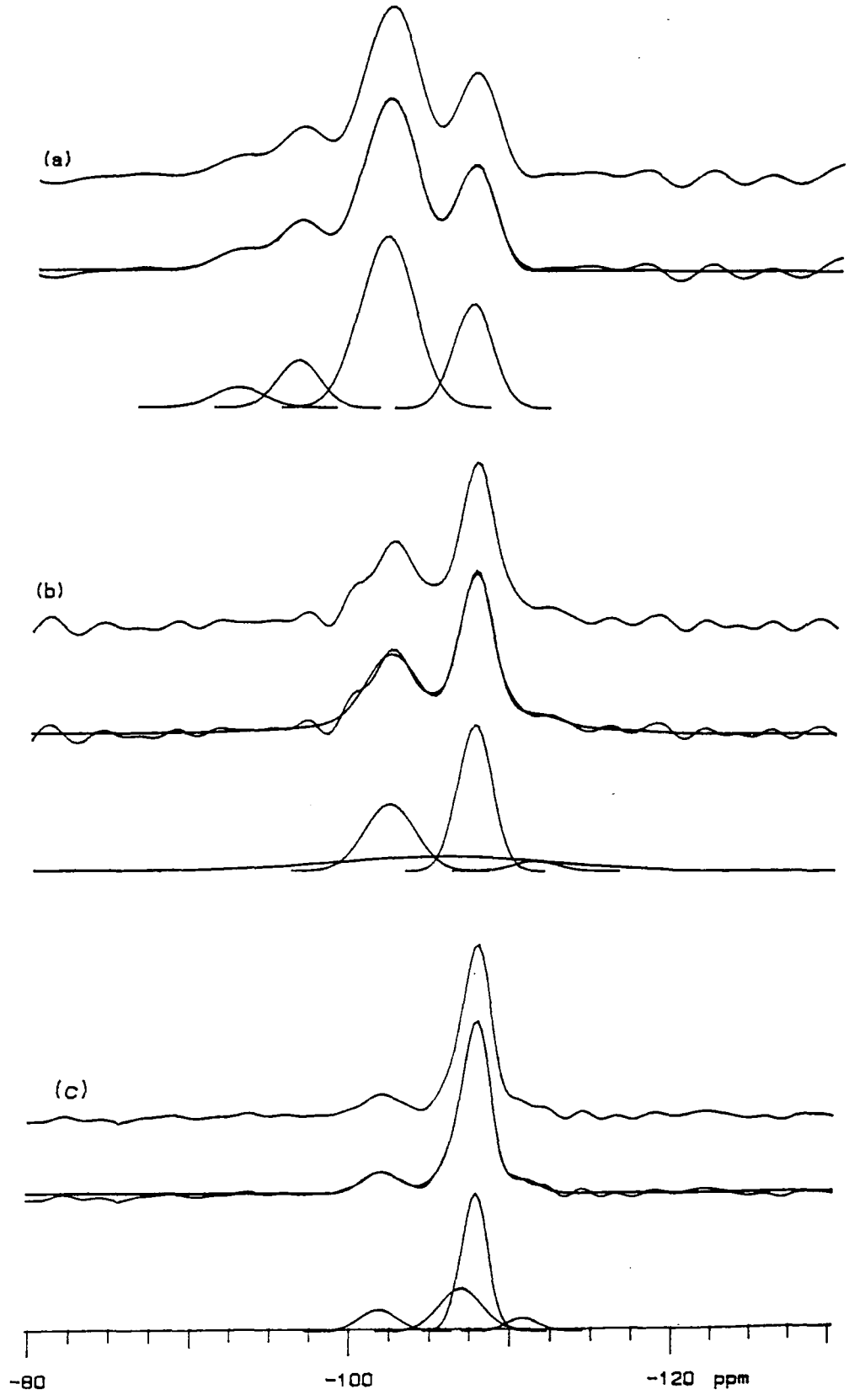

Figure 4.2: ^{29}Si CP/MAS spectra
(a) NH_4Y NT=2300 RD=2s CT=5ms
(b) HY–C550 NT=2300 RD=2s CT=10ms
(c) HY–C650 NT=3500 RD=2s CT=10ms

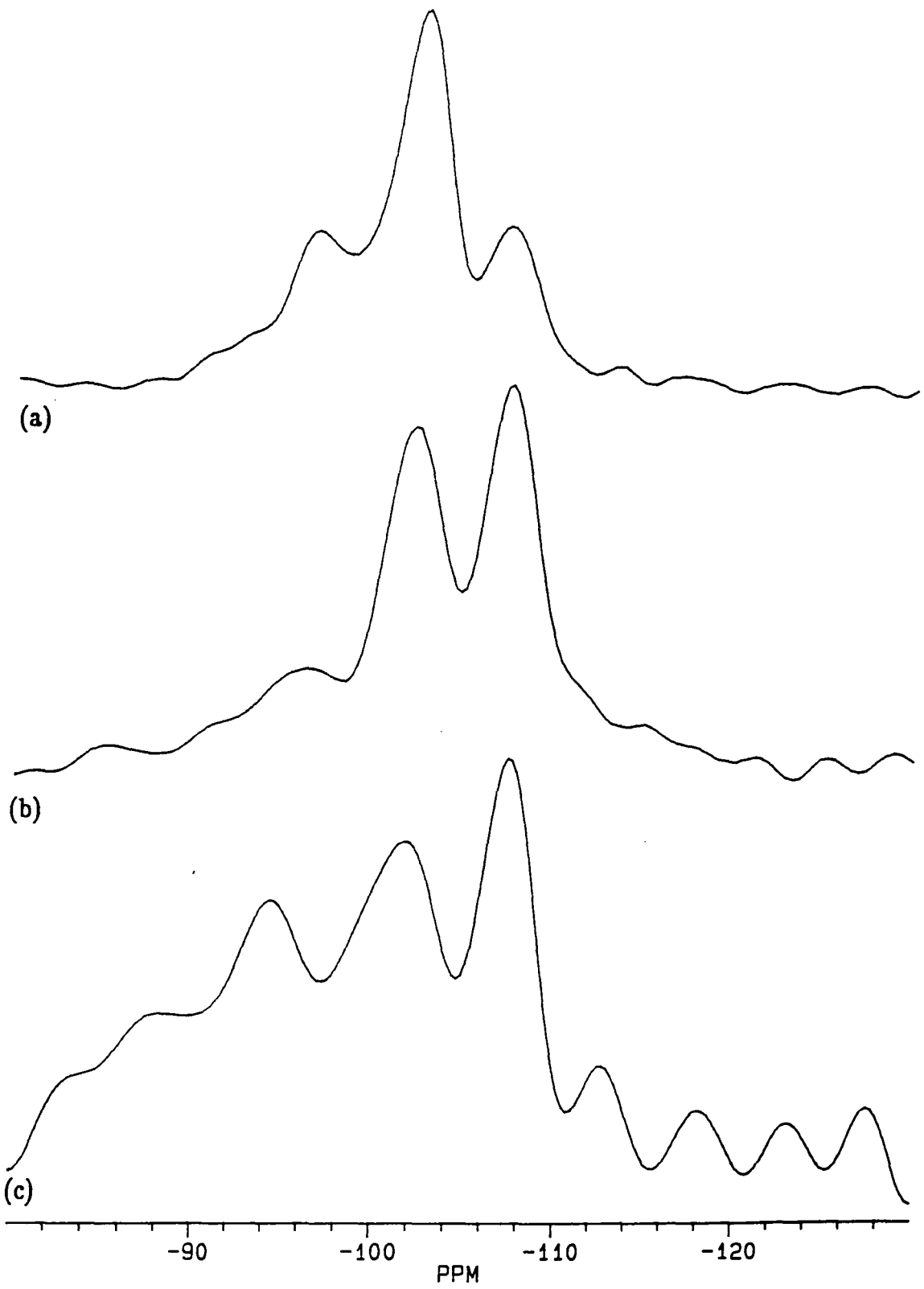

distinguish; (ii) possibly has more support in the literature, as described earlier. The suggestion that each lost lattice Al is replaced by four OH groups attached to the four silicons surrounding its site may also find support in the general similarity in site distribution between the single–pulse spectrum of NH_4Y[1] and the CP/MAS spectrum of HY–C650. One cannot, however, read too much significance into CP/MAS signal intensities, as discussed in Chapter 2; furthermore, the absence of significant $Si(OH)_n$ population seen in the quantitative single–pulse spectrum of HY–C650 indicates that widespread annealing or Si migration takes place. Furthermore, the difference between the CP/MAS spectra of HY–C550 and HY–C650 is not explained by this theory.

There is some evidence to support proposal (iii), that the high frequency peaks arise from non–lattice silicon. Table 4.1 shows that the lattice Si/Al ratio of HY–C550 found by measurement of the unit cell size is 7.93, and for HY–C650 11.8. The ^{29}Si NMR estimates are respectively 10.01 and ~32, as reported above. These show that ^{29}Si NMR is detecting more Si than the UCS measurement, which registers only lattice atoms. If the high–frequency peaks arose from lattice SiOH groups, the ^{29}Si NMR estimate of the Si/Al ratio would be lower than that obtained from the UCS measurement, since lattice SiOH is thought to resemble Si–O–Al in the ^{29}Si NMR spectrum. The conclusion may therefore be drawn that a significant amount of low–Q^n Si is in a non–lattice environment in these samples. The deconvolution results from the ^{29}Si single–pulse spectra shown in Figure 4.1 suggest that both calcined samples contain a little 'ordered' non–lattice silica (indicated by the small peak to low frequency of –110 ppm) but only HY–C550 contains a good deal of 'disordered' material (broad peak centred on –108 ppm). It may be that, in HY–C650, the non–lattice material is just as abundant but more ordered, and so does not appear as a single broad peak. Then the difference between the ^{29}Si CP/MAS spectra of the two calcined samples

could be explained by suggesting that the spectrum of HY–C550 arises mainly from lattice Si but that of HY–C650 (which is actually much weaker in total intensity) arises substantially from non–lattice material. This requires the assumption that lattice nuclei are much less strongly coupled to ^{1}H in HY–C650 than in HY–C550, a view supported by ^{27}Al results described later.

Figure 4.3 shows the ^{27}Al single–pulse spectra of the three samples. NH_4Y[1] shows a single peak due to lattice Al. The calcined samples additionally show the expected octahedral NLA peak in the range 0 to –7 ppm. Comparison of traces (b) and (d) in Figure 4.3 shows that full hydration of these samples increases the signal intensity and narrows the lines; this is due to the charge–dispersion effect of solvation.

The influence of ^{1}H–decoupling on these spectra is of particular interest. The ^{1}H–coupled spectrum of HY–C550 (Figure 4.3(c)) differs from the decoupled spectrum (b) in the virtual disappearance of the spinning sideband at 110.4 ppm and the attenuation of the octahedral NLA peak at –6.5 ppm. The loss of the latter peak shows that some NLA is coupled to ^{1}H, probably either from tightly–bound water or in AlOH groups. The spinning sideband is narrower than the overall band shape at 54.3 ppm, showing that it arises from one or more of many components superimposed in this band shape. The strongly coupled components may arise from tetrahedral NLA, or perhaps from lattice Al in an environment which is geometrically suited to strong coupling to immobile ^{1}H, *e.g.* on SiOH.

Turning off the ^{1}H decoupler has a substantially different effect on the ^{27}Al spectrum of HY–C650 (see Figure 4.3(e) and (f)). In this case, the spinning sidebands around the tetrahedral peak remain, but the octahedral NLA peak almost disappears. This suggests that, in contrast to HY–C550, *all* the NLA is coupled to ^{1}H; the unusually small linewidth of the signals indicates also that all

Figure 4.3: ^{27}**Al SP spectra** PA=3π/40 RD=200ms RO=4500Hz

(a)	NH_4Y decoupled	NT=2000
(b)	HY–C550 decoupled	NT=10000
(c)	HY–C550 coupled	NT=10000
(d)	HY–C550 hydrated, decoupled	NT=4000
(e)	HY–C650 hydrated, decoupled	NT=1000
(f)	HY–C650 hydrated, coupled	NT=1000

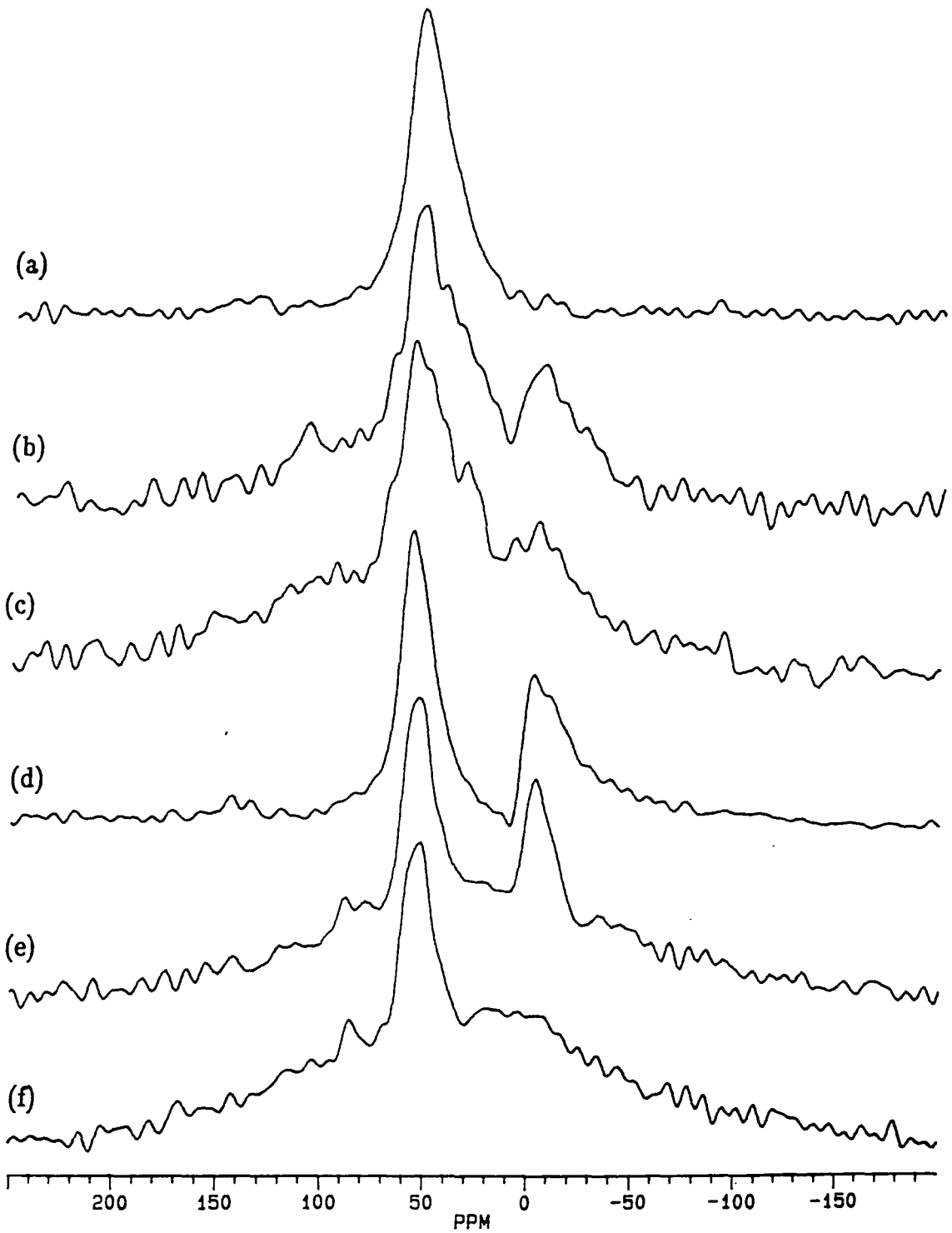

Al present, both lattice and non–lattice, is in well–defined and relatively symmetrical environments. This ties in with the conclusion drawn earlier that the non–lattice *silica* in this sample is also in a well–defined form. The dramatic attenuation of the tetrahedral peak in HY–C650 compared with the modest loss in HY–C550 suggests that the NLA in the former is richer in –OH groups, although this may be due to the greater hydration level (as discussed further in Chapter 6).

Deconvolution was performed on the ^{27}Al spectra of the fully hydrated calcined samples to enable the estimation of the ratio (R) of octahedral to tetrahedral Al present, assuming that the intensities within a given spectrum are comparable under the quantitative conditions mentioned earlier. The observed ratios were 0.753 for HY–C550 and 0.516 for HY–C650. Using these values, it is possible to estimate the amount of tetrahedral NLA per unit cell (T_N) as follows. The total number of *lattice* Al per unit cell (T_L) can be found from UCS or ^{29}Si NMR measurements of lattice Si/Al ratios, as above; the total NLA content per unit cell (N) is equal to the difference between the lattice Al content for NH_4Y[1] and for the calcined sample, since all the dislodged Al remains in the sample. The total amount of tetrahedral Al is $T_N + T_L$. If P is the octahedral Al content per unit cell, $R = P/(T_N + T_L)$ by definition. P can be found by subtracting T_N from N; substitution and rearrangement gives

$$T_N = \frac{N - RT_L}{R + 1}$$

Table 4.3 shows the T_L values, the derived N and hence T_N and the fraction of tetrahedral Al that is non–lattice, for the two calcined samples. Irrespective of whether UCS– or NMR–derived estimates of T_L are used, the results show that HY–C550 contains only a small fraction of tetrahedral NLA, whereas HY–C650 contains much more: there is approximately the same amount of tetrahedral NLA as lattice Al in this sample. The paucity of tetrahedral NLA in HY–C550

Table 4.3: Analysis of Al content in Calcined Samples

Sample	T_L		N	
	(UCS)	(^{29}Si)	(UCS)	(^{29}Si)
HY–C550	21.5	17.4	16.5	20.6
HY–C650	15.0	5.9	23.0	32.1

Sample	T_N		$\frac{T_N}{T_N+T_L}$	
	(UCS)	(^{29}Si)	(UCS)	(^{29}Si)
HY–C550	0.18	4.28	0.01	0.20
HY–C650	10.07	19.17	0.40	0.76

mitigates against the assignment of the spinning sideband at 110.4 ppm to NLA. It is reasonable to suggest, therefore, that the corresponding sidebands in HY–C650 also arise from lattice rather than non–lattice Al. This indicates that the coupling between ^{1}H and lattice Al is weak in HY–C650 but stronger in HY–C550. This result is in agreement with the assumption made earlier that ^{1}H–^{29}Si coupling is weaker in HY–C650.

3. Steaming of Calcined Samples

Figure 4.4 shows the ^{29}Si single–pulse spectra of HY–C550–S and HY–C650–S. Both show only a single narrow peak at –108 ppm, indicating the loss of all lattice Al. The deconvolution performed on HY–C550–S suggests the

Figure 4.4: ^{29}Si SP MAS spectra of steamed samples
(a) HY–C550–S RO=2160Hz RD=20s NT=7700
(b) HY–C650–S RO=3000Hz RD=20s NT=3019 AQ=25ms. Note sinc wiggles due to insufficiently long acquisition time

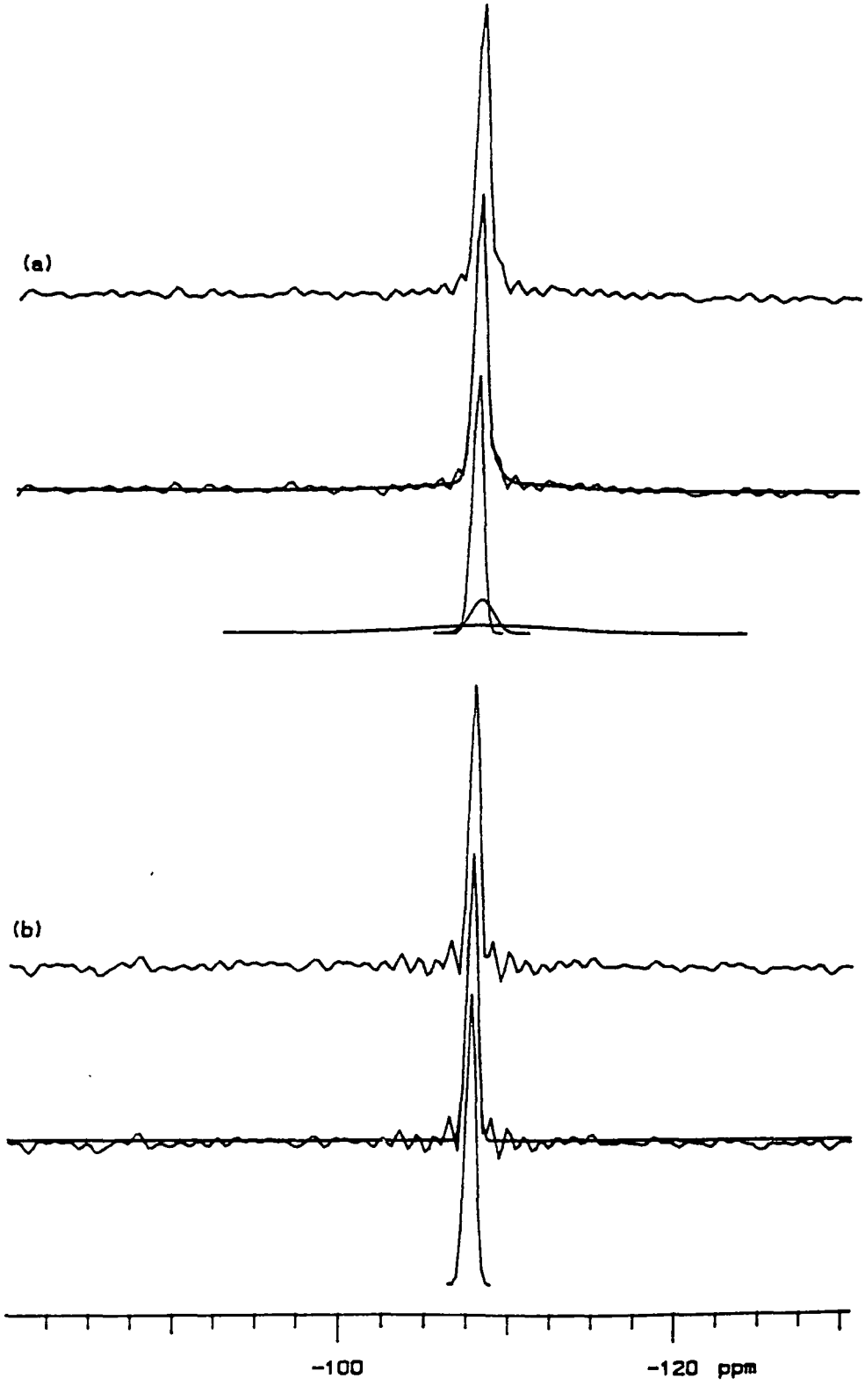

occurrence of some non–lattice silica by a broad peak underlying the narrow one. This material may be that left over from the previous calcination.

The ^{27}Al spectra shown in Figure 4.5(a) and (c) show a three–peak structure which, as discussed in Section A, may arise from overlap of two broad quadrupolar line shapes, indicating a very unsymmetrical environment for the ^{27}Al nuclei. On hydration, the spectrum reduces to the familiar two–peak structure attributed to tetrahedral and octahedral Al. Nearly all the Al present must be in a non–lattice form since the ^{29}Si single–pulse spectra show that very little lattice Al exists, if any.

Some ^{1}H spectra of HY–C550–S appear in Figure 4.6. The material as synthesized, which is in a partially hydrated form, shows an intense peak in the normal position of SiOH groups, equivalent to about 12 OH groups per unit cell. It is unlikely that these are all attached to the lattice, since only a Q^4 peak is visible in the ^{29}Si single–pulse spectrum. It seems reasonable to suggest that some of them are attached to non–lattice silicon; since the non–lattice species are amorphous, the ^{29}Si signals for such SiOH groups would be dispersed over a wide chemical shift range, as observed (Figure 4.4(a)). The ^{1}H spectrum also shows a narrow peak at 4.0 ppm, which is the normal position for Brönsted acidic protons in Zeolite Y. These might be Brönsted sites on non–lattice silica–alumina. There is also a broader underlying peak which may be attributed to AlOH in NLA.

The same sample after full hydration shows only free water at 5.0 ppm (0.3 ppm higher in frequency than the usual position, so possibly exchanging on Lewis acid sites) and a little SiOH at 1.5 ppm. Complete *dehydration* of this sample (by the method described in Chapter 3) gives the spectrum shown in Figure 4.6(c), where a number of SiOH and AlOH species, plus hints of more acidic groups (shoulders at 5.0 and ~7 ppm – perhaps the elusive superacid site?),

Figure 4.5: ^{27}Al MAS spectra of steamed samples
PA=3π/40 RD=200ms RO=4500Hz
(a) HY–C550–S as made NT=20000
(b) HY–C550–S fully hydrated NT=10000
(c) HY–C650–S as made NT=20000

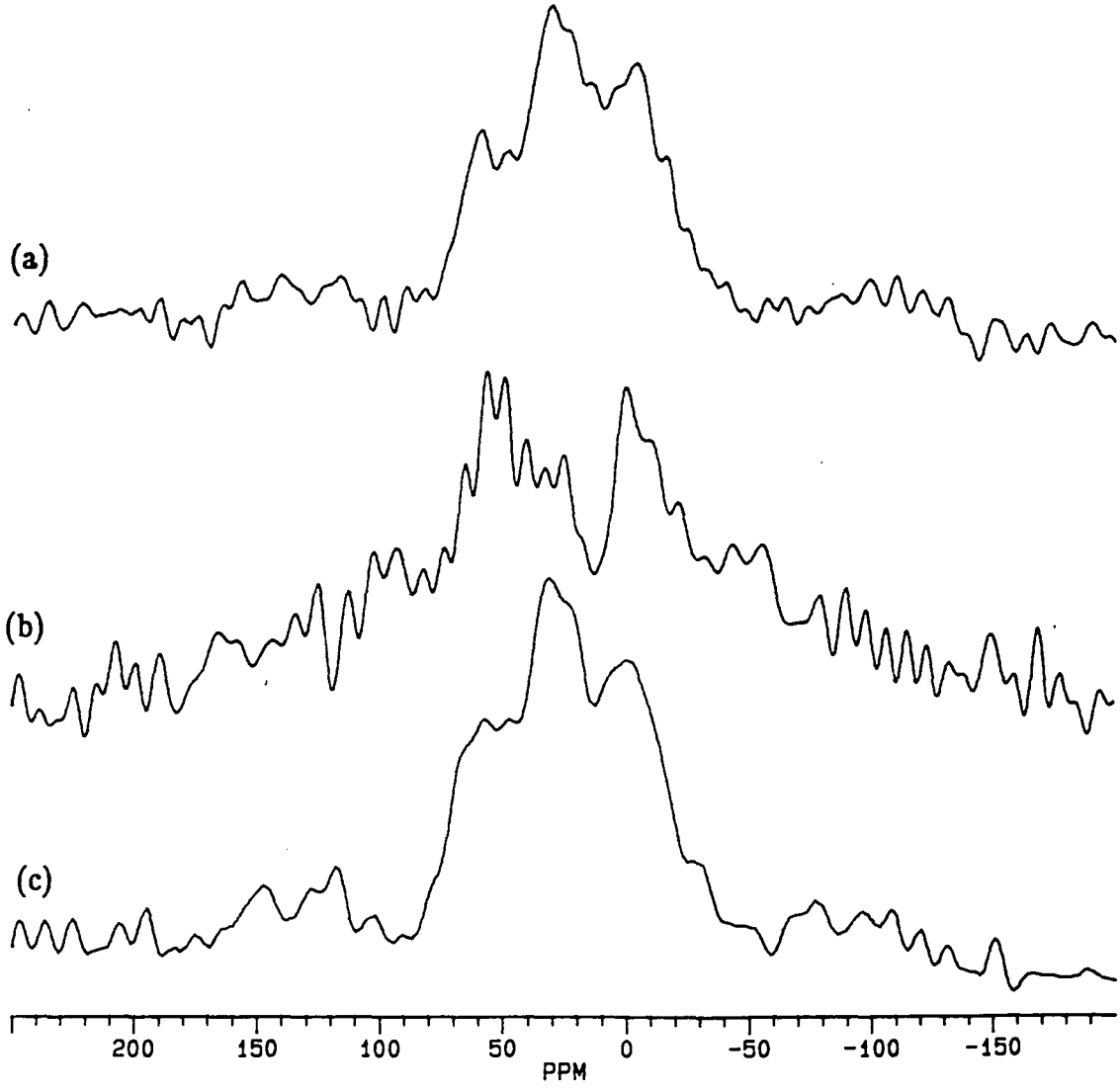

Figure 4.6: ^{1}H SP MAS spectra of steamed sample HY–C550–S
(a) As made PA=π/2 RD=3s NT=64 AQ=100ms RO=4500Hz
(b) Hydrated NT=32 RO=1834Hz RD=3s
(c) Dried NT=200 RO=3000Hz RD=5s

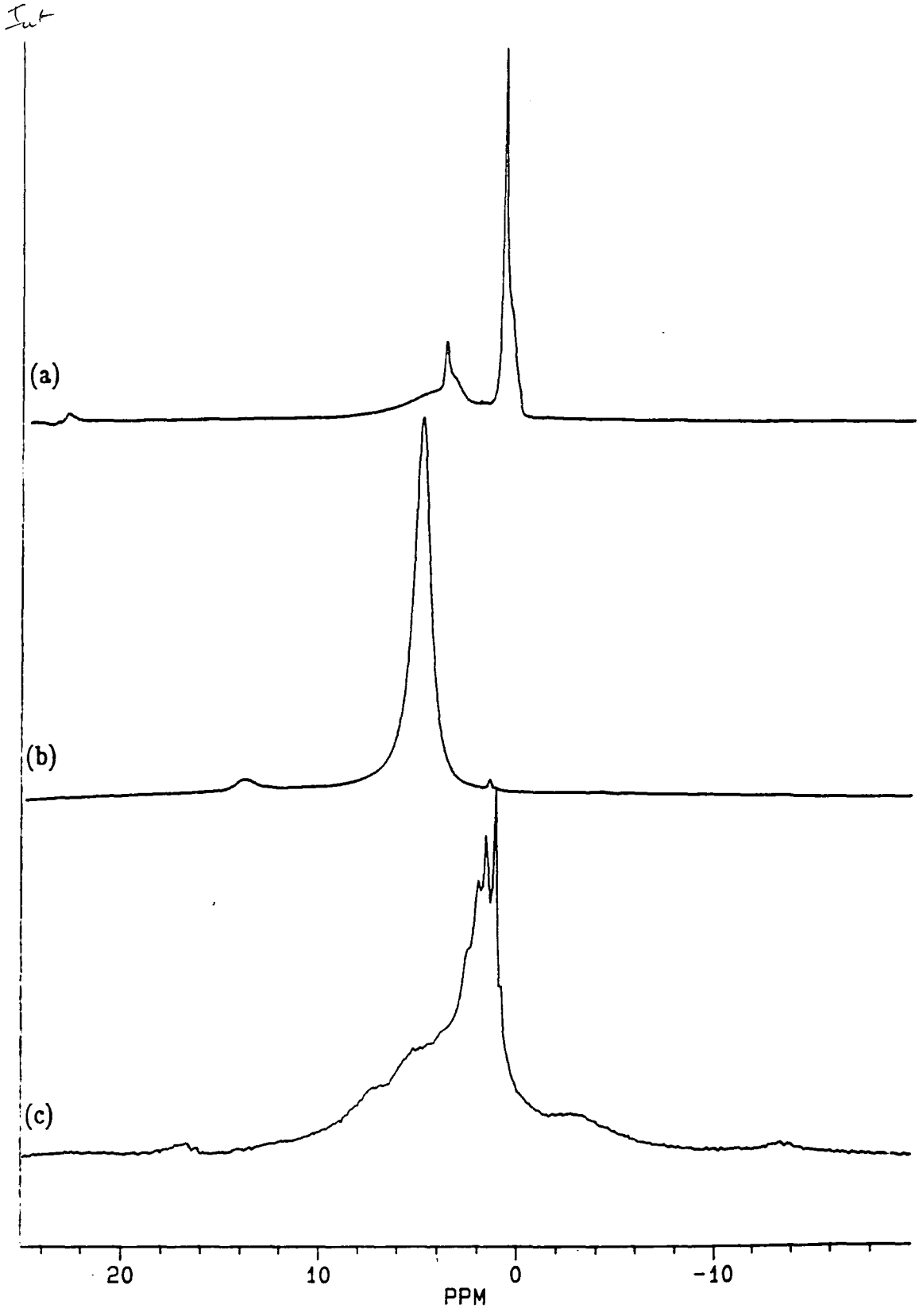

are visible.

The ^{29}Si CP/MAS spectra of HY–C550–S and HY–C650–S (Figure 4.7) are in dramatic contrast to the simplicity of the single–pulse spectra. These spectra, which are very weak in intensity, apparently show a host of overlapping peaks in the range –85 to –107 ppm. The spectra suggest that a range of sites with Q^n values varying from 1 to 4 are present in non–lattice and possibly also lattice environments. The –107 ppm peak is remarkably weak, showing an astonishing degree of rejection of lattice Q^4 sites. This demonstrates that there is no strong coupling between ^{1}H and lattice Q^4 Si; if water is associated with such lattice sites, its residence time must be short on the NMR time scale.

4. Chemically Dealuminated Sample

The ^{29}Si single–pulse spectrum of NH_4Y–CS is shown in Figure 4.8, together with a deconvolution into four Gaussian peaks. If the broad peak at –101 ppm is neglected in the calculation, the Si/Al ratio can be estimated to be 5.9, in good agreement with the value of 6.11 found by XRD (Table 4.1). Evidence that the lattice Al is inhomogeneously distributed arises indirectly from the deconvolution trace in Figure 4.8. The spectrum proved more difficult than most to simulate by means of single Gaussian band shapes for each Q^n site; had the Al distribution been homogeneous, a Gaussian distribution of next–nearest–neighbour occupancies would have been expected, generating a Gaussian band shape.

Figures 4.9 and 4.10 show the ^{27}Al SP and ^{29}Si CP/MAS spectra of NH_4Y–CS respectively. The sharpness of the ^{27}Al spectrum shows that there is very little damage to the lattice; the lost Al is removed completely, not residing

Figure 4.7: ^{29}Si CP/MAS spectra of steamed samples
(a) HY–C550–S NT=90000 CT=10ms RD=2s RO=1400Hz
(b) HY–C650–S NT=83050 CT=10ms RD=2s RO=1080Hz

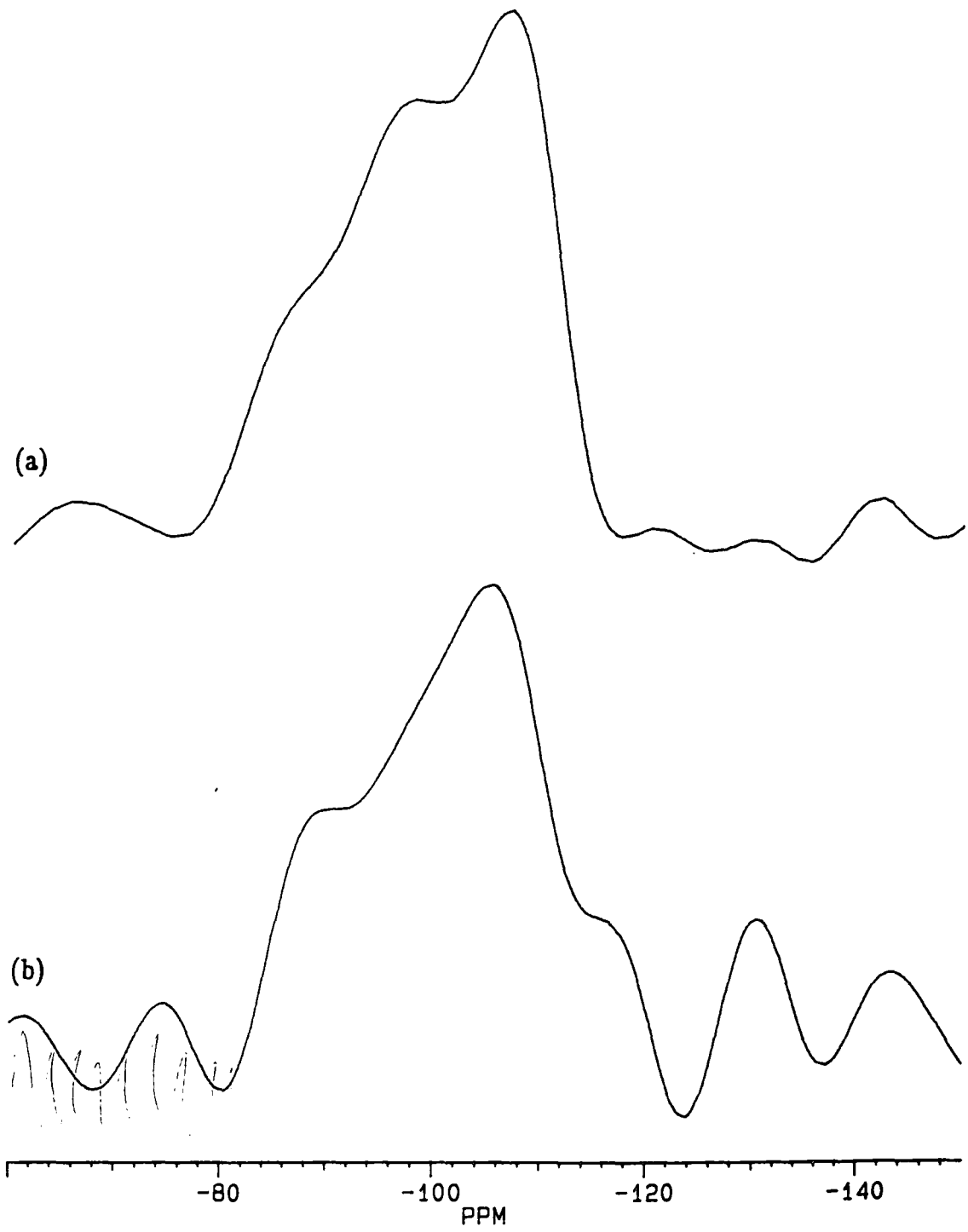

Figure 4.8: ^{29}Si SP MAS spectrum of NH_4Y–CS with Gaussian deconvolution
NT=3915 RD=20s RO=3000Hz

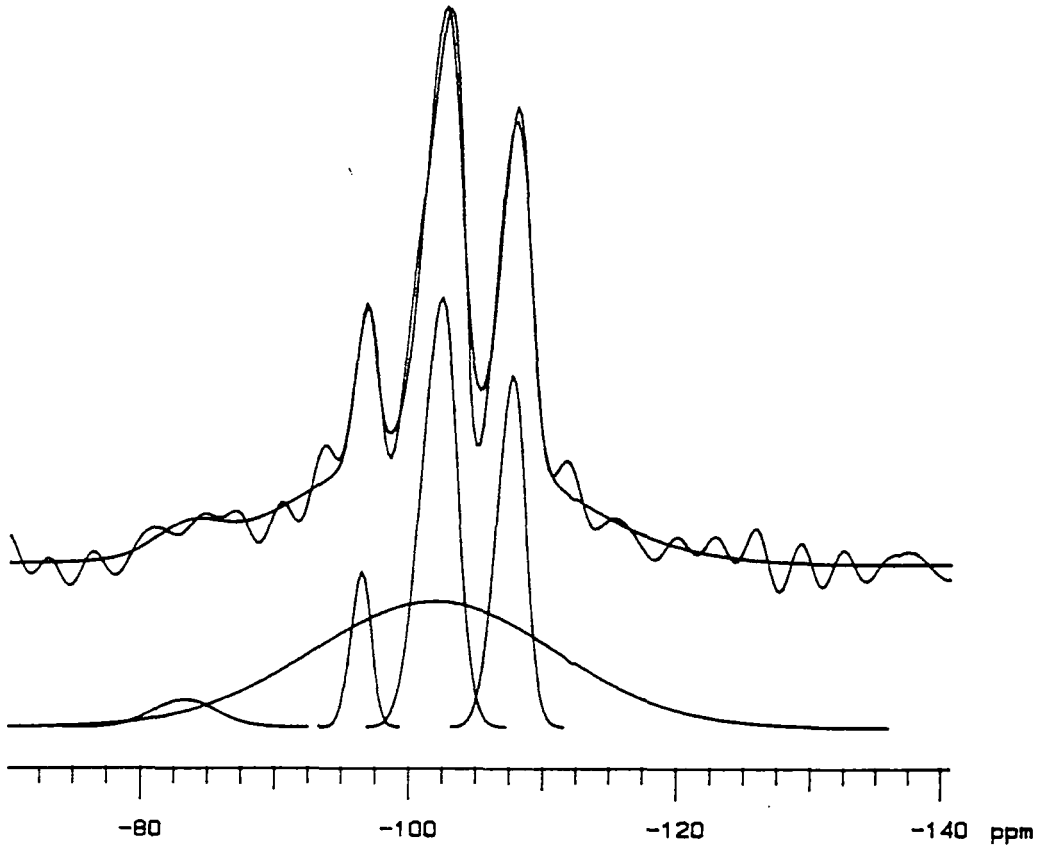

in the pores. ^{1}H decoupling has little effect on this spectrum showing that there is no strong association between water and lattice Al. The ^{29}Si CP/MAS spectrum strongly resembles the single–pulse spectrum, suggesting that CP/MAS is detecting intact lattice sites, very little defect SiOH or non–lattice silica being present. This indicates, then, that the broad peak at –96 ppm in the ^{29}Si SP spectrum arises on this occasion from *lattice* Si, and may be taken as further evidence for the inhomogeneity of the lattice Al distribution.

After steaming, HY–CS–S gives the ^{29}Si spectra shown in Figure 4.11.

Figure 4.9: ^{27}Al SP MAS spectra of NH_4Y–CS NT=2000 PA=3π/40 RO=4500
(a) Decoupled (b) Coupled

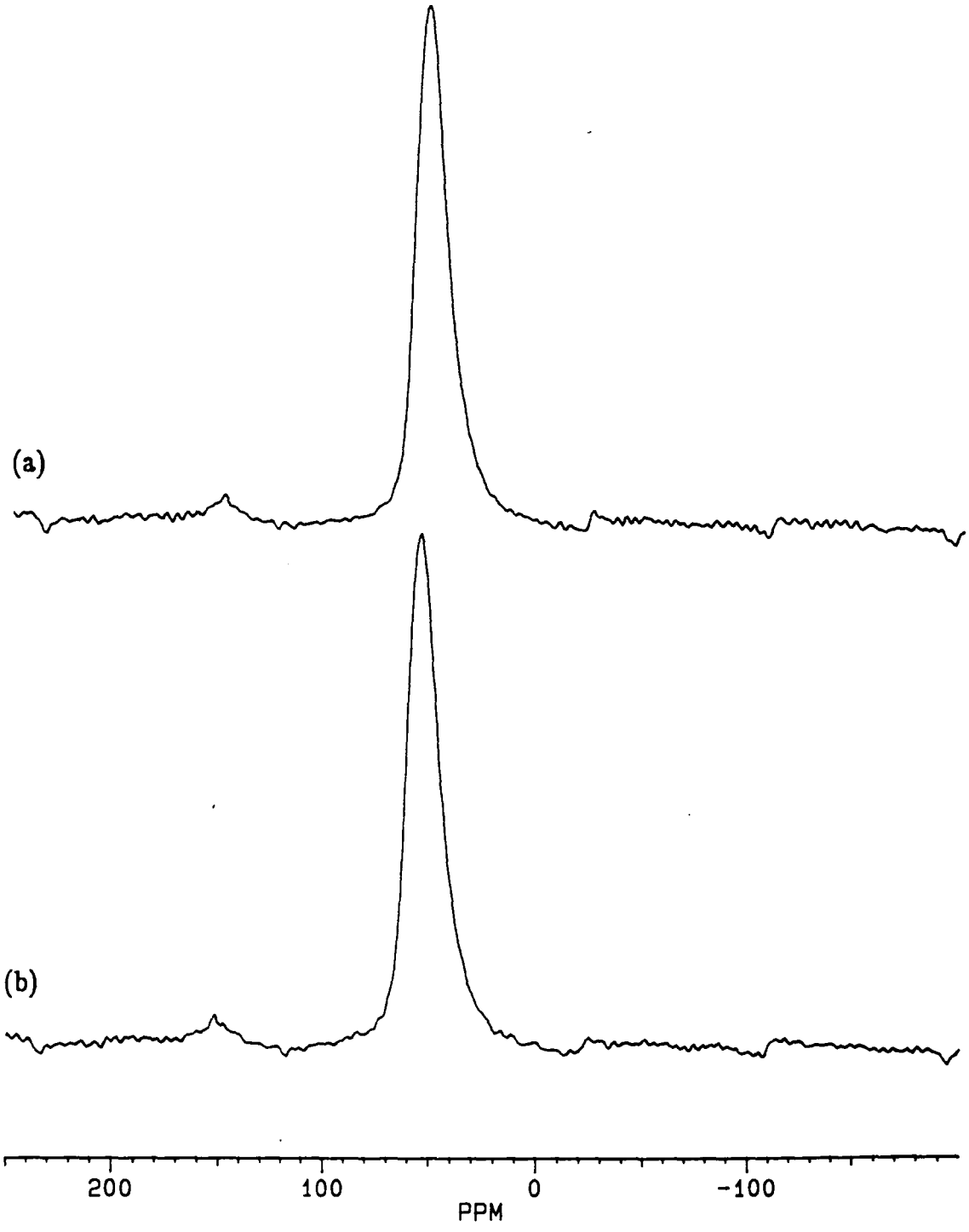

Figure 4.10: ^{29}Si CP/MAS spectrum of NH_4Y–CS
NT=22100 RO=1150Hz CT=10ms

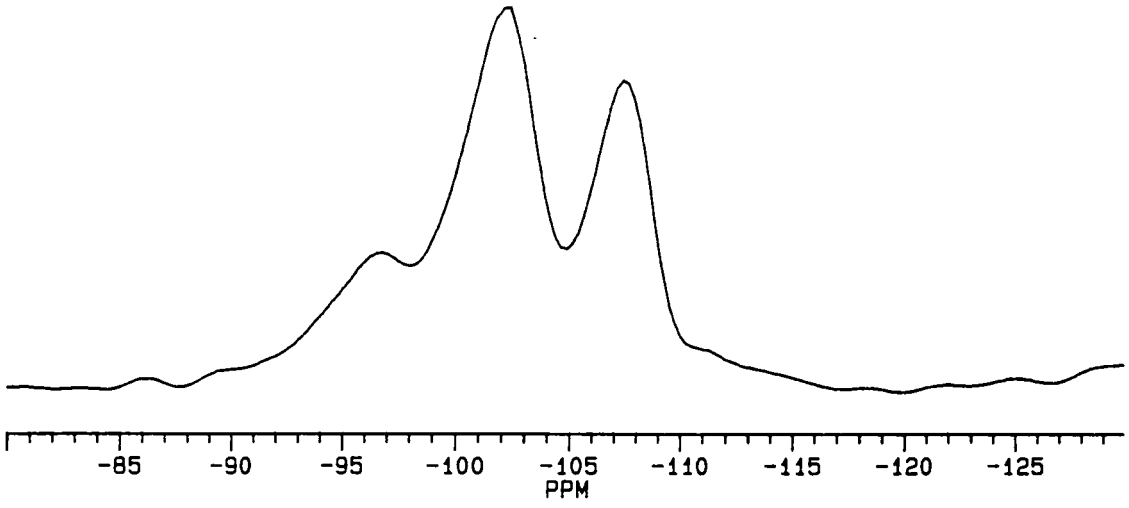

Figure 4.12: ^{27}Al SP MAS spectrum of hydrated HY–CS–S with decoupling
NT=6000 RO=4500Hz PA=3π/40 RD=200ms

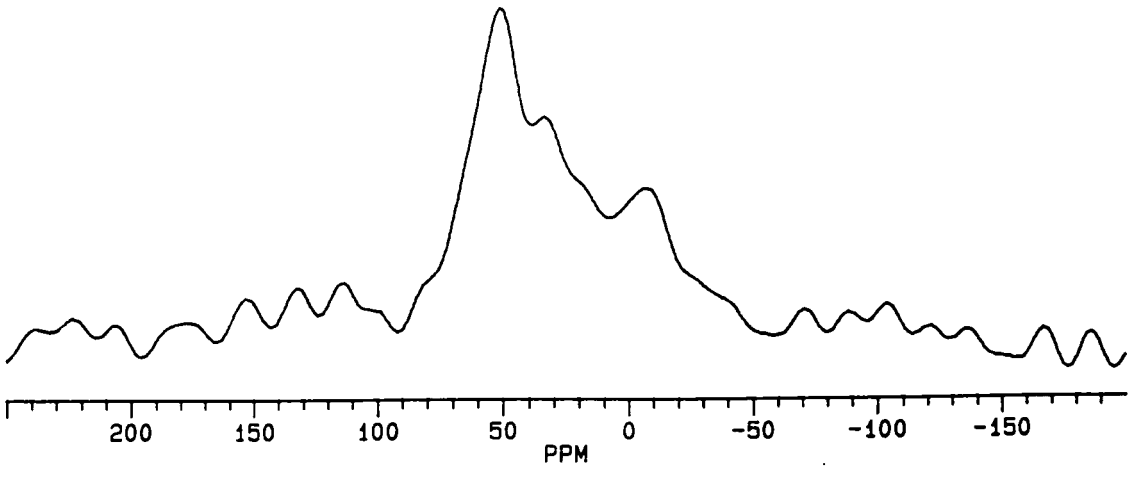

Figure 4.11: ^{29}Si MAS spectra of HY–CS–S
(a) SP with decoupling and Gaussian deconvolution RD=20s NT=2974 RO=3050Hz (b) CP/MAS RD=2s NT=90000 RO=1270Hz CT=10ms

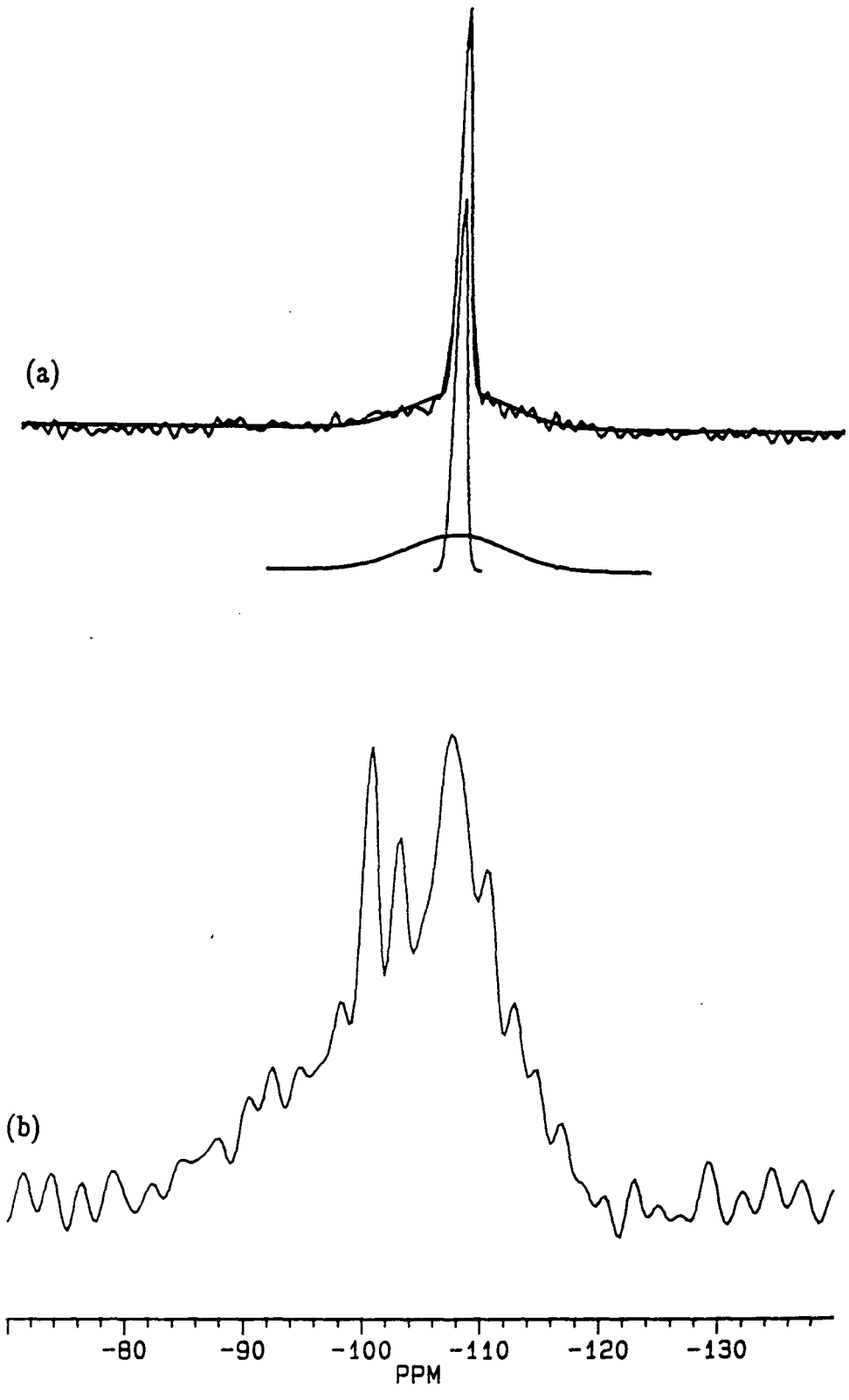

The CP/MAS spectrum (b) resembles that for HY–C550–S (Figure 4.7(a)) but shows even greater intensity for lower–Q^n sites, especially Q^3 (–100.1 ppm), and a marked dispersion of the Q^4 peak (–106.8 ppm). Amorphous (presumably non–lattice) material is also clearly visible in the single–pulse spectrum as shown by the deconvolution plot in Figure 4.11(a). Also, the sample crystallinity measured by XRD (quoted in Table 4.1) is much lower for HY–CS–S than for the HY–C*xxx*–S pair. It seems, then, that steaming results in greater damage to the lattice than for calcined samples, removing much more Si into a non–lattice environment (and perhaps leaving a significant concentration of lattice Q^3 SiOH groups). The greater damage may be due either to the absence of NLA (which might stabilize the lattice by delocalizing charges) or to the larger lattice Al content, which might result in collapse of regions of the crystal as steam attacks Al–O linkages. However, consideration of the surface area measurements given in Table 4.1 shows that the latter effect cannot be very significant, as such a large–scale collapse would result in a substantial decrease in intracrystalline surface area, whereas in fact the surface areas of HY–C650–S and HY–CS–S are found to be almost equal.

Figure 4.12 gives the ^{27}Al spectrum of HY–CS–S, which shows the presence of octahedral and tetrahedral NLA in a range of relatively unsymmetrical environments. In contrast to the spectra of the calcined samples, ^{1}H decoupling has a negligible effect, showing that the NLA is deficient in strongly coupled ^{1}H (*e.g.* AlOH groups), suggesting a high degree of condensation.

5. Conclusions

These results are clearly in broad agreement with the evidence cited from the literature in Section A concerning changes occurring in the lattice during

calcining, chemical dealumination and steaming. However, very little direct evidence has arisen for the widespread occurrence of lattice SiOH groups, except from the ^{1}H spectrum of HY–C550–S (Figure 4.6(a)). In particular, peaks are not observed in ^{29}Si single–pulse spectra in lower–Q^n positions in samples in which SiOH groups might be expected to occur. The ^{29}Si CP/MAS spectra of the calcined samples do seem to suggest the occurrence of some form of lower–Q^n sites, but, as discussed earlier, circumstantial evidence favours their assignment to non–lattice species in some samples. Certainly, if such peaks do arise from lattice $Si(OH)_x$, their abundance is very much less than four per lost lattice Al, and so we must conclude anyhow that widespread annealing ($2SiOH \longrightarrow SiOSi + H_2O$) or healing by Si migration takes place. The loss of 16.5 Al per unit cell from the lattice during calcination at 550^{o}C represents 2.9% of all lattice atoms, which is rather less than the value of 5% by which the crystallinity (measured by XRD and quoted in Table 4.1) decreases. For 650^{o}C calcination, 23 Al per unit cell, or 4.0% of lattice atoms, are lost; however, the crystallinity again declines by 5%. This provides support for the theory proposed earlier that the non–lattice material is more disordered in the sample calcined at the lower temperature.

The spectra quoted above enable details of the nature of non–lattice material to be deduced. There is much evidence to suggest that Si is dislodged from the lattice during thermal treatments, as well as Al. The Al has been shown to exist in both octahedrally and tetrahedrally coordinated environments, with some but not all nuclei strongly coupled to ^{1}H (*e.g.* in AlOH groups). The Si appears as a broad band in the $Q^2 - Q^4$ region and/or a narrower peak at –110 ppm or below (attributed to Al–free silica) in the ^{29}Si single–pulse spectrum, whilst better–resolved Q^n sites appear in the CP/MAS spectrum. Steamed samples show a particularly wide range of sites, including one around

–103 ppm which (as indicated in Section A) has been attributed by other workers to Si(1OH).

Samples containing non–lattice material show, in their ^{29}Si CP/MAS spectra, remarkably little signal from lattice ^{29}Si, in contrast to NLA–free samples such as NH_4Y[1] and NH_4Y–CS, where the SP and CP spectra are alike. It must be assumed, therefore, that whatever mechanisms of CP are active in NLA–free samples do not occur in NLA–containing samples. The NLA–free samples were NH_4^+–form zeolites, whereas those containing NLA had H^+ as the lattice cation; therefore it may be that NH_4^+ cations provide most of the CP to lattice silicon, which would require them to be relatively immobile and not exchanging freely with water. Alternatively, CP could occur from water itself coordinated to Brönsted sites; this might not occur in the NLA–containing samples either because of their lower lattice Al content (a weak argument, since the calcined samples still contain some) or because the water present forms a stronger complex by binding to the non–lattice material instead. The fact that, in other sets of samples, the CP appearance of uncalcined samples is found to be independent of the cation form of the zeolite would tend to disfavour the former explanation. Whatever ^{1}H–^{29}Si dipolar coupling does occur in these systems, however, cannot be very strong, since the application of dipolar dephasing procedures ('non–quaternary suppression') was found to have no effect on the CP/MAS spectrum.

The NLA itself has also been probed by a range of NMR experiments. It has been shown that a higher calcination temperature generates NLA which is less aggregated, has more OH groups and contains more Al nuclei in a tetrahedral environment. Deconvolution of ^{27}Al spectra has been shown to enable estimation of the amount of tetrahedral NLA present; no other technique is able to provide this information.

Finally, chemical dealumination has been shown to raise the lattice Si/Al ratio without generating any non–lattice material. Steaming of the chemically dealuminated sample resulted in loss of all remaining lattice Al and substantial destruction of the lattice, to a much greater degree than for calcined samples (as shown by the ^{29}Si single–pulse and XRD crystallinity measurements).

4C: MEASUREMENT OF Si/Al RATIOS

1. Literature

There is no single method available for measuring the Si/Al ratio of the zeolite lattice that is reliably applicable to all samples. A wide range of techniques has been used, each having advantages and shortcomings. The approach that is probably the most trusted is the measurement of the crystalline unit cell size (UCS). Since the Al^{3+} cation is larger than Si^{4+}, an aluminium–rich lattice has a larger UCS than a siliceous one. The UCS of a sample can be measured with great precision by XRD, even for only moderately crystalline samples. A linear correlation between UCS and lattice Al content per unit cell has been established for each type of zeolite lattice;[38,90] for Zeolite Y this is[45]

$$\text{Al/u.c.} = 10.71\ (a_0/\text{Å} - 24.238)$$

where a_0 is the UCS. For samples carefully prepared by chemical dealumination under conditions controlled to maintain maximum crystallinity, the confidence in the result is believed to be within ±1 Al/u.c.; however, steamed samples are also found to fit the correlation acceptably well.[45] The UCS method appears to be useful for a range of samples, then, but its accuracy may decline when the sample

contains a lot of lattice defects (whose lattice space occupancy is thought to be intermediate between Si and Al, as mentioned in Section A), amorphous material, coke, or any other adsorbate which may 'pillar' the structure, holding it open. Further, it is to be expected that the hydration level of the sample will affect the UCS by altering the extent of lattice charge delocalization.

Another widely–used technique is the measurement of relative Q^n site populations by ^{29}Si NMR, as described in Chapter 2. For most samples, the spectra have to be deconvoluted into individual Q^n bands; this procedure is somewhat subjective, especially when amorphous silicon–containing material is present (appearing as a broad underlying peak), or when the lattice Al distribution is not homogeneous, since the shape of the Q^n peaks is then distorted from Gaussian. Furthermore, it is believed by some workers that SiOH defects strongly resemble SiOAl linkages in the ^{29}Si NMR spectrum, resulting in incorrectly low Si/Al ratios being measured in defect–rich samples. The technique is best applied to samples whose Si/Al ratio is neither very high (>10) or very low (close to 1), since beyond these limits the intensities of peaks other than Q^4 or Q^0 respectively become very small and difficult to measure with confidence. Difficulties arise with zeolites which have inequivalent lattice T–sites (such as ZSM–5), for which deconvolution into Q^n peak groups becomes much more complex. Finally, ^{29}Si NMR also suffers from low sensitivity; the spectra used for deconvolution may have poor signal–to–noise ratios unless large amounts of spectrometer time are available. Despite these difficulties, Si/Al ratio measurement from ^{29}Si NMR peak areas is widely used and trusted and seems to give acceptable results.

Newsam[58] found a good correlation between the ^{29}Si NMR *chemical shifts* of Q^n peaks and the lattice Al content for a wide range of data published by other workers, and suggested that the correlation could be used to estimate

Si/Al ratios of samples with very high or very low Al contents. For example, the lattice Al content per unit cell can be found from the shift of the Q^4 peak (σ) by the relation Al/u.c. = 1700 + 15.63σ. This approach, however, appears to have severe limitations. It relies on small changes in measured quantities (close to the confidence limits of the measurement) to deduce large differences in lattice composition (*e.g.* a shift of –1 ppm in the Q^4 peak of Zeolite Y represents the loss of 16 lattice Al atoms). Small shifts can arise not only from changes in lattice composition but also from the presence of adsorbates, amorphous material, coke, water or cations other than the Na^+ and H^+ used in the correlation analysis, and also from referencing procedures or instability in the spectrometer. Furthermore, asymmetry in the band shape (arising from inhomogeneous Al, cation or water distribution or underlying broad peaks) may distort the position of maximum intensity. Prone as it is, then, to interference from a range of external influences, this technique is unlikely to be of great value.

^{27}Al NMR has also been used as a means of measuring the lattice Al content of a sample. In order to achieve this, the signal from lattice Al must be acquired under quantitative conditions:[59] the recycle time must be sufficiently long to avoid saturation of the magnetization; the dead time must be much shorter than T_2; the use of MAS should be avoided, to ensure that no intensity is lost to spinning sidebands; solid–state intensities should be multiplied by 35/9 for comparison with solution–state signals, to account for the usual excitation of only the central transition ($-\frac{1}{2} \leftrightarrow \frac{1}{2}$) in solids (see Chapter 2); and a small pulse angle must be used. Normally the tetrahedral peak area is measured, although it has been suggested[59] that using the initial gradient of a plot of peak intensity *vs.* pulse angle would advantageously eliminate the problem of signal loss during dead time. Another approach is to measure the peak intensity for the pulse angle at which it is maximized,[12] eliminating the problem of distorted intensities for

sites of different symmetry (see Chapter 2 for a discussion). With care, results reliable to within 5% can reportedly be obtained. The advantages of this technique include its accuracy and the ability to measure quite low levels of lattice Al.[21] However, there are many attendant difficulties. It is highly dependent on the use of appropriate operating conditions. Simple single–pulse ^{27}Al NMR is unable to distinguish between lattice and tetrahedral non–lattice aluminium. The sample must be hydrated to enable observation of ^{27}Al signals at all. Moreover, some workers[66] believe that not all Al present even in a fully hydrated zeolite is visible unless a complexing agent such as acac is present. Another complication is that the exact amount of zeolite sample used must be known to enable calculation of the content of Al per unit cell; this requires a knowledge of the amounts of water, cations and other adsorbates present and an approximate value of the lattice Si/Al ratio to enable estimation of the relative molar mass (RMM) of the sample.

An alternative approach to the measurement of the lattice Al concentration involves the application of infra–red spectroscopy.[9] A number of studies have demonstrated a correlation between the positions of some infra–red bands and the lattice Al content.[38,42] The band used may be a Brönsted O–H stretch or a lattice O–Al–O bending.[45] In the latter case, the band intensity can also be used.[9,72] This technique, however, is subject to distortion from cations or adsorbates, particularly water, which H–bond to the Brönsted site.

Several other physical techniques have been employed. Elemental analyses (chemical, atomic absorption or X–Ray Fluorescence) give a reliable *bulk* Si/Al ratio easily, but these techniques cannot distinguish between lattice and non–lattice material, and so are only appropriate for as–synthesized or chemically dealuminated samples (which are free from non–lattice components). Other approaches used include TPD of NH_3 (to measure Brönsted

concentration), assay of NH_4^+ in ammonium–exchanged samples by Kjeldahl's method,[26] and measurement of sample catalytic activity (which varies with Si/Al ratio in a known manner).

It is clear, then, that no single method can be applied reliably in every case; to obtain a Si/Al ratio for a given sample, several different techniques must be used and the results interpreted with consideration of the nature of the sample. In the following paragraphs results are presented and discussed of several measurements of Si/Al ratios for the samples under study in this Chapter.

2. Comparison of Si/Al Ratios Measured for Samples Studied

The Si/Al ratios of the samples studied were measured by five techniques as follows:

(i) Unit Cell Size (UCS) measurement;

(ii) X–Ray Fluorescence (XRF);

(iii) ^{29}Si NMR intensities by deconvolution;

(iv) ^{29}Si NMR Q^4 signal positions. The Si/Al ratio was calculated both from the Q^4 maximum in the ^{29}Si spectrum and from the position of the centre of the deconvoluted Gaussian line assigned to Q^4 sites;

(v) ^{27}Al NMR intensities, by deconvolution where necessary. The spectra were obtained using MAS and a $3\pi/40$ pulse angle. The sample water contents were measured by ^{1}H NMR as described in Chapter 2. The ^{27}Al intensity standard was a good–quality sample of $NaAl(SO_4)_2.12H_2O$.

The results obtained are collected in Table 4.4. The UCS and ^{29}Si intensity values are in good agreement except for the two HY–C*xxx* samples. Influences possibly resulting in a distortion of the ^{29}Si NMR estimate may be analyzed as follows. The presence of SiOH defects would tend to yield a measured ratio *below*

that given by UCS. The only phenomena which could give rise to an *elevation* of the measured ^{29}Si NMR value are (i) a substantial increase in T_1 of all Q^n sites other than Q^4 or (ii) large–scale loss of Si from the lattice. The former is hard to justify and has never been explicitly reported; the latter is disproved by the retention of crystallinity (as measured by XRD, Table 4.1) and the lack of signals from large amounts of amorphous material appearing in the ^{29}Si NMR spectrum. Therefore, it seems likely that it is the UCS value that is in error, not the ^{29}Si NMR value. This may result from the 'propping–open' or 'pillaring' of the structure by the non–lattice material present.

The values obtained from Q^4 signal positions in the ^{29}Si spectrum are disappointing. The fitted and spectral–peak values do not agree well, presumably due to the mis–shaping of the peaks and distortions due to amorphous material underlying the signals. Although the values for the three samples NH_4Y[1], HY–C550 and HY–C650 show the correct trend, the values obtained are not in very good agreement with those from other techniques. In

Table 4.4: Si/Al Ratio Estimates from Different Techniques

(a) UCS; (b) ^{29}Si Q^n signal areas; (c) ^{29}Si Q^4 chemical shifts obtained directly from spectra; (d) ^{29}Si Q^4 chemical shifts obtained by deconvolution; (e) ^{27}Al tetrahedral band signal areas; (f) X–Ray Fluorescence (±0.2).

Sample	(a)	(b)	(c)	(d)	(e)	(f)
NH_4Y[1]	4.1±0.1	4.0±0.2	7.7±0.6	6.4±0.5	90	2.5
HY–C550	7.9±0.4	10.0±0.9	10.3±1.0	12.3±1.3	200	2.5
HY–C650	12±1	32±2	11.4±1.2	16.3±2.2	200	2.9
HY–C550–S	∞	∞	11.2±1.2	11.2±1.2	–	–
HY–C650–S	95±48	∞	12.2±1.3	9.3±0.8	–	–
NH_4Y–CS	6.1±0.3	5.9±0.2	10.2±1.0	7.0±0.5	10	4.6
HY–CS–S	∞	∞	10.2±1.0	8.6±0.7	–	–

addition, the values for the highly siliceous samples are clearly much too low. It is clear, then, that while the peak positions may be used to provide a general indication of the Al content of the lattice, the influences described earlier distort the observed chemical shifts sufficiently to prevent calculation of quantitatively reliable Si/Al ratios.

Similarly, the values measured by ^{27}Al NMR are very poor. The NMR clearly failed to detect a large fraction (even as much as 95%) of the lattice Al present, despite the adoption of precautions such as the use of a small pulse angle and fully hydrated samples and explicit inclusion of any spinning sidebands in the intensity analysis (MAS was generally used to resolve peaks from tetrahedrally and octahedrally coordinated atoms). The measurements were compared also to a second intensity standard, a sample of highly crystalline Zeolite NaY, with similarly poor results. Extreme care is therefore necessary and extensive checks must be made to ensure that quantitative ^{27}Al NMR intensities are being measured.

Finally, the XRF measurements show that the technique cannot distinguish between the lattice and non–lattice Al in the calcined samples. It also underestimates the Si/Al ratio in NH_4Y–CS, for reasons which are not understood at present.

^{29}Si NMR Linewidths. As discussed earlier, aluminium–rich zeolites tend to exhibit broader ^{29}Si NMR lines than silicon–rich ones, since there is a greater dispersion of NNN environments in the former case. Thus, a sample of Zeolite Y containing no lattice Al is expected and observed to give a single narrow line (see Figure 4.4 for examples). The same is true for samples with a very high Al content (close to the 50% limit) in which Q^0 sites with nine NNN Si atoms will predominate. Intermediate cases might be expected to show a smooth increase in

linewidth as the Al content drops, passing through a maximum and declining to the Si–only value. As discussed in Chapter 2, dispersive effects dominate the ^{29}Si linewidth, and so for samples not too close to the extremes of the composition range, it may be possible to detect sufficiently consistent behaviour to enable use of the linewidth for one of the Q^n signals as an estimate of lattice Al content.

Table 4.5 shows the half widths at half height (HWHH) of the Q^4 and Q^3 signals obtained by deconvolution of the ^{29}Si single–pulse spectra. Where deconvolutions were repeated with different numbers of Gaussian lines, the figures used were those obtained from the fit to the greatest number of lines, in the expectation that such a fit would give the best representation of the signals. Where two superimposed peaks were fitted to a single Q^n band, the width of the narrowest component is quoted, based on the assumption that broader components largely represent amorphous or defective material.

Table 4.5: ^{29}Si NMR Linewidths (HWHH)

Sample	(Linewidth±1)/Hz		Si/u.c.	
	Q^4	Q^3	(UCS)	(NMR)
NH_4Y	69	96	154±1	153.6±1.5
HY–C550	53	88	170±1	174.6±1.3
HY–C650	46	65	177±1	186.1±0.5
HY–C550–S	18	–	192±1	192.0±0.5
HY–C650–S	16	–	190±1	192.0±0.5
NH_4Y–CS	60	73	165±1	164.2±0.8
HY–CS–S	26	–	192±1	192.0±0.5

Figure 4.13: Plots of deconvoluted Q^4 ^{29}Si linewidths *vs.* lattice Si content for all samples. Data far from best–fit straight lines were not included in the linear least–squares analysis.
(a) Unit Cell Size–derived lattice Si content (x)
(b) ^{29}Si Q^n intensity derived Si content (+)

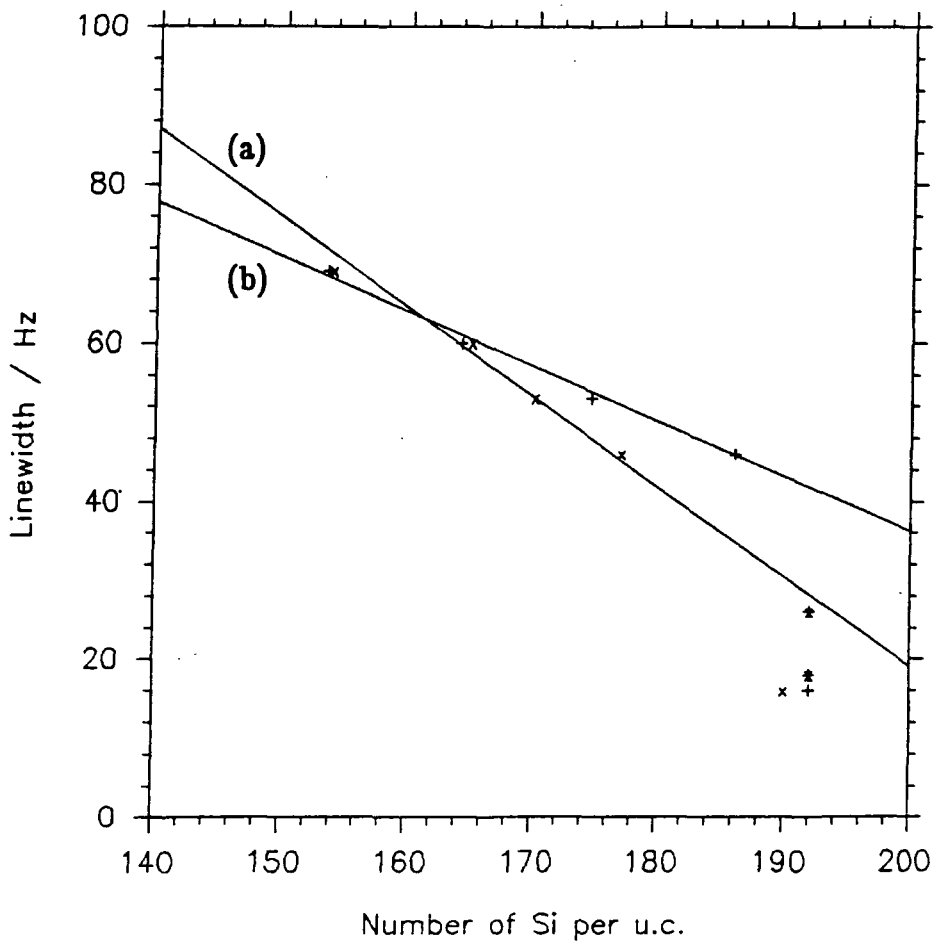

The correlation between lattice Si content and Q^3 linewidth is poor, showing no more than a general trend to lower widths as the lattice becomes silicon–rich. The Q^4 widths, however, show this trend clearly and appear to lie on a well–defined curve. Figure 4.13 shows the correlation between linewidths and lattice Si contents as estimated from UCS measurement (a) and ^{29}Si NMR intensities (b). Apart from those corresponding to the highly siliceous samples, all the points lie acceptably close to a straight line. For the UCS measurement, the correlation is

$$\text{HWHH} = (245.7 \pm 12.6) - (1.133 \pm 0.073)\ \text{Si/u.c.}$$

with a correlation coefficient of –0.994; the NMR intensity measurement gives

$$\text{HWHH} = (175.0 \pm 5.5) - (0.694 \pm 0.033)\ \text{Si/u.c.}$$

with a coefficient of –0.997.

These results suggest, then, that within the composition range 155–185 Si/u.c., the correlation between ^{29}Si NMR deconvoluted linewidth of the Q^4 site and the lattice composition is sufficiently good to permit its use as a supplementary technique for measuring Si/Al ratios of calcined and chemically dealuminated samples. Clearly many more samples need to be considered to verify the relationships deduced above, as the amount of data used here is very small.

3. Conclusions

The two most reliable techniques for measuring lattice Si/Al ratios of calcined and chemically dealuminated samples appear to be ^{29}Si NMR signal areas and unit cell size measurement. These methods gave very similar results for samples with a low amorphous content, but the presence of non–lattice material appears to distort the UCS value, due perhaps to pillaring of the lattice. No evidence was found for disturbance of the ^{29}Si value by SiOH groups.

^{27}Al NMR failed to detect all the ^{27}Al present and so could not be used as a quantitative technique. ^{29}Si NMR peak positions were found to correlate poorly with lattice compositions; however, a better relation was established between composition and linewidth of the deconvoluted Q^4 peak in the ^{29}Si NMR spectrum, which, after consideration of a number of other samples, may prove valuable as a novel addition to the range of techniques available.

REFERENCES

1. L M Parker, D M Bibby, G R Burns, *Zeolites* **11**, 293 (1991).
2. For a review, see G T Kokotailo, C A Fyfe, Y Feng, H Grondy, *Prepr. – Am. Chem. Soc., Div. Petroleum Chem.* **35**, 669 (1990).
3. L Kubelkova, S Beran, A Malecka, VM Mastikhin, *Zeolites* **9**, 12 (1989).
4. J Dwyer, K Karim, W J Smith, N E Thompson, R K Harris, D C Apperley, submitted.
5. Q L Wang, M Torrealba, G Giannetto, M Guisnet, G Perot, M Cahoreau, J Caisso, *Zeolites* **10**, 703 (1990).
6. G Garralón, A Corma, V Fornés, *Zeolites* **9**, 84 (1989).
7. A Martin, U Wolf, S Nowak, B Lucke, *Zeolites* **11**, 85 (1991).
8. See, for example, K Hashimoto, T Masuda, T Mori, *Chem. Eng. Sci.* **43**, 2275 (1988).
9. T Chevreau, A Chambellan, J C Lavalley, E Catherine, M Marzin, A Janin, J F Hemidy, S Khabtra, *Zeolites* **10**, 226 (1990).
10. A K Ghosh, R A Kydd, *Zeolites* **10**, 766 (1990).
11. H Pfeifer, D Freude, M Hunger, *Zeolites* **5**, 274 (1985).
12. E G Derouane, L Baltusis, R M Dessau, K D Schmitt, in *Catalysis by Acids and Bases* (*Stud. Surf. Sci. Catal.* **20**; B Imelik *et al.*, eds.; 1985), 135.
13. S Namba, K Yamagishi, T Yashima, *Chem. Lett.* 1987, 1109.
14. P E Eberly jr, C N Kimberlin jr, in *Chemical Reaction Engineering* (*Adv. Chem. Ser.* **109**; 1972), 506.
15. D Freude, M Hunger, H Pfeifer, W Schwieger, *Chem. Phys. Lett.* **128**, 62 (1986).
16. U Lohse, E Löffler, M Hunger, J Stöckner, V Patzelová, *Zeolites* **7**, 108 (1987).
17. A Janin, J C Lavalley, A Macedo, F Raatz, *ACS Symp. Ser.* **368**, 117 (1988).
18. S Beran, *J. Mol. Catal.* 10, 177 (1981).
19. R J Mikovsky, J F Marshall, *J. Catal.* **44**, 170 (1976).
20. B Chauvin, P Massiani, R Dutartre, F Figueras, F Fajula, T Des Courieres, *Zeolites* **10**, 174 (1990).
21. B L Meyers, T H Fleisch, G J Ray, J T Miller, J B Hall, *J. Catal.* **110**, 82 (1988).
22. G Engelhardt, U Lohse, V Patzelová, M Mägi, E Lippmaa, *Zeolites* **3**, 233 (1983).
23. Z Guo, K Wang, D Zhou, D Ding, J Wang, H Li, *Huaxue Wuli Xuebao* **3**, 100 (1990).

24. K Yamagishi, S Namba, T Yashima, *J. Catal.* **121**, 47 (1990).
25. G J Ray, B L Meyers, C L Marshall, *Zeolites* **7**, 307 (1987).
26. D Freude, E Brunner, H Pfeifer, D Prager, H–G Jerschkewitz, U Lohse, G Oehlmann, *Chem. Phys. Lett.* **139**, 325 (1987).
27. Y Sendoda, Y Ono, *Zeolites* **8**, 101 (1988).
28. A Macedo, A Auroux, F Raatz, E Jacquinot, R Boulet, *ACS Symp. Ser.* **368**, 98 (1988).
29. V Patzelová, E Drahordova, Z Tvaruzkova, U Lohse, *Zeolites* **9**, 74 (1989).
30. E Loeffler, U Lohse, C Peuker, G Oehlmann, L M Kustov, V L Zholobenko, V B Kazanskii, *Zeolites* 10, 266 (1990).
31. V B Mastikhin, I L Madrakovsky, S V Filimonova, *Zeolites* **10**, 593 (1990).
32. R D Shannon, K H Gardner, R H Staley, G Bergeret, P Gallezot, A Auroux, *J. Phys. Chem.* **89**, 4778 (1985).
33. H Hamdan, J Klinowski, *ACS Symp. Ser.* **398** (*Zeolite Synth.*), 465 (1989).
34. E Brunner, H Ernst, D Freude, M Hunger, C B Krause, D Prager, H Reschetilowski, W Schwieger, K H Bergk, *Zeolites* **9**, 282 (1989).
35. J W Akitt, W Gessner, M Weinberger, *Magn. Reson. Chem.* **26**, 1047 (1988).
36. V Bosácek, D Freude, *Stud. Surf. Sci. Catal.* **37**, 231 (1988).
37. V Bosácek, V M Mastikhin, *J. Phys. Chem.* **91**, 260 (1987).
38. Kubelkova et al. *J. Chem. Soc., Faraday Trans. 1* **84**, 1447 (1988).
39. R B Borade, A Adnot, S Kaliaguine, *J. Chem. Soc., Faraday Trans.* **86**, 3949 (1990).
40. E Brunner, H Ernst, D Freude, M Hunger, H Pfeifer, *Stud, Surf. Sci.* Catal. **37**, 155 (1988).
41. J R Sohn, S S Lee, *Bull. Korean Chem. Soc.* **10**, 390 (1989).
42. V Mavrodina, V Penchev, U Lohse, T Gross, *Zeolites* **9**, 203 (1989).
43. A Corma, M Faraldos, A Martinez, A Mifsud, *J. Catal.* **122**, 230 (1990).
44. W C Cheng, A W Peters, K Rajagopalan, *Prepr. – Am. Chem. Soc., Div. Petroleum Chem.* **34**, 719 (1989).
45. J R Sohn, S J DeCanio, J H Lunsford, D J O'Donnell, *Zeolites* **6**, 225 (1986).
46. J–P Gilson, G C Edwards, A W Peters, K Rajagopalan, R F Wormsbecher, T G Roberie, M P Shatlock, *J. Chem. Soc., Chem. Commun.* 1987, 91.
47. P P Man, J Klinowski, *J. Chem. Soc., Chem. Commun.* 1988, 1291.
48. G J Ray, private communication.
49. A Samoson, E Lippmaa, G Engelhardt, U Lohse, H–G Jerschkewitz, Chem. *Phys. Lett.* **134**, 589 (1987).
50. R H Meinhold, D M Bibby, *Zeolites* 10, 146 (1990).
51. R H Meinhold, D M Bibby, *Zeolites* 10, 74 (1990).
52. M Hunger, J Kärger, H Pfeifer, J Caro, B Zibrowius, M Bülow, R Mostowicz, *J. Chem. Soc., Faraday Trans. 1* **83**, 3459 (1987).
53. K Yamagishi, S Namba, T Yashima, *J. Phys. Chem.* **95**, 872 (1991).
54. B Kraushaar, J W de Haan, J H C van Hooff, *J. Catal.* **109**, 470 (1988).
55. B Kraushaar, L J M van de Ven, J W de Haan, J H C van Hooff, *Stud. Surf. Sci. Catal.* **37**, 167 (1988).
56. V Bosácek, V Patzelová, Z Tvaruzková, D Freude, U Lohse, W Schirmer, H Stach, H Tharum, *J. Catal.* 61, 435 (1980).
57. R M Dessau, K D Schmitt, G T Kerr, G L Woolery, L B Alemany, *J. Catal.* **109**, 472 (1988).
58. J M Newsam, *J. Phys. Chem.* **89**, 2002 (1985).
59. C Fernandez, F Lefebvre, J B Nagy, E G Derouane, *Stud. Surf. Sci. Catal.* **37**, 233 (1988).
60. G J Ray, A G Nerheim, J A Donohue, *Zeolites* **8**, 458 (1988).
61. P J Grobet, P A Jacobs, H K Beyer, *Zeolites* **6**, 47 (1986).

62. G L Woolery, L B Alemany, R M Dessau, A W Chester, *Zeolites* **6**, 14 (1986).
63. G Engelhardt, U Lohse, A Samoson, M Mägi, M Tarmak, E Lippmaa, *Zeolites* **2**, 59 (1982).
64. J Sauer, A Bleiber, *Catal. Today* **3**, 485 (1988).
65. M Hunger, D Freude, H Pfeifer, *Catal. Today* **3**, 507 (1988).
66. P J Grobet, H Geerts, J A Martens, P A Jacobs, *J. Chem. Soc., Chem. Commun.* 1987, 1688.
67. J Perez–Parient, J Sanz, V Fornés, A Corma, *J. Catal.* **124**, 217 (1990).
68. C E Bronnimann, R C Zeigler, G E Maciel, *J. Am. Chem. Soc.* **110**, 2023 (1988).
69. P Fejes, I Hannus, I Kiricsi, H Pfeifer, D Freuse, W Oehme, *Zeolites* **5**, 45 (1985).
70. N–Y Topsoe, K Pedersen, E G Derouane, *J. Catal.* **70**, 41 (1981).
71. M W Anderson, J Klinowski, *Zeolites* **6**, 455 (1986).
72. F Goovaerts, E F Vansant, P De Hulsters, J Gelan, *J. Chem. Soc., Faraday Trans. 1* **85**, 3687 (1989).
73. Z Gao, Y Tang, Y Zhu, *Appl. Catal.* **56**, 83 (1990).
74. S Bao, Q Yu, Q Xu, *Huaxue Xuebao* **48**, 42 (1990).
75. J Caro, M Bulow, M Derewinski, J Haber, M Hunger, J Kärger, H Pfeifer, W Storek, B Zibrowius, *J. Catal.* **124**, 367 (1990).
76. B Kraushaar, J W de Haan, L J M van de Ven, J H C van Hooff, *Chem. Lett.* 1986, 1523.
77. R M Dessau, K D Schmitt, G T Kerr, G L Woolery, L B Alemany, *J. Catal.* **104**, 484 (1987).
78. P E Eberly jr, *J. Phys. Chem.* **71**, 1717 (1967).
79. J H Lunsford, *Prepr. – Am. Chem. Soc., Div. Petroleum Chem.* **35**, 654 (1990).
80. H Kawakami, S Yoshida, T Yonezawa, *J. Chem. Soc., Faraday Trans. 2* **80**, 215 (1984).
81. D G Blackmond, J G Goodwin, J E Lester, *J. Catal.* **78**, 34 (1982).
82. J Dwyer, *Stud. Surf. Sci. Catal.* **37**, 333 (1988).
83. S Kowalak, J B Moffat, *Appl. Catal.* **36**, 139 (1988).
84. E Dima, L V C Rees, *Zeolites* **10**, 8 (1990).
85. P O Fritz, J H Lunsford, *J. Catal.* **118**, 85 (1989).
86. C Mirodatos, D Barthomeuf, *J. Chem. Soc., Chem. Commun.* 1981, 39.
87. E A Lombardo, G A Sill, W K Hall, *J. Catal.* **119**, 426 (1989).
88. M Guisnet, Q L Wang, G Giannetto, *Catal. Lett.* **4**, 299 (1990).
89. B H W S de Jong, C M Schramm, V E Parziale, *Geochim. et Cosmochim. Acta* **48**, 2619 (1984).
90. G T Kerr, *Zeolites* **9**, 350 (1989).

CHAPTER 5: NMR STUDIES OF WATER AND ACID SITES IN ZEOLITE Y

5A: BACKGROUND

The acid character of zeolites is at the heart of their effectiveness as catalysts. They are remarkable in their capacity for variation of acid nature, strength and concentration whilst retaining the original lattice structure, as discussed in Chapter 4. Proton NMR is a technique particularly suited to the study of zeolite acidity,[6] since it readily distinguishes the different types of hydroxyl group present, ranging from non–acidic SiOH defect sites to Brönsted sites and hydroxyls associated with non–lattice alumina. However, these sites are generally not visible in the ^{1}H NMR spectrum unless a substantial fraction of the intracrystalline water that is normally present has been removed. The intense affinity for water exhibited by most zeolite samples would tend to indicate a strong interaction between water and the lattice, and so it is perhaps to be expected that removal of water should result in side–effects such as the transfer of a fraction of lattice Al into a non–lattice environment. The study considered in this Chapter describes findings that appear to demonstrate the occurrence of changes such as this during drying which are critically dependent on the details of the drying procedure employed. There is also a brief consideration of the character of zeolitic water itself. Studies of the behaviour of the zeolite lattice during thermal dehydration are by no means peripheral to an understanding of their catalytic performance, since typical zeolite–catalyzed processes are carried out at elevated temperatures under anhydrous conditions.

The remainder of this Section is devoted to a consideration of results concerned with zeolite acidity previously published by other workers. Section B describes the samples used in the present study. Zeolite water and the effect of

dehydration and complete rehydration are considered in Section C, whilst Section D covers the appearance, assignment and interpretation of the ^{1}H NMR spectra of dried zeolites. Finally there is a gathering–together of the principal conclusions from the work presented.

1. ^{1}H NMR Studies

In addition to its capacity to resolve signals arising from different types of OH group in a zeolite sample, ^{1}H NMR is able to provide information concerning the location, mobility and dynamic behaviour of water and other hydrogen–containing species. However, it has not been very extensively exploited, probably on account of the practical difficulties of preparing a sample at a specified hydration level and keeping it in this condition during a measurement which may require magic–angle spinning. In addition, resolution and reproducibility are often not very good. A brief discussion of previously–published work in these areas follows.

The appearance of the ^{1}H NMR spectrum of a zeolite differs dramatically between a wet sample and a dry one, as demonstrated in Chapter 2. In particular, the linewidths of the signals are usually far greater in wet samples, with little narrowing being achieved by MAS even at speeds greater than the linewidth, suggesting that the broadness arises from rapid exchange between water molecules (*i.e.* lifetime broadening) or possibly from chemical shift dispersion.[1] However, in dried samples, the mobility of the zeolitic H atoms is greatly diminished, and dipolar coupling between ^{1}H and ^{1}H [2,4] (reduced by deuteration) or ^{1}H and lattice ^{27}Al [3] (narrowed by MAS and broken up into spinning sidebands) may become a significant line–broadening influence (although the ^{1}H nuclei are often too dilute for this effect to be of significance). Chemical exchange *between species* in zeolites must be slow on the NMR time

scale, since even H_2O and NH_4^+ appear as separate peaks in wet NH_4^+–zeolite samples.[4]

The presence or absence of spinning sidebands is a useful indication of the mobility and/or environmental anisotropy of a ^1H–containing species.[4] Addition of water tends to increase mobility (presumably by solvation and H–bonding) and so leads to diminished sideband intensity.[5] T_2 values can also indicate ^1H mobility: rigid species have stronger dipolar couplings, which give rise to quicker cross–relaxation and hence shorter T_2's.

^1H NMR Peak Assignments.[11] In general, several peaks appear in the ^1H NMR spectra of dried zeolites. The earliest studies were barely able to distinguish just two species at ≃2 ppm (assigned to SiOH and AlOH) and ≃7 ppm (Brönsted sites).[7,9] (Another worker assigned a peak at 7 ppm to water H–bonded to lattice SiOH groups.[4]) Later, as both NMR and sample–handling techniques improved, the SiOH and non–lattice AlOH species were assigned separate peaks at around 1.5 – 2 ppm and 3 ppm respectively,[8] and two distinct Brönsted peaks were identified (only in Zeolite Y) at 4.0 and 5.2 ppm.[10,18] The Brönsted signal generally only appears in H–type zeolites and can be destroyed by back–exchange with Na^+ [17] or by addition of a small basic adsorbate such as NH_3.[23] Its intensity is also found to be linearly related to the lattice Al content, further confirming the peak assignment.[17,28] The peak is absent in silicalite, which is isostructural with HZSM–5 but has no lattice Al and hence no Brönsted sites.[28] The SiOH peak assignment is based on its non–acidic behaviour (*e.g.* it does not disappear on treatment with pyridine–d_5 or another base) and on its similarity to SiOH peaks in silica gel. The remaining peak is assigned to AlOH by elimination and also on the grounds that it appears only when NLA is present.

2. **Nature of Brönsted and Other Sites.** The zeolitic lattice Brönsted site, which may loosely be designated as $SiO\diagdown^{H}_{Al}$, is widely recognized as the principal seat of catalytic activity.[22] It is capable of protonating many hydrocarbons to generate carbocations which undergo rearrangement, cyclization, hydrogen–transfer, oligomerization, aromatization and disproportionation reactions. The structure of the Brönsted site has been extensively investigated by spectroscopic and physical techniques (such as adsorption and desorption of bases) and modelled by quantum–mechanical studies of lattice fragments. It is known that the site's strong acidity arises from the interaction of the Si and the Al; both must be present, as SiOH and AlOH groups alone are found to be effectively non–acidic.[20] The Zeolite Y system has now been fully characterized in terms of bond lengths and angles,[21,24] with the H–Al distance measured as 2.48 Å.[22]

As already mentioned, the Brönsted H atoms in Zeolite HY are believed to give resonances at 4.0 and 5.2 ppm in the ^{1}H NMR spectrum. There is much evidence to suggest that the two signals arise from distinct types of Brönsted site; for example, they are found to bind Me_3P with different affinities,[12] and pyridine–d_5 adsorbs more rapidly to one of them.[10,14] This suggests that the sites have different accessibilities; the usual interpretation of this is that the 4.0 ppm signal arises from Brönsted sites in large cages (α– or *supercages*) and the 5.2 ppm signal from those in small (β– or *sodalite*) cages.[10,15,16] Two bands are also observed in the infra–red spectrum, at 3640 and 3550 cm^{-1}, [15,18] which correspond respectively to large and small cage sites.[26] The fact that separate peaks are visible for large and small cage sites demonstrates that the acidic ^{1}H nuclei undergo remarkably little exchange between cages under the conditions of measurement (the ^{1}H NMR peaks can only be observed in dried samples). ^{1}H NMR relaxation time studies support this view,[11,27] although one study showed that all sites were able to adsorb Me_3P despite the fact that it is too large to

enter the small cages,[12] indicating that the small cage ^{1}H atoms could migrate to the base under the conditions of measurement. Support is also found in a quantum–mechanical study which suggested that the barrier to ^{1}H jumps between sites was as large as 52 ± 10 kJ mol^{-1}.[42] As soon as a small amount of water is adsorbed, however, exchange becomes so rapid that the signals from Brönsted H atoms may no longer be visible at all.[29]

Whether the small cage sites are indeed more strongly acidic than those in large cages, as implied by their relative ^{1}H chemical shifts, is unclear. The small cage sites are found to bind pyridine[26] and water more strongly, requiring a higher temperature for desorption, but this may be due to the kinetic effect of slow escape from the small cages (as discussed below).

3. Intracrystalline Water

Most zeolites have an intense affinity for water; indeed, they have found widespread use as drying agents. The hydrophilicity of a given sample is closely linked with its Al content:[34] Al–free materials such as silicalite are hydrophobic, whereas aluminium–rich samples may reach equilibrium hydration at 25% or more water by weight in a humid atmosphere. Much attention has been focused on the behaviour and structure of intracrystalline water, since it reveals details of the structure of the lattice and the location and activity of polar sites and charge–balancing cations.

Proton NMR is a particularly useful technique for studying the dynamics and location of water molecules. A fully hydrated, highly crystalline Y zeolite generally exhibits a single broad peak at 4.7 ppm.[29] Infra–red stretching and bending (1636 cm^{-1}) bands also appear.[38] Under different conditions, however, a two–phase characteristic becomes apparent. Samples that have undergone thermal treatment frequently show two superimposed T_1 and T_2 values for water

^{1}H nuclei.[30] A few workers[31] attribute the shorter component to lattice Brönsted sites, but others have shown that the component is too intense, independent of lattice Al content and dependent on sample water content, refuting this assignment.[30] Another suggestion is that the components arise from sorption of water on Lewis and Brönsted acid sites.[37] Yet another is that the short and long components arise from bound and free water respectively. The commonly accepted view, however, is that the two components arise from water in small and large cages, with the T_2 of small–cage water being around $20 - 50$ μs and that of the large–cage water $1 - 40$ ms.[32] These assignments are confirmed by observing that the T_2 of water in silicalite (which has small cages only) is short, around 25 μs, and that of Zeolite ZK–5 (which has large cages only) is much longer.[33]

The visibility of two distinct relaxation components implies slow spin–diffusion between them, indicating that water does not pass rapidly between the cages, which are linked by windows circumscribed by four T–sites and their bridging oxygen atoms. Detailed studies have shown that the small cages fill rapidly from the dry state,[32,33] but empty slowly during dehydration,[35] requiring a higher temperature to desorb their water.[36] One interesting study[3] showed that the ^{29}Si single–pulse signals in a sample shifted on partial drying, due to the exposure of lattice charges introducing strain; by contrast, the CP signals did not shift, indicating that they arose from a region of the lattice that was still hydrated (probably corresponding to the small lattice cages).[3] It has been proposed that the affinity of cations for solvation by water contributes to the effect of different hydration character of the two cages;[36] however, it is not easy to appreciate why a small–cage cation should bind water more strongly than a large–cage one. Some of the cations are believed to be located in the four–ring windows mentioned above, and these may hinder the transport of water by

coordinating to it; again, the reason why the hindrance to leaving the small cage should be much greater than for entering is not clear. A possible explanation is that there is a strong interaction between water and Brönsted sites and the small–cage sites are more strongly acidic than the large–cage sites, as suggested by their relative ^{1}H NMR and IR band positions.

Intermolecular ^{1}H exchange between water molecules within each of the two cage systems is thought to occur rapidly on the NMR time scale under most conditions, as shown by deuteration studies.[32] (One study, however, found that exchange was slow in LiX zeolite.[39]) The predominant mechanism of relaxation here is by chemical exchange;[29] homonuclear dipolar couplings are generally not thought to be important, on account of the isotropic tumbling of water,[29] although water strongly bound to a cation may be sufficiently immobile to experience effective ^{1}H–^{1}H coupling.[32,33]

Large–cage water is considered to be intermediate in character between pure water in the neat liquid and tightly–bound water (*e.g.* in a salt crystal).[40] Some studies have suggested H–bonded chains of water molecules running through the zeolite channels. Opinions differ on the strength and lability of cation–water complexes; systems such as $Na(H_2O)_6^{+}$ [4] [and possibly $H(H_2O)_6^{+}$ by analogy][41] undoubtedly exist transiently, but no change in water chemical shift is observed on changing the cation, unlike the case in aqueous solutions of cations, suggesting that any association is weak.[40] (Results presented later imply, however, that the cation does indeed have a significant effect on the chemical shift of water.) The activation energy for a water molecule to jump from one Na^+ to another in NaX has been measured as 20 kJ mol^{-1}, which is significant in magnitude.[39] The average strength of association of water with lattice Al seems to rise on dehydration, as indicated by a fall in T_1,[40] but the water cannot be too close to Al or too rigidly held, since the spinning sideband

manifold observed is small.[5] Some workers have reported a rise in intensity of cross–polarization between water ^{1}H and lattice ^{29}Si during dehydration as the water becomes less mobile.[3] A peak at 9.2 ppm in the ^{1}H NMR spectrum has been assigned to $Al(H_2O)_6^{3+}$ complexes.[5]

A peak has often been reported at 6.5 ppm in the ^{1}H NMR spectrum of samples containing a small amount of water.[43] This is generally attributed to water adsorbed on Lewis sites, which have been shown to have greater affinity for hydration than other sites by means of quantum–mechanical calculations.[5] The peak usually grows with progressive addition of water and reaches a maximum intensity at 2–10 H_2O per unit cell.[29,43] The peak has been reported to have a long T_1, which suggests a rigid environment.[5]

Silanol groups at defect sites do not appear to exchange H atoms with water, nor to be strongly solvated. Maciel[19] showed there to be weak spin–mixing between SiOH and H_2O in silica gels, presumably mediated *via* transient dipolar couplings. This was manifest by the measurement of only one T_1 value for the system. In zeolites, however, where the SiOH groups are probably more scarce, such couplings are not generally found to be significant.

4. Sample Dehydration and Its Effect

Most of the fine structure in the ^{1}H NMR and IR spectra of zeolites is unobservable unless the sample is almost free of water. Samples which have been kept under atmospheric conditions for longer than a few minutes usually require dehydration to enable study of the lattice sites described above.[28] The usual method employed is heating under vacuum for several hours, then sealing the sample (in a cylindrical ampoule for MAS if required[5]). At least 300^{o}C must normally be attained to achieve sufficient eviction of water.[5,38]

It has often been assumed that the lattice undergoes very little structural

change during this process. This is perhaps a surprising presumption in view of the known solvating effect (described above) of water to distribute the charges on the lattice and on extra–lattice cations. When the water is removed, these charges will become highly localized and intense electrostatic forces will develop between parts of the lattice. These could lead to distortion of the lattice or even to the breaking of bonds under strain. Some studies have identified effects arising from dehydration. One group[28] found that the single–line appearance of the ^{1}H NMR spectrum of HZSM–5 was not restored by rehydration after the sample had been dried, even after many days. Recent studies by other workers have identified definite loss of lattice Al during a dehydration–rehydration cycle of a calcined sample, but not of an uncalcined one.[5] It has been suggested[38] that the bond–breaking between Al and the lattice occurs during the rehydration step, although there is little evidence to support this view. Studies described in this Chapter and the one following aim to clarify this area of uncertainty.

It is known that the nature of NLA formed depends critically on the treatment used for drying or calcining. In particular, the sample depth has been identified as an important parameter. A deeply–packed sample will experience 'steaming' of the upper layers by the water released from the lower ones during dehydration, resulting in substantial loss of lattice Al.. This does not occur when the sample bed is shallow.[13] Deep–bed samples are also thought to contain NLA which is highly condensed into polynuclear clusters; these contain few Lewis–acidic sites and give rise to a broad underlying hump in the ^{27}Al NMR spectrum.[25] Chapter 6 is devoted to a consideration of the dependence of the character of NLA on the treatment used to prepare the sample.

5B: CHARACTERIZATION OF SAMPLES STUDIED

The six basic samples used in the studies described in this Chapter and the one following are considered in this Section. Unlike those discussed in Chapter 4, they are not of common origin, although all were derived from precursors provided by Unilever Research Port Sunlight Laboratory.

1. NaY

This is a standard sample of as–synthesized zeolite Y with Na^+ as the charge–balancing cation. Figure 5.1 shows ^{29}Si, ^{27}Al and ^{1}H NMR spectra of the sample after exposure to atmospheric moisture. The ^{29}Si single–pulse spectrum shows, by the abundance of low–Q^n intensity, that the lattice is aluminium–rich. Deconvolution of the spectrum permits estimation of the Si/Al ratio to be 2.2. This may be compared with the value obtained from unit cell size measurement (UCS = 24.69 Å; Si/Al ratio = 3.3). XRD shows the sample to be 100% crystalline. The ^{29}Si SP and CP spectra in Figure 5.1 are remarkably similar, which suggests an absence of non–lattice silica, as demonstrated in Chapter 4. A possible clue to the solution of the problem is to be found in the ^{1}H NMR spectrum (Figure 5.1(c)) which contains, in addition to a rather narrow water signal at 4.7 ppm, a small SiOH peak at 1.0 ppm. If the lattice contains a significant population of SiOH groups, the Si/Al ratio obtained from ^{29}Si NMR will be an underestimate, since SiOH are thought to resemble SiOAl linkages in the ^{29}Si spectrum. It may be, therefore, that the UCS estimate (3.29) is a truer representation of the lattice Si/Al ratio of this sample. The ^{27}Al spectrum of this sample (Figure 5.1(d)) shows only a single narrow peak at 56.9 ppm arising from tetrahedral lattice Al, strongly suggesting the absence of NLA.

Figure 5.1: Spectra of hydrated NaY
(a) ^{29}Si SP Coupled RD=20s NT=2000 RO=3068Hz PA=$\pi/2$
(b) ^{29}Si CP/MAS RD=1s NT=3200 RO=1239Hz CT=10ms
(c) ^{1}H SP RD=400ms NT=32 RO=3120Hz PA=$\pi/2$
(d) ^{27}Al SP Coupled RD=100ms NT=1000 PA=$\pi/4$ RO=3595Hz

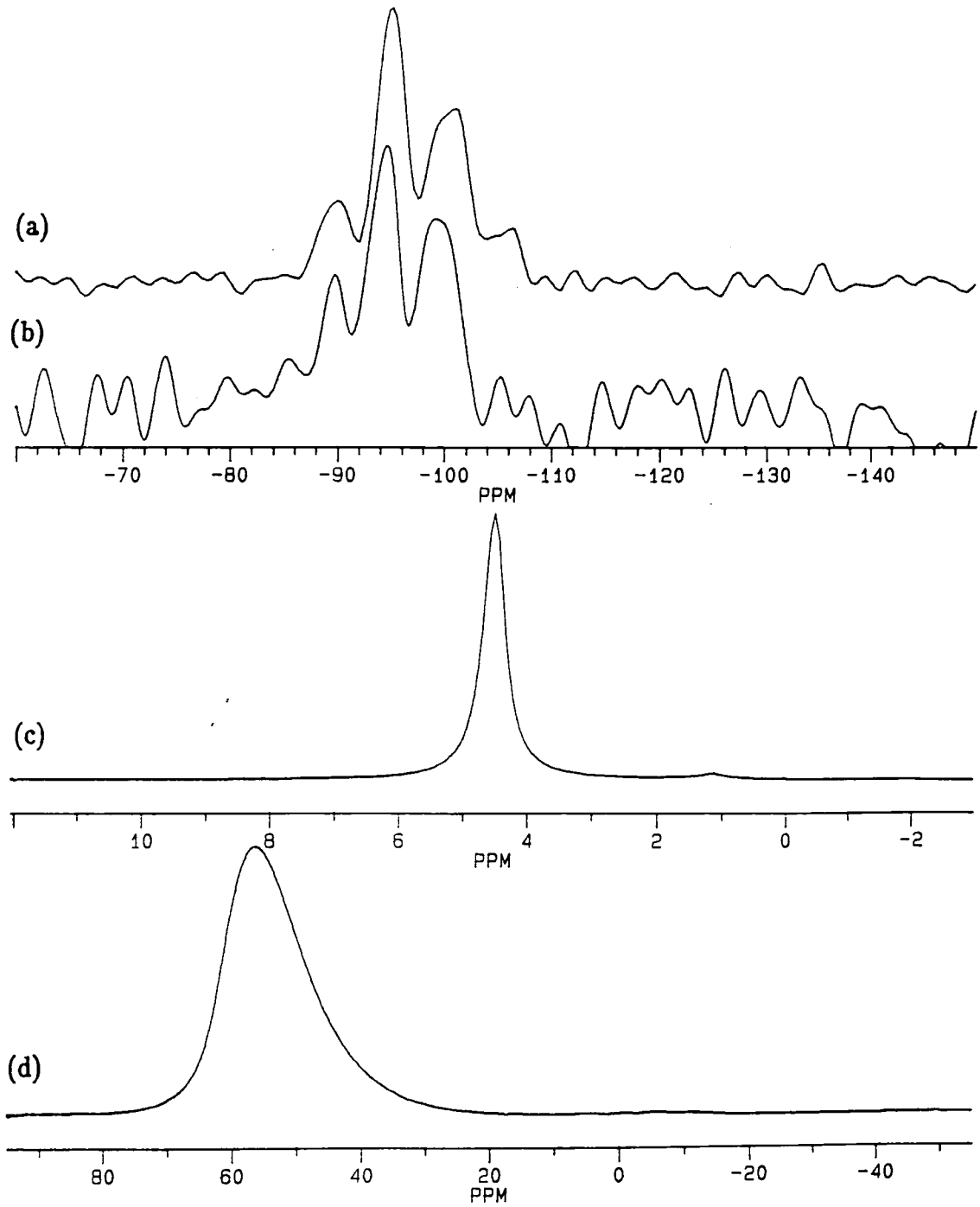

Relaxation times for this sample have been measured as follows. The ^{29}Si T_1 value of the Q^3 site is 6.7 s, with 6.1 s for Q^2 and 5.8 s for Q^1. Their similarity indicates the validity of quantitative intensity measurements from spectra obtained with a recycle delay less than five times the longest ^{29}Si T_1 present, as discussed in Chapter 2. The ^1H T_1 of the intracrystalline water is 12.7 ms at 200 MHz and 7.8 ms at 60 MHz; a single $T_{1\rho}$ value of 5.8 ms at 20 kHz was also measured. The ^1H T_2 decay exhibits double exponential character, with 70% at around 4 ms and 30% at 90 μs. This is thought to arise from water in the two different lattice cages, as discussed in Sections A and C.

2. NH_4Y[2]

This was prepared from a different sample of NaY (not the one described above) by aqueous cation–exchange. Figure 5.2 shows ^{29}Si, ^1H and ^{27}Al single–pulse spectra and the ^1H CRAMP spectrum. The ^{29}Si spectrum again shows the sample to be rich in lattice Al and highly crystalline, with well–resolved Q^4, Q^3, Q^2 and Q^1 peaks visible. The Si/Al ratio can be estimated by deconvolution to be 2.4. The unit cell size is 24.69 Å, which yields a Si/Al ratio estimate of 3.3. In addition, the deconvoluted ^{29}Si Q^4 linewidths can be used to estimate the Si/Al ratio, as described in Chapter 4, yielding values of 3.1 and 2.4 for the UCS and ^{29}Si NMR correlations respectively. The ^1H single–pulse and CRAMP spectra of the fresh sample (Figure 5.2(b) and (d)) show the occurrence of some lattice SiOH, which may distort the ^{29}Si NMR estimate as in the case of NaY discussed above. Accordingly, the true value of the lattice Si/Al ratio may be estimated as being close to 3. The ^{27}Al spectrum (Figure 5.2(e)) again shows the absence of NLA. XRD measurements show the sample to be 97% crystalline, and the ^{29}Si deconvolution shows there to be no broad peak due to non–lattice silica.

Figure 5.2: Spectra of hydrated NH_4Y

(a)	^{29}Si SP	RD=20s PA=$\pi/2$ NT=4000
(b)	^{1}H SP (fresh)	RD=400ms RO=3125Hz NT=32
(c)	^{1}H SP (aged)	RD=2s RO=1600Hz NT=32
(d)	^{1}H CRAMPS (fresh)	MREV-8 NT=32 RD=10s
(e)	^{27}Al SP	NT=2000 RD=200ms PA=$\pi/2$

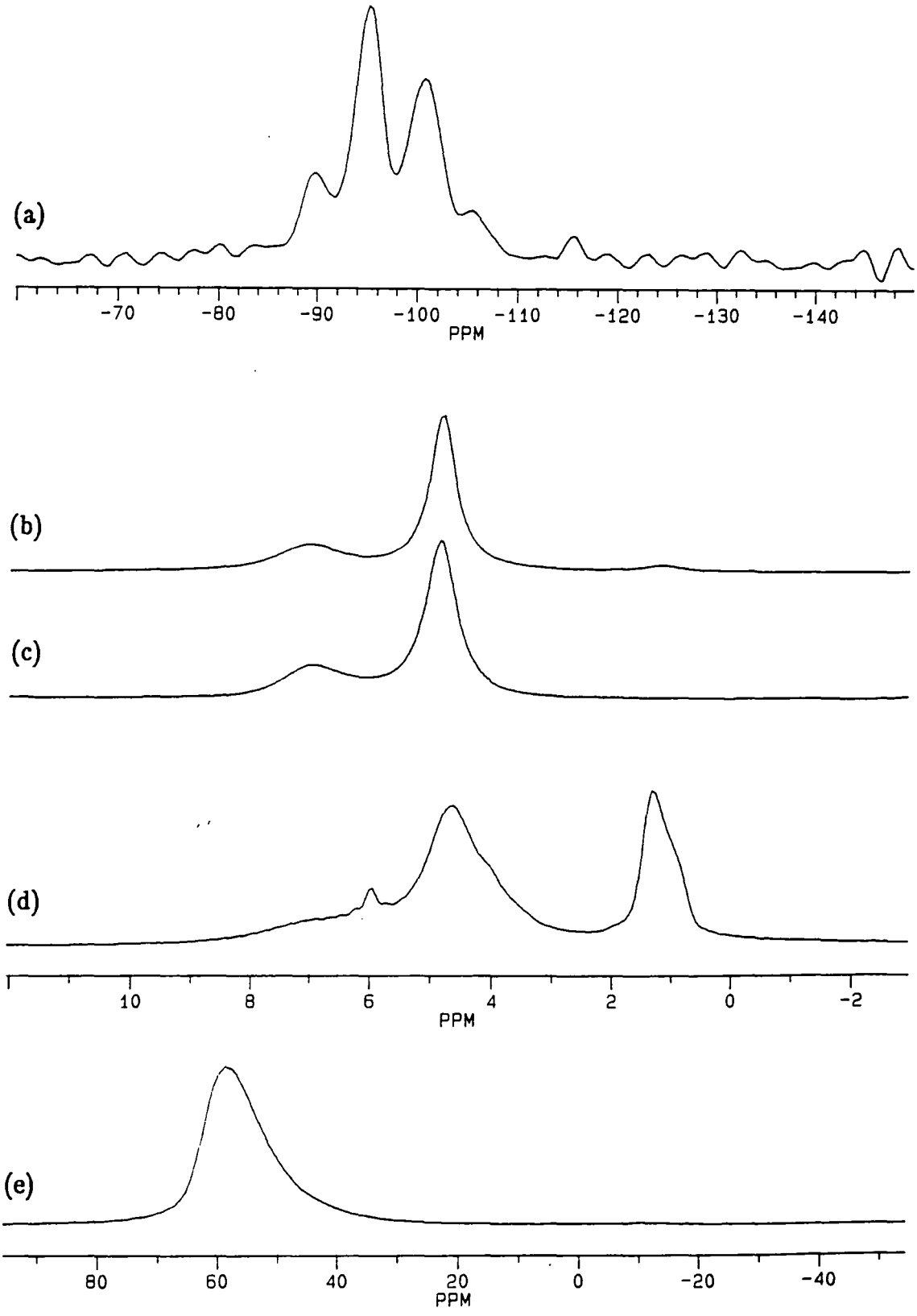

The ^1H SP spectrum of the fresh material, that is, not long after preparation (Figure 5.2(b)) shows three peaks at 7.0, 4.7 and 1.0 ppm, assigned respectively to NH_4^+, intracrystalline water and lattice SiOH groups. The same three peaks are visible also in the CRAMP spectrum, with substantial enhancement of the SiOH peak. It is to be expected that the ^1H nuclei in some SiOH groups, being non–acidic and relatively static, would undergo significant homonuclear dipolar couplings; these would be averaged out by the CRAMPS technique, increasing the intensity of the narrow peak. After the material had been kept for 18 months, the ^1H SP spectrum showed no sign of the SiOH peak at all; see Figure 5.2(c). It is unclear whether this is due to disappearance of SiOH groups (*e.g.* by annealing) or by their redistribution into an arrangement encouraging even greater dipolar coupling, resulting in broadening of the whole signal beyond the limits of observability.

Figure 5.3 shows ^{29}Si CP spectra obtained on the CXP–300 instrument at Unilever Research Port Sunlight Laboratory. Trace (a) shows the normal CP spectrum, which resembles the SP spectrum in Figure 5.2(a). Traces (b) and (c) show the selective CP spectra obtained after annulling the magnetization of the NH_4^+ and H_2O ^1H nuclei respectively (see Chapter 2 for a discussion of this experiment). The ^1H T_1 values of these two species are 12.5 and 19.6 ms respectively (see Table 5.1); the corresponding recovery times used in the pulse sequence (Figure 2.3) were 8.7 and 13.6 ms. All spectra were obtained with similar numbers of averages. The substantially lower signal–to–noise ratio of (c) indicates that the ^1H nuclei on water molecules are more important in cross–polarization to lattice Si than those on NH_4^+ ions. This may arise simply from the somewhat greater population of water in the sample; alternatively, water may bind more strongly and more rigidly to lattice sites, enhancing the heteronuclear coupling required for CP. The spectra may also indicate that NH_4^+

Figure 5.3: ^{29}Si Selective CP spectra of hydrated NH_4Y (CXP-300)
NT=25000 RO=1950Hz RD=1s CT=20ms
(a) Normal CP/MAS
(b) NH_4^+-annulled
(c) H_2O-annulled NT=18379

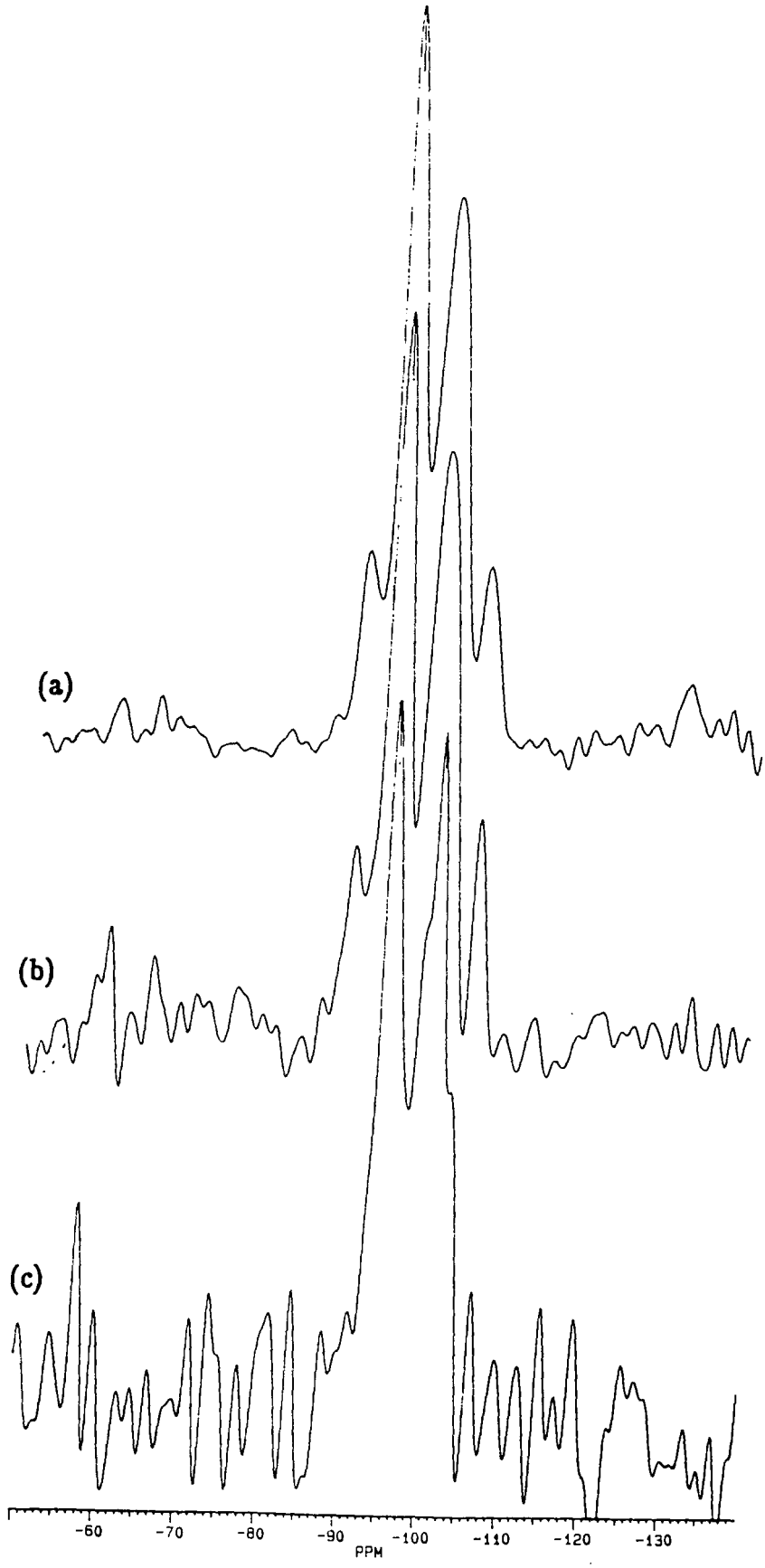

does not cross–polarize to Q^4 sites, as shown by the absence of a Q^4 peak in trace (c). This would suggest that NH_4^+ associates more strongly with lattice Al (necessarily nearer to low–Q^n sites) than with lattice Si.

The ^1H relaxation times for this sample are shown in Table 5.1 below. Approximately 85% of the hydrogen present is in water molecules. Figure 5.4 shows the relaxation curves obtained from the inversion–recovery experiment used to obtain the estimates of T_1 on the CXP–200 spectrometer, plus the best–fitting exponential curves; the signal–to–noise ratio and quality of fit are both high and exemplary of most of the relaxation time data quoted in this Chapter.

Table 5.1: ^1H Relaxation Times of NH_4Y[2], in ms

Time Constant	Field	Ammonium	Water
T_1	60 MHz	9.3	1.1
	200 MHz	16.5	16.2
	300 MHz	12.5	19.6
$T_{1\rho}$	20 kHz	3.0	6.6
	62.5 kHz	≃2.9	4.8
T_2	60 MHz	5	1

3. HY

This sample was made from a sample of NH_4Y similar to that described above by calcination at 650°C, driving off NH_3 and dislodging some lattice Al. Figure 5.5 shows ^1H, ^{29}Si and ^{27}Al NMR spectra of the material. The ^{29}Si SP spectrum clearly shows that much lattice Al has been lost during the deammoniation process; the Si/Al ratio can be estimated as 5.33, which is in

Figure 5.4: Relaxation curves obtained from inversion–recovery measurement of NH_4Y[2]: the crosses are experimental data, whilst the continuous line is the best–fitting exponential curve. Top: NH_4^+ peak; bottom: H_2O peak. The vertical scale is in arbitrary intensity units.

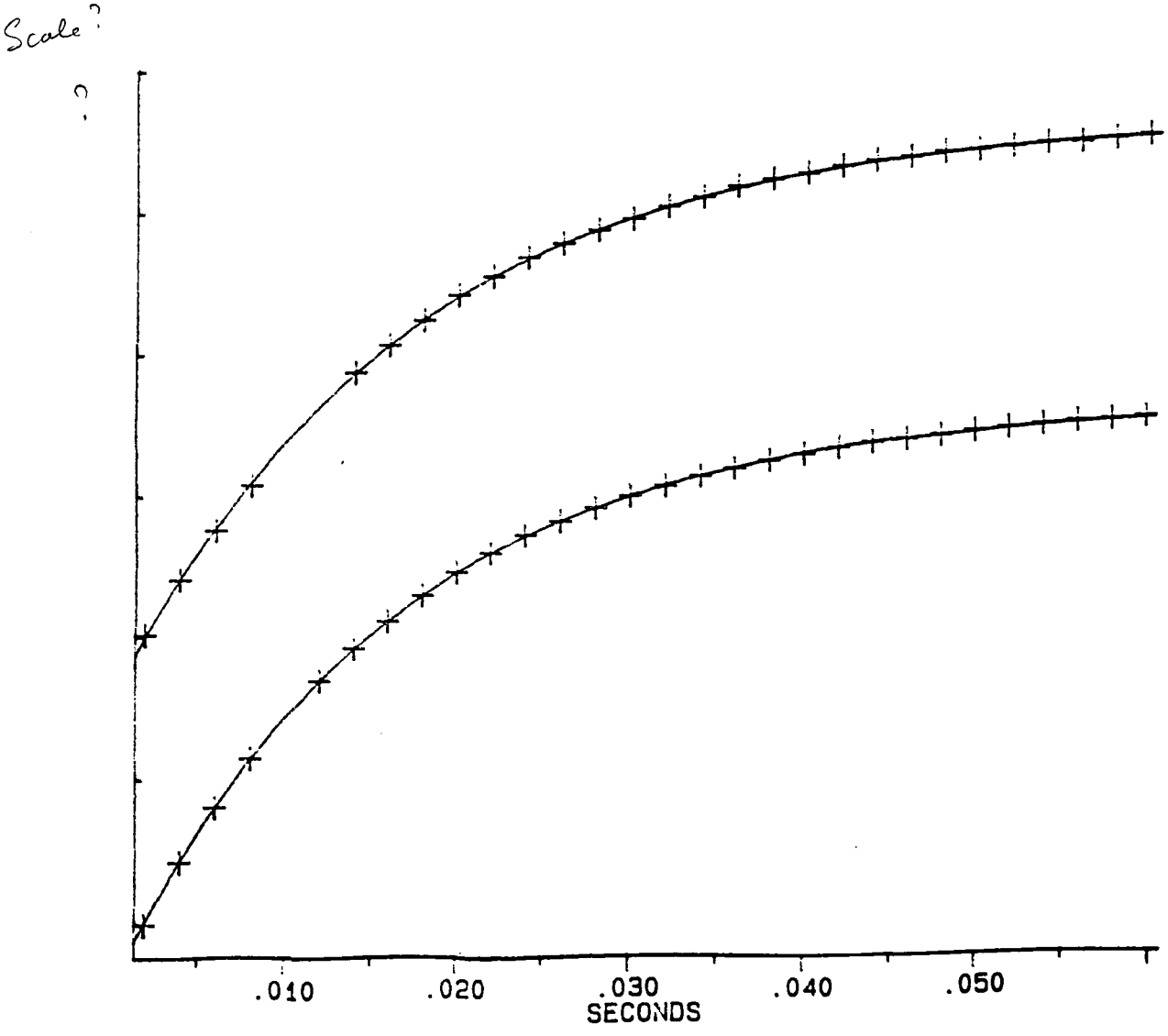

Figure 5.5: Spectra of hydrated HY

(a) ^{29}Si SP RD=60s NT=1000 RO=3130Hz
(b) ^{29}Si CP/MAS RD=2s NT=5000 RO=1200Hz CT=10ms
(c) ^{1}H SP RD=200ms NT=32 RO=3000Hz
(d) ^{1}H CRAMPS MREV–8 RD=10s NT=32
(e) ^{27}Al SP RD=100ms NT=4000 RO=3000Hz PA=3π/40
(f) As (e) except RO=4455Hz
(g) ^{27}Al CP/MAS (VXR–300) RD=500ms NT=3000 CT=500μs

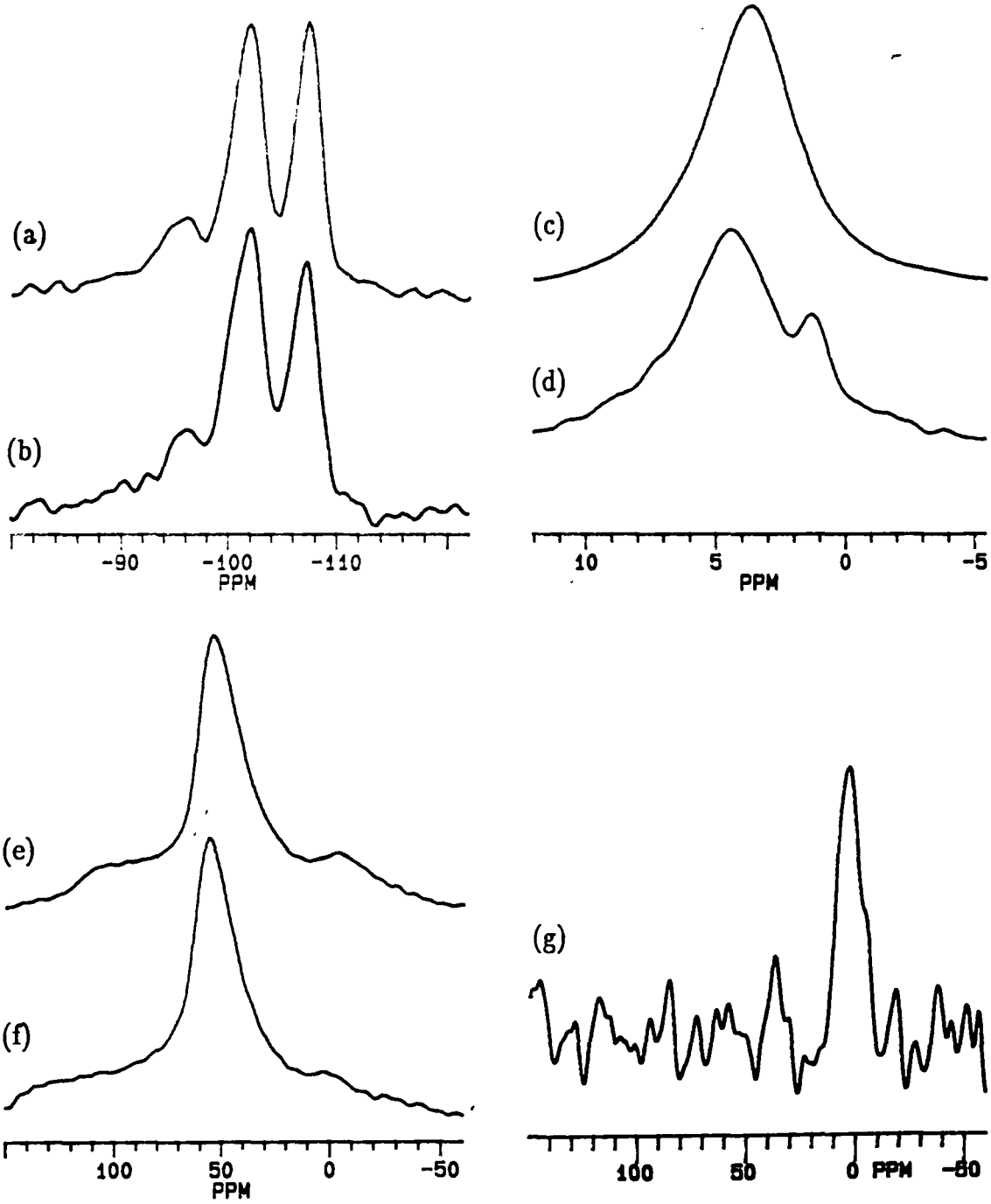

excellent agreement with the value of 5.32 obtained from the unit cell size (UCS = 24.54Å). In addition, the crystallinity has dropped substantially to 81%, and ^{27}Al NMR shows (in Figure 5.5(e) and (f)) the presence of a small amount of octahedral NLA. Deconvolution of the ^{29}Si single–pulse spectrum into Gaussian components requires the inclusion of two broad peaks (half–width > 250 Hz, all others < 110 Hz) of significant intensity which account for 37% of the total ^{29}Si population of the sample, supporting the view that extensive amounts of non–lattice silica are present. Deconvolution of the CP/MAS spectrum (Figure 5.5(b)) also requires an amorphous component accounting for 37% of the total intensity. However, as the amorphous material is clearly not strongly enhanced by CP (unlike that in corresponding samples discussed in Chapter 4), it may be concluded that the non–lattice material is quite condensed and carries relatively few –OH groups.

The 0 ppm NLA peak is strongly enhanced by CP, as seen in Figure 5.5(g), indicating that NLA is coupled to relatively static ^{1}H nuclei, presumably on non–lattice AlOH groups. Variable contact–time measurements permitted estimation of the cross–polarization time T_{CP} to be 0.7 ms for the 50 ppm (lattice Al) peak, where visible, and 1.5 ms for the 0 ppm (NLA) peak.

The ^{1}H single–pulse MAS spectrum in Figure 5.5(c) shows a single peak at 4.7 ppm due to intracrystalline water. The peak is remarkably broad compared with the corresponding peaks in NaY and NH_4Y[2], suggesting a significant ^{1}H–^{27}Al dipolar interaction between water and NLA. Homonuclear couplings cannot be responsible for the broadening, since the peak is not narrowed by CRAMPS (see Figure 5.5(d)). The CRAMP spectrum also shows a clear signal due to SiOH groups which is entirely invisible in the single–pulse spectrum. This is one of very few known cases in which CRAMPS results in a significant improvement in spectral resolution in a zeolite.

^{1}H relaxation times proved difficult to measure with confidence, varying with the exact water content of the sample. Two distinct components were always seen, in the approximate intensity ratio 4:1, with the larger component arising presumably from supercage water. Much longer times were measured for SiOH groups. The results are shown in Table 5.2. Variation of the recycle delay during measurement of the ^{29}Si single–pulse spectrum showed that no ^{29}Si T_1 value in the sample exceeded 12 s.

A variable–contact ^{29}Si cross–polarization measurement showed that the rate of cross–polarization to different Q^n sites increased as n decreased, with T_{CP} values ranging from 1.1 ms for Q^1 to 2.8 ms for Q^4, as expected from the relative populations of Brönsted ^{1}H atoms around these sites. The CP behaviour of the sample was found to be invariant over the temperature range –60 to +22^{o}C, suggesting that the mobilities of water molecules and Brönsted ^{1}H atoms do not change substantially in this range.

Table 5.2: ^{1}H Relaxation Times of HY in ms

Time Const	Field Strength	Supercage Water	Small cg. Water	SiOH
T_1	200 MHz	≃5	≃22	≃170
	300 MHz	≃3	≃14	≃60
	20 MHz	2.3	21	
$T_{1\rho}$	62.5 kHz	1.5	1.5	
	20 kHz	1.4	6.0	
T_2		≃2	≃0.027	0.47

Figure 5.6: Spectra of hydrated HY–S

(a)	^{29}Si SP	NT=8000 RD=20s RO=1221Hz
(b)	^{29}Si CP/MAS	NT=40000 RD=2s RO=2980Hz CT=10ms
(c)	^{1}H SP (fresh)	NT=128 RD=1s RO=4011Hz
(d)	^{1}H SP (aged)	NT=32 RD=1s RO=2955Hz
(e)	^{1}H CRAMPS (fresh)	MREV–8 NT=32 RD=20s
(f)	^{1}H CRAMPS (aged)	MREV–8 NT=32 RD=10s
(g)	^{27}Al SP Decoupled	NT=30500 RD=100ms RO=4500Hz PA=3π/40

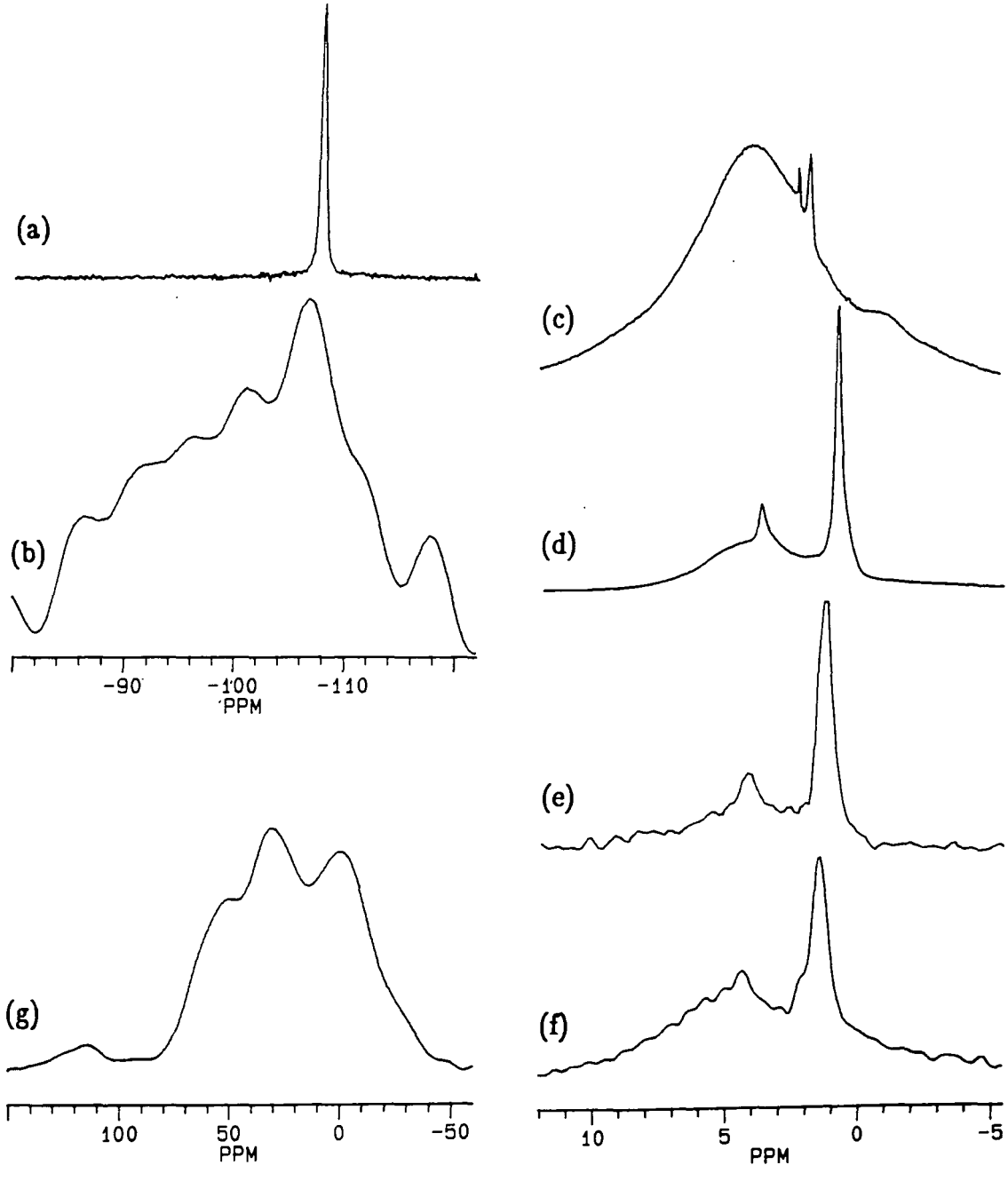

4. HY–S

This sample was made by steaming a low–sodium calcined NH_4Y at 816^{o}C for 5 hours. It contains hardly any lattice Al, as shown by the ^{29}Si single–pulse spectrum (Figure 5.6(a)) which contains a single narrow peak in the Q^4 position. As with the steamed samples described in Chapter 4, however, the ^{29}Si CP/MAS spectrum (Figure 5.6(b)) shows a mass of broad peaks indicating the presence of non–lattice silica–alumina; this is supported by the multiple peaks in the ^{27}Al spectrum and the SiOH and AlOH peaks visible, in addition to water, in the ^{1}H spectra in Figure 5.6.

The ^{1}H SP and CRAMP spectra of the fresh material show signals from water (4–5 ppm) and AlOH (2.2 ppm). The water signal is substantially narrowed by CRAMPS, suggesting that the water is fairly immobile. After keeping for 8 months, the CRAMP spectrum is largely unchanged (Figure 5.6(f)) but the SP spectrum now shows an intense SiOH peak, presumably arising from slow hydrolysis of SiOSi strained linkages, and the AlOH signal has apparently shifted to 3.8 ppm. One possible explanation for these changes is that the non–lattice silica–alumina is originally coordinated to the lattice at defect sites, and the complex is slowly destroyed by hydrolysis or solvation of the non–lattice material, resulting in the development of SiOH groups at the newly–released lattice vacancies and Brönsted–acidic AlOH groups at the sites on the non–lattice material previously occupied by coordination to the lattice. Such slow hydrolysis, in a slightly different form, is also proposed elsewhere in this Chapter and in Chapter 6.

The ^{1}H relaxation times all exhibit two–component character, with the components approximately in the ratio 30:70. The T_1 values at 60 MHz are 23 and 6.2 ms; the $T_{1\rho}$ values at 20 kHz are 17 and 1.4 ms; and the T_2 values are 2.3 ms and 640 μs. These measurements were made when the sample was about 5

months old. After aging, the sample is estimated to be 0.17% water by weight – a remarkably low figure by comparison with those quoted in Section C for other fully–hydrated zeolites, further indicating that the hydrophilicities of zeolite samples are associated with their lattice Al content.

5. NaY–ex

This sample was made from the HY described above (Section 3) by aqueous cation–exchange. The ^{29}Si single–pulse MAS spectrum (Figure 5.7(a)) is very similar to that of the parent HY (Figure 5.5(a)) except perhaps for a slight narrowing of the Q^1 and Q^2 peaks, showing that the lattice has undergone virtually no change in the ion–exchange. The ^{1}H single–pulse (aged sample) and CRAMP spectra in Figure 5.7(c) and (d) show water and SiOH peaks; the similarity of these two spectra shows that there is very little homonuclear dipolar coupling, as in the NaY sample. The ^{27}Al spectrum shows lattice and non–lattice peaks similar to the HY precursor; this indicates that ion–exchange under non–acidic conditions does not affect non–lattice alumina significantly. The Si/Al ratio estimate obtained from the ^{29}Si spectrum is 4.0, whilst the Q^4 linewidth correlation described in Chapter 4 gives estimates of 4.3 and 4.6. A value close to that obtained for HY, *i.e.* 5.3, might be expected for this sample; the low estimate from ^{29}Si NMR intensities may arise again from SiOH groups, which appear abundantly in the ^{1}H spectrum after aging.

The effect of storage for several months after preparation is seen in the difference between the ^{1}H spectra obtained before and after aging (Figure 5.7(b) and (c)). The fresh material appears to show two distinct and overlapping peaks of differing width in the region generally assigned to water. After aging, a single Gaussian band shape is visible. This may be caused by slow diffusion of Na^+ into the small cages; in the fresh material, the water in the two cages would

Figure 5.7: Spectra of hydrated NaY–ex

(a)	^{29}Si SP Decoupled	RO=3030Hz NT=3400 RD=20s
(b)	^{1}H SP (fresh)	RO=3000Hz NT=64 RD=5s
(c)	^{1}H SP (6 months old)	RO=1770Hz NT=32 RD=2s
(d)	^{1}H CRAMPS (3 months old)	MREV–8 NT=32 RD=10s
(e)	^{27}Al SP (VXR–300)	RO=2910Hz NT=10000 RD=100ms PA=$\pi/6$

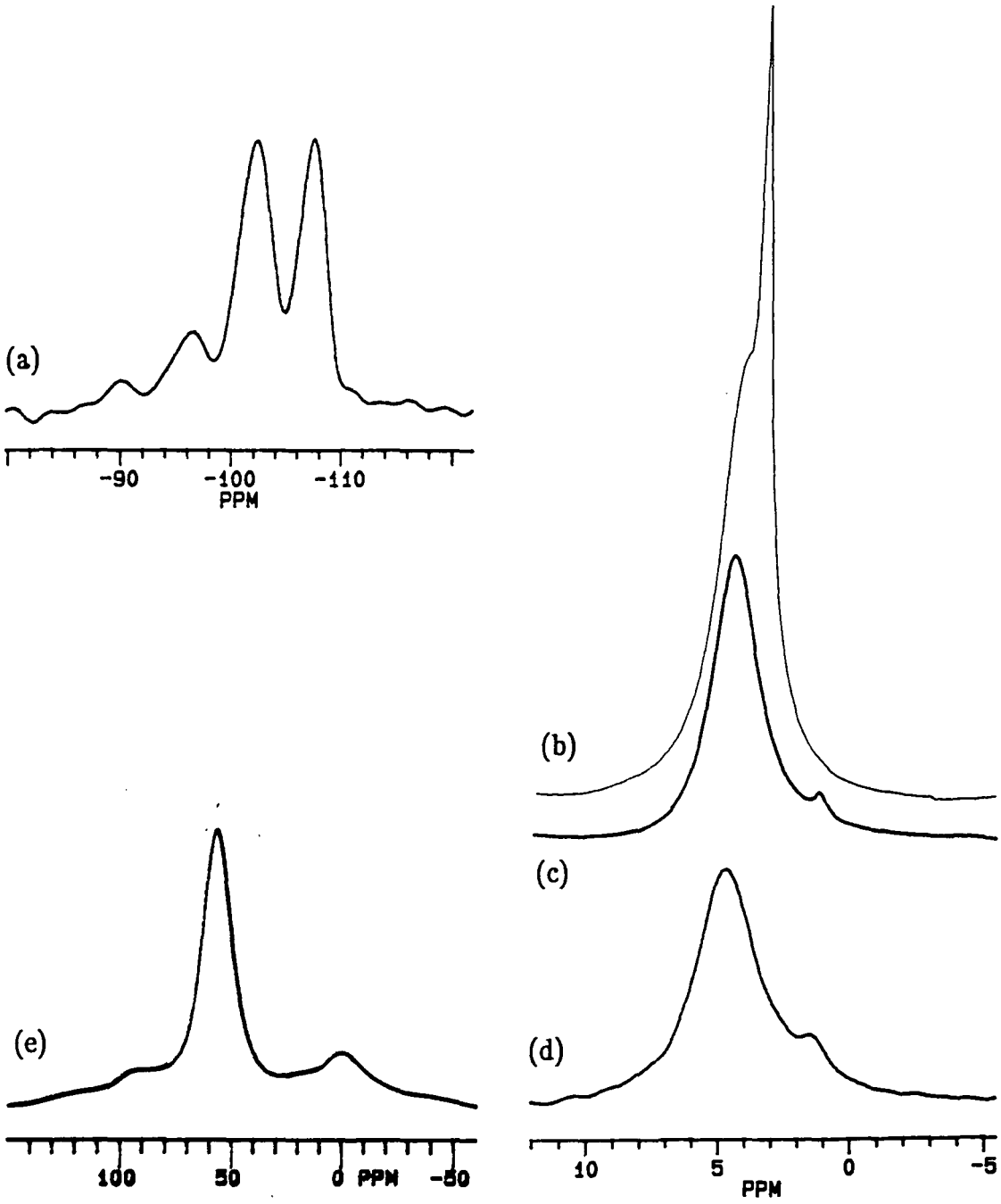

experience substantially different ionic environments, but after distribution of Na^+ (which would be slow because of the hindrance of the small windows between cages to the passage of large $Na(H_2O)_6^+$ clusters) the environments would become much more similar. Also, the SiOH groups are absent in the fresh material, suggesting that they are formed by slow hydrolysis, perhaps after the manner of HY–S.

The ^1H T_1 values for this sample at 200 MHz were found to be 11 ms (water) and 34 ms (SiOH), whilst at 60 MHz the corresponding values were around 2 and 10 ms. Only a single component could be observed for water.

6. AgY–ex

This sample was made by ion–exchange from HY in a manner analogous to NaY–ex; the two samples were found to be very similar in character. The ^{29}Si CP/MAS spectrum resembles the single–pulse spectra of other similar samples, except for enhancement of lower–Q^n peaks. One interesting feature of this sample is the clear chemical–shift separation between the two water phases visible in the ^1H spectrum (Figure 5.8), even without MAS. The water peak is clearly composed of a broad line at 4.8 ppm superimposed on a narrow one at 4.5 ppm. There is also another peak at 2.3 ppm, whose assignment is uncertain, which is very much broader in the static spectrum. Elemental analysis found the wet sample to contain 13% Ag by weight, showing that a substantial degree of ion–exchange had taken place during the preparation of this sample.

5C: NMR STUDIES OF ZEOLITE WATER

The first part of this Section considers general aspects of the affinity of

Top: Figure 5.8: ^{1}H SP MAS spectrum of hydrated AgY–ex
NT=32 RO=1730Hz RD=5s

Bottom: Figure 5.14: ^{1}H SP MAS spectrum of AgY–ex–68 dried and hydrated NT=32 RO=2987Hz RD=3s

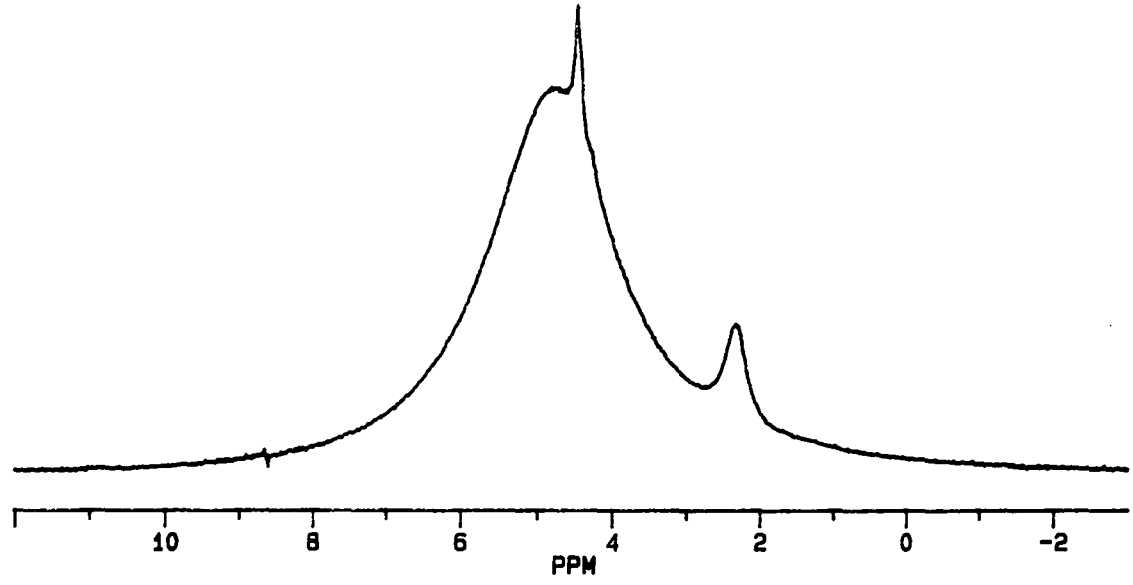

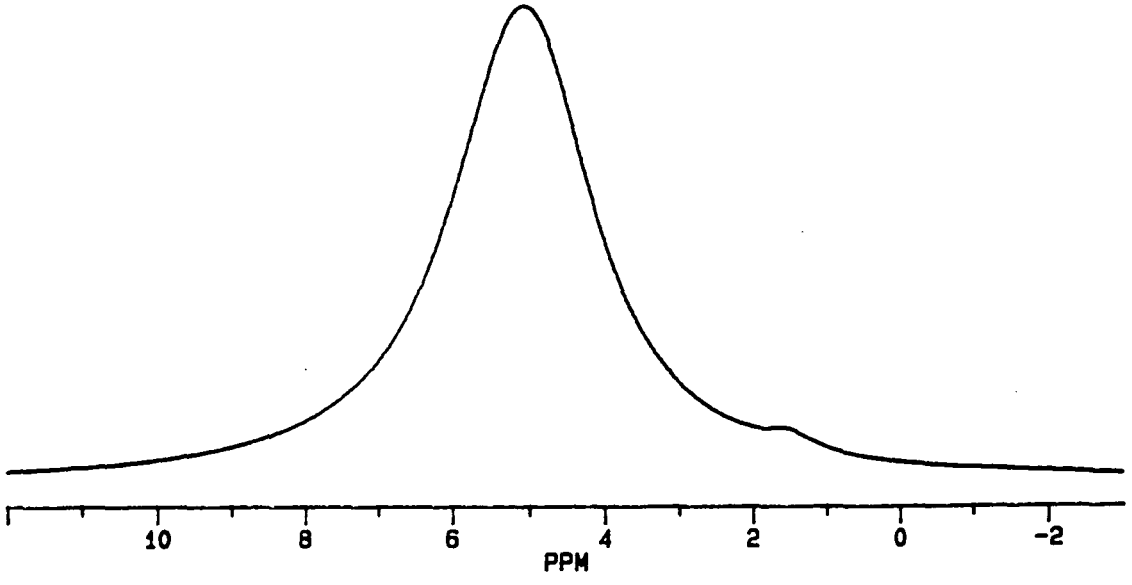

Zeolite Y samples for water. Then a consideration of the appearance of water in ^{1}H NMR spectra is given, followed by a discussion of the effect of complete dehydration and rehydration on the water itself and on the zeolite lattice.

1. Hydrophilicity of Zeolite Y

Any sample of Zeolite Y containing aluminium (either lattice or non–lattice) has a strong affinity for polar sorbates, especially water, because of their capacity to 'solvate' charges on the lattice, charged or polar non–lattice species, and charge–balancing cations. Unlike close–packed crystals, however, zeolites do not confine individual water molecules in small spaces; rather, sorbates are able to move in the channel and cage network, subject to constraints of molecular size. Thus, the amount of water adsorbed by a sample is affected not only by its composition but by external influences such as temperature and humidity of the ambient conditions.

This may be illustrated by measurements of the water content of HY made using the ^{1}H NMR spin–counting technique described in Chapter 3. The sample was kept in a plastic container with a moderately well–fitting screw lid. Measurements of the water content of the sample on separate occasions, with little care taken over sample handling, yielded results of 3.0 wt% and 1.4 wt%. However, a portion of this sample which was allowed to equilibrate in an atmosphere of 85% relative humidity (RH) for six days and then packed for MAS without further exposure to ambient conditions yielded a result of 22.7 wt%.

Some of the samples studied in Chapter 4 were assayed for water content after prolonged exposure to a controlled 85% RH atmosphere, yielding water contents by weight as follows: HY–C550, 59.4%; HY–C650, 23.5%; NH_4Y–C550 [HY–C550 after exchange with NH_4^+], 30.6%; NH_4Y–C650, 33.6%; HY–C550–S, 13.6%; NH_4Y–CS, 55.5% and 58.5% (two measurements);

HY–CS–S, 20.1%. Apart from the value for HY–C550, the samples containing NH_4^+ generally have a greater affinity for water than those with H^+, suggesting that the NH_4^+ ions themselves help to bind water by ionic interactions. Also, the steamed samples have a lower affinity for water, as expected from their very low lattice Al content; the same result was reported in Section B for HY–S.

In order to overcome the problem of varying water content, sample of which a known mass was required were always kept in an 85% RH atmosphere for several days before use, to ensure the attainment of a known hydration level.

2. NMR Character of Intracrystalline Water

Several results have already been presented which demonstrate that the intracrystalline water in many samples exists in two distinct phases, between which exchange is slow on the NMR time scale; these phases are associated with water in small and large cages of the crystal lattice. Some samples show the two–phase character directly in the ^1H spectrum (MAS or static). Figure 5.7(b) shows the ^1H spectrum of freshly–made NaY–ex, which clearly contains overlapping peaks at 4.5 and 3.5 ppm. It was suggested in Section B that the chemical shift difference between these peaks, which is not visible in normal NaY or HY, arose from the presence of Na^+ in large cages only. Coordination of water to Na^+ would cause deshielding of the ^1H nuclei in the water molecule, and so it seems reasonable to assign the high–frequency (4.5 ppm) peak, the broader of the two, to supercage water. The broadness of the 4.5 ppm peak may arise from chemical shift dispersion due to rapid motion of the water molecules in and out of the Na^+ coordination sphere, whilst the small–cage water band may be narrower than usual because the lack of strong coordination sites results in enhanced water mobility and hence decreased homonuclear dipolar coupling. The two peaks, broad and narrow, are also clearly visible in the ^1H spectrum (MAS

or static) of AgY–ex as shown in Figure 5.8, although in this case the shift difference is only 0.35 ppm instead of 1 ppm in NaY–ex, reflecting the lower polarizing effect of the softer Ag^+ ion on the water molecule.

Some samples show equivalent two–phase character in their ^1H relaxation times. A number were reported in Section B, and are in agreement with published findings that small–cage water ^1H has a T_2 of around 25–100 μs and that in the supercage around 3–5 ms (or sometimes longer).

Figure 5.9 shows the results obtained from a measurement of the T_2 values in hydrated HY by the CPMG pulse sequence. The upper part of the Figure is a semi–logarithmic deconvolution diagram, showing the original data (uppermost line of dots) and that resulting from successive subtraction of the three best–fitting exponential components (solid lines). The intercept of the three lines on the vertical axis give the relative intensities of the corresponding relaxation components at zero time. The lower part of the plot shows the integrated residue resulting from subtraction of all three components from the original data. Apart from the large feature near the end, which probably results from spectrometer instability, the residue shows little but noise, indicating that the three–component fit is a good representation of the original data. One point of interest arising from the deconvolution diagram is that the shortest T_2 component is characterized by only a few data points; this highlights the difficulty of measuring such short relaxation times with confidence.

The short T_2 component has not been observed in NH_4Y[2]; instead, a separate component (T_2 = 1 ms) is observed which could be an average value resulting from rapid exchange between NH_4^+ and H_2O in the small cages. Most samples also show two T_1 and $T_{1\rho}$ phases for water, although only one has been observed in NaY. The two–phase T_1 character can sometimes be seen clearly during inversion–recovery experiments, where one of the superimposed peaks

Figure 5.9: Deconvolution and residue plots obtained from T_2 measurement of hydrated HY. See text for full description. On the residue plot, the horizontal axis is the same as that on the deconvolution plot, whilst the vertical axis is in arbitrary intensity units.

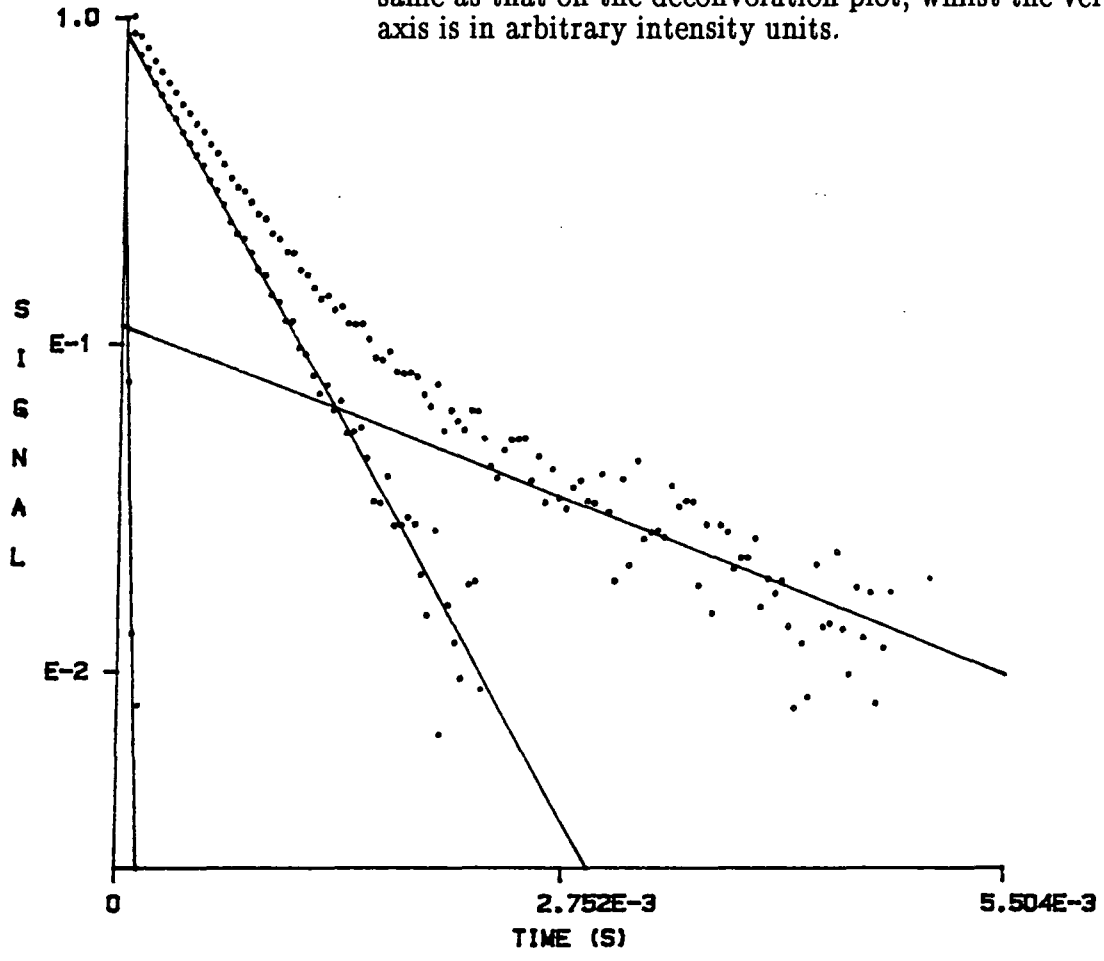

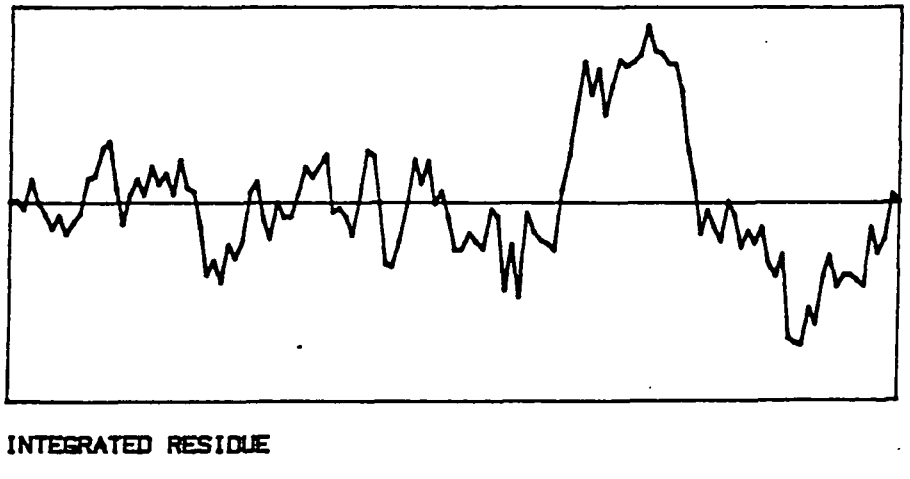

Figure 5.10: Series of ^1H MAS spectra of hydrated HY acquired using the inversion–recovery pulse sequence. The recovery time runs from 1 ms (bottom) to 15 ms (top) in steps of 1 ms.

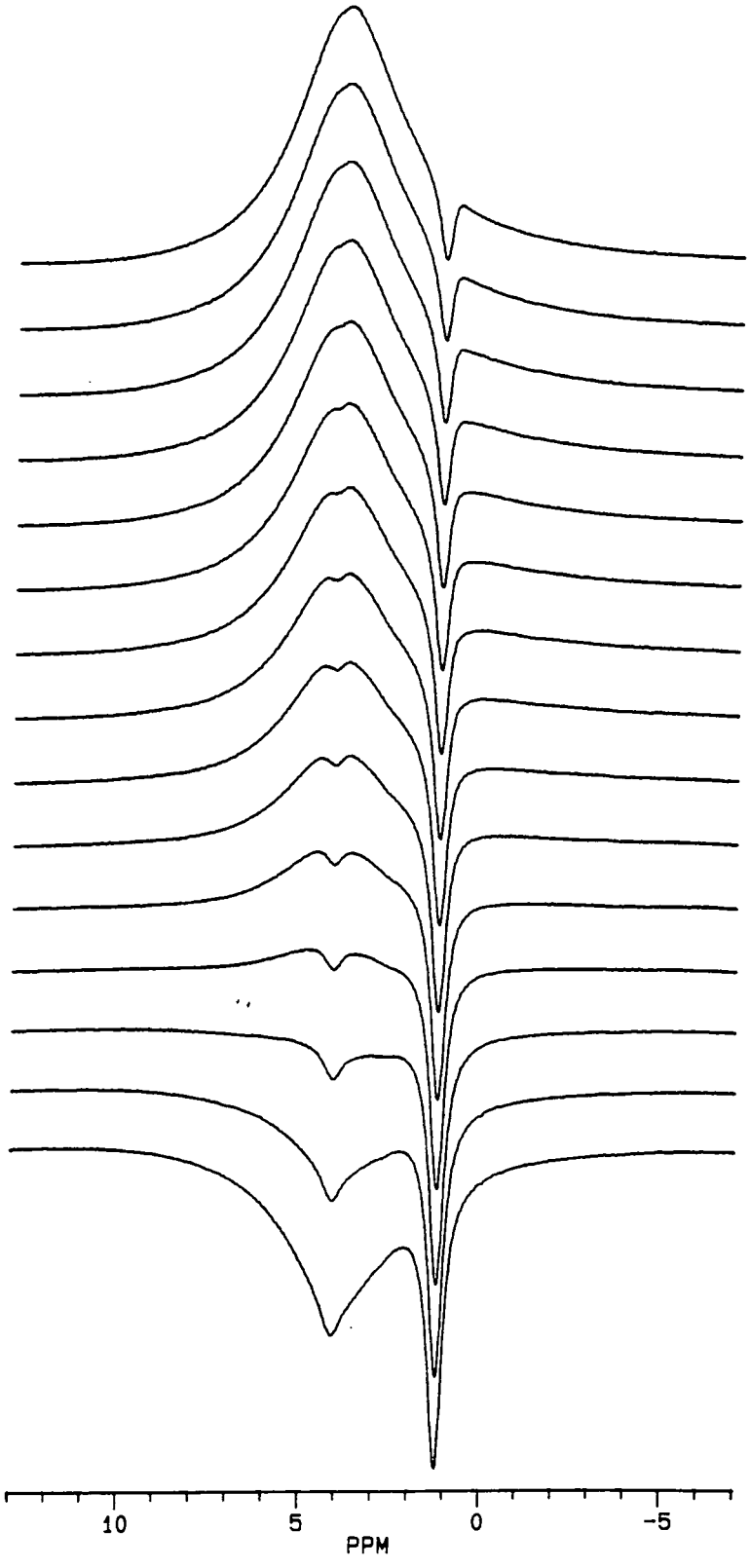

inverts before the other. Figure 5.10 shows an example of this for HY.

Relaxation Times of Samples in Chapter 4. Some T_1 (200 MHz) and $T_{1\rho}$ (62.5 kHz) relaxation times measured for the samples described in Chapter 4 in their fully hydrated forms are shown in Table 5.3. The times shown here for NH_4Y–CS do not differ greatly from the values for NH_4Y[2] shown in Table 5.1; the other T_1 values, however, are much higher than those found for samples of the same cation form described in the present Chapter. The differences may arise from binding of water to NLA, reducing its mobility and hence increasing the T_1 values observed, as suggested earlier. The $T_{1\rho}$ values are not greatly affected by this, suggesting that the water is still mobile on the tens–of–kilohertz time scale. It can therefore be deduced that the correlation time of water on NLA lies in the range 5×10^{-9} to 2×10^{-5} s.

Table 5.3: ^{1}H Relaxation Times of Fully Hydrated Samples in ms

Sample	Relax time	NH_4^+	H_2O	SiOH
HY–C650	T_1 $T_{1\rho}$		75.0 4.8	250.6
NH_4Y–C550	T_1 $T_{1\rho}$		103.3 5.9	
NH_4Y–C650	T_1 $T_{1\rho}$		90.1 6.2	220(66%) 20(34%) 23(66%) 2(34%)
NH_4Y–CS	T_1 $T_{1\rho}$	25.9 2.7	21.9 3.3	

3. Water Contents During Dehydration and Rehydration

Several experiments have been performed to assess the water contents of samples during various dehydration and rehydration treatments. In particular, the effect of exposure to the atmosphere and the rate of equilibration have been investigated, with the aim of ensuring that the hydration behaviour of samples used in other experiments is sufficiently well–understood to endue confidence in the results.

Exposure of HY to Humid Atmospheres. Two portions of HY (typically containing around 2% water by weight) were drawn from the reasonably airtight container in which the HY had been kept since preparation. The first, initially weighing 0.7607 g, was exposed to an 85% RH controlled atmosphere for several days and reweighed periodically; then it was left in the open atmosphere and again weighed at intervals. The second, initially weighing 0.9937 g, was exposed to the open atmosphere first and then to the 85% RH controlled atmosphere, with periodic weighing. Both samples reached an equilibrium mass within six days of exposure in the 85% RH atmosphere, adsorbing 136 and 127 mg per gram of starting material respectively. The total uptake of water from the atmosphere was measured repeatedly at intervals of at least 24 hours; the readings were as follows (in milligrams of water per gram initial sample):

First sample: 113, 110, 105, 111, 94, 93, 99

Second sample: 88, 97, 83, 87, 88

The fluctuations in these values, arising from ambient humidity changes, and the variation between the two samples, highlights the importance of using samples equilibrated in a controlled–humidity atmosphere. The readings taken during exposure to the fixed humidity were somewhat less variant:

First sample: 134, 137, 137

Second sample: 132, 124

They also demonstrate that more water was adsorbed in the higher humidity atmosphere than in the open laboratory, as intuitively expected.

Rate of Dehydration of HY. A sample of HY from the usual container, initially weighing 229 mg, was heated under vacuum to 400^{o}C for 16 hours using the procedure described in Chapter 3, then allowed to cool, still under vacuum. It was weighed without exposure to the atmosphere, then heated for two further periods, reweighing after each. The mass loss, normalized to units of milligrams sorbate lost per gram of initial sample, is shown in Figure 5.11. From this it can be seen that the mean *rate* of loss after 16 hours is only about 10% of that before

Figure 5.11: Desorption from HY during heating under vacuum. Vertical axis: total mass loss in mg per g initial sample. Horizontal axis: heating time in hours.

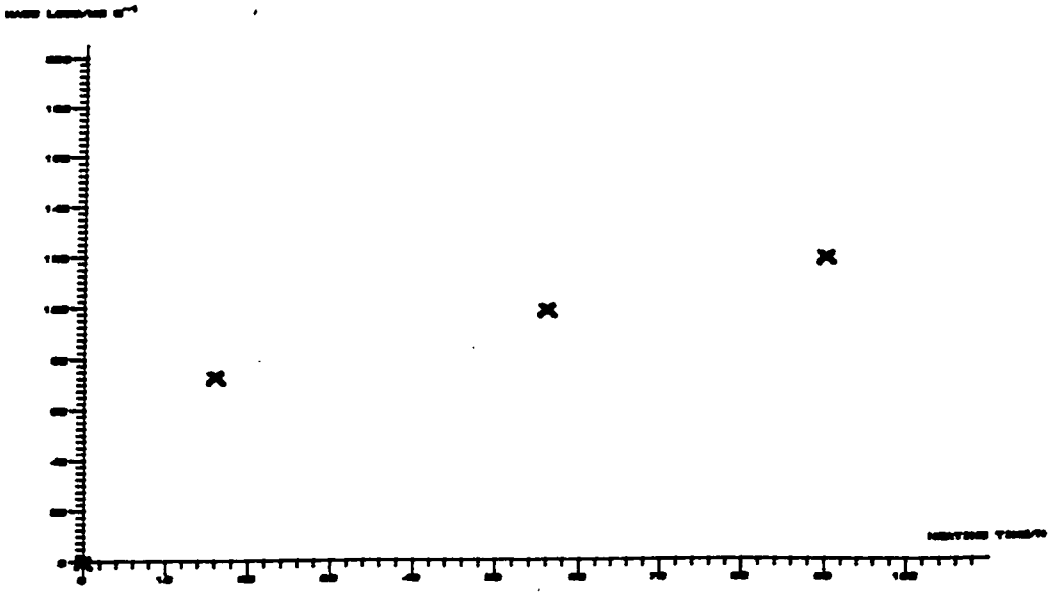

16 hours; thus, nearly all sorbates are lost in the first few hours. The continuing desorption after long periods of heating may be due to condensation of lattice defects, releasing water ($2\ SiOH \longrightarrow SiOSi + H_2O$), similar processes involving non–lattice alumina, or possibly release of sorbates from small cages, which is known to be a slow process: see Section A.

Rate of Rehydration of Dried HY Samples. The dried sample described above was transferred first to a capped glass jar overnight and then exposed to the open atmosphere, with periodic weighing. The total uptake at equilibrium with the atmosphere was about 410 mg/g initial sample; this is over three times as much as was lost during the heating experiment. Similar phenomena have been observed by other workers,[28] although they did not report whether the sample was equilibrated in the atmosphere prior to drying; the present HY sample was not equilibrated, and this may account for some, if not all, of the apparent excess adsorption of water on rehydration. The sample initially adsorbed about 0.2% of its final water uptake per minute of exposure to the atmosphere; this shows that great care must be taken during handling of dried samples for study by ^1H NMR, since the ^1H content of dry materials is very low by comparison with hydrated ones.

Another sample was dried by heating under vacuum to 400°C for $36\frac{3}{4}$ hours to form HY–3; this was then rehydrated by exposure to an atmosphere of 20% relative humidity with periodic weighing as before. The rate of uptake of water was steady at around 0.4 mg (g dry sample)$^{-1}$ h^{-1} for the first 12 days, after which the sample was still not at equilibrium and had adsorbed 120 mg H_2O per gram of dry sample. After exposure to the open atmosphere for a further 12 days, the sample reached an equilibrium water content of 147 mg/g. The lower final uptake of water compared with the sample discussed earlier could

be due to the shorter heating time employed, suggesting that changes occur after prolonged heating which increase the sample's hydrophilicity.

4. Effect of Dehydration and Rehydration on the Zeolite Lattice

As mentioned in Section A, it has generally been assumed that dehydration has little effect on the zeolite lattice. Any changes which do occur in the lattice should be visible in the ^{1}H, ^{29}Si and ^{27}Al NMR spectra of the sample. One may envisage a scenario in which, during drying, Al atoms might be lost from the lattice, leaving SiOH nests at the vacancies which immediately heal or condense to form new SiOSi linkages. This change would be visible in the ^{29}Si spectrum as a diminution of the intensities of low–Q^n peaks (*i.e.* an increase in the lattice Si/Al ratio); the ^{27}Al spectrum would show an increase in the intensity of the octahedral (0 ppm) peak after rehydration (this would not be visible before rehydration, since ^{27}Al spectra cannot be obtained from dry materials). In the ^{1}H spectrum, there may be a certain amount of SiOH and AlOH visible while dry, but these might be expected to be unobservable after rehydration, as in the original materials, unless they are highly abundant.

NMR measurements carried out on various dried and rehydrated samples of HY do indeed show that some largely irreversible changes take place on drying. ^{29}Si is the only one of the three nuclei studied here for which the NMR spectra of wet and dry materials are directly comparable (although the signal–to–noise ratio obtained from dried samples is poorer because the Kel–F rotor inserts have a smaller internal volume than the normal rotors). This provides a useful indication of the changes taking place in the lattice during the drying part of the dehydration–rehydration process. Figure 5.12 shows the ^{29}Si single–pulse spectrum of the original HY (as in Figure 5.5(a)), plus the spectra of

Figure 5.12: ^{29}Si SP MAS spectra of HY wet and dry with Gaussian deconvolutions (a) hydrated RD=60s NT=1000 RO=3130Hz
(b) HY–2 dry RD=20s NT=3100 RO=1029Hz
(c) HY–18 dry (VXR) RD=10s NT=22400 RO=2120Hz

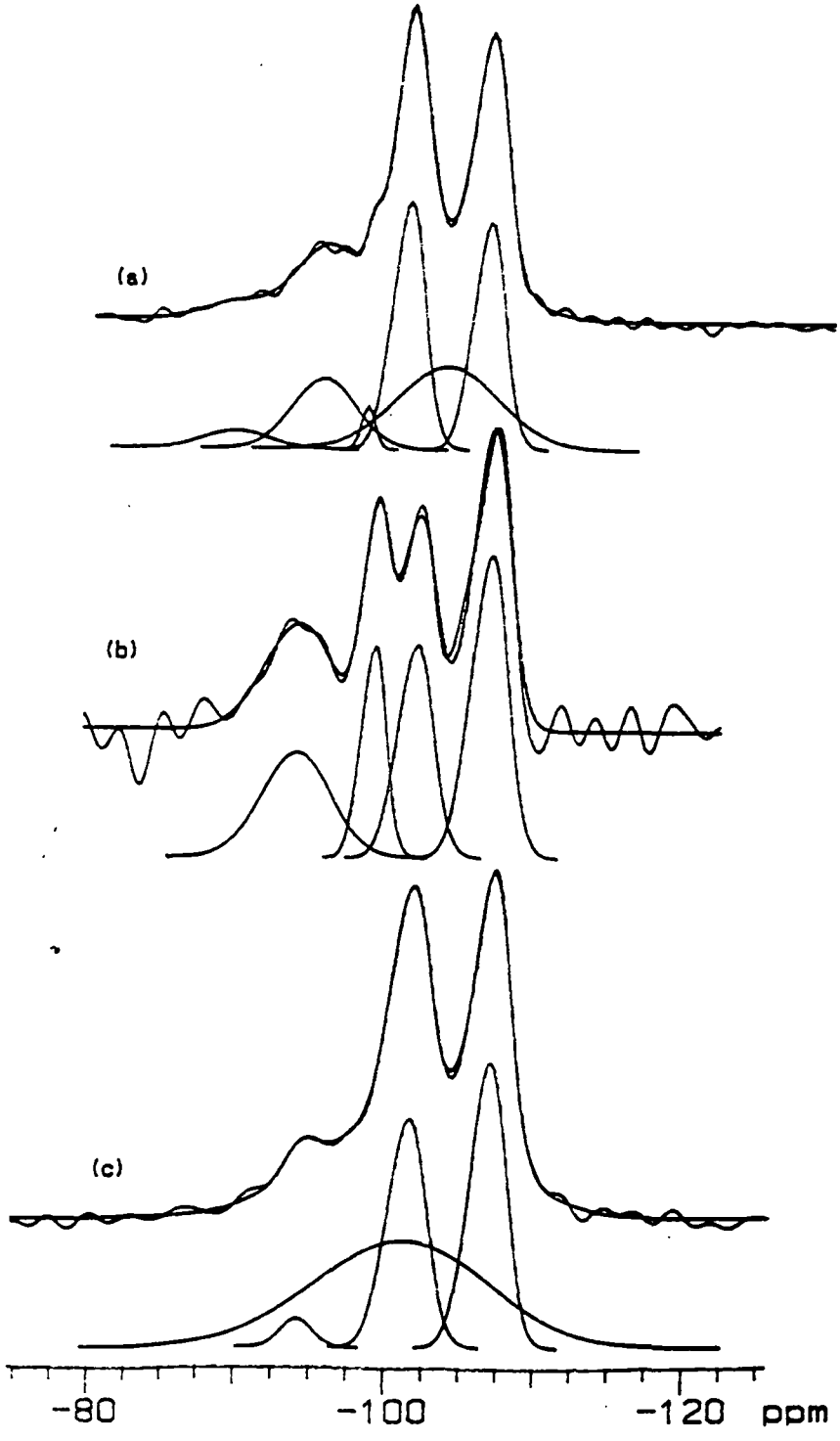

two dried samples, HY–2 and HY–18 (see Chapter 3 and Appendix B for a description of the nomenclature). These samples were both dried by heating to 400^{o}C under vacuum in a bed depth of approximately 10 mm, holding for 72 h in the case of HY–2, and 17 h for HY–18; then the samples were cooled under vacuum and packed into the MAS rotors under dry N_2. The spectrum of HY–2 (trace (b)) broadly resembles that of the untreated material (a) except in the appearance of an unusual extra peak in the Q^3 region. This may arise from the formation of Q^3 SiOH sites by loss of lattice Al. Deconvolution into four narrow Gaussian bands, taking both peaks close to –100 ppm as Q^3, yields an estimate for the Si/Al ratio of 4.59, which is *lower* than that found for the original material (5.23). However, there must be a substantial uncertainty margin on the lower value on account of the poor signal–to–noise ratio of the spectrum. If the higher–frequency Q^3 peak (–99.0 ppm) is assumed to arise solely from SiOH and neglected from the calculation, the Si/Al ratio obtained is 4.74. Similar omission of the low–frequency peak (–101.9 ppm) yields a value of 4.82. The rather small differences between these three estimates may suggest that the presence of Q^3 SiOH in the ^{29}Si single–pulse spectrum does not greatly perturb the Si/Al ratio calculation. The low figures obtained for the dried sample could arise from the presence of Q^2 SiOH superimposed on the Q^2 SiOAl band.

The spectrum of HY–18 shown in Figure 5.12(c) (acquired on the VXR–300 spectrometer) has a better signal–to–noise ratio, but shows no sign of the splitting; this suggests that the longer heating time used in the preparation of HY–2 may be required to develop the lattice changes observed. Acceptable deconvolution of this spectrum requires the inclusion of a broad peak, underlying the others, centred on –101.0 ppm, which accounts for 48% of the total intensity of the spectrum. If this component corresponds to amorphous material displaced from the lattice, the drying process must dislodge 11% of lattice T–atoms in

addition to those lost in the calcination step used to make the HY sample, which yielded an amorphous content of 37% (as quoted in Section B). Estimation of the Si/Al ratio of the lattice from the other three peaks yields a value of 7.59, well above that for HY (5.23), providing a further indication of the loss of lattice atoms and, presumably, annealing of the vacancies. The rise in Si/Al ratio implies a change from 30.8 to 22.4 lattice Al atoms per unit cell, a loss of 8.4/u.c. The total loss of lattice T–atoms is 11% of all Si and Al present, *i.e.* 21.1 per unit cell. Thus, there is at least as much Si lost from the lattice as Al, although the Al is still displaced selectively (the ratio of Si to Al atoms displaced is about 1.5).

The ^{29}Si CP/MAS spectra of dried HY samples (not shown) strongly resembles those obtained from the wet material, except that contact times generally need to be longer, with peaks still growing in intensity after 20 ms of contact between spins. It has been suggested in the literature (see Section A of this Chapter and of Chapter 4) that samples rich in SiOH groups should experience significant enhancement of the lower–Q^n peaks in ^{29}Si CP/MAS spectra; no evidence of this phenomenon has been seen in dried HY samples (eight separate samples have been studied). However, the Q^3 peak is frequently observed to be substantially broader than the Q^4; this may arise from the same origin as the splitting shown in Figure 5.12(b).

^{1}H NMR Spectra. The ^{1}H spectra of dried samples are only comparable with the starting material after rehydration, since the principal species visible therein is water. (^{1}H spectra of dry samples are presented and discussed in Section D and Chapter 6.) The spectra of many samples show an overall change after drying and rehydration, as reported by other workers.[28] The ^{1}H spectra of all samples which were rehydrated are shown in Figure 5.13, along with the starting material (as in Figure 5.5(c)). All samples were dried under vacuum at 400^{o}C with a 24

Figure 5.13: ^{1}H SP MAS spectra of HY wet and dry

(a)	hydrated	RD=200ms NT=32 RO=3000Hz
(b)	HY–3 dry	RD=500ms NT=128 RO=2507Hz
(c)	HY–5 dry (CXP–300)	RD=5s NT=64 RO=3000Hz
(d)	HY–7 dry	RD=5s NT=128 RO=2223Hz
(e)	HY–23 dry	RD=3s NT=100 RO=1000Hz

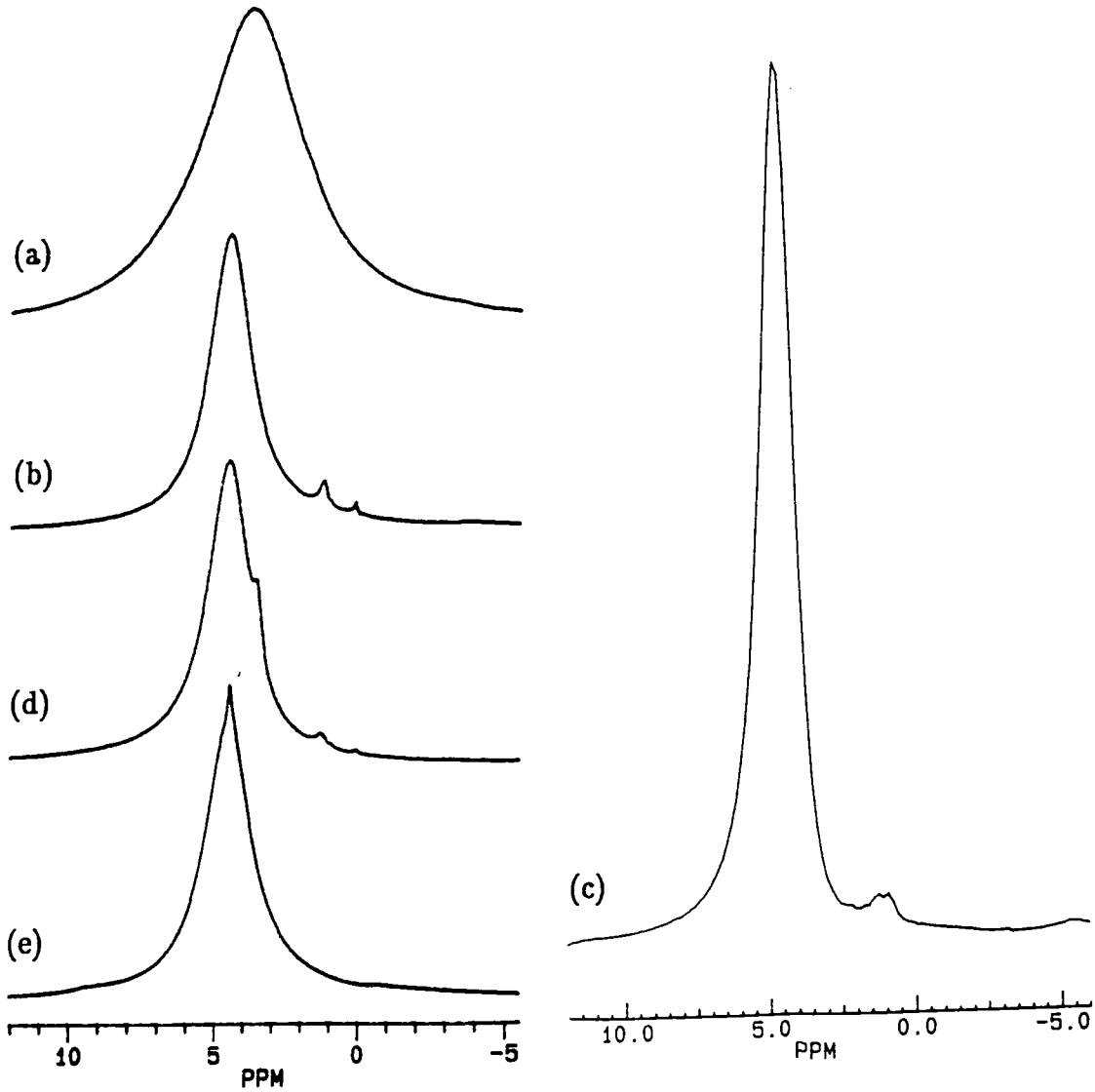

hour hold time for all except HY–23, which was heated under vacuum to 400^{o}C and then cooled immediately. The samples were rehydrated as follows: HY–3, 15% RH atmosphere only; HY–5, 15% RH atmosphere for 12 days, then in the open laboratory; HY–7, 23% RH atmosphere only; and HY–23, open laboratory only.

The spectra of all the samples which were rehydrated initially under controlled conditions show the appearance of peaks assigned to SiOH groups at 1.1 ppm and, in HY–3 and HY–7, a peak at 0.0 ppm. The SiOH groups might occur at newly–created lattice vacancies, or be formed by the hydrolysis of strained –O– linkages at previously existing defects. In the light of the evidence already presented for loss of lattice T–atoms during drying, the former proposal seems plausible. The sample rehydrated only under uncontrolled conditions (HY–23) shows no signal due to SiOH, but clearly exhibits two–phase character in the water peak: there is a smaller, narrow peak superimposed on the main broader signal. This is reminiscent of the spectra of NaY–ex and AgY–ex presented in Figures 5.7(b) and 5.8 respectively, although in the present case there is little sign of a chemical shift difference between the two peaks (except perhaps in HY–7, trace(d)). This adds further weight to the suggestion made in Section B that any shift difference arises from differing degrees of interaction between water and the cation in the two cages. The absence of any SiOH signal in this sample suggests that the new defects form relatively slowly during the hold at 400^{o}C.

Figure 5.14 shows the ^{1}H spectrum of AgY–ex after drying and rehydration in an 85% RH atmosphere (sample name: AgY–ex–68). This spectrum differs from that of the untreated material (Figure 5.8) in the absence of the two–phase water peak. This may be attributed to enhanced mobility of the Ag^{+} cations during the heating. A newly–formed SiOH peak is also visible

at 1.6 ppm, whilst the water peak is at 5.1 ppm, 0.4 ppm to high frequency of its usual position in HY, suggesting a Lewis acid–Lewis base interaction between Ag^+ and water. The previous 2.3 ppm peak has also disappeared, or perhaps shifted to form the peak at 1.6 ppm.

Effect of Heating HY at Atmospheric Pressure. As a demonstration that high temperature *and* vacuum conditions are required to dry a sample of HY fully, two portions were heated in an oven under atmospheric pressure. The first, denoted HY–71, was heated at 60^oC for 18 hours, then packed for MAS while hot and allowed to cool in the rotor before measurement of the ^1H spectrum. The second (HY–72) was treated similarly, with heating at 200^oC for 45 hours. The ^1H MAS spectra are shown in Figure 5.15(a) and (b). Sample HY–71 shows almost no change from the wet material, except a shift of the water peak 0.7 ppm to lower frequency. HY–72 shows a further shift to 1.9 ppm to low frequency of the original position, plus the appearance of intense spinning sidebands (not shown), suggesting that the remaining water is greatly reduced in mobility. The low–frequency shifts may arise from interaction with NLA: in HY–72, the peak position (2.9 ppm) is close to that normally assigned to AlOH, which generally also shows intense spinning sidebands; therefore, possibly the remaining water molecules in the sample are largely in a dissociated state attached to NLA. There is also a shoulder at around 6.5 ppm, which is similar to signals discussed in Chapter 7 and may be assigned to water strongly interacting with Lewis–acidic sites. Rehydration of HY–72 yields the spectrum shown in Figure 5.15(c), which is similar to the starting material shown in Figure 5.5(c) (the band observed here is a little narrower). Clearly, then, any changes which occurred under the mild conditions used are substantially reversible; in particular, no dealumination of the lattice has taken place.

Figure 5.15: ^{1}H SP MAS spectra of HY oven–dried
(a) HY–71 (60° C) RD=3s NT=32 RO=3010Hz
(b) HY–72 (200° C) RD=2s NT=100 RO=3000Hz
(c) HY–72 rehydrated RD=3s NT=32 RO=3035Hz

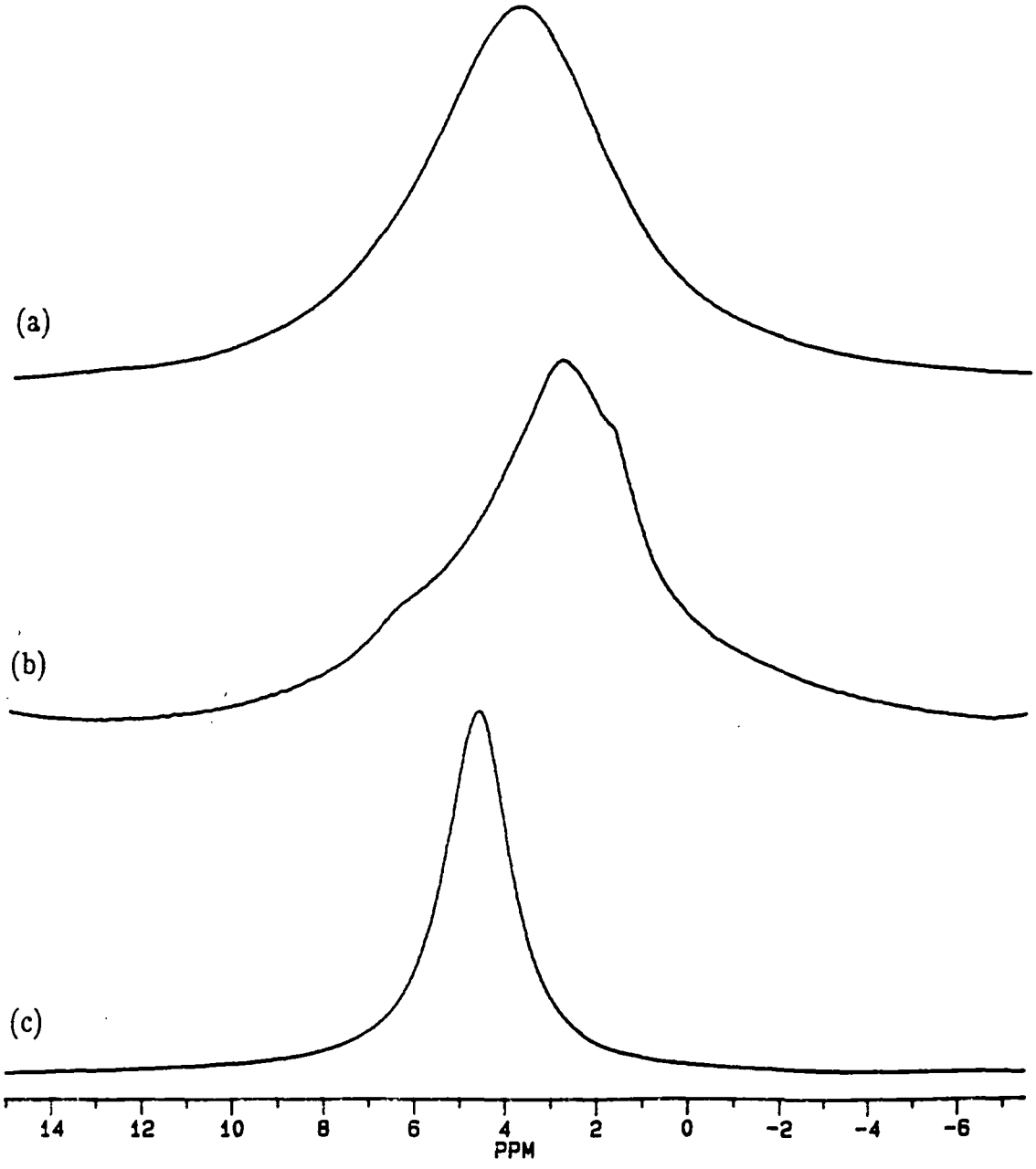

Figure 5.16: Spectra of HY–62 rehydrated
(a) ^{1}H SP MAS RD=3s RO=4485Hz NT=32
(b) ^{27}Al SP MAS RD=200ms RO=4485Hz NT=5000 PA=3π/40

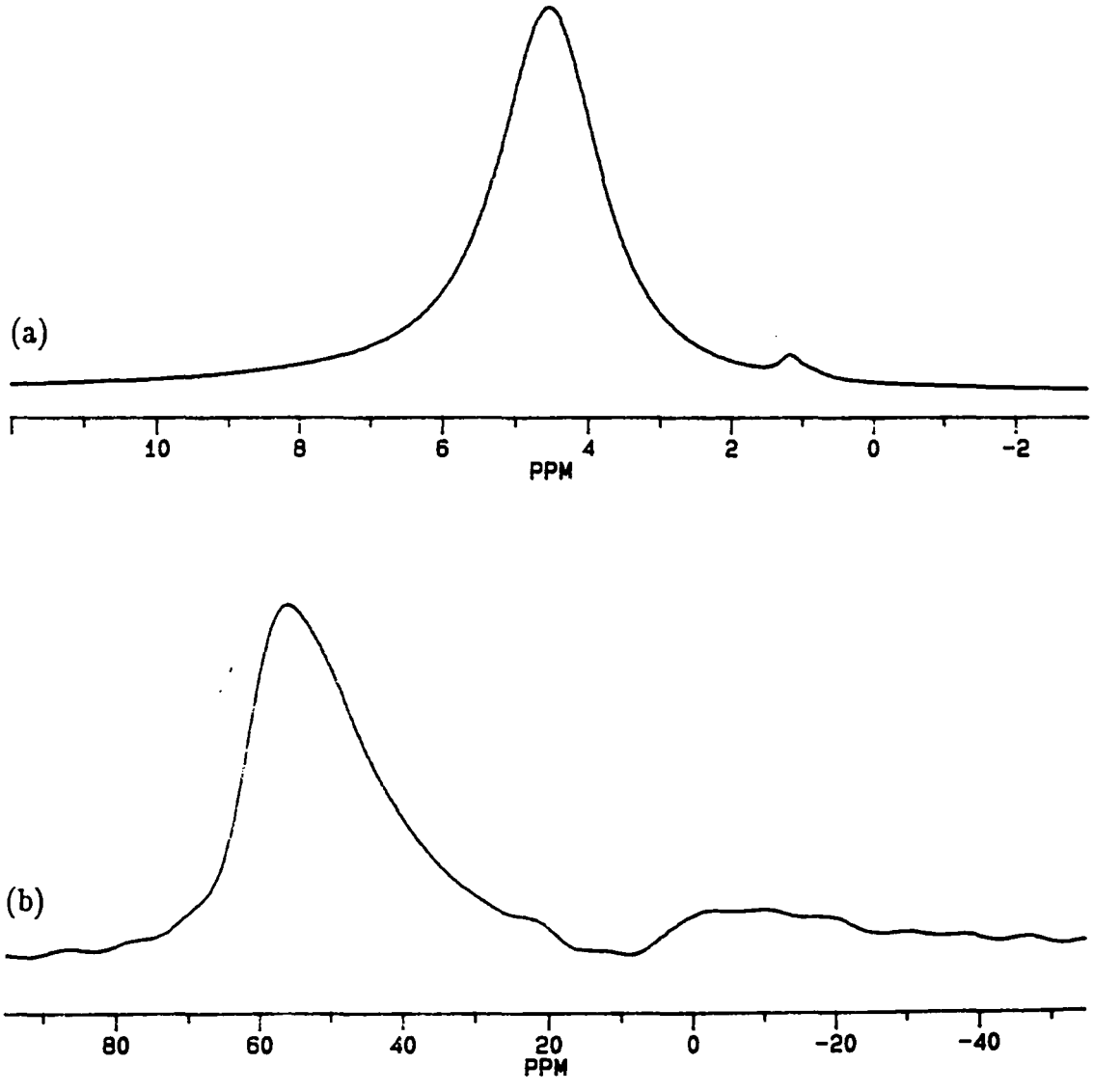

Multinuclear Studies of Dried and Rehydrated HY. A sample of HY was dried by heating to 400^{o}C for 4 hours under vacuum, then rehydrated in an 85% RH atmosphere to form HY–62. The ^{1}H and ^{27}Al spectra of the rehydrated material are shown in Figure 5.16. The ^{1}H spectrum, obtained after 3 days of rehydration, shows the familiar, Lorentzian water peak close to its normal position at 4.5 ppm, plus a significant SiOH signal at 1.1 ppm. The ^{27}Al spectrum shows a slightly enhanced concentration of octahedral Al, presumably freshly displaced from the lattice, by comparison with the starting material (Figure 5.5(f)). Deconvolution of the ^{27}Al spectra of the starting and final samples shows that the octahedral Al content rose from 3.0% to 10.5% of the total Al population. It is to be suspected that a substantial amount of tetrahedral NLA exists in addition to the octahedral material, since it has already been suggested that drying and rehydration of sample HY–18 generated 8.4 new non–lattice Al atoms per unit cell (much more than 10.5% of the total Al population).

Another sample, HY–66, was prepared in a similar manner, except that it was kept hot for slightly longer during the drying procedure. The ^{1}H spectra of rehydrated HY–66 obtained after 1 and 14 days of rehydration are shown in Figure 5.17. The SiOH peak only appears (weakly) in the latter. This suggests that the process of hydrolysis by which the SiOH groups are formed from SiOSi or SiO–$Al_{non-lattice}$ linkages is slow. ^{29}Si and ^{27}Al spectra of this sample (not shown) also suggest that the changes occurring in the lattice were very slight by comparison with those observed in HY–62. The shift to high frequency of the water peak between traces (a) and (b) implies an increased interaction between Lewis–acidic sites and water in the older sample.

Top: Figure 5.17: ^{1}H SP MAS spectra of HY–66 rehydrated
(a) 1 day old RD=3s NT=64 RO=4510Hz
(b) 14 days old RD=3s NT=32 RO=1648Hz

Bottom: Figure 5.20: ^{13}C CP/MAS spectrum of HY–32
RO=3040Hz NT=41900 RD=2s CT=5ms Transmitter Offset=6kHz

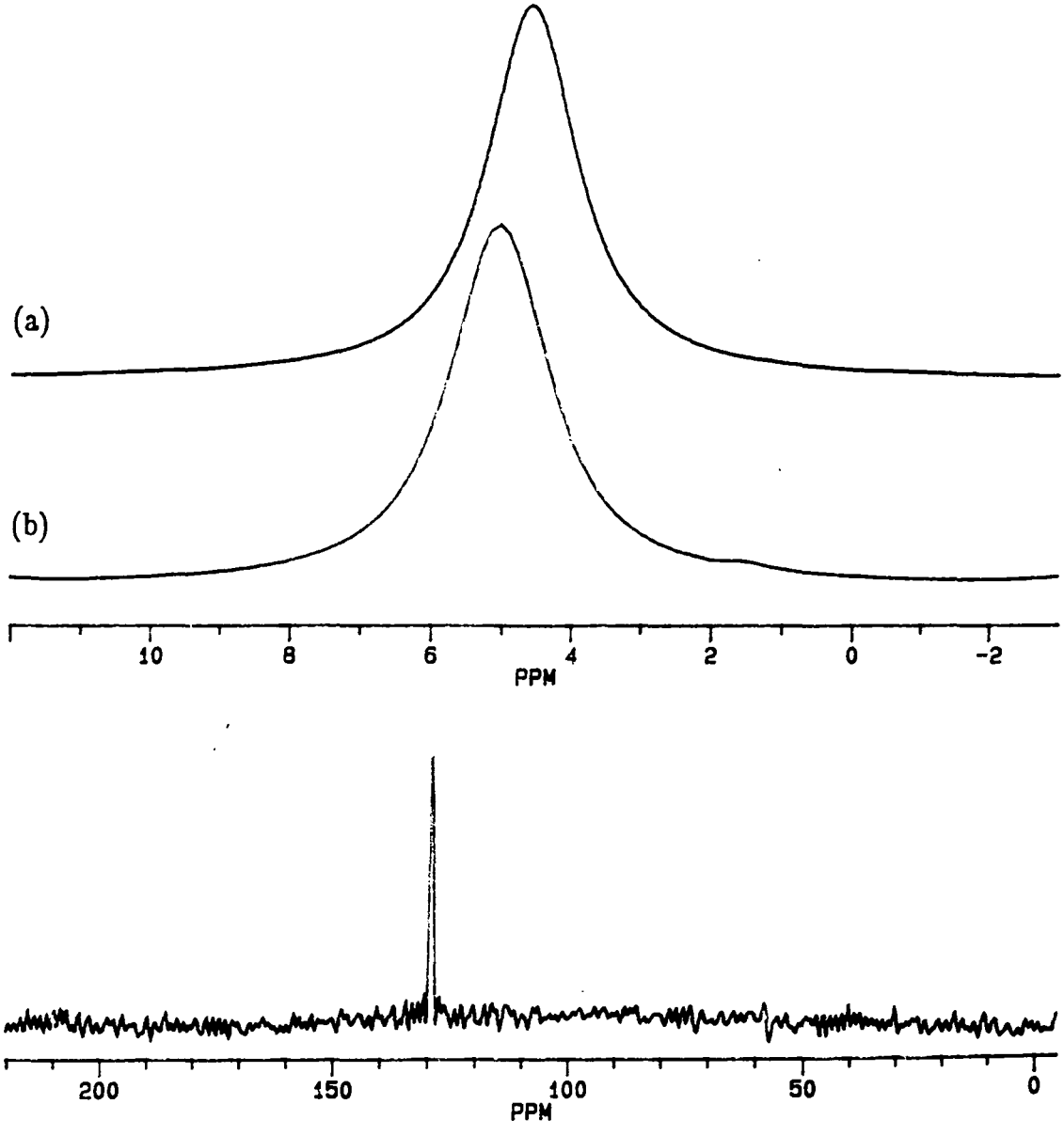

5D: ^{1}H NMR STUDIES OF FULLY DEHYDRATED HY

One of the principal aims of the research presented in this thesis was to develop a reliable procedure for preparing dehydrated samples of zeolites and to demonstrate that useful information can be derived from the study of these samples by magic–angle–spinning NMR. The following pages discuss the results obtained from some of the sixty–eight samples prepared using the technique described in Chapter 3. It is shown here that, with suitably careful sample–handling methods, exceptionally well–resolved ^{1}H NMR spectra of dried samples can be obtained. Then the assignment of the peaks and their relaxation times are considered. Finally, deconvolution techniques are employed to permit estimation of the concentrations of individual ^{1}H–containing species in the samples; the information gained is used to throw further light on the changes occurring in the lattice during degradation. Chapter 6 follows directly from this Section, discussing the influence of subtle changes in handling procedures on the ^{1}H–containing species present, with particular consideration of the non–lattice alumina.

All samples are identified as before by the nomenclature HY–x, where x is an experiment number. The details of the preparation procedures used are given in the text where appropriate, and are listed in detail in Appendix B.

1. Signal Assignments

Figure 5.18 shows a collection of ^{1}H MAS–NMR spectra of dried HY samples in Kel–F capsules, as described in Chapter 3. The success of the handling procedure in achieving thoroughly dry, well–defined samples is apparent. The resolution in many of the spectra far exceeds that of any

Figure 5.18: ^{1}H SP MAS spectra of HY dried

(a)	HY–4	RD=500ms NT=128 RO=4004Hz
(b)	HY–14	RD=2s NT=128 RO=3003Hz
(c)	HY–26	RD=5s NT=32 RO=2988Hz
(d)	HY–27	RD=2s NT=48 RO=2720Hz
(e)	HY–29	RD=5s NT=48 RO=3000Hz
(f)	HY–41	RD=5s NT=128 RO=3040Hz
(g)	HY–54	RD=3s NT=100 RO=3000Hz
(h)	HY–58	RD=3s NT=100 RO=2994Hz

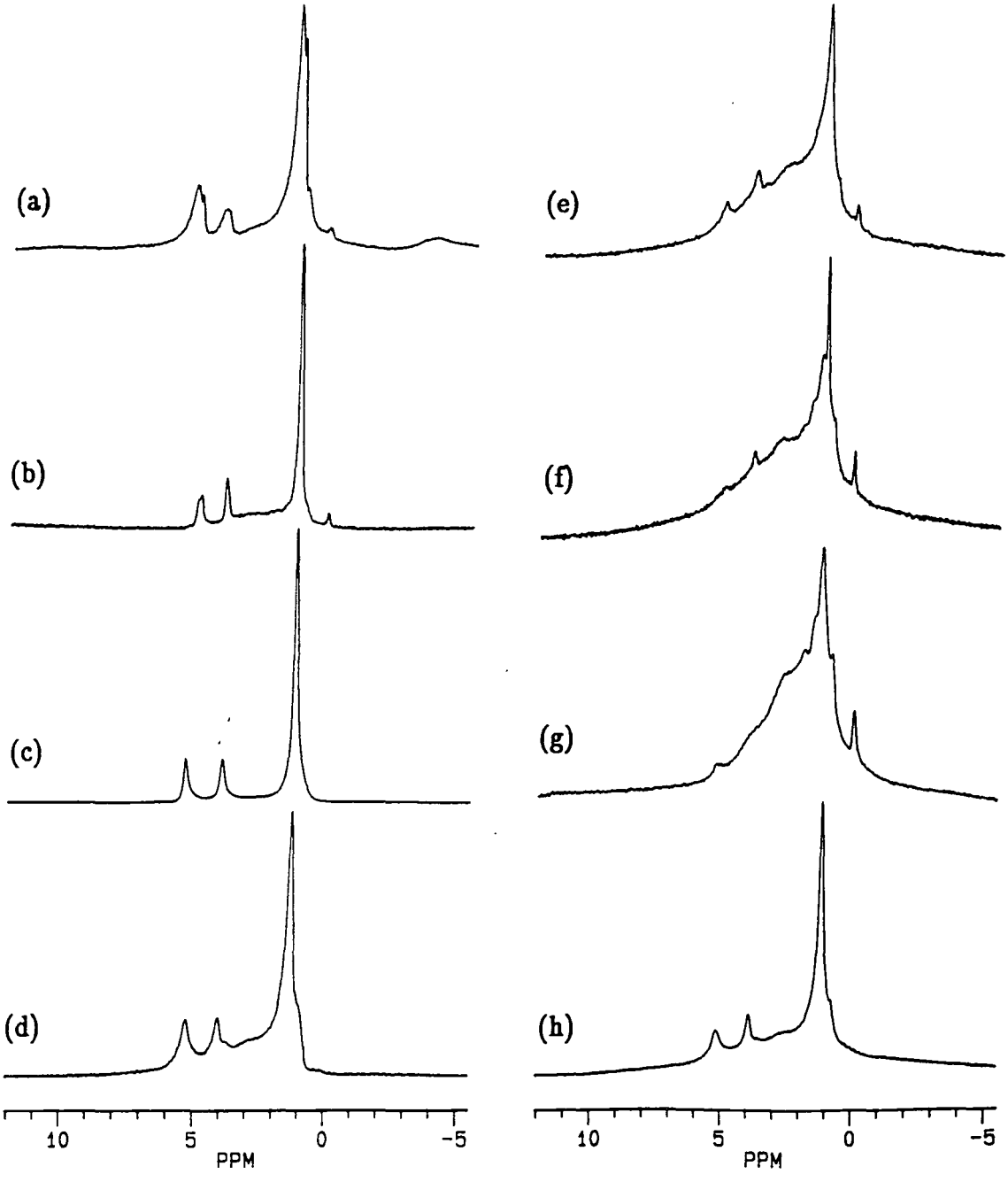

previously published. It was not possible to obtain CRAMP spectra of dried samples because the rotors used with the CRAMPS probe were too small to accommodate the Kel–F inserts; attempts were made to obtain spectra by filling the CRAMPS rotor with a freshly–dried sample in an inert atmosphere, but without success.

Several common features are observable in some or all of the spectra in Figure 5.18. Most show signals at 4.0 and 5.2 ppm, which are often quite narrow. These are assigned to Brönsted acidic sites in large and small cages, respectively; the assignments have been verified by many workers, as discussed in Section A. Another common feature is the occurrence of a broad band, often underlying other peaks, usually centred on 2.3 ppm and accompanied by intense spinning sidebands (not shown), showing the presence of significant shielding anisotropy. The constituent peaks in this band, which may be deconvoluted by computer, are assigned to AlOH groups attached to, or H_2O strongly associated with, non–lattice alumina. Chapter 6 is devoted to further consideration of this signal. Two other common features remain: a cluster of narrow peaks at $1.0 - 1.3$ ppm, assigned to lattice SiOH groups, and an unassigned band very close to 0.0 ppm. This latter peak does not disappear when the transmitter frequency is varied by a few hundred Hertz, proving it to be a true NMR signal and not an artifact arising from the RF electronics. The only remaining signal is a weak, broad peak at around –4 ppm, which is visible only in HY–4 (Figure 5.18(a)). This peak is also seen in some spectra of dried AgY–ex and has been reported by other workers,[28] but there is no explanation available for it at present.

All the peaks, with the exception of the one at 0 ppm, show clear evidence that they are composed of several individual bands superimposed. This can be seen by eye for the Brönsted peaks in HY–4 (Figure 5.18(a)), HY–25 (c) and HY–27 (d), and for the SiOH peaks in HY–4 (a), HY–41 (f) and HY–54 (g)

for example; deconvolution results (presented later) show this to be true for the AlOH band also. It is easy to conceive of a range of local environments for each of these species, with variations possible in the local connectivity, next–nearest–neighbour Si/Al occupancy and twinning (geminal –OH groups) and H–bonding effects all possible, subject to varying geometry. For SiOH groups, substantially differing T_1 times can be observed in the same sample in the inversion–recovery experiment, as different component peaks invert after different recovery times.

The treatments by which the samples were prepared differ in terms of maximum temperature, time held at that temperature and rate of cooling. Detailed discussion of the influences of varying conditions are reserved for Chapter 6; it is clear, however, that the amount of AlOH visible varies substantially from one sample to another. Furthermore, consideration of the spectra in Figure 5.18 reveals two general trends concerning this. Firstly, the intensity and clarity of the Brönsted peaks is inversely related to the amount of AlOH visible. This may be seen by comparing HY–26 (c), which shows scarcely any AlOH, with HY–54 (g), where the AlOH is intense and the Brönsted peaks are virtually absent (they are barely detectable by deconvolution), whilst HY–58 (h) is an intermediate case. A possible explanation for this phenomenon is that samples such as HY–26 contain much less NLA than HY–54, and the NLA in the latter sample coordinates to Brönsted sites, deprotonating them. Another explanation is that there are similar amounts of NLA in both samples, but the NLA in HY–26 is highly condensed and polynucleated (therefore carrying few AlOH groups) and so has little unsatisfied Lewis acidity to interact with a deprotonated lattice Brönsted site. Evidence presented in Chapter 6 tends to favour the latter explanation. Another related observation is that the intensity of the unidentified peak at 0 ppm is also linked with that of the AlOH band;

comparison of HY–26 with HY–54 again shows this clearly, although there are exceptions, such as HY–27 and HY–58, in which the 0 ppm peak is very weak or absent whilst the AlOH band is clearly visible.

All the peaks in these spectra are significantly narrowed by magic–angle spinning, showing that there is a degree of residual dipolar interaction and/or shielding anisotropy in their environments. However, only the AlOH band exhibits spinning sidebands of greater intensity than 10% of the centreband. Spinning rates of 3 kHz (corresponding to 15 ppm at 200 MHz) were nearly always used to avoid the appearance of sidebands in the region of interest.

An attempt was made to measure the effect on the ^1H spectrum of adsorbing small, controlled quantities of D_2O and pyridine–d_5 on dried samples of HY. It was hoped that pyridine–d_5 would exchange with supercage Brönsted sites but not with small–cage ones, whilst adsorption of D_2O would be expected to destroy all signals associated with exchangeable ^1H, indicating whether SiOH and AlOH groups were susceptible to such exchange. The resulting spectra, however, show disappointingly little detail, except for an intense band in the AlOH region; it is suspected that the vacuum line used for the controlled adsorption was insufficiently airtight to prevent ingress of atmospheric water whilst the line was shut off from the vacuum pump.

2. Hydrocarbon Contamination

Figure 5.19 shows a further selection of ^1H MAS spectra of dried HY samples. These spectra differ from those shown in Figure 5.18 in that they all contain a signal at 7.4 ppm. In some samples (HY–35, HY–36) this signal coexists with the Brönsted peaks, whereas in others, when the 7.4 ppm peak is generally more intense, the Brönsted signals are absent. The fact that there appears to be little relation between the intensity of this new signal and that of

Figure 5.19: ^{1}H SP MAS spectra of dried HY contaminated with hydrocarbon sorbate

(a) HY–18 RD=5s NT=128 RO=3010Hz
(b) HY–30 RD=5s NT=48 RO=3000Hz
(c) HY–35 RD=2s NT=32 RO=1540Hz
(d) HY–36 RD=10s NT=32 RO=3000Hz
(e) HY–40 RD=3s NT=128 RO=3040Hz

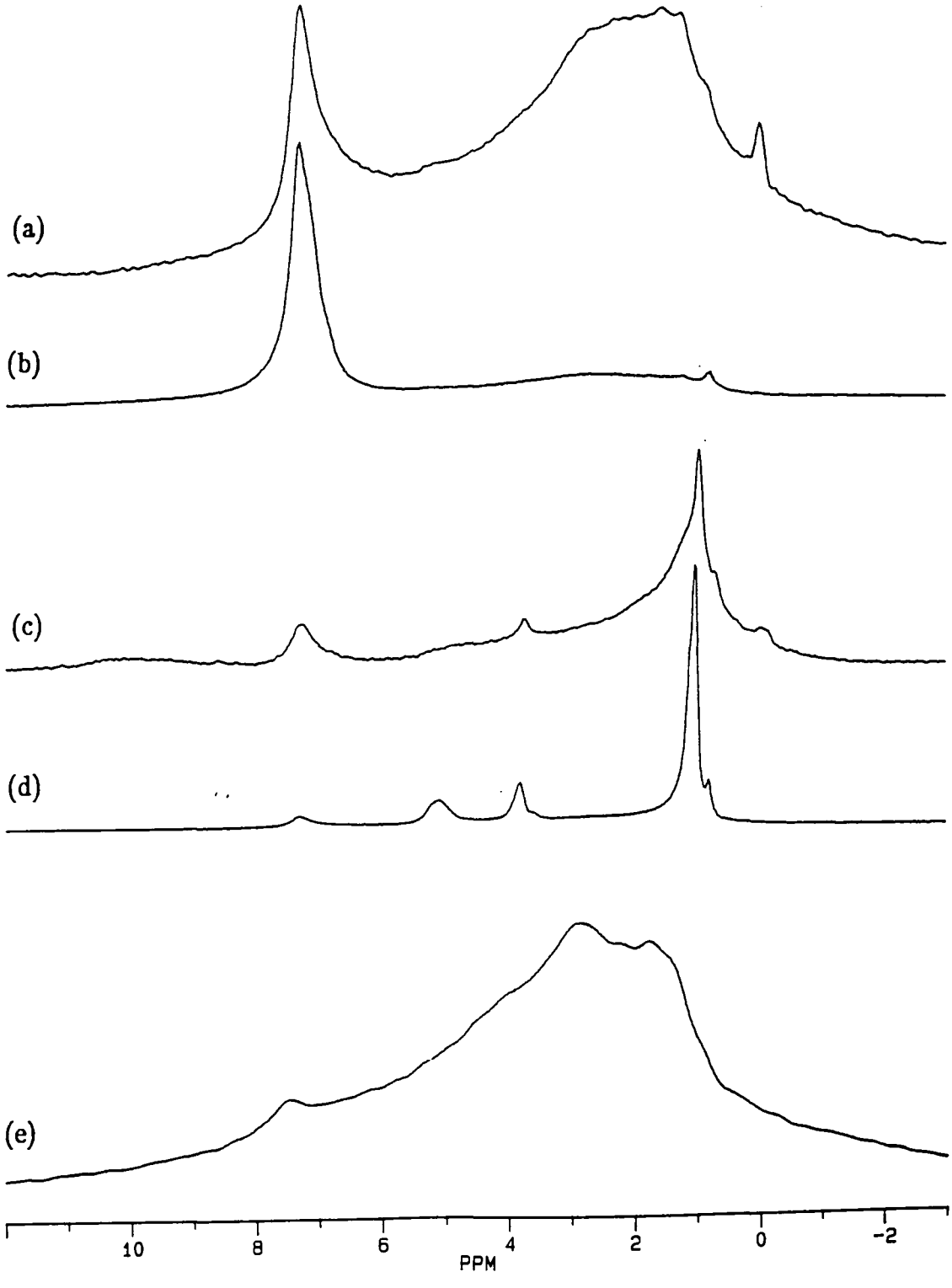

the AlOH groups tends to suggest that the peak does not represent the superacid sites often proposed (see Chapter 4) but never reported in the ^{1}H spectrum. Consideration of the methods of preparation of the samples shown in Figures 5.18 and 5.19 reveals that, after drying at high temperature under vacuum, all samples in Figure 5.18, which do not exhibit the new peak, were cooled in a closed tube; by contrast, those in Figure 5.19, which all show the new peak, were cooled under a 'live' vacuum – that is, whilst connected to the vacuum line and pumped. It is therefore proposed that the new signal arises from adsorption of (possibly aromatic) hydrocarbons present in the vacuum pump oil, either as part of its composition or as a contaminant from an earlier experiment. It was found that the peak did not appear when the trap on the vacuum line was immersed in liquid air during cooling of the sample (a dry ice/acetone slush was, however, insufficient to trap the contaminant). This procedure had not normally been used because heating and cooling operations were carried out automatically overnight. The Brönsted peaks were observed to be absent in all spectra containing an intense hydrocarbon signal (only two of several such samples made are shown in Figure 5.19); this suggests that the hydrocarbon chemisorbs on Brönsted sites. All other species are clearly unaffected by its presence (see HY–18, trace (a)).

A ^{13}C CP/MAS spectrum was obtained from another contaminated sample known as HY–32. The ^{1}H spectrum of this sample is not shown but strongly resembles that of HY–30 (Figure 5.19(b)), containing an intense hydrocarbon peak and little else. The ^{13}C CP/MAS spectrum (Figure 5.20) is very weak; over 40,000 averages were required to obtain even the poor signal–to–noise ratio observed. There is a clear peak at 129.0 ppm which appears to be genuine (neither background nor artifact). There is no background signal. No signal was observed in the absence of cross–polarization.

Figure 5.21: ^{29}Si SCP spectra of HY–18 (CXP–300)

(a) Normal CP/MAS (scale x $\frac{1}{4}$)
CT=4ms NT=1000 RO=2731Hz RD=2s

(b) SCP hydrocarbon–annulled
NT=10000

(c) SCP AlOH–annulled
NT=10000

(d) SCP, non–selective nulling time
NT=10000

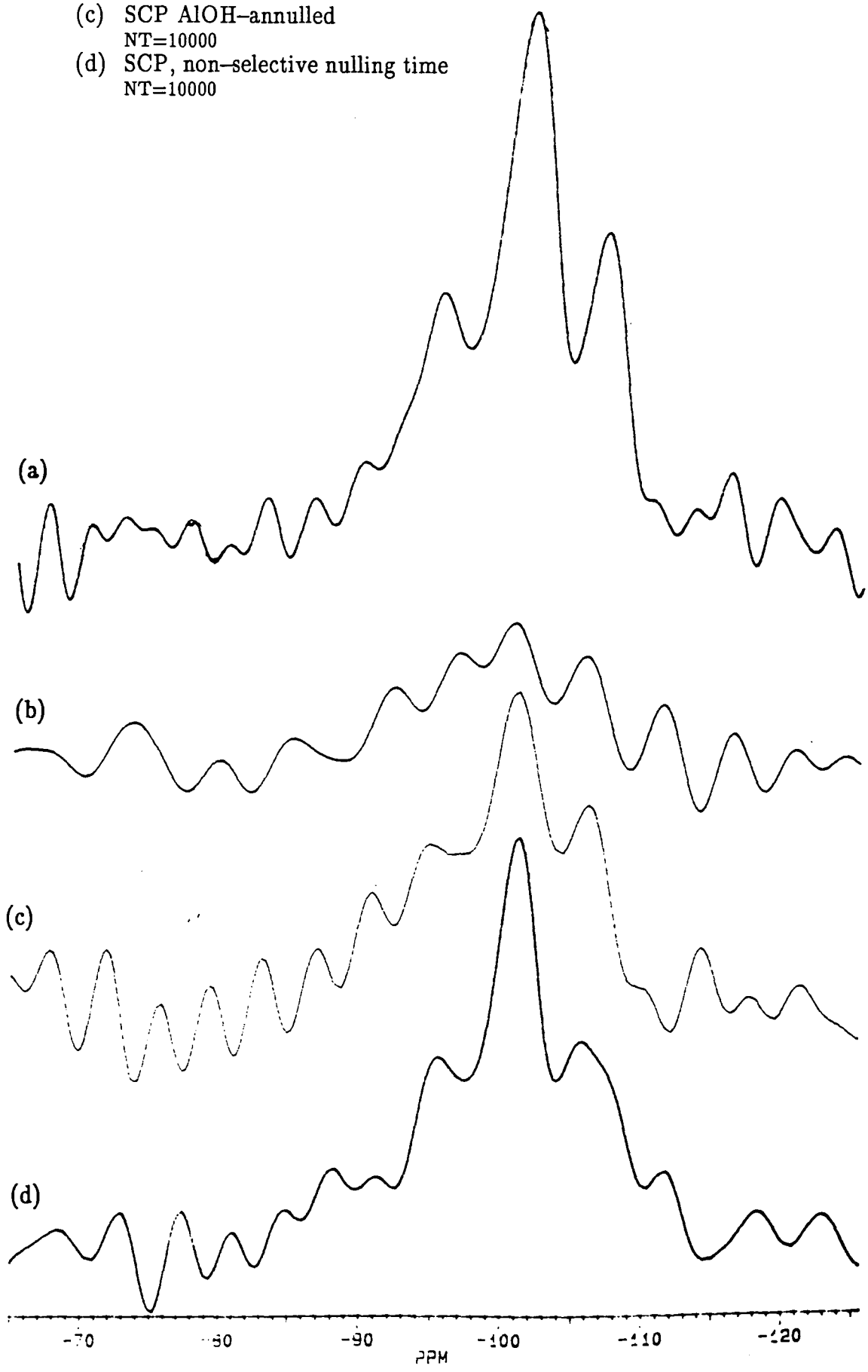

In addition, a ^{29}Si selective cross–polarization (SCP) experiment was carried out on HY–18. The ^{1}H spectrum of this sample appears in Figure 5.19(a) and shows two major signals: hydrocarbon and AlOH. Figure 5.21 shows the results of the ^{29}Si SCP experiment, with the normal CP/MAS spectrum in trace (a) (scaled down by a factor of four), the spectrum obtained after annulment of the hydrocarbon ^{1}H magnetization in trace (b), that obtained after annulment of AlOH magnetization in trace (c), and that after a non–selective (100 μs) nulling time in trace (d). The weakness of the signal in trace (b) clearly shows that the hydrocarbon ^{1}H nuclei contribute substantially to CP in lattice ^{29}Si, whereas those in AlOH do not. This suggests that the hydrocarbon is largely immobilized on lattice Brönsted sites, whereas the association between the NLA and the lattice is weak in this sample. The ^{29}Si spectroscopy in this experiment was carried out on the CXP–300 instrument at Unilever Research Port Sunlight Laboratory.

3. Relaxation Times

The ^{1}H relaxation times of many dried HY samples have been measured using MAS to resolve the peaks. T_1 and $T_{1\rho}$ were measured on the CXP–200 at 200 MHz and 62.5 kHz respectively. T_2 values were measured on the WRAC at 60 MHz without MAS.

The T_1 values obtained are collected in Table 5.4. Although there is much variation, some general trends can be discerned. The Brönsted–acidic ^{1}H nuclei (5.2 and 4.0 ppm) usually have T_1 relaxation times of around $200 - 300$ ms and $300 - 500$ ms respectively. The T_1 of the small–cage site (4.0 ppm) is always the higher, suggesting less local motion (of remaining sorbates, SiOH groups, NLA *etc.*) and is also more variable, suggesting that it is more sensitive to the preparation treatment; this is plausible in view of the fact

Table 5.4: ^{1}H Spin–Lattice Relaxation Times (T_1) of Dried HY Samples at 200 MHz in ms

Sample	Chemical Shift of Signal/ppm					
	7.4	5.2	4.0	2.3	1.0	0.0
HY–4		278	487		528	≃500
HY–14*		230	494		[474] [130]	>700
HY–18	134				141	1090
HY–26		226	299		258	
HY–27		304	741		871	
HY–29		≃170	≃300	≃200	≃300	≃300
HY–30	215	371	≃720		≃170	
HY–35	216		93		198	
HY–40	61			152	150	
HY–58		188	283		264	

*This sample has two distinct components for the SiOH band at 1.0 ppm.

that any remaining adsorbates are more likely to be located in the small cages and so the environment of small–cage Brönsted sites will vary more widely than those in large cages. The SiOH groups show even greater variability, presumably being highly sensitive to the proximity of NLA. Some of the variability can be explained by noting from Table 5.4 that all SiOH with T_1 values below 250 ms occur in samples contaminated by hydrocarbons; the sorbate presumably enhances SiOH ^{1}H relaxation by means of its intramolecular motions whilst bound to a nearby Brönsted site. The 0 ppm species exhibits some very long T_1 times in certain samples. Not surprisingly, all the T_1 times observed in dry samples are much longer than those found in wet zeolites; it may be that the

Figure 5.22: Relaxation curves obtained from inversion–recovery measurement of HY–4: the crosses are experimental data, whilst the continuous line is the best–fitting exponential curve. Top: 5.2 ppm Brönsted peak; middle: 4.0 ppm Brönsted peak; bottom: SiOH peak. The vertical scale is in arbitrary intensity units.

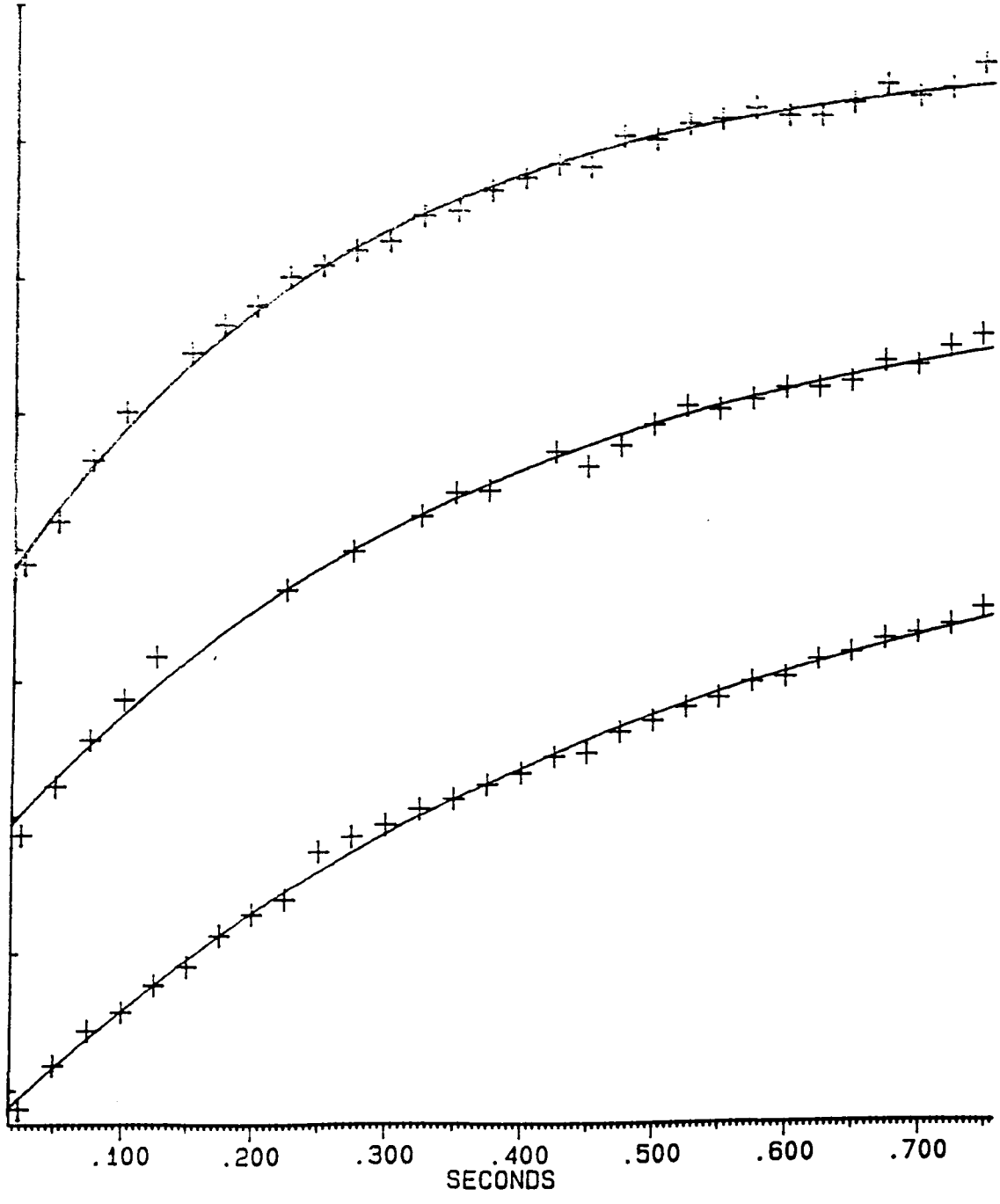

general level of T_1 values in a given sample could be used as an assessment of its dryness. Figure 5.22 shows some T_1 relaxation measurements obtained from HY–4, as an example to demonstrate the typical quality of the experimental data and fitted curves.

The $T_{1\rho}$ values observed, collected in Table 5.5, show much greater variability than the T_1 values; again, however, lower times are generally observed in contaminated samples, due to molecular motions of the sorbate.

The T_2 times, which were obtained without MAS, cannot be directly related to individual resonances in the MAS spectrum. The measured values are presented in Table 5.6, shown as population (as a percentage of the total in each sample) with T_2 values close to the centre of given bands. Figure 5.23 shows the deconvolution plots arising from measurement of T_2 in sample HY–24 (see Section C for a discussion of this type of plot). Generally the values within each band deviate from the central value by less than 15%. Of the samples shown, only HY–24 and HY–25 were contaminated; it is reasonable to assume that the most intense component, at 15 ms in both samples, arises from the contaminant. The short (0.2 ms) component in all samples except HY–25 and HY–26 may be assigned to AlOH on the grounds of its high intensity and the observation that the corresponding signal in the MAS spectrum must be very broad. The amount of AlOH observed in the MAS spectrum of all the samples listed shows a qualitatively good correlation to the percentage populations quoted for this component, except HY–14, which has rather little AlOH visible. Other components present must, by elimination, arise from SiOH, Brönsted and 0 ppm species. Of the samples listed in Table 5.6, only HY–4, HY–13 and HY–14 show the 0 ppm signal; in conjunction with the findings discussed earlier that its T_1 relaxation time is generally long, and that the signal is narrow and weak, we may perhaps assign the 35 and 52 ms components in HY–4 and HY–13 to it. Only

Table 5.5: ^{1}H Relaxation Times ($T_{1\rho}$) of Dried HY Samples at 62.5 kHz in ms

Sample	Chemical Shift of Signal/ppm					
	7.4	5.2	4.0	2.3	1.0	0.0
HY–4		40	52		69	
HY–18	70				≃27	≃30
HY–26		54	50		51	
HY–29				5.6	30	≃37
HY–30	8.1	≃15	≃11		≃10	
HY–35	8.0		≃7		≃10	
HY–41			≃60			

Table 5.6: ^{1}H Transverse Relaxation Times (T_2) of Dried HY Samples at 60 MHz

shown as % of total ^{1}H population within each band of T_2 values

Sample	Approximate T_2/ms						
	52	35	15	6	3	1.5	0.2
HY–4		4%		14%		28%	54%
HY–13	Trace				10%		90%
HY–14				40%			60%
HY–23			33%		23%		45%
HY–24†			55%			18%	26%
HY–25†			79%		21%		
HY–26		36%			27%		37%

Figure 5.23: Deconvolution and residue plots obtained from T_2 measurement of HY–24. On the residue plot, the horizontal axis is the same as that on the deconvolution plot, whilst the vertical axis is in arbitrary intensity units.

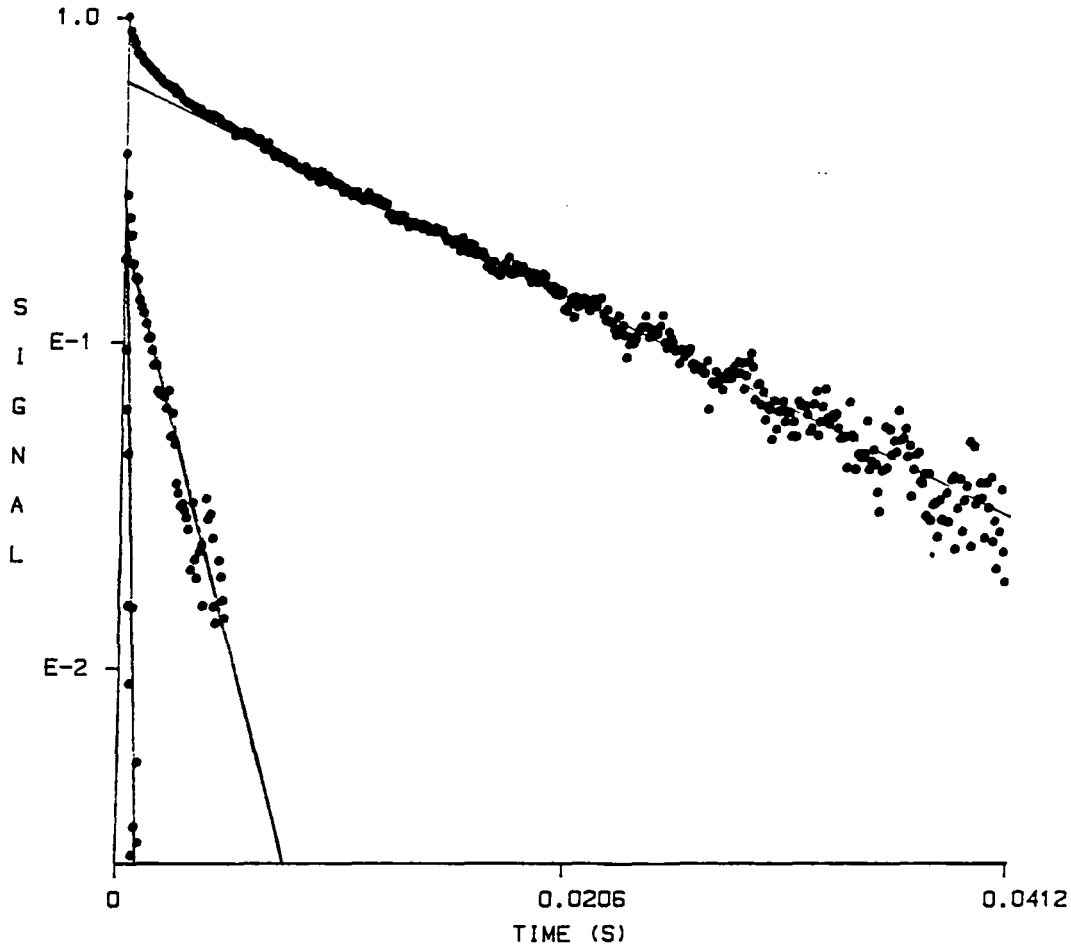

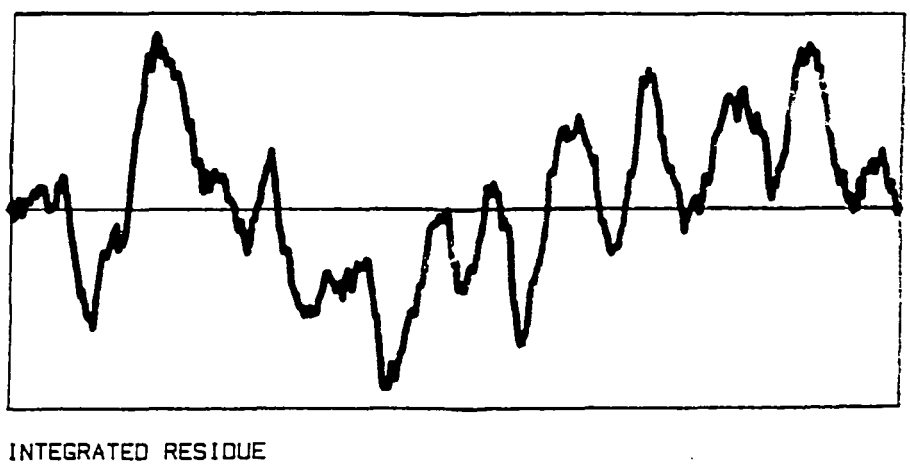

HY–4, HY–14 and HY–26 show significant Brönsted peaks; the 6 ms component in HY–4 and HY–14 may be assigned to this. All components at 1.5 and 3 ms may be assigned by elimination to SiOH. There remains just the 15 ms component in HY–23 and the 25 ms component in HY–26, the latter of which may be tentatively assigned to Brönsted sites. In summary, the proposed assignments are as follows: hydrocarbon, 15 ms; Brönsted, 6/35 ms; SiOH, 1.5 – 3 ms; AlOH, 200 μs; and the 0 ppm species, >30 ms. The short T_2 of AlOH sites presumably arises from strong coupling to ^{27}Al and the proximity of other relatively immobile AlOH groups for efficient spin–diffusion.

Additional measurements were performed on the HY–4 sample using the WRAC spectrometer as follows. The T_1 and $T_{1\rho}$ values of the sample were measured (at 60 MHz and 20 kHz respectively). The T_1 relaxation curve showed double exponential character, with decay times of 159 ms (57%) and 26 ms (43%); the corresponding $T_{1\rho}$ results were 11 ms (54%) and 2.9 ms (46%). Then the T_2 measurement was repeated, preceded by annulment of the longer of the two T_1 components, using the following pulse sequence: $\pi - \tau - \pi/2$ – CPMG; τ was set to ℓn 2 times 159 ms. The resulting T_2 relaxation curve, shown in Figure 5.24, contained only the two shorter components (1.2 ms and 200 μs) seen in the original experiment; the longer components (39 ms and 6.5 ms) were lost. This indicates that the 159 ms T_1 component corresponds to the 0 ppm species (T_2 = 39 ms) and the Brönsted sites (T_2 = 6.5 ms); the relative populations, and the long T_1 measured at 200 MHz, would suggest that the SiOH groups should also be included in this component. The remaining component, therefore (T_1 = 26 ms; $T_{1\rho}$ = 2.9 ms; T_2 = 200 μs; ≃50% population), arises from AlOH groups. A similar T_1–nulling experiment ($\pi - \tau - \pi/2$ – spinlock – acquire) was used to demonstrate that the 26 ms T_1 and the 2.9 ms $T_{1\rho}$ components arise from the same spins.

Figure 5.24: Deconvolution and residue plots obtained from T_2 measurement of HY–4 with annulment of the 159 ms T_1 component. See text for full description. On the residue plot, the horizontal axis is the same as that on the deconvolution plot, whilst the vertical axis is in arbitrary intensity units.

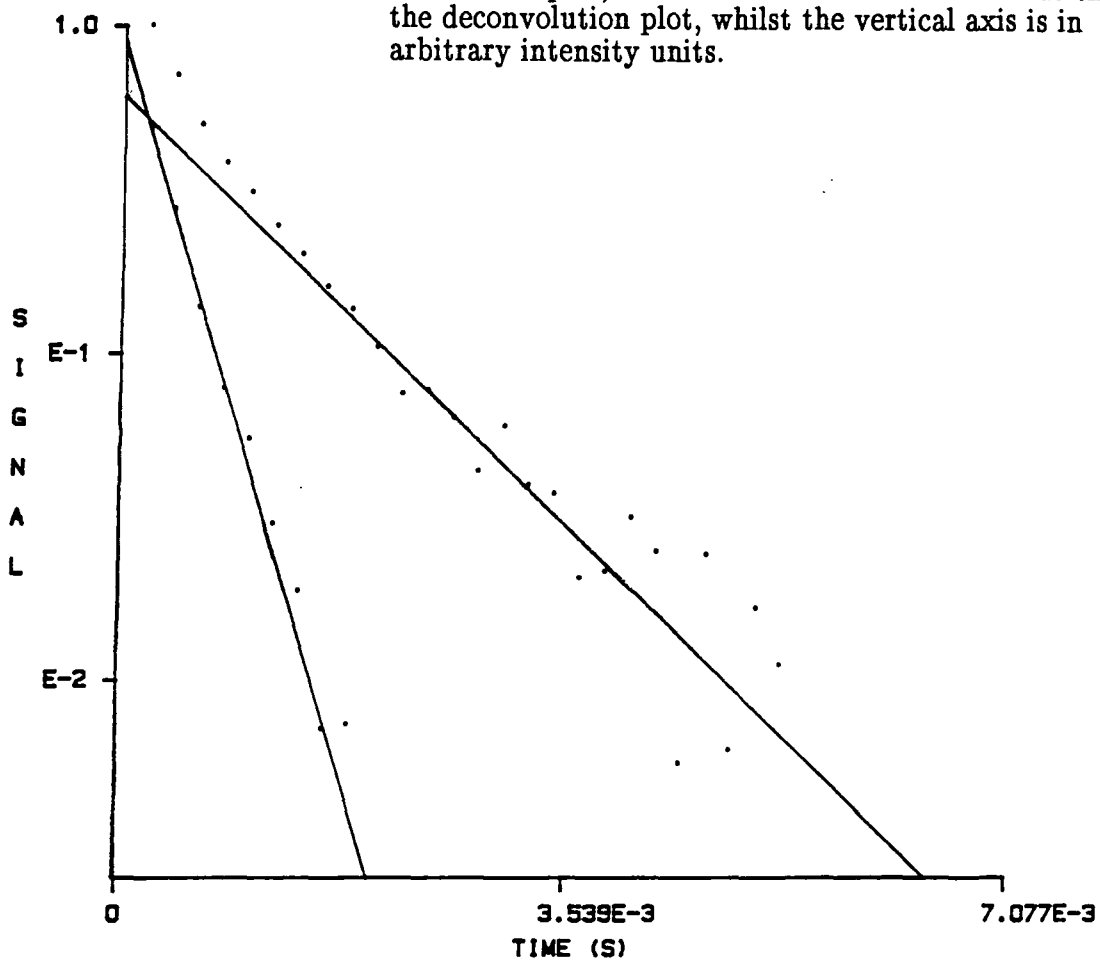

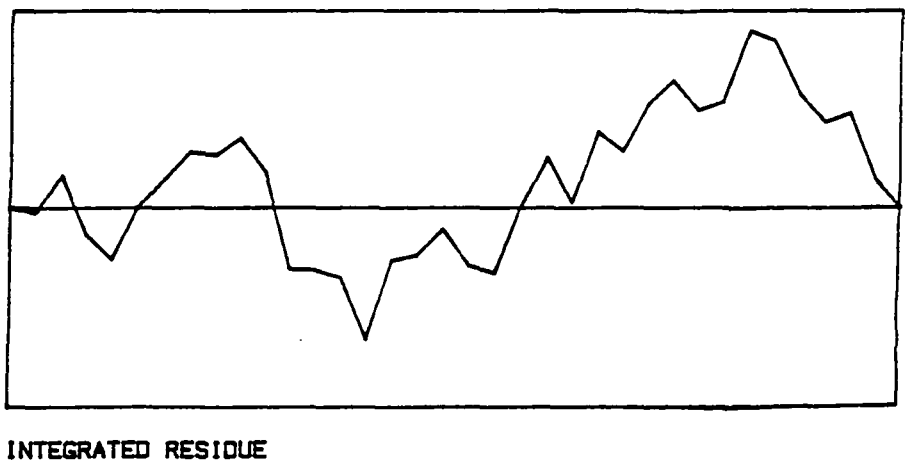

Figure 5.25: ^{1}H SP MAS spectra of HY dried, with Gaussian deconvolutions
(a) HY–26 RD=5s NT=32 RO=2988Hz
(b) HY–29 RD=5s NT=48 RO=3000Hz
(c) HY–43 RD=2s NT=32 RO=1625Hz
(d) HY–58 RD=3s NT=100 RO=2994Hz

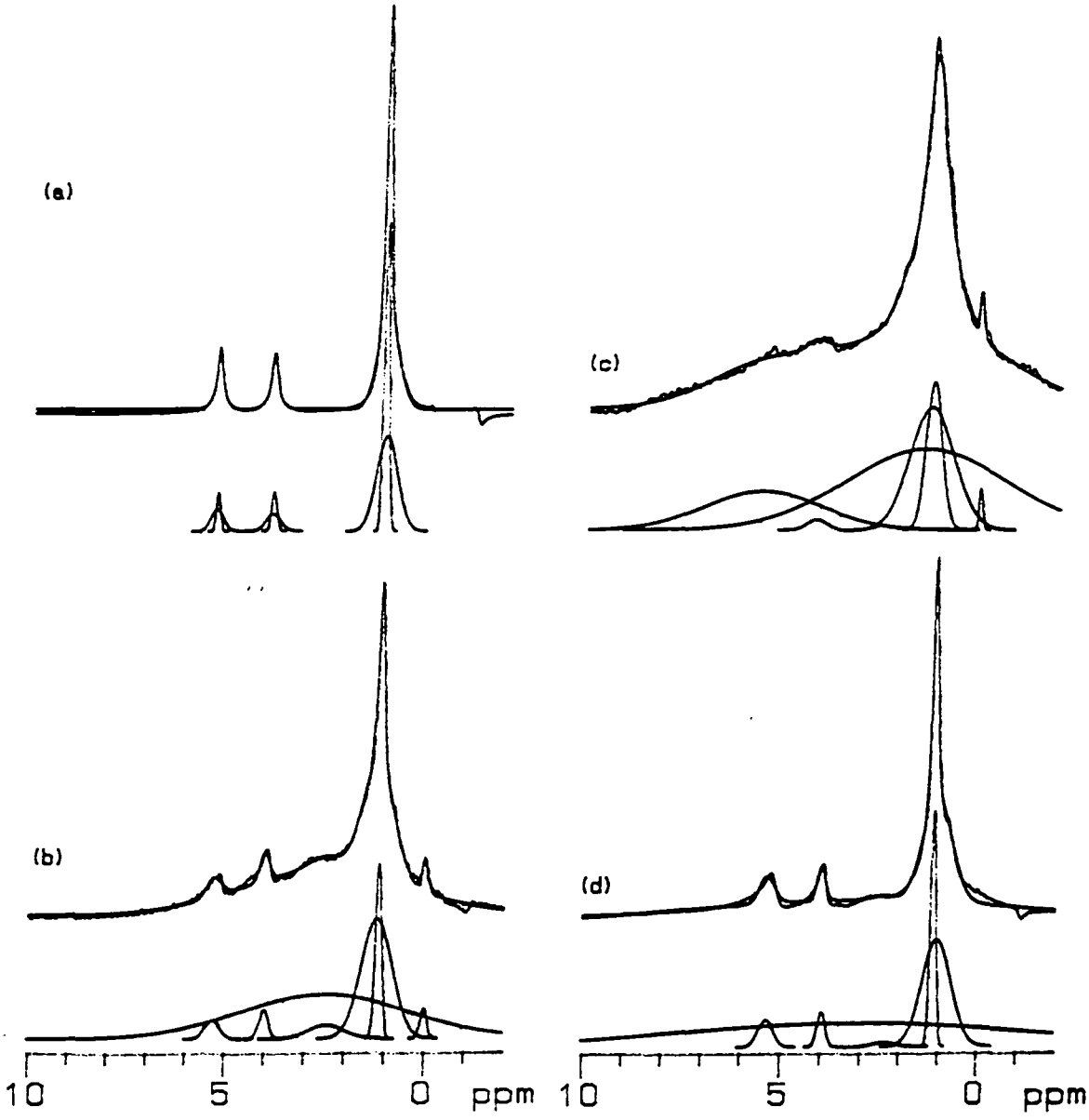

4. Spectral Deconvolution

The ^{1}H spectra of several dried HY samples were deconvoluted into Gaussian components using the SpecMan software described in Chapter 3. The deconvoluted spectra of four samples (HY–26, HY–29, HY–43 and HY–58) are shown in Figure 5.25. By comparison with a standard sample of silicone rubber, the absolute ^{1}H concentrations of each component were calculated in terms of hydrogen atoms per zeolite unit cell.

The intensities, linewidths and concentrations of all the deconvoluted peaks are shown in Table 5.7. It is clear that all the samples other than HY–26 have a much lower total ^{1}H content than expected; one might have predicted a total concentration of the order of 1 H atom per lattice Al, *i.e.* 31 per unit cell. The total figures obtained were checked by integration relative to a known standard and found to be correct to within 15% (there was always a small deficit in the results obtained by deconvolution, which was attributed to intensity lost to spinning sidebands). It must therefore be assumed that, in HY–29, HY–43 and HY–58, extensive dehydroxylation has taken place during the drying procedure. It is interesting to note that the one sample which exhibits a high ^{1}H concentration (HY–26) is also the only sample in the set to show very little evidence of AlOH groups. Nevertheless, this latter sample contains a total Brönsted ^{1}H concentration (including spinning sideband intensity) of only 15.1 per unit cell; the starting material was thought to contain 30.6 lattice Al per unit cell, and one must therefore presume either significant dealumination of the lattice or limited dehydroxylation, as in the other samples. No direct evidence is available from ^{27}Al NMR, since the signals cannot be observed in dried samples. One may, however, surmise a possible scenario taking into account also the observation of 57.8 SiOH per unit cell. The loss of 7.5 Al per unit cell would be sufficient for the disappearance of 15.5 Brönsted H atoms, since the number of

Table 5.7: Deconvolution of ^{1}H NMR Spectra of Dried HY

(*a*) *HY–26* (*including corrections for spinning sidebands*)

Peak	δ/ppm	Intensity/ arbitrary units	HWHH/ Hz	Concentration/ ^{1}H per u.c.
Brönsted 2	5.4	0.0962	16.1	] 7.5
		0.0548	46.5	
Brönsted 1	4.0	0.0974	19.7	] 7.6
		0.0424	52.5	
SiOH	1.2	0.7638	18.2	] 57.8
		0.2374	74.1	

(*b*) *HY–29*

Peak	δ/ppm	Intensity/ arbitrary units	HWHH/ Hz	Concentration/ ^{1}H per u.c.
Brönsted 2	5.3	0.0519	52.8	0.19
Brönsted 1	4.0	0.0791	33.3	0.18
AlOH	2.5	0.1217	597.5	] 5.2
		0.0374	124.7	
SiOH	1.2	0.4786	21.1	] 3.1
		0.3285	108.7	
0 ppm	0.0	0.0828	24.0	0.14

(*c*) *HY–43*

Peak	δ/ppm	Intensity/ arbitrary units	HWHH/ Hz	Concentration/ ^{1}H per u.c.
Brönsted 1	4.3	0.0274	70.6	0.10
AlOH [1]	1.5	0.2148	582.3	] 8.2
AlOH [2]	5.6	0.1028	415.0	
SiOH	1.3	0.3918	58.8	] 3.1
		0.3245	161.1	
0 ppm	0.1	0.1079	14.4	0.08

(*d*) *HY–58*

Peak	δ/ppm	Intensity/ arbitrary units	HWHH/ Hz	Concentration/ ^{1}H per u.c.
Brönsted 2	5.4	0.0718	53.4	0.63
Brönsted 1	4.0	0.0920	28.3	0.42
AlOH [1]	3.1	0.0632	1268.7	] 13.3
AlOH [2]	2.4	0.0116	85.9	
SiOH	1.1	0.6334	19.5	] 6.9
		0.2824	104.5	

Brönsted sites will decline by 7.75 and the released Al (in the form AlO^+) may charge–balance a further 7.75 sites, deprotonating them (no new AlOH band is visible, so the new non–lattice Al has not formed AlOH–containing clusters). The 7.75 newly–created vacancies could contain as many as four times their number of new SiOH groups, accounting for 31.0 in total. The CRAMP spectrum of the untreated HY sample (Figure 5.5(d)) shows that some SiOH was present before dehydration, and this could account for the remaining 26.8 SiOH detected after treatment. This result is in good agreement with that quoted in Section C concerning sample HY–18 for which it was found by deconvolution of the ^{29}Si spectrum after drying and rehydration that 8.5 Al per unit cell were lost from the lattice.

Consideration of the measurements discussed above also serves to highlight the difficulty of achieving a high degree of reproducibility with these samples. The treatments of HY–26 and HY–29 were designed to be identical (see Appendix B for details), whilst their ^1H spectra and concentration clearly differ substantially. The treatment for HY–43 was also similar except for a shorter hold at 400^oC. There is clearly further understanding to be developed concerning the interaction of these materials with their environment when they are extremely dry. Furthermore, it is apparent from the deconvolution plots shown in Figure 5.25 that the spectral simulations obtained, although reasonable, clearly fail to account for all components present, especially in samples rich in AlOH. The spectra often suffered from rolling baselines and artifacts such as folded spinning sidebands like those observable in the –1 to –5 ppm region in HY–29.

5E: CONCLUSIONS

The results presented in this Chapter demonstrate that solid–state magic–angle–spinning NMR, in particular of the ^{1}H nucleus, is an effective technique for the investigation of acid sites and other species in Zeolite Y. In addition to assessing their occurrence and concentration, ^{1}H NMR is capable of probing their mobility and interactions with other components of the system; particular attention has been focused in this study on the interactions between water and charge–balancing cations.

Section B of this Chapter discussed the NMR appearance of the hydrated starting materials. As–synthesized NaY was found to contain a significant population of lattice SiOH groups, which affected the estimate of the Si/Al ratio obtained from ^{29}Si NMR. Similar groups visible in fresh NH_4Y[2] could not be observed in the ^{1}H spectrum of this material after 18 months, perhaps because of rearrangement into a more strongly dipolar–coupled geometry.

HY made by calcination of NH_4Y at 650^{o}C was found to have extensive amounts of non–lattice material rich in both Si and Al. Evidence from a range of techniques suggested that this material was similar in composition to the lattice. Hydroxyl groups attached to non–lattice Al could be observed and were found to cross–polarize efficiently to this Al. Steamed HY also contained non–lattice silica–alumina, which appeared to be associated with the lattice; slow hydrolysis of the linkages over a period of months gave rise to the formation of new SiOH groups.

The water signal in most hydrated samples was shown to be composed of two distinct phases, arising from water molecules in small and large lattice cages. Usually separate T_1 and T_2 values were observed; characteristic T_2 components of $3-5$ ms for large–cage water and $25-100$ μs for small–cage water were

measured. In most samples the two component signals appeared at the same chemical shift in the ^1H MAS spectrum, but in HY samples back–exchanged with Na^+ or Ag^+, the two regions exhibited different chemical shifts. This was attributed to the presence of cations in large cages only. The chemical shift difference observed was 1.0 ppm in NaY–ex and 0.3 ppm in AgY–ex. Keeping of the samples for long periods, or heating strongly, allowed the cation to reach an equilibrium concentration in both cages, and the two signals appeared at the same frequency once more.

Section C discussed additional studies focusing on the intracrystalline water itself. The affinity of zeolite samples was shown to be linked to the lattice Al content; the predominant charge–balancing cation also has a significant influence, with NaY and NH_4Y having a greater water uptake than HY under the same conditions. The water content of a given sample is highly dependent on its history, and reproducible water levels can only be achieved if the sample is equilibrated for several days in a controlled–humidity atmosphere.

During heating under vacuum, most of the water and other volatile sorbates are lost in the first few hours. Dried samples rapidly rehydrate in the open atmosphere, adsorbing about 0.2% of their total capacity per minute. The drying procedure used (described in Chapter 3) does not leave the crystal lattice unchanged; some Al is displaced from the lattice – up to 8 atoms per unit cell in one case. The population of SiOH groups formed during this process is not very large; a few can be seen in the ^1H spectrum after rehydration. They appear to be formed slowly, perhaps by a process of gradual hydrolysis of strained Si–O–Si linkages or removal of partially dislodged lattice Al. Heating HY in an oven at atmospheric pressure is insufficient to develop these changes.

In Section D a series of results was presented to show that reasonably consistent and highly–resolved ^1H MAS spectra could be obtained from carefully

dried HY samples. Of particular interest was the broad peak at 2.3 ppm assigned to AlOH; this band, which was accompanied by intense spinning sidebands, varied widely in intensity from one sample to another, probably due to varying degrees of condensation of the non–lattice alumina present. (Detailed consideration of this subject is reserved for Chapter 6.) Hydroxyl–rich NLA was found to coordinate to lattice Brönsted sites.

A narrow, intense peak at 7.4 ppm was observed in many samples; evidence was presented to suggest that it arose from a hydrocarbon contaminant adsorbed from the vacuum system. The contaminant sorbed strongly to lattice Brönsted sites; its ^{1}H nuclei cross–polarized efficiently to lattice Si.

The ^{1}H T_1 relaxation times observed in dried samples were much longer than those found in hydrated materials. Brönsted–acidic ^{1}H atoms had a T_1 of 200 – 300 ms and 300 – 500 ms for large– and small–cage sites respectively. The T_1 of SiOH varied widely depending on the presence of other species; the range observed was 130 – 900 ms. T_2 values were measured as follows: Brönsted sites, 6 ms and 35 ms; SiOH, 1.5 – 3 ms; AlOH, 200 μs.

Absolute concentrations of individual ^{1}H–containing species were measured by deconvolution. Most dried samples were found to be highly deficient in ^{1}H, suggesting that extensive dehydroxylation took place during drying. Results were presented to support the theory suggested earlier that about 8 Al per unit cell were displaced from the lattice as a result of the drying procedure employed.

REFERENCES

1. E Brunner, *J. Chem. Soc., Faraday Trans.* **86**, 3957 (1990).
2. E Brunner, D Freude, B C Gerstein, H Pfeifer, *J. Magn. Reson.* **90**, 90 (1990).
3. A J Vega, Z Luz, *J. Phys. Chem.* **91**, 365 (1987).
4. R Challoner, Ph.D. Thesis, University of Durham, p.239–45 (1989).
5. M Hunger, D Freude, H Pfeifer, *J. Chem. Soc., Faraday Trans.* **87**, 657 (1991).
6. H Ernst, *Z. Phys. Chem.* **269**, 1073 (1988).
7. M Hunger, D Freude, H Pfeifer, H Bremer, M Jank, K–P Wendlandt, *Chem. Phys. Lett.* **100**, 205 (1983).
8. E Brunner, H Ernst, D Freude, M Hunger, C B Krause, D Prager, W Reschetilowski, W Schwieger, K H Bergk, *Zeolites* **9**, 282 (1989).
9. C E Bronnimann, I–S Chuang, B L Hawkins, G E Maciel, *J. Am. Chem. Soc.* **109**, 1562 (1987).
10. D Freude, M Hunger, H Pfeifer, W Schwieger, *Chem. Phys. Lett.* **128**, 62 (1986).
11. For a review, see H Pfeifer, D Freude, M Hunger, *Zeolites* **5**, 274 (1985).
12. J H Lunsford, W P Rothwell, W Shen, *J. Am. Chem. Soc.* **107**, 1540 (1985).
13. D Freude, T Fröhlich, M Hunger, H Pfeifer, G Scheler, *Chem. Phys. Lett.* **98**, 263 (1983).
14. M Hunger, D Freude, T Fröhlich, H Pfeifer, W Schwieger, *Zeolites* **7**, 108 (1987).
15. M W Anderson, J Klinowski, *Zeolites* **6**, 455 (1986).
16. W L Earl, P O Fritz, A A V Gibson, J H Lunsford, *J. Phys. Chem.* **91**, 2091 (1987).
17. G Engelhardt, H–G Jerschkewitz, U Lohse, P Sarv, A Samoson, E Lippmaa, *Zeolites* **7**, 289 (1987).
18. D Freude, M Hunger, H Pfeifer, G Scheler, J Hoffmann, W Schmitz, *Chem. Phys. Lett.* **105**, 427 (1984).
19. C E Bronnimann, R C Zeigler, G E Maciel, *J. Am. Chem. Soc.* **110**, 2023 (1988).
20. L Kubelková, S Beran, A Malecka, V M Mastikhin, *Zeolites* **9**, 12 (1989).
21. J Klinowski, H Hamdan, *Chem. Phys. Lett.* **149**, 355 (1988).
22. D Freude, J Klinowski, *J. Chem. Soc., Chem. Commun.* 1411 (1988).
23. N–Y Topsoe, K Pedersen, E G Derouane, *J. Catal.* **70**, 41 (1981).
24. P A Jacobs, J B Uytterhoeven, *J. Chem. Soc., Faraday Trans. 1* **69**, 359 (1973).
25. V M Mastikhin, I L Mudrakovsky, S V Filimonova, *Zeolites* **10**, 593 (1990).
26. H P Wang, B A Garland, A Gerhard, J Liang, E M Eyring, *Appl. Spectrosc.* **43**, 1370 (1989).
27. P J Grobet, P A Jacobs, H K Beyer, *Zeolites* **6**, 47 (1986).
28. K F M G J Scholle, W S Veeman, J G Post, J H C van Hooff, *Zeolites* **3**, 214 (1983).
29. Z Luz, A J Vega, *J. Phys. Chem.* **91**, 374 (1987).
30. H Pfeifer, *Surf. Sci.* **52**, 434 (1975).
31. Z Guo, K Wang, D Zhou, D Ding, J Wang, H Li, *Huaxue Wuli Xuebao* **3**, 100 (1990): Chinese.
32. W D Basler, in *Properties & Applications of Zeolites* (*Chem. Soc. Special Publ. 33*; R P Townsend, ed.), 174 (1979).
33. W D Basler, W Maiwald, *J. Phys. Chem.* **83**, 2148 (1979).

34. J R Sohn, S G Ryu, *Hwahak Konghak* **27**, 168 (1989): Korean.
35. A Gedeon, T Ito, J Fraissard, *Zeolites* **8**, 376 (1988).
36. A K Aboul–Gheit, M F Menoufy, *Thermochim. Acta* **160**, 193 (1990).
37. A Jentys, G Warecka, M Derewinski, J A Lercher, *J. Phys. Chem.* **93**, 4837 (1989).
38. L M Parker, D M Bibby, G R Burns, *Zeolites* **11**, 293 (1991).
39. W D Basler, *Z. Phys. Chem.* **152**, 199 (1987).
40. P H Kasai, P M Jones, *J. Mol. Catal.* **27**, 81 (1984).
41. B Beagley, J Dwyer, T K Ibrahim, *J. Chem. Soc., Chem. Commun.* 493 (1978).
42. J Sauer, C M Koelmel, J R Hill, R Ahlrichs, *Chem. Phys. Lett.* **164**, 193 (1989).
43. E Brunner, H Ernst, D Freude, M Hunger, H Pfeifer, *Stud. Surf. Sci. Catal.* **37**, 155 (1988).

CHAPTER 6: ^{1}H NMR STUDIES OF NON–LATTICE ALUMINA

In the preceding Chapter results were presented which demonstrated the possibility of achieving sufficiently well–resolved ^{1}H NMR spectra of dried samples of Zeolite Y to permit the identification and quantification of a number of distinct ^{1}H–containing species. It was also shown that the drying procedure does not leave the lattice unchanged, but displaces a fraction of lattice atoms (predominantly Al) into a non–lattice environment.

It was commented that the intensity of the peak assigned to AlOH groups in the ^{1}H spectrum varied depending on the treatment used to dry the material. In this Chapter, the relationship between AlOH peak intensity and sample history is developed more thoroughly. Although the results show a degree of variability (which may probably be ascribed to the inadequacies in the vacuum system employed for these experiments), there are clear indications that the nature of the NLA, and in particular its degree of condensation (*i.e.* how polymerized or polynucleated it is), can be linked to the exact details of the drying treatment used. In addition, evidence is presented to support the hypothesis that polymerized NLA can be affected *after* drying by the attack of water slowly encroaching from the atmosphere through the walls of the sample container over a period of months, and by the rearrangement of hydroxyl groups inside the sample within a time scale of several weeks.

The first Section of this Chapter describes an experiment involving removal of the NLA from a steamed HY sample which was intended to enable investigation of the state of the lattice alone after steaming. This is followed by a description of the results obtained from experiments involving variation of the drying treatment used for HY. There follows a discussion of observations made

on dried samples which have aged or slowly adsorbed water from the atmosphere; the Chapter closes with a gathering–together of the conclusions drawn. The relevant literature is discussed in the first Section of Chapter 5.

6A: REMOVAL OF NON–LATTICE ALUMINA WITH EDTA

A portion of the HY–S steamed sample discussed in Chapter 5 was treated with $(NH_4)_2H_2EDTA$ under carefully controlled conditions designed to extract non–lattice alumina from the sample without attacking any residue of lattice Al. (The details of the experimental procedure are given in Chapter 3.) This Section describes and aims to explain the differences observed by NMR between HY–S and the EDTA–leached material, designated HY–S–L (although it is actually an NH_4Y zeolite). Figure 6.1 shows the ^{29}Si single–pulse and CP/MAS and ^{27}Al single–pulse spectra of the two samples. Consideration of the ^{29}Si single–pulse spectra before and after leaching demonstrates that removal of NLA by this technique has a substantial effect on the remaining ^{29}Si: the narrow signal corresponding to Q^4 lattice sites in a highly siliceous environment in HY–S is apparently replaced by a broad pattern of many overlapping signals in HY–S–L. The point of maximum intensity in the latter spectrum is at an unusually low frequency, appearing at –111.0 ppm. Lattice Si has never been observed in Zeolite Y at such a position, and so it may be inferred that a substantial part of the signal in HY–S–L arises from non–lattice material. It has already been discussed in Chapter 4 that the ^{29}Si CP/MAS spectra of steamed samples suggest the presence of small but significant quantities of such material. The ^{29}Si CP/MAS spectrum of HY–S (Figure 6.1(c)) shows the same effect; on leaching, the pattern changes as shown in trace (d), with the emergence of peaks

Figure 6.1: MAS Spectra of hydrated HY–S and HY–S–L

(a)	HY–S ^{29}Si SP	RO=1221Hz NT=8000 RD=20s
(b)	HY–S–L ^{29}Si SP	RO=3040Hz NT=2352 RD=20s
(c)	HY–S ^{29}Si CP/MAS	RO=2980Hz NT=40000 RD=2s CT=10ms
(d)	HY–S–L ^{29}Si CP/MAS	RO=1500Hz NT=2000 RD=1s CT=5ms
(e)	HY–S ^{27}Al SP	RO=3569Hz NT=5035 RD=100ms PA=π/4
(f)	HY–S–L ^{27}Al SP	RO=3200Hz NT=2000 RD=100ms PA=π/4

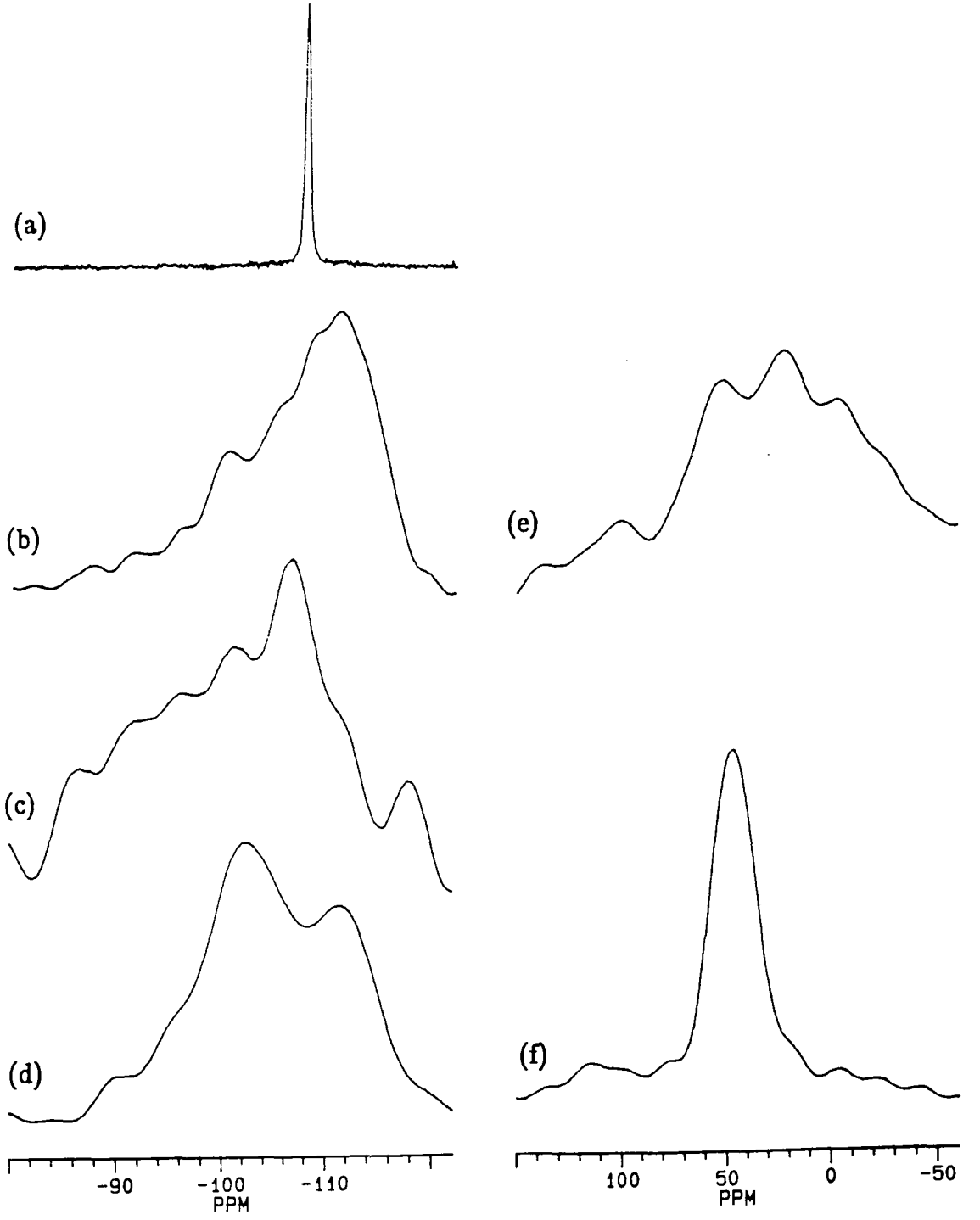

at –111.9 ppm (not far from the single–pulse position) and –101.5 ppm, assigned respectively to non–lattice silica and Q^3 groups [as $(SiO)_3SiOH$ or $(SiO)_3SiOAl$].

Further evidence concerning the changes taking place arises from the ^{27}Al single–pulse spectra in Figure 6.1(e) and (f). The spectrum of HY–S shows a broad cluster of peaks in the region 60 to –20 ppm characteristic of a wide range of local environments and the presence of four–, six– and possibly five–coordinate Al. After leaching, the spectrum narrows substantially to yield a single, well–defined peak close to 52 ppm; this resembles the spectra of highly ordered systems such as NaY and NH_4Y[2] (see Figures 5.1(d) and 5.2(e)) and may thus be taken as an indication that all Al present is in a reasonably symmetrical four–coordinate environment. All the NLA has been chelated by EDTA and presumably also removed entirely from the sample, since EDTA generally forms six–coordinate complexes with metal cations and no six–coordinate Al is visible in the ^{27}Al spectrum. It may therefore be deduced that all the remaining Al in HY–S–L is in the lattice.

The question arises as to whether any Al has re–inserted into the lattice during the EDTA treatment. The high signal–to–noise ratio of the ^{27}Al spectrum of HY–S–L (Figure 6.1(f)) suggests the presence of a significant quantity of lattice Al. Furthermore, elemental analysis gives a bulk Si/Al ratio measurement of 6.4. If it is accepted that no non–lattice aluminium is present, this figure represents an *upper* limit for the lattice Si/Al ratio; if there is any non–lattice silicon, the lattice Si/Al ratio must be lower than 6.4 to keep the bulk ratio at this value. By contrast, the ^{29}Si SP spectrum of HY–S (Figure 6.1(a)) shows that the lattice Si/Al ratio of this sample is far in excess of this, and probably over 50. Unless the elemental analysis result is substantially in error, then, it is necessary to conclude that a large amount of Al is present in HY–S–L in an ordered tetrahedral environment, possibly having been re–inserted

into the lattice. The elemental analysis figure could be distorted by deposition of aluminium in an extracrystalline environment; one would have to assume, however, that such Al occurs in an ordered, tetrahedrally coordinated form (which would not be characteristic of an EDTA complex) or that it is highly disordered and thus invisible to ^{27}Al NMR.

A deconvolution of the broad ^{29}Si SP spectrum of HY–S–L is shown in Figure 6.2. The dispersive feature near –100 ppm is almost certainly an artifact from the transmitter, since it occurs at exactly –4 kHz, which was the carrier offset employed on this occasion. Apart from this, the band deconvolutes remarkably well into four relatively broad Gaussian peaks at –95.0, –101.7, –106.6 and –111.9 ppm, assigned respectively to lattice Q^2, Q^3 and Q^4 sites and non–lattice silica. Assuming that no lattice SiOH is present, the lattice Si/Al ratio can be estimated from the first three peaks to be 4.75; this is consistent with the observation above that the lattice Si/Al ratio must be below 6.4. The fourth peak, assigned to non–lattice silica (alumina–free, since the sample contains no non–lattice aluminium), accounts for 50.0% of the total intensity of the spectrum. Given that the bulk Si/Al ratio is 6.4 by elemental analysis, the lattice Si/Al ratio might therefore be estimated to be half of this value, *i.e.* 3.2. The disparity between these two estimates of the lattice Si/Al ratio indicates that the figure of 50.0% for the fraction of Si present which is non–lattice may be an overestimate arising from the inclusion of signal from lattice Si in the intensity assigned to the non–lattice material, or perhaps from variations in T_1; nevertheless, the evidence as a whole suggests the re–insertion of a substantial amount of Al (perhaps as much as 30 atoms per unit cell) into the lattice.

The ^{29}Si CP/MAS spectrum of HY–S–L (Figure 6.1(d)) is also consistent with this view, showing a significant enhancement of the newly–formed Q^3 sites at –101.5 ppm (*cf.* –101.7 ppm by deconvolution, above)

Figure 6.2: ^{29}Si SP MAS spectrum of hydrated HY–S–L with Gaussian deconvolution RO=3476Hz NT=3252 RD=20s

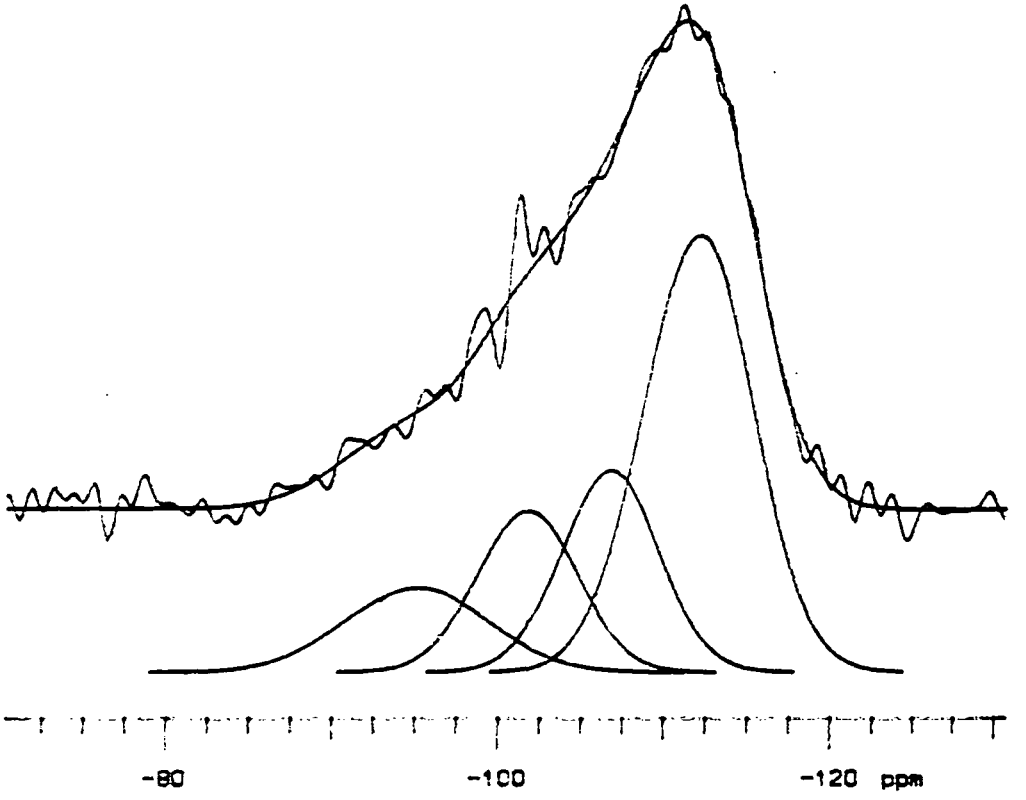

Figure 6.5: ^{1}H MAS spectrum of HY–S–L–16
RO=3476Hz NT=128 RD=5s

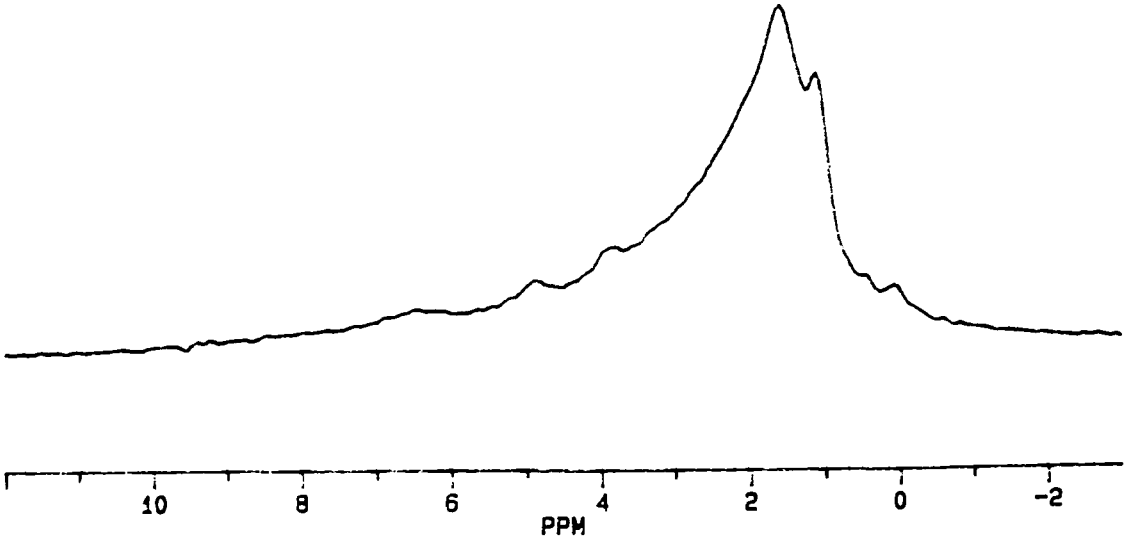

plus a clear signal at –111.9 ppm arising from the non–lattice material. The difference between the spectra of HY–S and HY–S–L could be explained either by re–insertion of Al into the lattice or by the formation of a substantial population of $(SiO)_3SiOH$ groups in lattice or non–lattice material. Evidence presented later from ^1H NMR is consistent with the latter proposal; since compelling grounds for the re–insertion of Al into the lattice have already been given, then, it may be appropriate to consider both of these processes to be active.

^1H NMR Measurements. The ^1H MAS spectra of wet HY–S and HY–S–L are shown in Figure 6.3. The SP spectra both show water peaks, at 4.0 ppm in HY–S (a lower frequency than normal for Zeolite Y, presumably due to interaction with NLA, as discussed in Chapter 5) and 4.7 ppm in HY–S–L. The latter sample shows an additional signal at 4.0 ppm which may arise from water in cation–free small cages, as discussed before. AlOH signals around 2 ppm are present in HY–S but absent in HY–S–L, whereas only the latter shows an intense SiOH signal at 1.1 ppm. This indicates that some of the ^{29}Si peaks to high frequency of –105 ppm may arise from $(SiO)_3SiOH$ and $(SiO)_2Si(OH)_2$ species. The CRAMP spectrum of HY–S (trace (b)) differs remarkably from the single–pulse spectrum, particularly in the presence of the strong SiOH signal in the latter, suggesting that these species are actually quite abundant in this sample. The SP and CRAMP spectra of HY–S–L. however, are much more similar.

No NH_4^+ signal is visible in either SP or CRAMP spectra of HY–S–L. This would be expected if the sample contained no lattice Al; it is rather surprising, however, in view of the evidence presented above for re–insertion of Al into the lattice.

Figure 6.3: ^{1}H MAS spectra of hydrated HY–S and HY–S–L

(a)	HY–S SP	RO=4011Hz NT=128 RD=1s
(b)	HY–S CRAMPS	MREV–8 RO=1400Hz NT=32 RD=20s
(c)	HY–S–L SP	RO=3156Hz NT=32 RD=2s
(d)	HY–S–L CRAMPS	MREV–8 RO=2257Hz NT=64 RD=10s

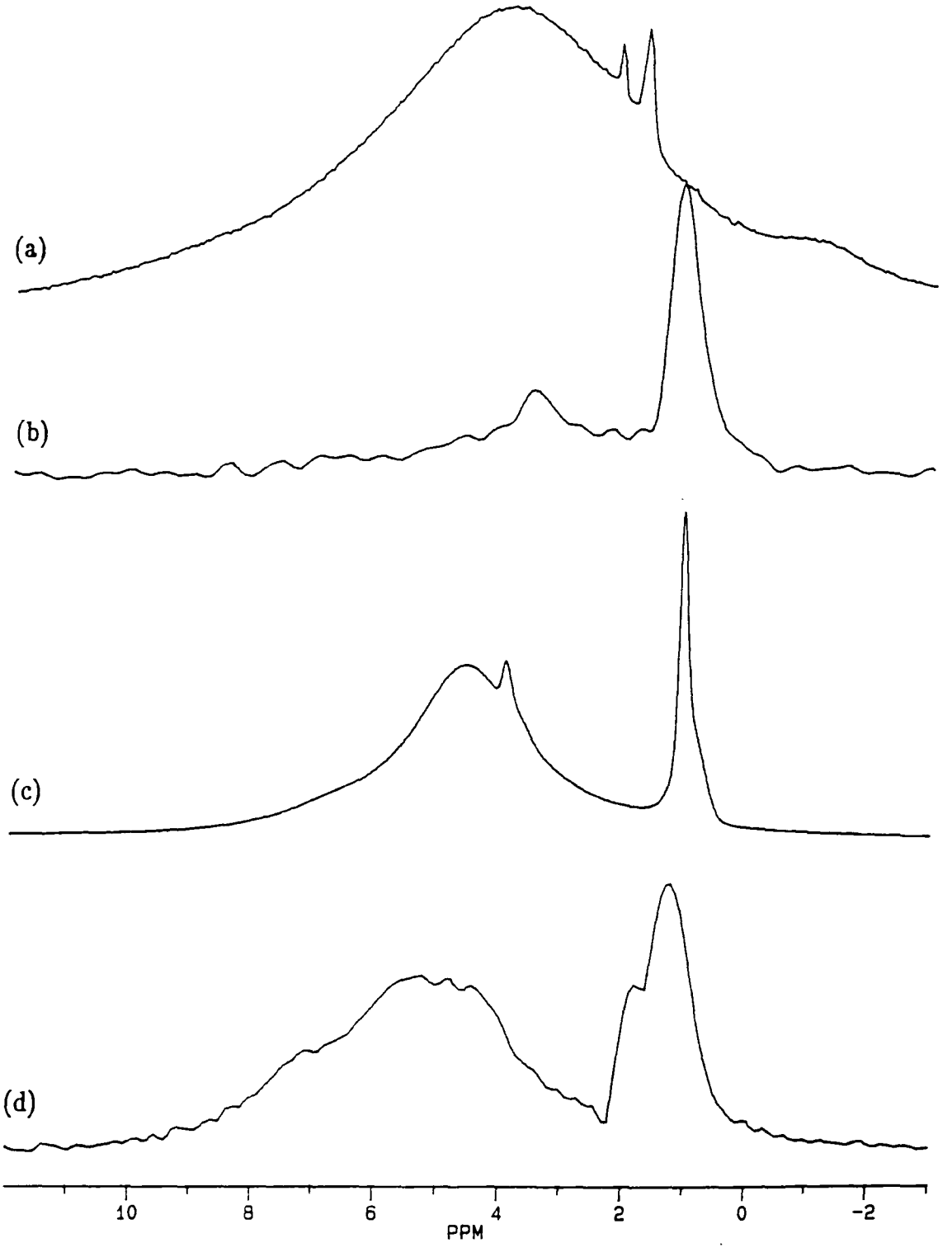

The ^{1}H relaxation times of these wet samples are collected in Table 6.1. By analogy with the samples in Chapter 5, the T_2 component at 6.3 – 6.4 ms may be assigned to large–cage water, and the other component to AlOH in HY–S and to SiOH in HY–S–L. By deduction from the populations, the 95 ms T_1 and 3.6 ms $T_{1\rho}$ components in HY–S–L may also be assigned to SiOH. It may therefore be assumed that the 17 ms $T_{1\rho}$ component in HY–S arises from the same species as the 14 ms component in HY–S–L, *i.e.* large–cage water; the same may also apply to the 22.8 ms T_1 component in HY–S.

The behaviour of the dried sample HY–S–10 (see Appendix B for details of preparation) over time was investigated by measuring the ^{1}H MAS spectrum at intervals. Three spectra obtained when the sample was 0, 9 and 11 months old are shown in Figure 6.4 along with deconvolution plots. They show, in varying quantities, an SiOH signal near 1 ppm, narrow AlOH peaks at 4 ppm, and a broad AlOH band centred on 4.1 ppm in trace (a), 3.3 ppm in (b) and 1.5 ppm in (c). Integration shows that the total ^{1}H content rose by a factor of 3.0 between acquisition of (a) and (b), and by a further factor of 4.5 between (b) and (c). It may be assumed that the additional nuclei arise from atmospheric water slowly penetrating the Kel–F rotor insert in which the sample was always kept; the insert itself was kept in a screw–top plastic bottle in the open laboratory when not in the NMR spectrometer. The populations of individual sites are shown (in ^{1}H nuclei per unit cell) in Table 6.2. They show that, in the first nine months, the SiOH and broad AlOH bands grew most, with the narrow AlOH band hardly growing at all. This may suggest that the narrow AlOH band corresponds to material which is not readily hydrolyzed to form extra –OH groups. During the period 9 – 11 months, however, all bands grew by approximately the same factor (around 4). This could result from all the readily hydrolyzable groups having already been attacked, allowing the water to hydrolyze (or adsorb to) the

Table 6.1: ^{1}H Relaxation Times of HY–S and HY–S–L wet, in ms

Sample	Time Constant	Field Strength	Relaxation Time/ms
HY–S	T_1	60 MHz	22.8 (29%) 6.2 (71%)
	$T_{1\rho}$	20 kHz	17 (24%) 1.4 (76%)
	T_2	200 MHz	6.3 (51%) 0.64 (49%)
HY–S–L	T_1	200 MHz	Water: 107; AlOH: 127; SiOH: 346
		60 MHz	95 (85%) 35 (15%)
	$T_{1\rho}$	20 kHz	14 (37%) 3.6 (63%)
	T_2	200 MHz	6.4 (14%) 0.80 (86%)

Table 6.2: ^{1}H Populations of Species in HY–S–10 Dried
in ^{1}H nuclei per unit cell

Sample Age /months	Population/^{1}H per unit cell			
	SiOH	AlOH (narrow)	AlOH (broad)	Total AlOH
0	0.7	1.5	1.2	2.7
9	11.3	2.9	16.3	19.2
11	45.3	12.6	56.4	69.1

Figure 6.4: ^{1}H MAS spectra of HY–S–10 during aging, with Gaussian deconvolutions RD=5s

(a) Fresh
RO=2878Hz NT=128

(b) 9 months old
RO=1600Hz NT=32

(c) 11 months old
RO=3000Hz NT=128

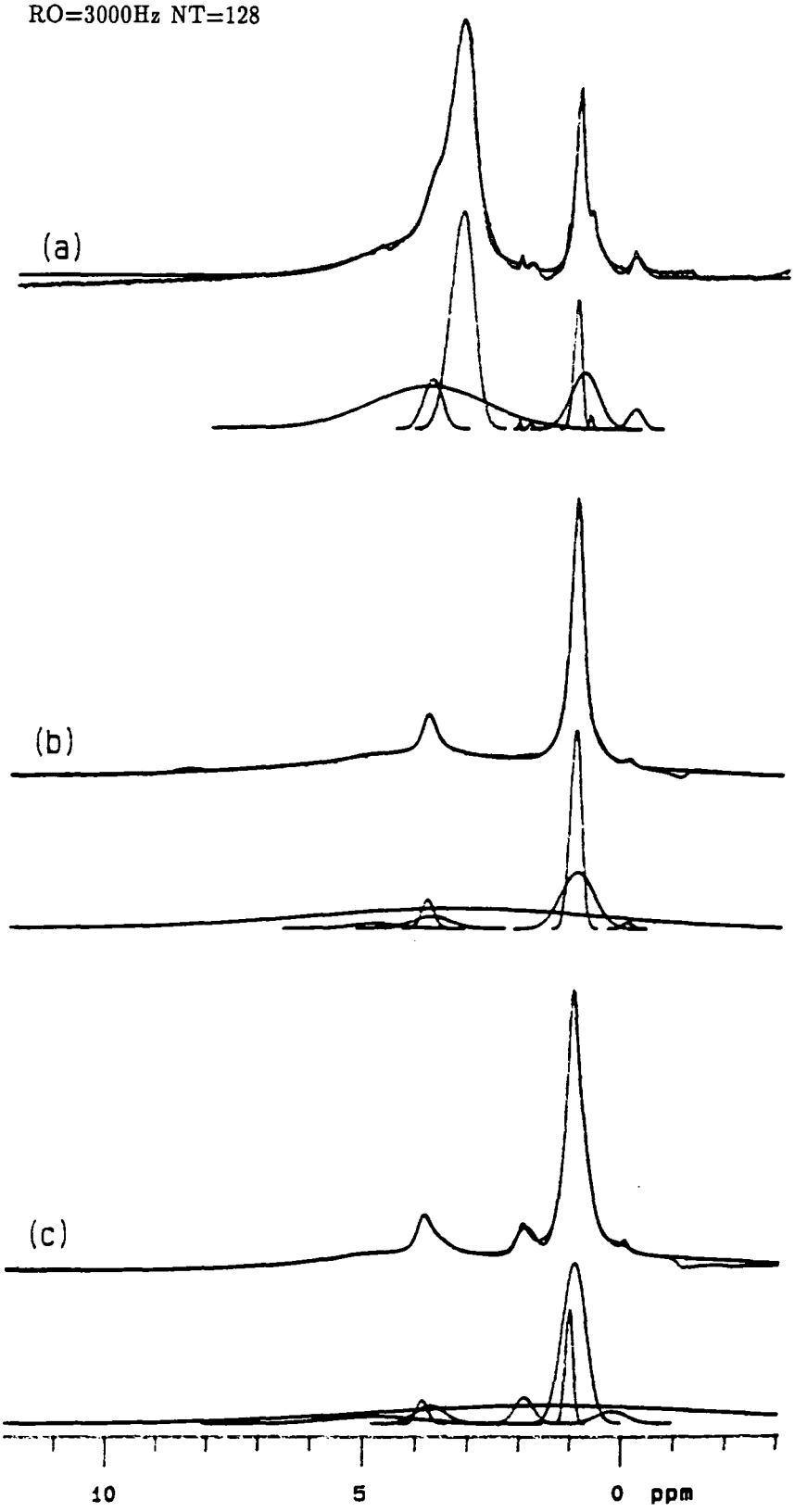

remaining sites to equal extents. One point of particular interest is that, despite the large amount of water that has been adsorbed (about 56 molecules per unit cell in total), there is no evidence for a free water peak; this demonstrates that substantial *chemical* changes (*i.e.* bond breaking and forming) occur during the drying and rehydration process, not just *physical* ones.

The figures given in Table 6.2 also permit estimation of the state of the NLA as follows. The bulk Si/Al ratio of HY–S given by elemental analysis is 3.64, as reported above. This is equivalent to 41.4 Al per unit cell. Comparing this value with the figures in the final column of Table 6.2, it is clear that the freshly–made sample has highly condensed NLA with only 0.07 OH groups per Al atom. If all the Al is in an oxyhydroxide form (as seems likely), this gives an empirical formula for the NLA of $Al_{15}O_{22}(OH)$, not counting any non–lattice Si present. Although based on many assumptions and approximations, this result serves to make the point that the non–lattice material must be in a highly polymerized and OH–deficient form. After 11 months, the ratio of AlOH to non–lattice aluminium has risen to 1.7, and the approximate empirical formula of the non–lattice alumina becomes $Al_5O_6(OH)_3$.

The ^1H relaxation times measured for this sample are shown in Table 6.3. During aging, T_1 generally falls as liberated –OH groups become less restricted in mobility. The times observed are mostly shorter than those reported in Table 5.4 for dried HY, suggesting that there are mobile components present, possibly small–cage water or NLA.

The ^1H MAS spectrum of HY–S–L dried (HY–S–L–16) is shown in Figure 6.5. It shows an intense cluster around 1.6 ppm assigned to SiOH groups (as seen in the wet spectrum, Figure 6.3(c)) plus peaks in the usual positions of Brönsted sites (3.9 and 4.9 ppm) and additional signals at 0.1 and 6.5 ppm. The appearance of Brönsted sites, albeit weakly, is further evidence for the

re–insertion of Al into the zeolite lattice, although they may occur in non–lattice silica–alumina also. Clearly, however, the intensity of the SiOH signal is such that there must be a substantial contribution to the lower–Q^n signals in the ^{29}Si spectra from –Si(OH)$_x$ species. Concerning the signal at 6.5 ppm, a peak in this position has been assigned by other workers to water coordinated to Lewis sites: see Chapter 4 for references. The T_1 values of some of these signals have been measured at 200 MHz, giving results as follows: 6.5 ppm, 88 ms; 3.9 ppm, 102 ms; 1.6 ppm (main peak), 127 ms. These values are rather lower than those quoted for dried HY samples in Chapter 5, suggesting the presence of some residual water.

Selective Cross–Polarization Study of HY–S–10. HY–S–10 was considered to be a good candidate for the selective cross–polarization experiment outlined in Chapter 2 on account of its two clearly–defined ^1H components differing

Table 6.3: ^1H Relaxation Times of HY–S–10 in ms

Time Constant	Field Strength	Age/ months	Relaxation Time 1.1ppm	3.5–4ppm
T_1	300 MHz	Fresh	188	46
	200 MHz	Fresh	110	29
		7	97	48
		11	87	43
		13	75	32
	60 MHz	Fresh	68	9
T_2	200 MHz	Fresh	≃30	≃4
	60 MHz	Fresh	≃30	≃4

Figure 6.6: ^{29}Si SCP spectra of HY–S–10 (not same vertical scale)
(a) Normal CP/MAS Spectrum
NT=65060
(b) SCP with AlOH annulled
NT=75000
(c) SCP with SiOH annulled
NT=75000

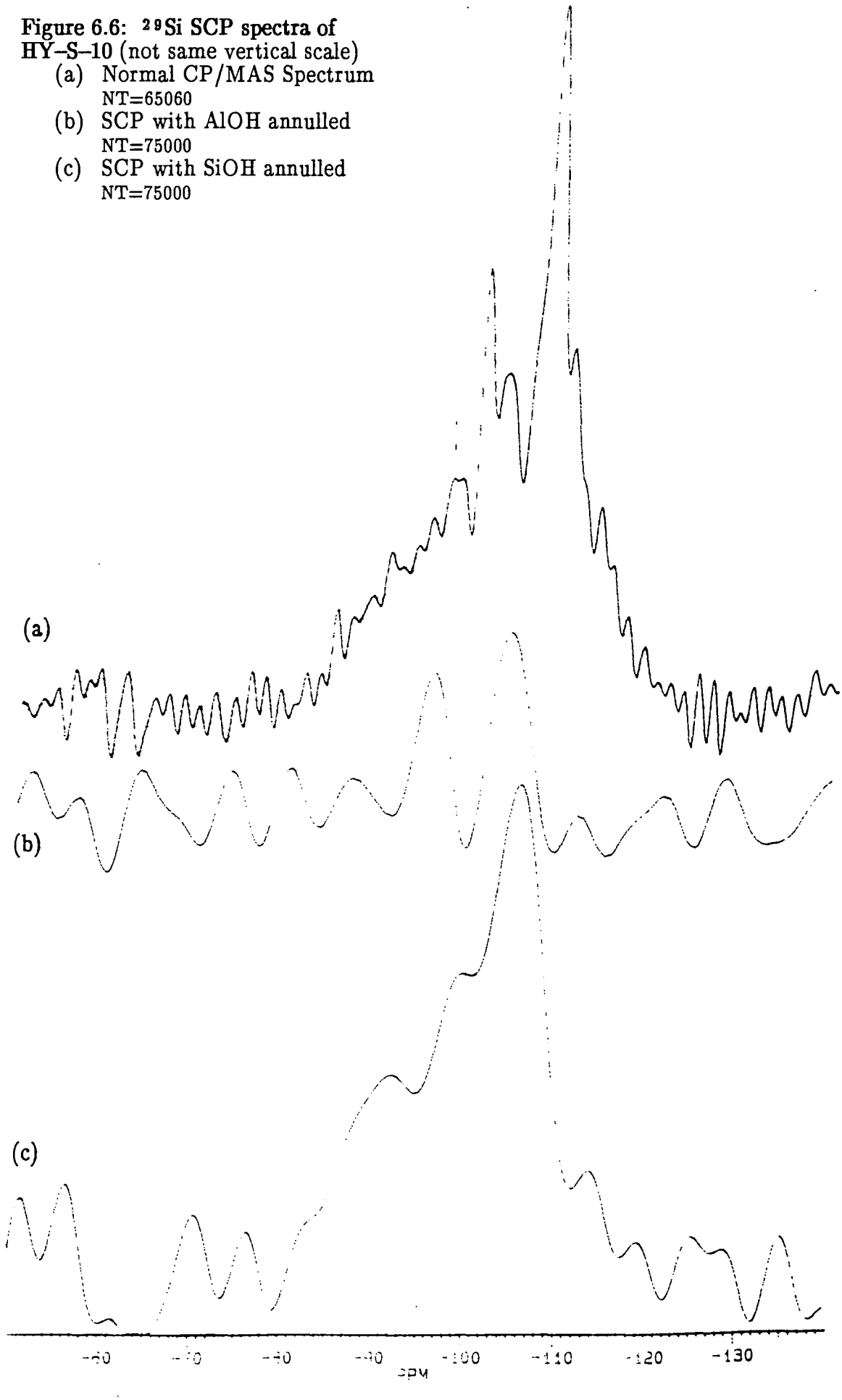

substantially in T_1. SCP results obtained at Unilever Research Port Sunlight Laboratory when the sample was 1 month old are shown in Figure 6.6. The spectrum obtained after annulment of the ^1H signal at 3.5 ppm (trace (b)) shows only a very weak signal by comparison with that obtained by annulment of the SiOH magnetization (trace (c)), despite their relative populations in the ^1H spectrum (Figure 6.4(a)). This indicates that the 3.5 ppm species is more strongly coupled to ^{29}Si than SiOH, which tends to suggest that it corresponds not to mobile water in small cages (by analogy with NaY–ex), but to water or OH groups associated with non–lattice material. This is in agreement with findings reported in Chapter 4 that most of the signals in the ^{29}Si CP/MAS spectra of steamed Zeolite Y samples arise from non–lattice material. The small signals which remain in the AlOH–annulled spectrum (Figure 6.6(b)) are narrow, suggesting that they correspond to well–defined lattice sites, perhaps $Si(OSi)_3(OH)$ and $Si(OSi)_2(OH)_2$. The chemical shifts of the two peaks are –104.5 and –96.0 ppm (both ± 0.5 ppm), which are in reasonable agreement with previously–reported positions for these species (see Chapter 4 for a review of the literature).

6B: EFFECT OF THERMAL TREATMENT CONDITIONS ON NON–LATTICE ALUMINA

This Section describes the changes observed in the ^1H MAS spectra of dried HY samples as a function of the heating programme used during the drying procedure. As mentioned in Chapter 5, some samples were found to have significantly different ^1H spectra even when the programme was supposedly identical; this was interpreted as an indication of the difficulty of maintaining the

integrity of very dry samples during handling. Nevertheless, some common trends in behaviour were observed during variation of the programme, as described in the following paragraphs. In general, it was found that relatively mild conditions were sufficient to dry HY to the point where the free water peak (4 – 5 ppm) was no longer visible; heating to 200^{o}C (at 2^{o}C per minute) and holding for half an hour, or to 400^{o}C with no hold, were adequate. (The same was not found to pertain for metal cation–containing samples, as described in Chapter 7.) However, as shown in Section A of this Chapter, non–lattice alumina and other species are capable of 'hiding' large amounts of water by the formation of high concentrations of internal–surface OH groups; often very mildly–treated samples showed large signals due to AlOH at around 2.5 ppm.

1. Effect of Quenching

A study was performed to consider the effect of generating rapid cooling of the sample from certain temperatures after the normal drying programme. The usual procedure was to leave the sample tube evacuating and embedded in the insulated aluminium heating block to cool slowly; six hours typically sufficed to return the sample from 400^{o}C to room temperature. This technique was varied by removing the block after a period of time and allowing the sample tube to cool rapidly in air, reaching room temperature in a few minutes. The sample was in a closed evacuated tube during this 'fast cooling' phase. It was expected that the procedure outlined should achieve a quenching of the sample in the state pertaining at the time of removal of the heating block.

Figure 6.7 shows the ^{1}H MAS spectra of samples HY–29, HY–27, HY–26 and HY–54. These samples were all heated to 400^{o}C and held there for four hours; thereafter, the treatments applied were varied as follows. HY–29 was quenched immediately; HY–27 was allowed to cool slowly (still attached to the

Figure 6.7: ^{1}H MAS spectra of dried HY samples, quenched from temperature shown

(a)	HY–29: 400° C	RO=3000Hz NT=48 RD=5s
(b)	HY–27: 340° C	RO=2720Hz NT=48 RD=2s
(c)	HY–26: 270° C	RO=2988Hz NT=32 RD=5s
(d)	HY–54: not quenched	RO=3000Hz NT=100 RD=3s

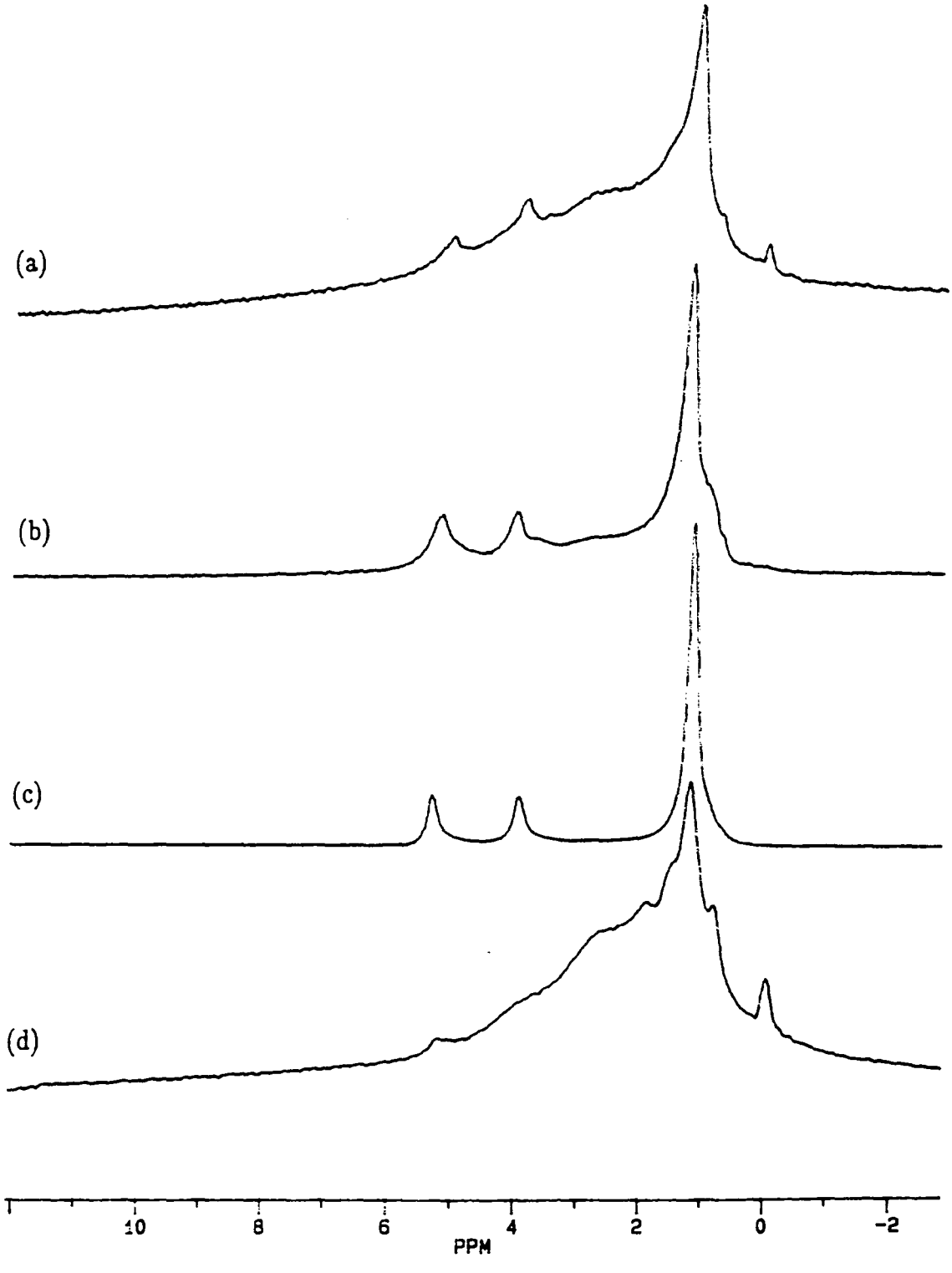

vacuum line) to 340^{o}C, then quenched; HY–26 was quenched similarly from 270^{o}C; and HY–54 was cooled slowly (with a liquid–air trap on the vacuum line) to room temperature. There is a clear progression though the first three members of the series, with the growth of the Brönsted peaks and the disappearance of the AlOH band (centred on 2.3 ppm) and its spinning sidebands (not shown) relative to the SiOH peak. The 0 ppm peak, as yet unassigned, also disappears. The loss of the AlOH band implies that either the non–lattice aluminium re–inserts into the lattice at lower temperatures, or that it forms a more highly condensed phase during slow cooling. The former suggestion is unlikely on account of the large amount of NLA visible in the unquenched sample HY–54 (Figure 6.7(d)), whereas the latter is reasonable on entropy grounds. Also, the formation of condensed NLA during slow cooling may be irreversible, since the water released would be pumped away almost immediately. It is not clear why the fourth sample, slow–cooled to room temperature, should show a high AlOH concentration. Another interesting feature of these spectra is the absence of any contaminant peak in HY–27 (b) and HY–26 (c), which were cooled without freezing of the trap. This may suggest that the contaminant only adsorbs at temperatures below 270^{o}C.

Figure 6.8 shows another two samples similarly treated. HY–35 (trace (a)) was heated to 400^{o}C, held for two hours, then slow–cooled with pumping to 300^{o}C and quenched. HY–36 (trace (b)) was quenched from 200^{o}C. On this occasion, the two samples were quenched while still connected to the vacuum line. It is clear that some contamination has occurred, although relatively little, especially in HY–36. Nevertheless, the same trend as before, towards a smaller concentration of AlOH and 0 ppm species, is evident. Surprisingly, the contaminant in HY–35 seems to have adsorbed selectively to small–cage Brönsted sites, destroying the expected peak at 5.2 ppm.

Figure 6.8: ^{1}H MAS spectra of dried HY samples, quenched from temperatures shown
(a) HY–35: 300° C RO=1540Hz NT=32 RD=2s
(b) HY–36: 200° C RO=3008Hz NT=32 RD=10s

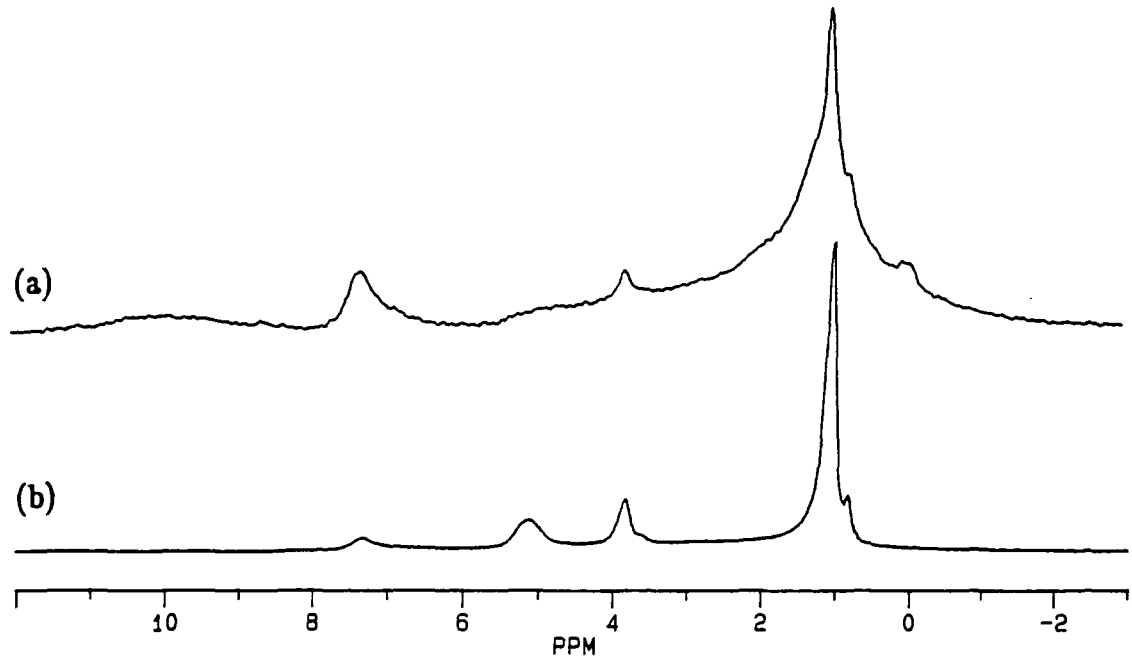

Figure 6.9: ^{1}H MAS spectra of dried HY samples
(a) HY–58 RO=3000Hz NT=100 RD=3s
(b) HY–59 RO=3030Hz NT=100 RD=3s

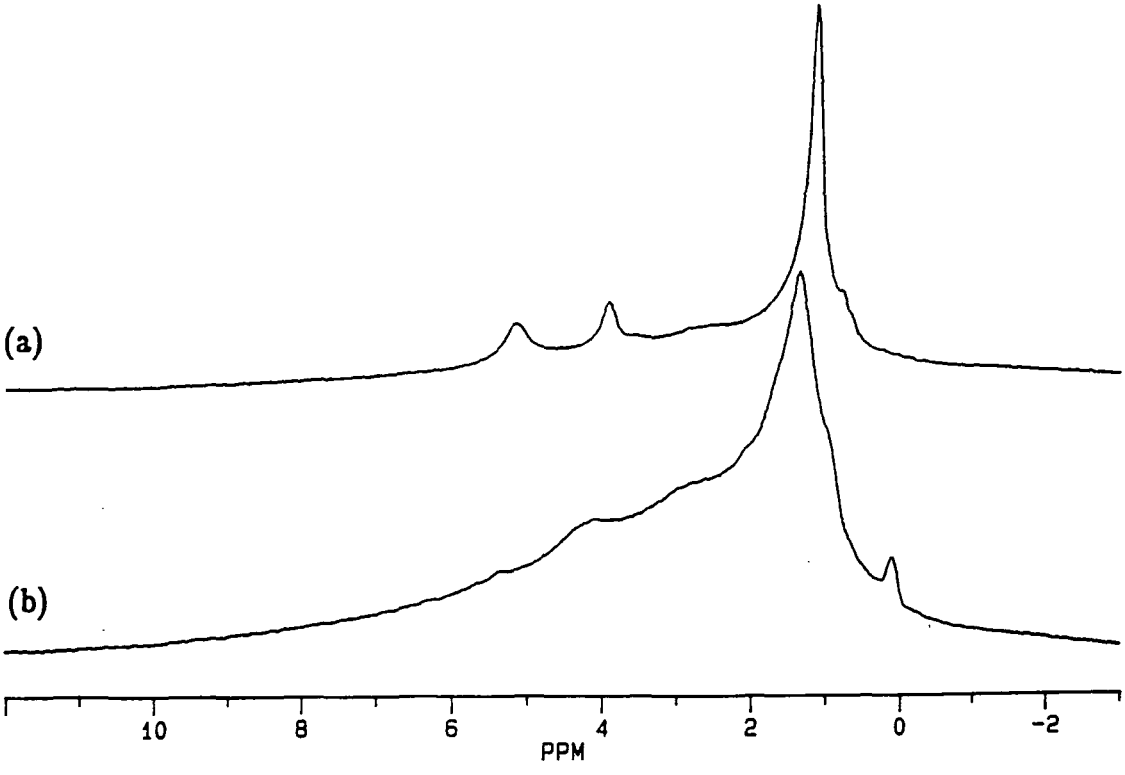

Another sample, HY–58, was heated to a higher temperature (500^{o}C) and quenched after a four–hour hold, in the expectation of generating an AlOH peak of greater intensity. However, the resulting spectrum, which appears in Figure 6.9(a), does not show any more NLA than, for example, the spectrum of HY–29 in Figure 6.7(a); the AlOH peak observed in HY–58 may, however, be broader, suggesting that the material has stronger homonuclear dipolar couplings.

2. Reheating of Dried Samples

A portion of sample HY–58 (described above) was retained in a dry N_2 atmosphere for 24 hours, then returned to the vacuum apparatus (without exposure to the open atmosphere) and heated again. The programme used involved heating to 400^{o}C under vacuum, holding for two hours and cooling slowly under vacuum to 220^{o}C; the sample was then quenched to room temperature in a closed tube. The resulting sample, designated HY–59, gave the ^{1}H MAS spectrum shown in Figure 6.9(b). It was anticipated that, if all the changes occurring in the NLA during slow cooling were reversible, the spectrum of HY–59 should resemble that of a sample such as HY–26, which was treated similarly to HY–59 except that the starting material was wet rather than dry. Clearly, however, the changes taking place under the two régimes must be quite different, since a substantial amount of AlOH is visible in HY–59. It is reasonable to suppose that the nature of the NLA present at the end of the heating time must differ substantially in the two cases of wet and dry starting material, since the former is likely to be more ^{1}H–rich. Although it is impossible to make further deductions from a single measurement, there is clear scope for further work to expand the understanding of NLA in such systems.

3. Varying Heating Time

The ^{1}H MAS spectra of a series of samples dried by similar methods appear in Figure 6.10. All the samples shown were heated under vacuum to $400^{o}C$, held for a certain time and quenched in a closed tube. The four samples (HY–23, HY–43, HY–29 and HY–52) were held at $400^{o}C$ for 0 h, 2 h, 4 h and 8 h respectively. Figure 6.10 demonstrates that the amount of AlOH visible decreases across the first three members of this series. This suggests that further condensation of NLA takes place over time, releasing water which is pumped away. The same phenomenon may indeed be responsible for the change in the series HY–29/27/26 discussed above (see Figure 6.7); in the latter series, cooling slowly to a lower temperature effectively results in a longer period spent at temperatures well above ambient. However, HY–26 was cooled slowly for only 45 minutes, which is short compared with the extra four hours of heating applied to HY–29 in the present series, and so the time scales of condensation appear to be different, *i.e.* gradual cooling encourages condensation to take place more quickly – possibly for entropic reasons as previously suggested. With the diminution of the AlOH peak, the Brönsted signals grow through this series, on account of the reduced tendency of highly–condensed NLA to coordinate to Brönsted sites.

After the extended heating time used for HY–52 (Figure 6.10(d)), more NLA is again visible, plus some broad features around the SiOH peak; this may suggest that, after long heating times, collapse of the lattice (to create further non–lattice silica and alumina) becomes significant.

Figure 6.10: ^{1}H MAS spectra of HY dried, variable duration of hold at 400° C as shown

(a)	HY–23: No hold	RO=3016Hz NT=128 RD=3s
(b)	HY–43: 2 hours	RO=1625Hz NT=32 RD=2s
(c)	HY–29: 4 hours	RO=3000Hz NT=48 RD=5s
(d)	HY–52: 8 hours	RO=3000Hz NT=16 RD=2s

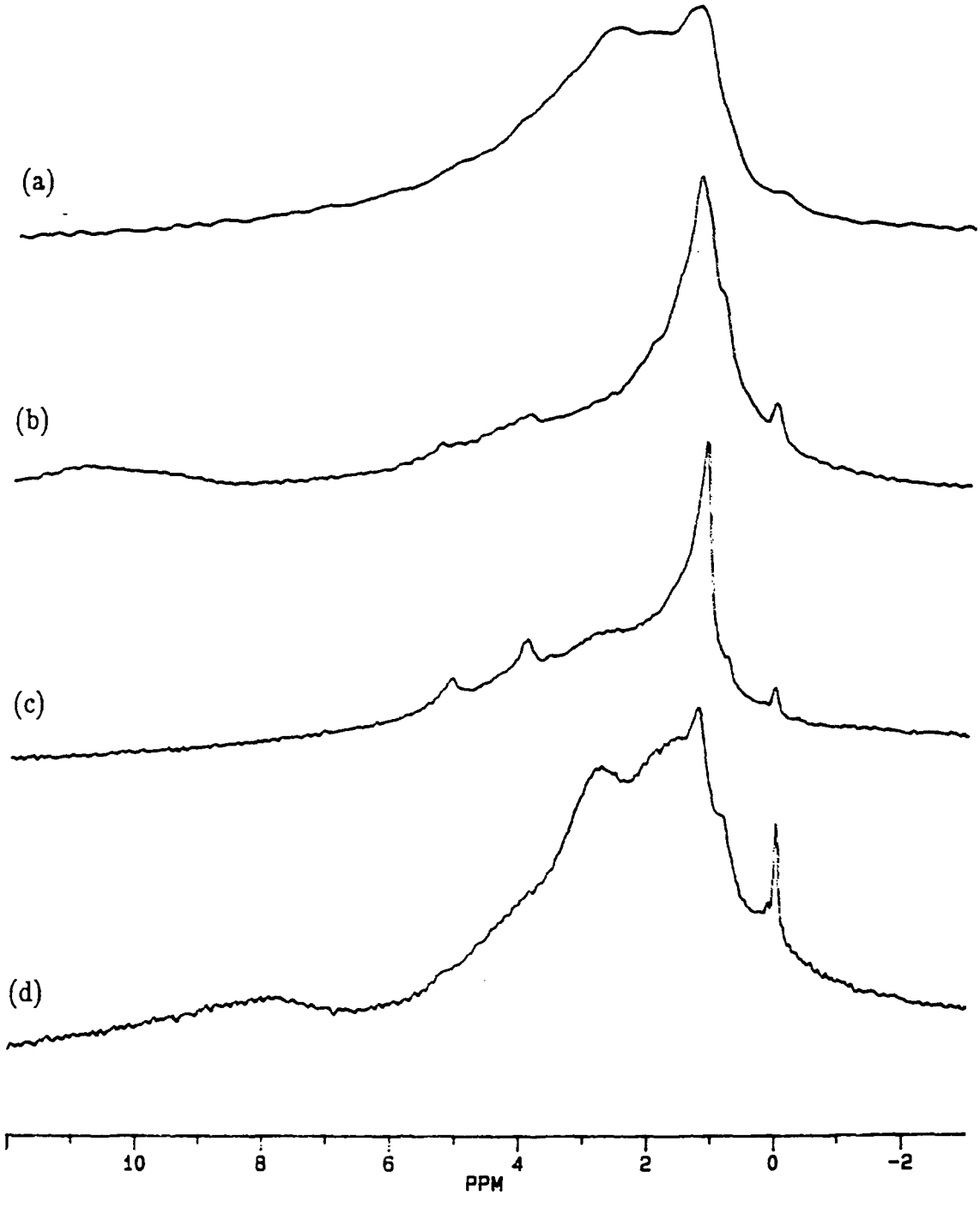

6C: AGING EFFECTS IN DRIED HY

Results were presented in Section A of this Chapter which showed that the slow adsorption of water on a sample of dried steamed HY resulted in a gradual increase in the population of AlOH and SiOH groups over a period of months, presumably by hydrolysis of X_1–O–X_2 linkages (X = Si, Al). This demonstrated that relatively subtle changes in the structure of a dried sample could be studied effectively by ^{1}H NMR. In this Section the results of similar aging experiments on dried HY samples are discussed, generally over a shorter time scale than the studies of HY–S. As before, they show that subtle changes are readily observed and quantified and provide information which can be used to begin to unravel the nature of non–lattice material in these very dry systems.

1. Sample HY–27

HY–27 was prepared by heating to 400^{o}C under vacuum, holding for 4 hours, cooling slowly under vacuum to 340^{o}C, then quenching to room temperature in a closed tube. The sample was packed as usual into a Kel–F rotor insert and the ^{1}H MAS spectrum shown in Figure 6.11(a) acquired almost immediately. The sample was kept in the rotor insert under ambient conditions for 24 days and the spectrum acquired again with identical spectrometer settings as shown in Figure 6.11(b). The spectra are dramatically different, with Brönsted peaks clearly visible in (a) but absent in (b), apparently having been swallowed by a substantial growth in the AlOH peak at around 2.6 ppm.

Integration shows the total areas of these two spectra to be equal to within the bounds of experimental error (trace (b) has a large amount of baseline undulation removed, introducing minor distortions in the integrals obtained). Thus, the changes observed cannot be attributed to adsorption of ^{1}H–containing

Figure 6.11: ^{1}H MAS spectra of HY–27 during aging (not same vertical scale)
(a) Fresh RO=2720Hz NT=48 RD=2s
(b) 24 days old RO=2983Hz NT=48 RD=2s

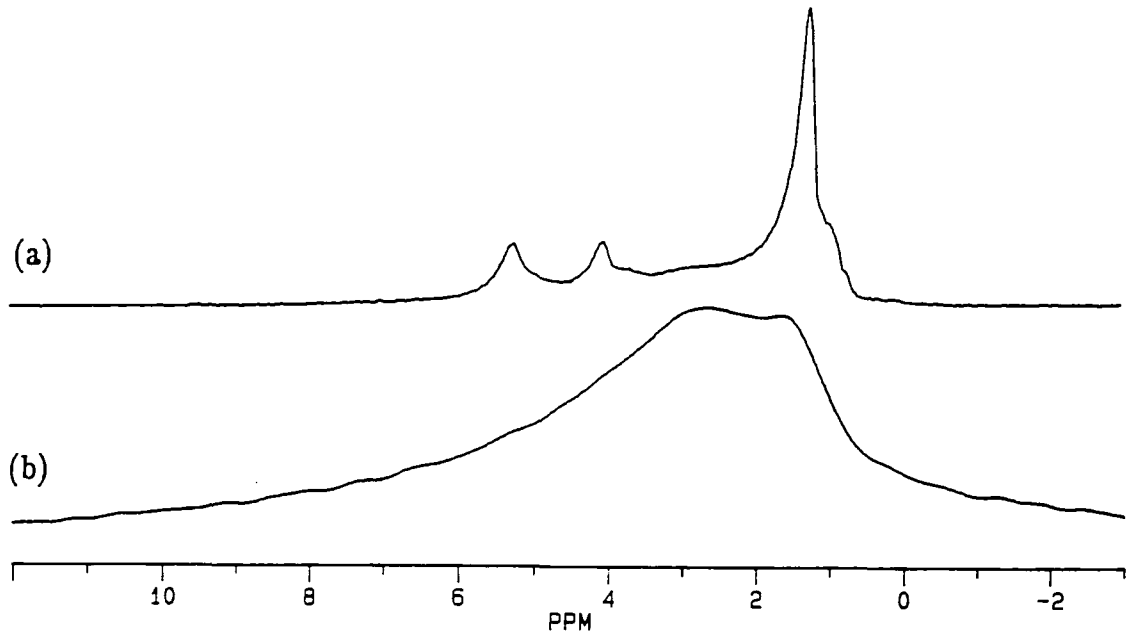

Figure 6.12: ^{1}H MAS spectra of HY–36 during aging
(not same vertical scale)
(a) Fresh RO=3008Hz NT=32 RD=10s
(b) 28 days old RO=3030Hz NT=64 RD=5s

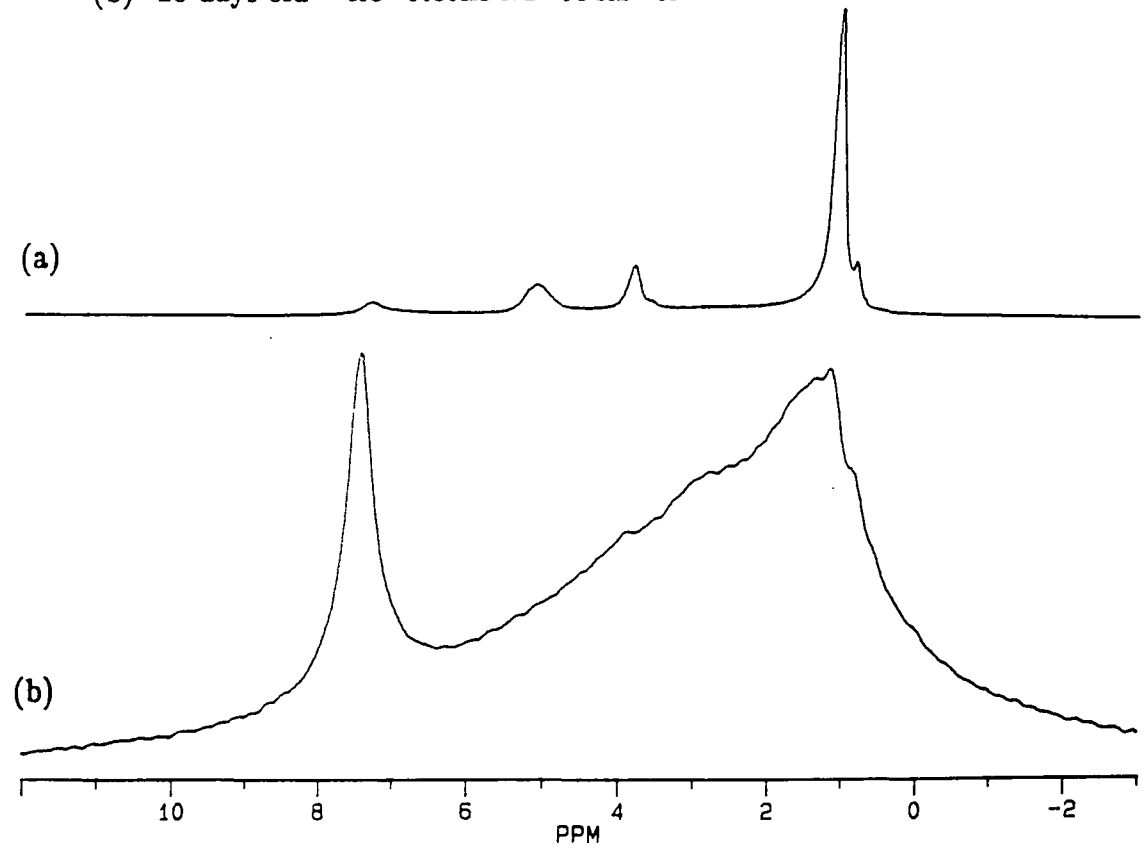

species such as water from the outside; rather, they must be explained in terms of re–distribution of ^{1}H within the sample. Deconvolution shows both spectra to contain narrow peaks at 1.2 ppm, assigned to SiOH; the peak has an intensity of 11.0 SiOH groups per unit cell in the fresh material, but only 2.1 after aging. The Brönsted peaks in the fresh sample account for a total of 1.9 ^{1}H per unit cell, whilst the AlOH signals contain 4.9 ^{1}H per unit cell, including the intensity in spinning sidebands. There must therefore be a total AlOH intensity of 15.7 ^{1}H per unit cell in the aged sample. It appears, then, that condensed NLA species have 'scavenged' OH groups from Brönsted and SiOH sites, forming new AlOH groups in their stead. This suggests that condensed NLA is quite reactive and has a significant capacity for absorption of water and other hydroxyl–containing material; this may be expected to influence its behaviour in a catalytic reaction.

2. Sample HY–36

This sample was prepared, as discussed earlier, by heating under vacuum to 400^{o}C, holding for 2 hours, then cooling slowly to 200^{o}C and quenching under vacuum. Figure 6.12 shows ^{1}H MAS spectra of the sample on the day it was made (trace (a)) and after storage in the rotor insert for 28 days (b). The fresh material shows SiOH and Brönsted peaks, plus a small signal at 7.4 ppm assigned to hydrocarbon contaminant. There is also a very weak, broad band under all these signals, which may be attributed to AlOH groups. After aging, this band has grown substantially, accompanied by the disappearance of the Brönsted peaks and the emergence of intense, broad spinning sidebands.

Integration of the spectra suggests that the total ^{1}H content of the sample has actually *fallen* by about half during the aging process. This observation may arise from two causes. Firstly, the aged spectrum has a substantial roll in the baseline (removed in Figure 6.12(b)), which must be

corrected to enable any attempt at integration. It may be that a significant amount of NMR signal contained in broad bands has been lost in this process. Secondly, there may be very broad components present in the AlOH signal, which integration has failed to distinguish from the baseline. Nevertheless, it is clear that the changes observed do not arise from the attack of water invading from the atmosphere. Further evidence that they result from rearrangement of the internal ^{1}H distribution, and support for the assignment of this peak to a contaminant, is found in the observation that the integral of the 7.4 ppm peak is unchanged within the bounds of experimental error. It is reasonable to suggest, then, that a hydroxyl–scavenging process very similar to that cited above for sample HY–27 has also occurred in the present case.

3. Sample HY–14

This sample was prepared at Unilever Research Port Sunlight Laboratory by drying overnight under vacuum at 430^{o}C. ^{1}H MAS spectra acquired after 3 and 6 months are shown in Figure 6.13. In this case, the total intensity of the spectrum has increased by a factor of about nine during aging, indicating that water has attacked from outside. As before, the AlOH and 0 ppm peaks have grown and the Brönsted sites diminished (perhaps due to rapid exchange with any free water present). There is also a new and rarely–observed signal at 6.5 ppm which other workers have attributed to water adsorbed on Lewis–acid sites (see Chapter 5). It is of interest to note, however, that the changes observed are generally similar to those in the other samples described above; this suggests that the NLA is capable of consuming hydroxyl groups from a range of sources to satisfy its desire to become less strongly condensed.

Figure 6.13: ^{1}H MAS spectra of HY–14 during aging (not same vertical scale)
(a) 3 months old RO=3000Hz NT=128 RD=2s
(b) 6 months old RO=3049Hz NT=128 RD=1s

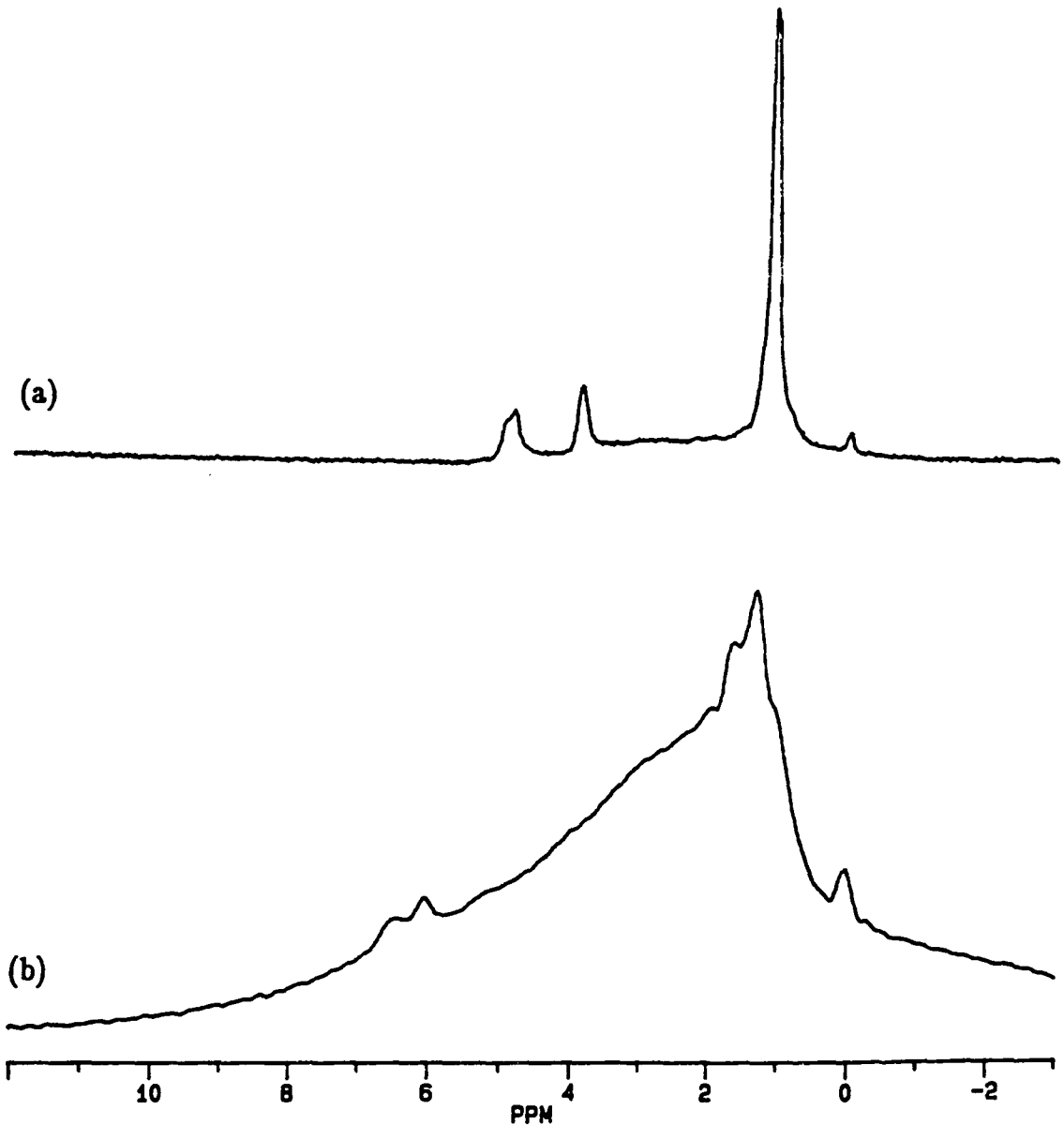

4. Controlled Hydration Studies

In the wake of the results obtained by rehydration over long periods of time, an experiment was devised to observe the effect of admitting a known amount of water to a dried HY sample using the controlled adsorption apparatus and technique described in Chapter 3. Limited success only was achieved, however, probably on account of the use of an inadequately airtight vacuum apparatus. Two samples were prepared thus: the first of these was Sample HY–60, which was heated under vacuum to 400^{o}C, held for 4 hours, then cooled slowly under vacuum with a liquid–air trap. When it reached room temperature, 10 moles of distilled and degassed H_2O were adsorbed per unit cell of the dried sample. The spectrum acquired when the sample thus made was five days old appears in Figure 6.14(a). It shows Brönsted, SiOH, 0 ppm and AlOH features all present. One interesting feature is that the Brönsted and AlOH signals are co–existent; in most other sample discussed in this Chapter and the one preceding, growth or appearance of the AlOH peak has been accompanied by attenuation or disappearance of the Brönsted peaks. This may suggest that the water adsorbed on the sample has hydrolyzed reactive NLA species which would otherwise attack and dehydroxylate Brönsted sites. It also indicates that there is no residual free water present, since this would be expected to render the Brönsted sites unobservable due to rapid ^{1}H exchange.

The second experiment involved the preparation of a dried sample, HY–63, made by heating to 400^{o}C under vacuum, holding for 4 hours and cooling slowly to 150^{o}C with a liquid–air trap, followed by a quench to room temperature in a closed tube. Part of the sample was removed and packed into a Kel–F rotor insert under dry N_2, while the remainder was returned to the vacuum line (without exposure to the open atmosphere) and hydrated with 20 mol water per unit cell. This second portion, HY–63–H (the final 'H'

Figure 6.14: ^{1}H MAS spectra of HY samples during controlled rehydration (not same vertical scale)

(a) HY–60 (10 mol H_2O adsorbed) RO=3030Hz NT=100 RD=3s
(b) HY–63 dry RO=3000Hz NT=100 RD=3s
(c) HY–63–H (20 mol H_2O adsorbed) RO=2980Hz NT=100 RD=3s

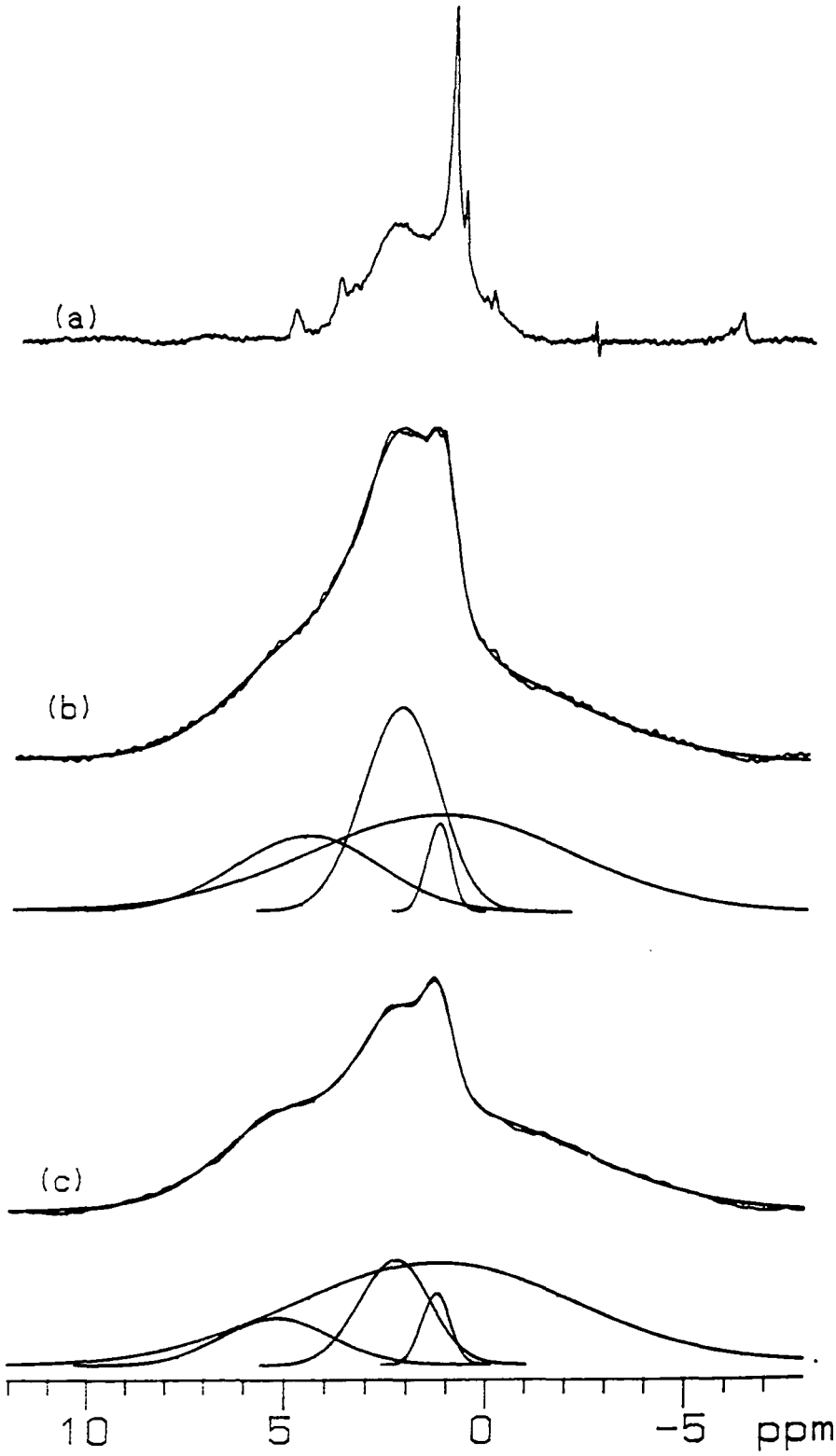

denoting 'hydrated'), was then packed into another rotor insert. ^{1}H MAS spectra of the two samples, acquired two days later, are shown with deconvolutions in Figure 6.14(b) and (c).

Table 6.4: Deconvolution of ^{1}H Spectra of HY–63 and HY–63–H

Sample	Intensity in ^{1}H atoms per unit cell			
	SiOH (1.2 ppm)	1.3 ppm	AlOH + ssbs (2.3 ppm)	≃5 ppm
HY–63	4.5	43.1	72.1	22.0
HY–63–H	6.8	93.2	49.2	16.7

The intensities of individual bands are shown in Table 6.4 in the form of ^{1}H population per unit cell of zeolite. The total ^{1}H population has risen by about 24 ^{1}H per unit cell (rather less than the expected value of 40) between HY–63 and HY–63–H. The results show a general increase in the populations of low–frequency bands, especially the broad peak centred on 1.3 ppm, and a decline in the populations of high–frequency bands. The broad peak at 1.3 ppm has not previously been observed, but it seems reasonable to assign it to SiOH groups (clustered, hence broadened by homonuclear dipolar coupling) on the grounds of its chemical shift; we may, therefore, be observing the hydrolysis of non–lattice silica or, perhaps, the complete dislodging of Al partly released from the lattice, forming a new NLA species and two lattice SiOH groups per Al atom displaced, as suggested in Chapter 4. The peak at around 5 ppm (4.6 ppm in HY–63, 5.2 ppm in HY–63–H) may be assigned to lattice Brönsted sites, which are slowly dehydroxylated by NLA as suggested before. The spectra presented above serve to accentuate the variability of results obtained from apparently

similar treatments (compare, for example, HY–63 with HY–26 and HY–54 as shown in Figure 6.7) and so it would be inappropriate to draw detailed conclusions on the strength of this measurement alone.

6D: CONCLUSIONS

The first Section of this Chapter described a study of the effect of treatment of a steamed HY sample with $(NH_4)_2H_2EDTA$. It has been considered by many workers that suitably controlled treatments such as this are capable of extracting non–lattice alumina from steamed zeolites without greatly affecting the lattice. The present study shows clearly, however, that the lattice undergoes significant changes during the EDTA–leaching procedure employed. Deconvolution of the ^{29}Si NMR spectrum suggests the formation of non–lattice silica, possibly accounting for up to 50% of all Si in the sample. There is, as expected, no non–lattice aluminium remaining, but elemental analysis and ^{1}H, ^{29}Si and ^{27}Al NMR results are all consistent with the re–insertion of Al into lattice sites. There is also a large population of SiOH groups in the leached material.

The effect of slow adsorption of water on a dried sample of steamed HY has also been investigated. The results show that the NLA is in a highly condensed form in the freshly–made sample, with only 1 OH per 15 Al non–lattice Al atoms present. After sorption of water over a period of 11 months, the NLA has been slowly hydrolyzed to a form containing 1.7 OH per Al.

A number of other experiments performed on dried HY samples serve to demonstrate that the NLA undergoes subtle changes in form depending on the

drying procedure and on the age of the sample. ^{1}H magic–angle spinning NMR coupled with computer deconvolution techniques have proved a powerful and effective tool for elucidation of these processes. It has been shown that extending the heating time of HY during the drying procedure generates a more highly–condensed NLA phase. The same effect can be observed on prolonged slow cooling of the sample. Both of these results suggest that condensation of the NLA at elevated temperature takes place within a time scale of hours, and is accelerated by gradual cooling, perhaps for entropic reasons.

Remarkable changes are also observed in dried HY samples which are kept in a water–free environment over a period of weeks. The condensation process appears to reverse slowly, with NLA attacking and dehydroxylating other OH–containing species in the sample such as Brönsted sites and SiOH groups. The NLA can also react with water slowly adsorbed through the walls of the container, as reported above for steamed HY. Controlled rapid sorption of water on a freshly–dried sample results in a growth of AlOH and possibly SiOH concentration without the disappearance of Brönsted sites, suggesting a more rapid reaction between water and AlOH in this instance. No evidence is seen for the presence of free water in these samples. Combination of these results with those presented in Section C of Chapter 5 may suggest a time scale of $1 - 2$ days for the dislodgement of partially displaced lattice Al atoms.

CHAPTER 7: DRYING OF CATION–CONTAINING ZEOLITE Y

The drying studies described in Chapters 5 and 6 are confined to the investigation of HY zeolites – that is, samples containing a very low level of charge–balancing cations. The present brief Chapter complements this by considering the effect of similar drying treatments on cation–containing samples of Zeolite Y; the cations Na^+, Ag^+ and NH_4^+ are considered in turn. Materials such as these are relevant to the investigation of lattice degradation in zeolite catalysts on account of the known behaviour of cations, in particular Na^+, in inhibiting such degradation under moderate conditions. The evidence for this, and a mechanism by which it might be considered to take place, are discussed in the first Section of Chapter 4. Thus, a sample containing Na^+ cations may well not undergo the same lattice changes found in HY (described in Chapter 5) during drying; that is, the lattice in dried NaY could be expected to resemble that in the wet material to a much greater extent than in the case of HY.

In addition, experiments attempting to prepare dried cation–containing zeolites act as a direct test of the widely–held belief that such cations are involved in strong attractive interactions with water. Thus, it is no surprise to find that drying procedures such as heating under vacuum to 400^oC for 2 hours, which is sufficient to remove almost all intracrystalline water from HY, are entirely inadequate for drying NaY and AgY, as shown in the following pages. In addition, the intense interactions alleged to take place between water and cations would be expected to result in reduced water mobility, especially as the sample becomes drier, leading to altered NMR characteristics for the ^1H nuclei on the water molecules. This prediction is also confirmed by the experimental results described below.

7A: DRYING OF NaY

Five portions of the standard NaY sample described in Chapter 5 were subjected to drying treatments of increasing severity. All were heated under vacuum to 400^{o}C; the hold times ranged from 24 to 63 hours. (Full details are given in Appendix B.) The ^{1}H MAS spectra of these samples are shown in Figure 7.1. Although some variability is apparent, a general trend may be discerned: the usual, rather narrow, water peak at 4.3 ppm seen in NaY–8 (trace (a)) apparently gives way to two broad signals, one centred on 1.3 – 2 ppm and the other on 7 – 8 ppm. In NaY–39, the high–frequency band is extremely broad and intense, but narrows and shrinks on progression though the series. It is absent in fresh NaY–31 (trace (e)), but reappears at 8.5 ppm in this sample after aging for eight days. (Integration shows that very little water, if any, has penetrated the Kel–F rotor insert from the outside atmosphere during this period.) It is reasonable to assign this signal to residual water. The strong binding to the cation which it is expected to undergo would result in deshielding of the ^{1}H nuclei on the water molecules, as observed; in addition, the reduced mobility of the water is likely to permit enhanced ^{1}H–^{1}H dipolar coupling (intra– and intermolecular), resulting in a broadening of the signal relative to the 'wet' sample (NaY–8).

The second signal resembles the peaks assigned to SiOH groups in spectra of dried HY, except in NaY–46 where it appears as a broader band centred on 2.1 ppm. It is generally too intense to be explained simply in terms of terminating SiOH on the exterior surfaces of the crystallites; the NaY sample used is known to be highly crystalline before heat treatment (see Chapter 5) and so, if the assignment of this band to intracrystalline SiOH groups is correct, it must be deduced that some degradation of the lattice takes place, especially after

Figure 7.1: ^{1}H MAS spectra of dried NaY samples

(a)	NaY–8	RO=3016Hz NT=128 RD=5s AQ=100ms
(b)	NaY–39	RO=1680Hz NT=32 RD=3s
(c)	NaY–46	RO=3040Hz NT=64 RD=5s
(d)	NaY–51	RO=3010Hz NT=64 RD=3s
(e)	NaY–31 fresh	RO=2990Hz NT=32 RD=5s
(f)	NaY–31 aged	RO=3030Hz NT=32 RD=2s

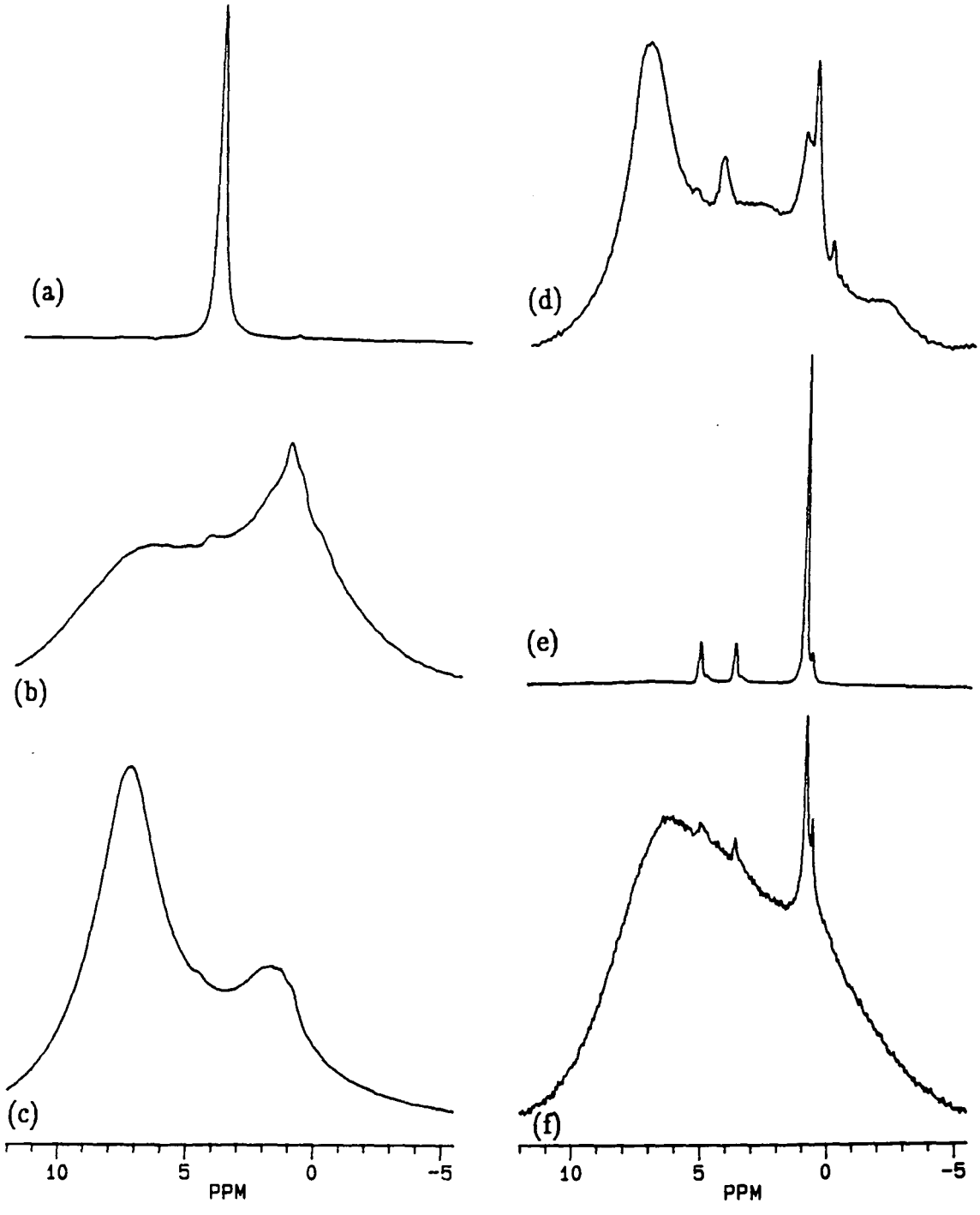

prolonged treatment (*e.g.* 48 hours in the case of NaY–51, Figure 7.1(d)). Two distinct SiOH peaks are visible in NaY–51 and NaY–31, at about 1.2 and 0.9 ppm, in varying proportions. These might correspond to surface and internal SiOH groups, or perhaps those in large and small lattice cages. They are destroyed at different rates during the aging of NaY–31 (see Figure 7.1(e) and (f)).

In addition to these signals, a further set of peaks is observed to emerge across the series. Small humps can be discerned at 4.6 ppm in NaY–39, NaY–46 and, much more strongly, in NaY–51. The peak has shifted to 3.9 ppm in NaY–31, the most severely–treated sample. This is very close to the position assigned to small–cage Brönsted sites in dried HY samples. Further small peaks at around 5.7 ppm can be seen in NaY–39 and NaY–51; a clear, narrow signal at 5.3 ppm is also visible in NaY–31, close to the large–cage Brönsted position in HY. The T_1 values measured in fresh NaY–31 at 200 MHz also resemble those found for Brönsted sites; the values are 547 and 952 ms for the 5.3 and 4.0 ppm peaks respectively. (The values in NaY–51 are difficult to measure, but seem to be around 100 and 25 ms respectively; the short times observed may arise from enhanced relaxation due to the motion of residual water.) The appearance of Brönsted–acidic ^{1}H in a NaY sample implies that Na^{+} cations are no longer strongly associated with all lattice Brönsted sites; ^{23}Na NMR might be able to reveal the environment in which the displaced cations are located.

Other T_1 values measured at 200 MHz are as follows. The 4.3 ppm signal attributed to free water in NaY–8 has an associated T_1 of 18.6 ms, close to the value of 12.7 ms measured for free water in untreated NaY (see Chapter 5). The poor resolution of the peaks in NaY–39 does not permit measurement of separate T_1 values; all peaks appear to have a value close to 120 ms. The 7.5 ppm peak in NaY–51 has a T_1 of 79.7 ms, and the SiOH cluster

(0.9 – 1.3 ppm) around 50 ms (see Figure 7.2 for a plot of the relaxation curves obtained for this sample). In contrast, the T_1 of the SiOH band in the very dry NaY–31 sample is estimated at 1.02 s, further supporting the belief that this sample contains very little free water. $T_{1\rho}$ values were estimated for this sample at 62.5 kHz to be around 14, 13, and 19 ms for the high– and low–frequency Brönsted and SiOH bands respectively.

Integration of the ^{1}H spectrum of fresh NaY–31 provides the following estimates of the site populations per unit cell: large–cage Brönsted, 15; small–cage Brönsted, 15; SiOH, 78. Data presented in Chapter 5 shows that this sample contains about 44 Al per unit cell. The ^{1}H NMR spectrum reveals, therefore, that about two–thirds of the Brönsted sites in this sample are protonated. There is no evidence for the presence of non–lattice material, whether in the dried sample or in the precursor NaY.

Sample NaY–ex–12. This sample, which was made from NaY–ex (prepared by exchanging Na^+ cations into the normal HY sample, as discussed in Chapter 5), was heated to 400^{o}C under vacuum for 24 hours and packed in a rotor insert for MAS. The ^{1}H MAS spectrum (acquired on the CXP–300) shows a single, fairly broad line at 3.6 ppm, strongly resembling the major signal in the spectrum of the wet sample (see Figure 5.7(b)). The ^{29}Si CP/MAS spectrum of NaY–ex–12 is identical to that of the starting HY, showing that no major changes have occurred in the lattice.

Figure 7.3 shows deconvolution plots of the T_1 and T_2 relaxation curves measured for this sample at 60 MHz. The T_1 profile contains three components as follows: 51 ms (13% of total population), 13 ms (23%) and 3.9 ms (64%). This pattern is very similar to that found for untreated HY (see Table 5.2), suggesting that the present sample contains much free water. The components

Figure 7.2: Relaxation curves obtained from inversion–recovery measurement of T_1 in NaY–51: the crosses are experimental data, whilst the continuous lines are the best–fitting exponential curves. Top: 4.5 ppm signal; middle: 0.9 ppm; bottom: 7.6 ppm. Note the poor fit to the top data; this probably arises from the superimposition of two peaks. The vertical scale is in arbitrary intensity units.

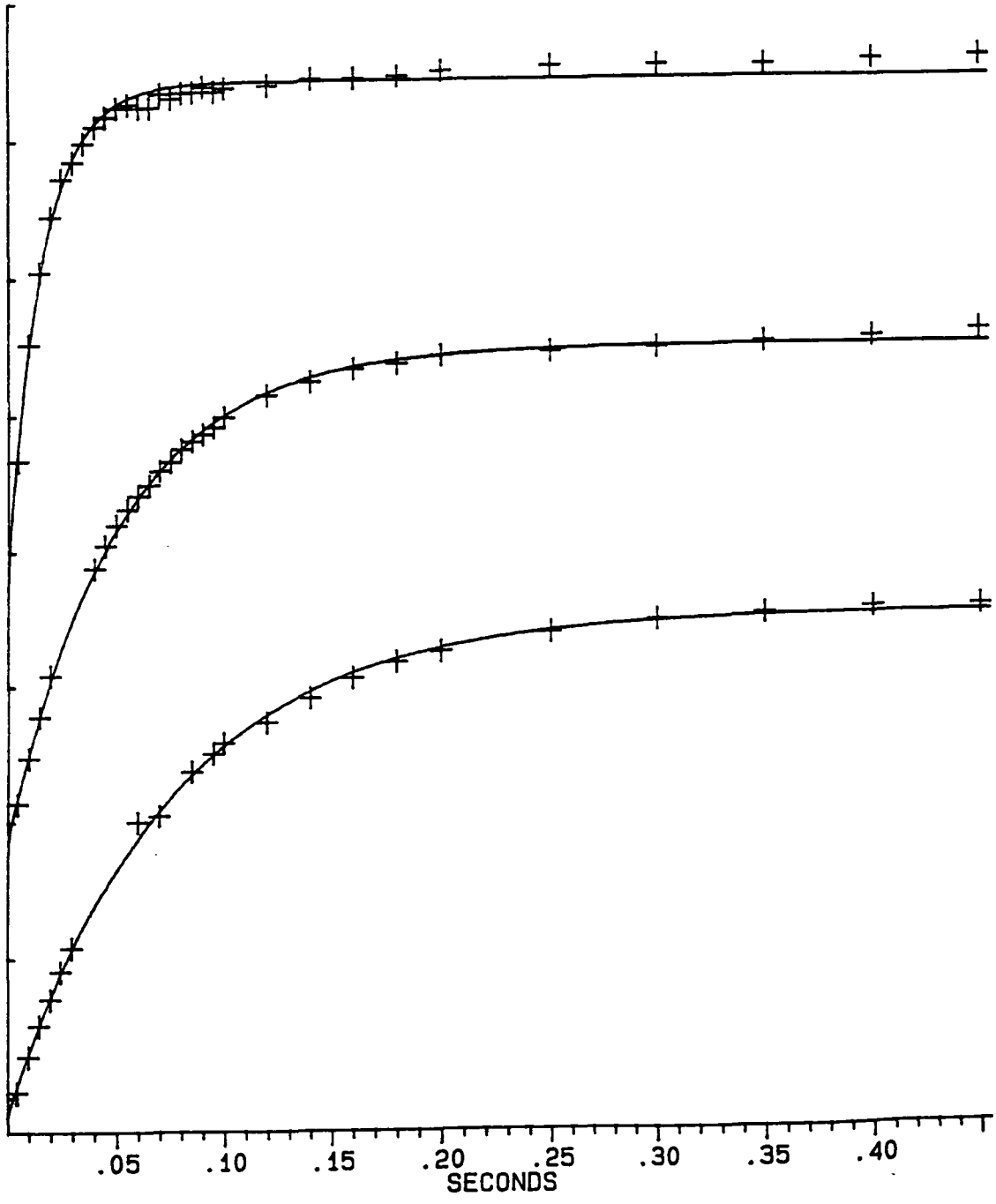

Figure 7.3: Deconvolution plots obtained from T_1 (top) and T_2 (bottom) measurements of NaY–ex–12. See Chapter 5 for a full description of this type of plot.

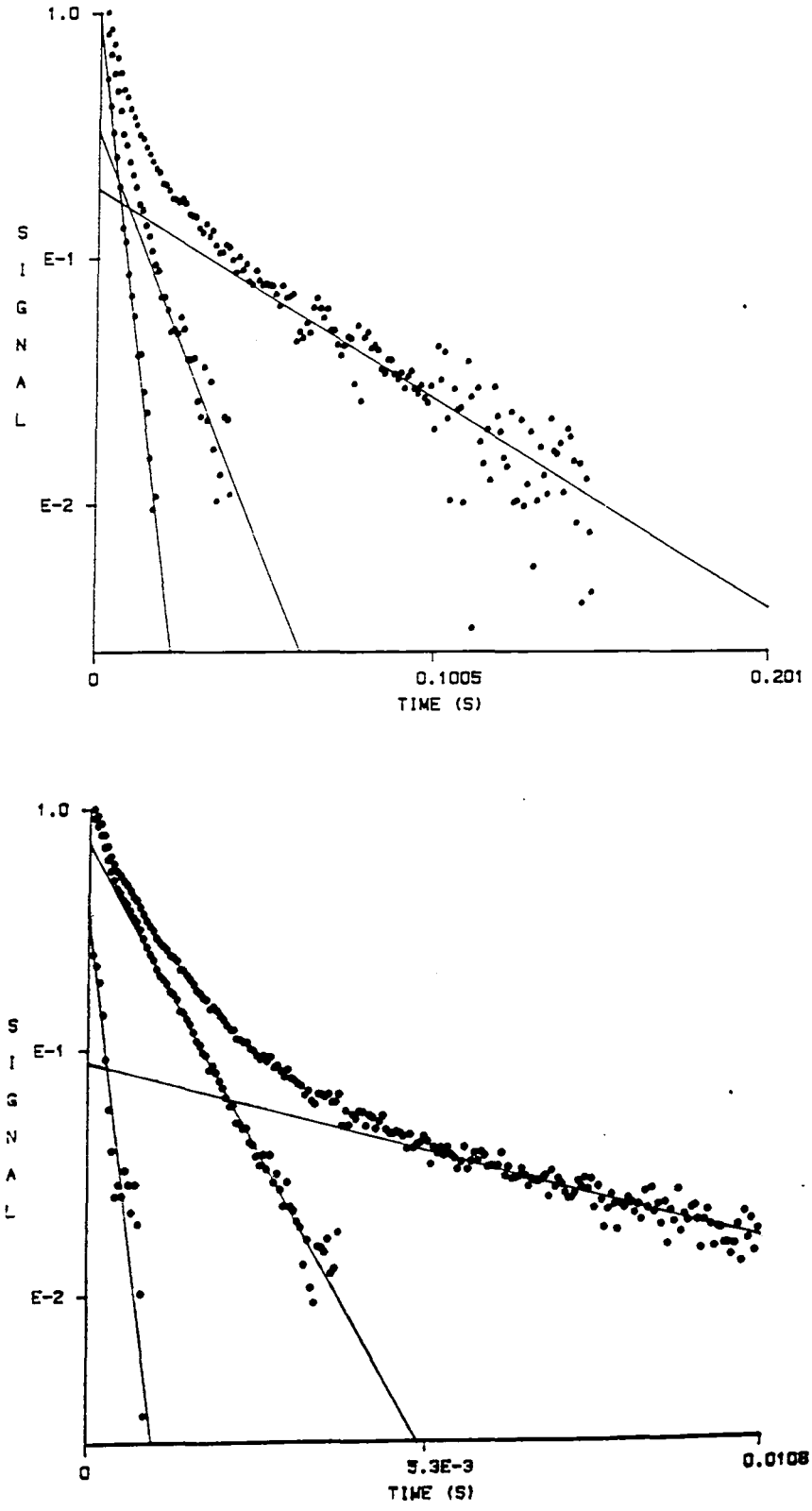

are assigned respectively to SiOH, small–cage and large–cage water (the latter, at least, presumably associated with Na^+). The T_2 profile measured at 60 MHz is 6 ms (7%), 900 μs (62%) and 210 μs (31%). Comparison of the populations with the T_1 values given above suggests the assignment of the 900 μs component to large–cage water and the 210 μs component to small–cage water. These values are rather different from those measured previously for HY: the small–cage value in the present sample is longer, and the large–cage value shorter, by a factor of about 4 in each case. It has already been suggested (see Chapter 5) that the small cages of NaY–ex are cation–free in the fresh sample (as used here), resulting in increased mobility of small–cage water (although it is surprising, perhaps, that the figures for HY and NaY–ex–12 differ so greatly, since HY also contains no metal ions). In addition, the loss of some water from the supercages will result in longer residence times on cation coordination sites, hence to enhanced homonuclear dipolar couplings, leading to a diminished T_2 value. Only two $T_{1\rho}$ components could be distinguished at 20 kHz: 10 ms (24%) and 1.8 ms (76%), which may be assigned to small– and large–cage water respectively. The latter value is close to that measured for HY (Table 5.2), but the former is longer than the value of 6 ms reported previously for HY, again pointing to reduced water mobility on the 10^{-5} s time scale.

7B: DRYING OF AgY–ex

This sample was prepared by ion–exchange of HY with aqueous Ag^+ in an attempt to generate a cation–containing material with a lower affinity for water than NaY. A dried sample of AgY–ex, known as AgY–ex–22, was prepared by heating under vacuum to 400^{o}C, holding for 18$\frac{3}{4}$ hours, cooling

Figure 7.4: ^{1}H MAS spectra of AgY–ex–22
(a) Fresh RO=3066Hz NT=128 RD=3s
(b) Aged RO=1000Hz NT=64 RD=1.5s

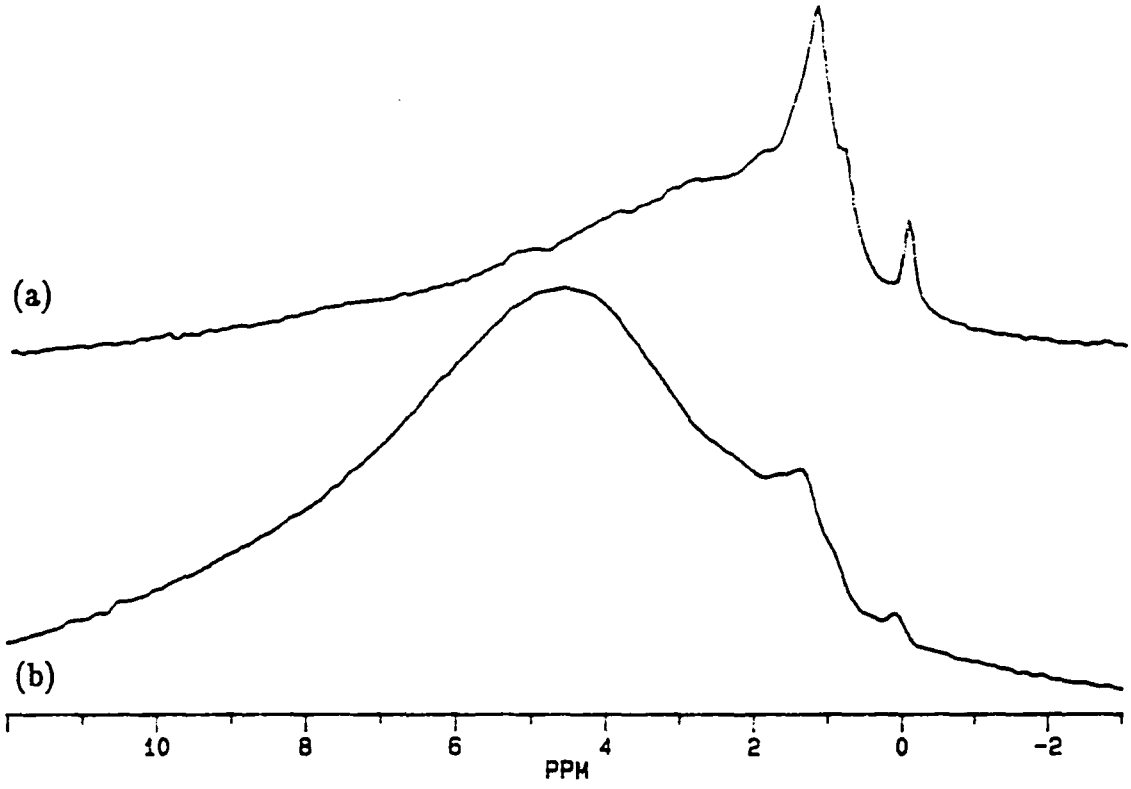

Figure 7.8: ^{1}H MAS spectrum of NH_4Y–47 aged RO=3020Hz NT=64 RD=5s

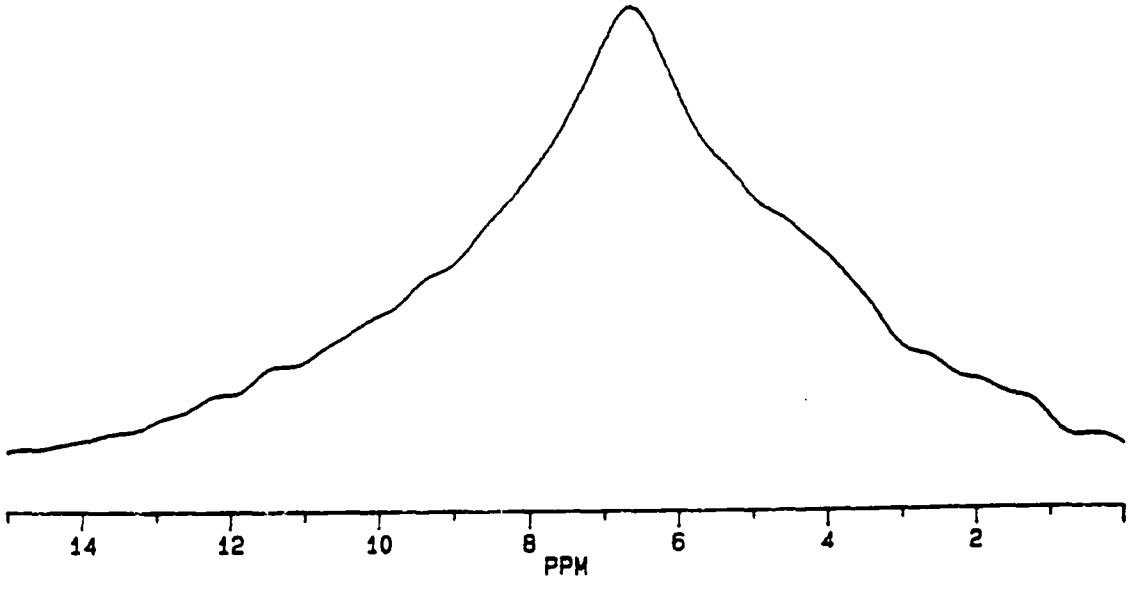

slowly to 200^{o}C and then quenching in a closed tube. The ^{1}H MAS spectrum given by this material is shown in Figure 7.4(a). It appears that the aim outlined above has been successful; there is little evidence for free water in this sample, whilst the SiOH, AlOH (broad) and 0.0 ppm signals familiar from dried HY (see Figure 5.18) are all clearly visible. Small bumps can just be distinguished at around 4.0 and 5.2 ppm, near the usual Brönsted site positions in dried HY samples, but they are clearly strongly attenuated compared with similar HY samples such as HY–29 (Figure 5.18(e)). It is reasonable to deduce, therefore, that Ag^{+} cations have replaced the readily exchangeable acidic ^{1}H atoms at these sites. All other sites, including the unassigned 0 ppm species, apparently remain intact and so do not exchange with Ag^{+}, confirming the assignments of the peaks concerned to predominantly non–acidic groups such as SiOH and AlOH.

Figure 7.4(b) shows the ^{1}H spectrum of the same sample after aging for 48 days. An intense band is visible at 4.6 ppm, which may be assigned as usual to free water (or possibly OH groups on non–lattice alumina, although the chemical shift is unusual for such species). As with the HY examples described in Chapter 6, however, integration shows that there has been no overall increase in sample ^{1}H content; it must therefore be assumed that internal OH groups have condensed to release water, which may then strongly adsorb to Ag^{+} ions, as suggested by the broadness of the water band, preventing the occurrence of the reverse process.

The T_1 values measured at 200 MHz for the freshly–dried sample are as follows (see Figure 7.5): 0 ppm, 424 ms; SiOH, 227 ms; AlOH, about 115 ms. These times are in broad agreement with those measured for dried HY (see Table 5.5).

Figure 7.5: Relaxation curves obtained from inversion–recovery measurement of T_1 in AgY–ex–22 (see Figure 7.2 for a description of this type of plot). **Top: 1.3 ppm signal; bottom: 0.0 ppm.** The vertical scale is in arbitrary intensity units.

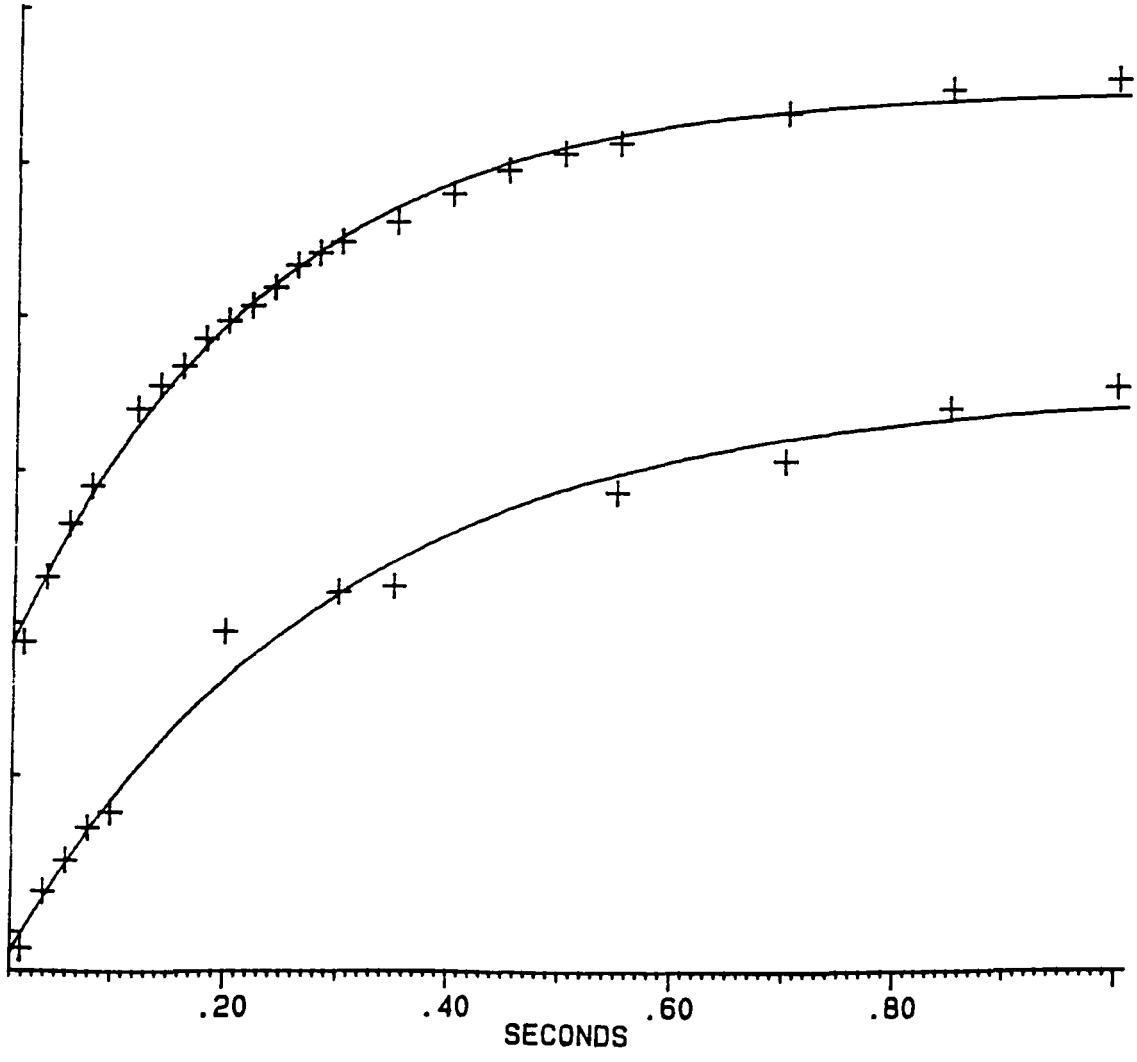

7C: DRYING OF NH_4Y

A number of standard procedures commonly employed in the preparation of Zeolite Y samples for study and for industrial applications involve a stage in which the material exists in the NH_4Y form as an intermediate. Such procedures include cation–exchange, catalytic activation (*en route* to the H–form), calcining, steaming and chemical treatments such as dealumination, which often yield an NH_4^+–zeolite as the final product. Accordingly, it would be useful to be able to study dried NH_4Y in the same manner as that described in earlier Chapters for HY. However, the complication of thermal instability of the NH_4^+ cation arises: it is generally considered (*e.g.* on the strength of temperature–programmed desorption and similar thermal experiments) that decomposition occurs at $250 - 300^oC$, yielding NH_3 (which desorbs) and H^+. If this process were to take place cleanly during the normal (400^oC) drying procedure, without concomitant damage to the lattice or other side reactions, the resulting material might be expected to resemble dried HY (excluding effects due to non–lattice material in the latter). Alternatively, any residual NH_4^+ or NH_3 might interact strongly with water or other species, or bind strongly to Brönsted sites or NLA, producing characteristic effects in the ^1H spectrum. The present study aims to investigate this underdeveloped area.

Nine samples of dried NH_4Y have been prepared from the NH_4Y[2] sample described in Chapter 5 by varying treatments, which are summarized in Appendix B. A representative selection of ^1H MAS spectra is shown in Figure 7.6, along with the spectrum obtained from the untreated precursor. The treatments applied were generally milder than those used for drying HY. The first sample, NH_4Y–37, was dried at only 100^oC for 4 hours and quenched. The ^1H spectrum (Figure 7.6(b)) shows a substantial diminution of the free water

Figure 7.6: ^{1}H MAS spectra of dried NH_4Y samples

(a)	NH_4Y hydrated	RO=3125Hz NT=32 RD=400ms
(b)	NH_4Y–37	RO=3011Hz NT=16 RD=2s
(c)	NH_4Y–45	RO=1000Hz NT=64 RD=3s
(d)	NH_4Y–47	RO=3020Hz NT=64 RD=5s
(e)	NH_4Y–55 (VXR–300)	RO=4260Hz NT=100 RD=2s
(f)	NH_4Y–53	RO=3000Hz NT=256 RD=5s
(g)	NH_4Y–56 (VXR–300)	RO=3290Hz NT=100 RD=3s
(h)	NH_4Y–61	RO=3000Hz NT=100 RD=3s

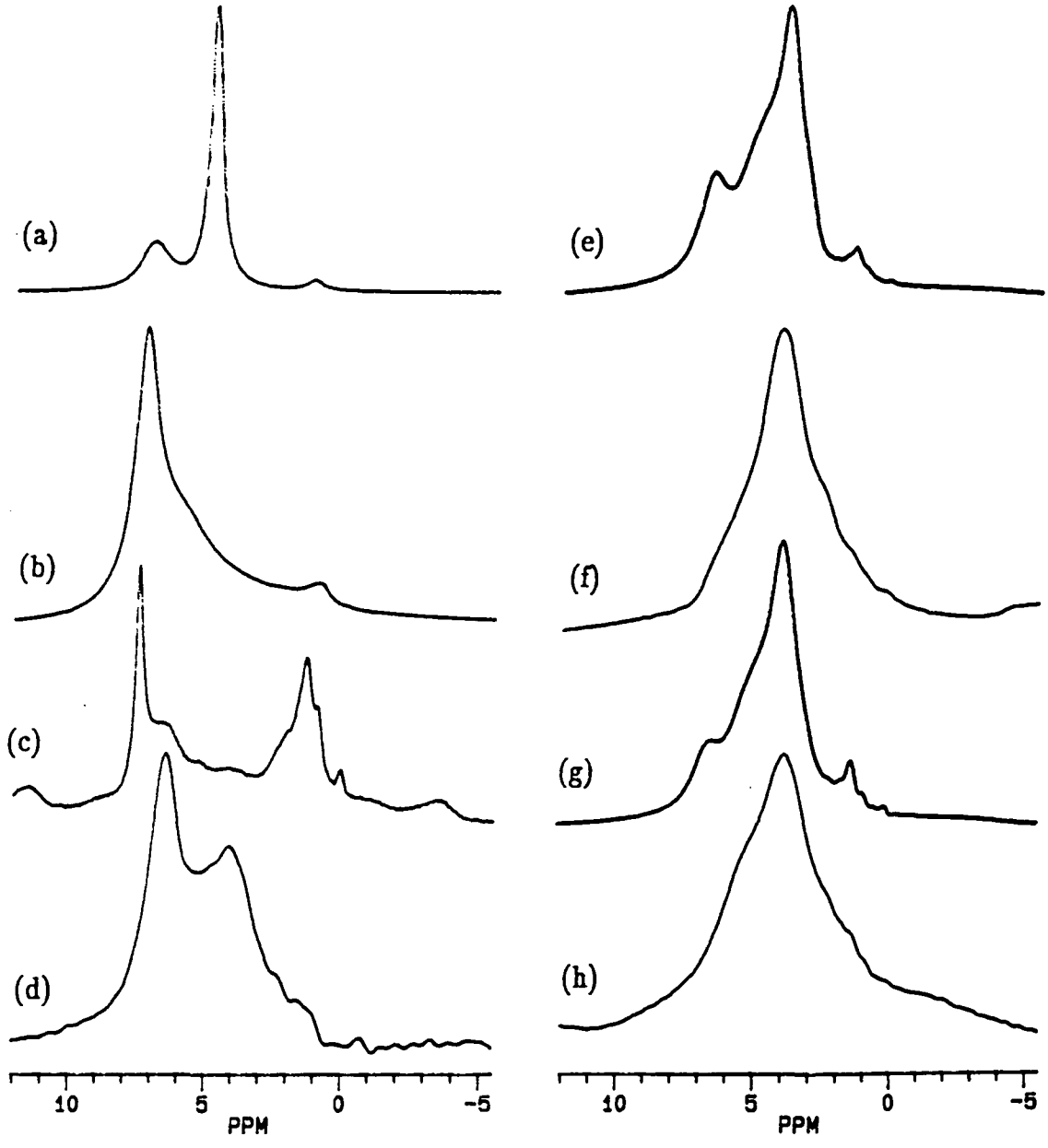

peak (4.8 ppm in the untreated material) relative to the NH_4^+ (7.3 ppm) and SiOH (1.1 ppm) signals. It also appears to shift to higher frequency, perhaps to around 6 ppm. A similar effect was found in the case of NaY discussed in Section A, and may be attributed to deshielding of the ^1H nuclei on water due to increased H–bonding between water O and ammonium H as water becomes scarce. The trend continues in NH_4Y–45 (Figure 7.6(c)) with the water signal now at around 6.5 ppm, accompanied by intense spinning sidebands (one of which underlies other peaks at about 1.6 ppm). The NH_4^+ peak (around 7 ppm) seems to remain strong until NH_4Y–47, which was heated to 250°C for 4 hours, but is severely attenuated in later samples, appearing only weakly in samples treated at 300°C (such as NH_4Y–56, Figure 7.6(g), and NH_4Y–57, not shown), and often shifted slightly to low frequency (*e.g.* 6.3 ppm in NH_4Y–56). The shift is unlikely to arise from rapid exchange between NH_4^+ and NH_3, since the signal is unaffected by cooling from room temperature to –50°C (this experiment was carried out on NH_4Y–55, 56 and 57: see Figure 7.7).

In place of the original water and NH_4^+ peaks there appears a broad band centred on approximately 4 ppm (4.1 ppm in NH_4Y–47, 3.7 – 3.9 ppm in NH_4Y–55/56/57, 4.1 ppm in NH_4Y–61). This band shifts about 0.2 ppm to high frequency on cooling to –50°C and often exhibits a shoulder on the high–frequency side, which is particularly apparent in NH_4Y–55. One possible interpretation of this band is that it arises from NH_3 remaining in the lattice, trapped perhaps in small cages; either the high–frequency shoulder or the shift on cooling could result from H–bonding to lattice oxygen. If this peak is assigned alternatively to residual water, it must be assumed that some NH_3 or NH_4^+ is still present to bind the water, since it would otherwise be expected to desorb as readily as from HY. The high–frequency shoulder to the main band is noticeably attenuated on cooling to –50°C, suggesting that it may arise from exchange

between NH_3 and NH_4^+ *via* interaction of NH_3 with Brönsted sites. Another point of interest concerning the 4 ppm band is that it usually exhibits strong spinning sidebands, suggesting that the corresponding species is bound to an appropriate site such as a Brönsted site or a lattice oxygen atom.

The only remaining signal not discussed so far is the SiOH band, which is detected at 1.2 ppm in the starting material and in several other samples shown in Figure 7.6. It is particularly intense in NH_4Y–45 (although part of the low–frequency cluster is a spinning sideband arising from the 6.5 ppm water peak); this sample was heated for 45 hours, much longer that the others in this study, which may have resulted in a degree of lattice degradation. Figure 7.7 illustrates that the SiOH peak shifts to higher frequency and almost vanishes on cooling to -50^oC, suggesting the occurrence of intense H–bonding amongst clustered SiOH groups, resulting in deshielding of the ^1H nuclei and the development of strong homonuclear dipolar coupling, which severely broadens the signal. The same effect is observed in NH_4Y–56 and NH_4Y–57.

Figure 7.8 shows the spectrum of NH_4Y–47 acquired under identical conditions to that shown in Figure 7.6(d), but after nine days of storage in the rotor insert. In place of the original peaks at 4.0 and 6.5 ppm, a single broad band centred on 6.8 ppm has appeared, with a hint of a shoulder on the low–frequency side. This suggests that NH_3 previously trapped in small cages has effused into the supercages, permitting rapid exchange of hydrogen with NH_4^+. There is clearly a preponderance of NH_4^+, on account of the population of H^+ required to balance anionic charges in the lattice.

^1H relaxation times have been measured on the CXP–200 as follows. The NH_4^+ peak has a T_1 of 17 ms in the wet sample, rising to 80 ms in NH_4Y–37 and to around 150 ms in dried samples, as the site residence time increases. The $T_{1\rho}$ value measured at 62.5 kHz rises similarly from around 3 to 14 ms. The T_1

Figure 7.7: ^{1}H MAS spectra of NH_4Y–55 (VXR–300) NT=100 RO=4300Hz RD=2s
(a) Room temperature (b) –50° C

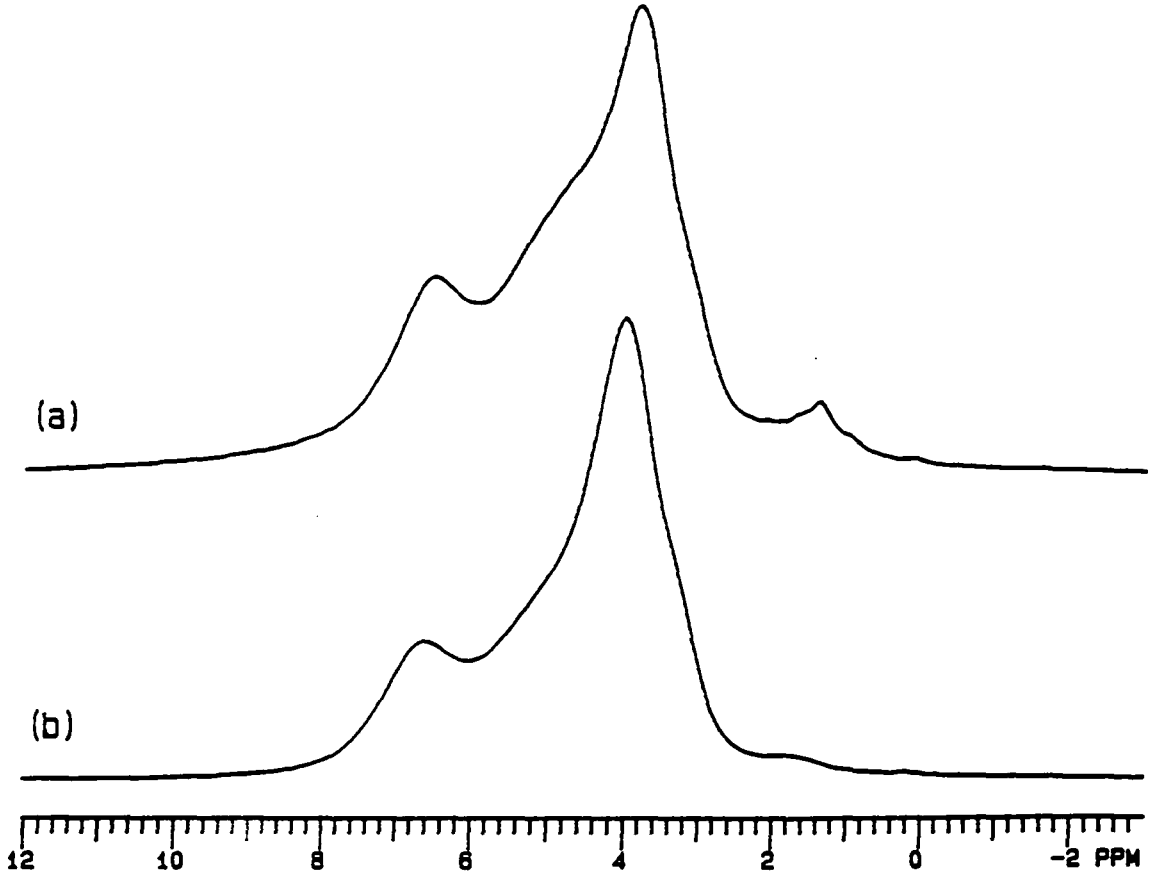

Figure 7.9: Relaxation curve obtained from inversion–recovery measurement of T_1 in NH_4Y–47, 6.8 ppm peak. See Figure 7.2 for a description of this type of plot. The vertical scale is in arbitrary intensity units.

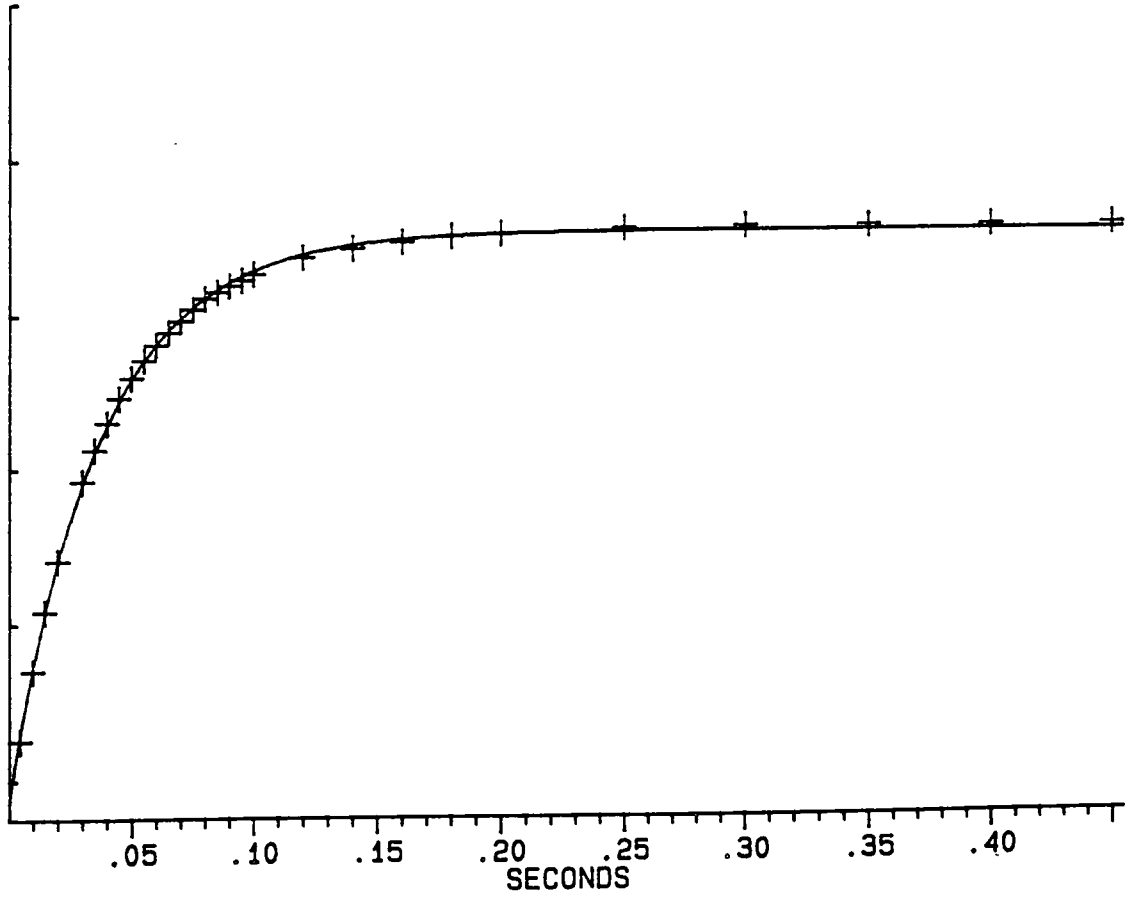

value measured for aged NH_4Y–47, however, is only 36.5 ms, indicating enhanced mobility as implied by the spectrum in Figure 7.8; see Figure 7.9 for a plot of the relaxation curve. The T_1 of residual water also increases from 16 ms ($T_{1\rho}$ = 4.8 ms) in wet NH_4Y[2] to 50 and then to 150 ms ($T_{1\rho}$ = 14 ms). The T_1 of SiOH groups is around 50 – 100 ms in mildly–treated samples, with 180 and 200 ms measured in NH_4Y–45. These values are shorter than those found in dried HY samples, which may again be attributed to the presence of mobile sorbate residues. The 4.0 ppm peak in NH_4Y–53, assigned to NH_3, has a T_1 of 247 ms and a $T_{1\rho}$ of 1.6 ms, suggesting that it is mobile on the tens–of–kilohertz time scale but static in the megahertz range. The corresponding T_1 measured in NH_4Y–61 is around 90 ms.

7D: CONCLUSIONS

The results presented in this Chapter clearly demonstrate that the dehydration behaviour of cation–containing Zeolite Y samples is quite distinct from that of HY. The differences observed can be attributed mainly to interaction between water and the cation. Na^+ is found to bind water tightly, as expected; whereas four hours or less of heating under vacuum is sufficient to dry HY, NaY requires up to 63 hours. The same is true for HY which has been back–exchanged with Na^+, demonstrating that the difference in hydrophilicity arises solely from the presence of the cation, not from the different lattice Al or site vacancy content, non–lattice material or any other cause. A well–dried sample of NaY exhibits signals arising from lattice Brönsted–acidic ^1H atoms; approximately two–thirds of the sites in one sample studied bore such ^1H atoms, showing that the Na^+ normally associated with them had been dislodged. The

rather, it becomes entrapped in small lattice cages, appearing at around 4.0 ppm in the ^1H spectrum. The intracrystalline water is easily desorbed under conditions as mild as those required to dry HY, while the NH_4^+ peak at around 7 ppm is gradually destroyed during treatment in the 200 – 300°C range. It is clear, then, that NH_4^+–containing zeolites must either be pre–calcined to yield the H–form, or subjected to a more severe drying treatment, with the concomitant risk of lattice damage, if clean spectra comparable with those arising from H–zeolites are to be obtained.

effect is observed in a chemically dealuminated sample free from non–lattice material. The rationalization suggested is that the intracrystalline water is largely responsible for CP and that this interacts more strongly with non–lattice species, when present, than with the lattice.

The non–lattice material generated by hydrothermal treatment is rich in Si as well as Al; the Si can be observed clearly by ^{29}Si CP/MAS NMR. There is evidence to suggest that the non–lattice material is more ordered and less aggregated (*i.e.* richer in –OH terminations) after calcination at 650^{o}C than at 550^{o}C. The Al in this material is coordinated both octahedrally and tetrahedrally; a technique has been proposed for measuring the ratio of Al atoms in the two geometries. Efficient CP between octahedral Al and attached OH groups has been observed. Some of the Si appears to be in an ordered, highly Al–deficient environment, giving rise to a narrow peak in the ^{29}Si single–pulse spectrum well to the low–frequency side of the lattice Q^4 sites.

Leaching of a sample rich in non–lattice alumina with a solution of EDTA is a widely–used method for removing the amorphous material without inflicting further damage on the lattice. However, careful study of a sample treated in this way revealed evidence to suggest that large amounts of non–lattice silica are created by this treatment, and that there may also be a significant degree of re–insertion of Al into the lattice.

Having demonstrated that the multinuclear approach revealed useful information about the effect of these treatments on the system as a whole, attention was then focused on ^{1}H NMR as a technique for investigation of the hydroxyl and adsorbate species present. ^{1}H MAS–NMR was shown to be capable of revealing a wealth of detail concerning population, mobilities and interactions. CRAMPS was rarely found to provide additional information, but relaxation time measurements proved useful, particularly in the study of

intracrystalline water. Two distinct water species could usually be detected, differing substantially in T_1 and T_2. They generally occurred at the same chemical shift except in samples back–exchanged with cations such as Na^+. It is proposed that, during the cation–exchange used to prepare these samples, the cations initially enter the supercages only, interacting with water there, and diffuse gradually into the sodalite cages over a time scale of months (or hours if strongly heated).

It was anticipated that important details of the hydroxyl population of the system would be revealed by total dehydration. As a preparation for this, a reliable drying procedure was developed and evaluated. It was found that heating a sample of calcined HY under vacuum to 400^oC for two hours was sufficient to remove all free water from the system, producing a sample generally containing fewer than 3 residual H atoms per lattice Al. The drying process may itself displace a few Al atoms from the lattice, but, more importantly, gives rise to extensive dehydroxylation of internal SiOH and AlOH species.

Particular attention was paid to the ^1H MAS–NMR signal at 2.3 ppm arising from non–lattice AlOH groups; it is distinctively broad, accompanied by intense spinning sidebands, and varies greatly in magnitude. The latter observation was attributed to varying degrees of aggregation of the non–lattice alumina; the more condensed and polymerized it is, the fewer terminating –OH groups are required. The condensation process seems to occur during the drying treatment, the longer heating times resulting in a more aggregated product; it appeared that condensation was also encouraged by gradual cooling. Particularly interesting and novel effects were observed when the samples were allowed to age in the airtight container used for MAS: the condensation appeared to reverse, with new AlOH groups appearing in the ^1H spectrum at the expense of other hydroxylated species present. When small amounts of water were admitted,

either deliberately or by slow diffusion into the container, the AlOH population again increased, this time without loss of other species; no free–water signal was observed.

Attempts to dehydrate cation–containing Zeolite Y samples revealed major differences between their behaviour and that of HY as discussed above. The presence of metal cations strongly increases the hydrophilicity of a sample, making it difficult to dry; prolonged heating of NaY under vacuum yielded a water–free sample which showed, surprisingly, that about half of the Brönsted sites in the sample were protonated, instead of being charge–balanced by Na^+. AgY was easier to dehydrate, and did not appear to contain any protonated Brönsted sites. The behaviour observed for NH_4Y was substantially different: dehydration was facile, but the expected decomposition of NH_4^+ to NH_3 and H^+ resulted in the appearance of a new broad band close to 4 ppm in the ^1H MAS–NMR spectrum, which was tentatively attributed to NH_3 trapped in sodalite cages. NH_4Y is commonly used by other workers as a starting material for the preparation of dried HY samples; this result shows that great care should be exercised to ensure that the sample is truly in the desired H–form after treatment.

These results demonstrate that solid–state NMR is a technique of enormous importance for the study of zeolites, particularly under non–equilibrium conditions such as those pertaining in fluidized catalytic cracking units. It is clear that, whilst there is a general understanding of the gross effects resulting from standard treatments such as calcination, knowledge of the concomitant subtler changes to the lattice and to non–lattice material remains incomplete. In particular, further work, perhaps involving chemical treatments such as deuteration, is required to elucidate the remarkable behaviour of non–lattice alumina which the work presented in this thesis has revealed.

APPENDIX A: SUMMARY OF SAMPLES USED

This Appendix details the preparation treatments employed for all hydrated samples discussed in Chapters 4 – 7. Detailed descriptions of the treatments are given in Chapter 3. The abbreviation SAR is used below to denote 'lattice Si/Al Ratio'.

CHAPTER 4

NH_4Y[1] Made from as–synthesized NaY by special route generating product with low Na^+ content. SAR ≃ 3.

HY–C550 NH_4Y calcined for 30 minutes at 550°C. SAR ≃ 10.

NH_4Y–C550 HY–C550 exchanged with aqueous NH_4Cl.

HY–C650 NH_4Y calcined for 30 minutes at 650°C. SAR estimated as 15–30.

NH_4Y–C650 HY–C650 exchanged with aqueous NH_4Cl.

HY–C550–S NH_4Y–C550 steamed at 816°C for 5 hours in 100% steam. No lattice Al present.

HY–C650–S NH_4Y–C650 steamed at 816°C for 5 hours in 100% steam. SAR > 90.

NH_4Y–CS NH_4Y chemically dealuminated with aqueous $(NH_4)_2SiF_6$. SAR ≃ 6.

HY–CS–S NH_4Y–CS steamed at 816°C for 5 hours in 100% steam. No lattice Al present.

CHAPTERS 5–7

NaY As–synthesized material with high crystallinity and SAR close to 2.7.

NH_4Y[2] NaY exchanged with NH_4Cl. Not the same sample as NH_4Y[1] discussed in Chapter 4 and listed above.

HY Made from a sample of NH_4Y very similar to NH_4Y[2] by calcination at 650°C for 30 minutes. SAR = 5.3.

HY–S Made from a sample of NH_4Y very similar to NH_4Y[1] by an identical route to HY–C650–S. No lattice Al present.

HY–S–L HY–S leached with $(NH_4)_2EDTA$. SAR estimated as <6.4.

NaY–ex HY back–exchanged with aqueous NaCl.

AgY–ex HY back–exchanged with aqueous $AgNO_3$.

APPENDIX B:
SUMMARY OF DEHYDRATED SAMPLES

This Appendix lists and describes the preparation treatments of all samples subjected to dehydration treatments. In each case, the starting material can be identified by deleting the numerical suffix from the sample identification.

The meanings of the column headings are as follows:

TMP = Maximum temperature in degrees Celcius

TIM = Hold time at TMP in hours

QT = Temperature from which the sample was quenched (see Chapter 3 for a description of this technique). An entry *nq* denotes *not quenched.*

P = Whether connected to the vacuum line (*i.e.* pumped) during cooling. The following codes are used: A = pumped continuously; B = pumped only until quenched; C = not pumped during cooling; T = liquid air applied to trap during cooling; NP = not pumped at all during experiment.

REH = Rehydration treatment: *n*% = rehydrated in controlled atmosphere at a relative humidity of *n*%; *atm* = rehydrated in the ambient atmosphere.

DISC = Section(s) of thesis in which sample is considered.

Sample	TMP	TIM	QT	P	REH	DISC
HY–2	400	72	nq	A	–	5C
HY–3	400	$36^3/_4$	nq	A	15%	5C
HY–4	400	24	nq	A	–	5D
HY–5	400	$36^3/_4$	nq	A	21%	5C
HY–6	400	16	400	C	atm	5C
HY–7	400	24	nq	A	21%	7A
NaY–8	400	24	nq	A	–	5C
HY–9	400	24	nq	A	47%	5C
HY–S–10	400	24	nq	A	–	5D, 6A
NaY–ex–12	400	24	nq	A	–	7A
HY–14	430	16	430	A	–	5D, 6C
HY–S–L–16	400	16	400	C	–	6A
HY–18	400	17	400	C	–	5C, 5D
HY–19	–	–	–	NP	90%	5C
NH_4Y[2]–20	250	13	nq	A	–	7C
HY–21	–	–	–	NP	atm	5C
AgY–ex–22	400	$18^3/_4$	200	B	–	7B

(Table continued overleaf)

Sample	TMP	TIM	QT	P	REH	DISC
HY–23	400	0	400	C	–	5C, 6B
HY–26	400	4	nq	A	–	5D, 6C
HY–27	400	4	270	B	–	5D, 6B, 6C
HY–29	400	4	400	C	–	5D, 6B
HY–30	400	2	nq	A	–	7A
NaY–31	400	63	nq	A	–	7A
HY–32	400	2	400	A	–	5D
HY–35	400	2	300	A	–	5D, 6B
HY–36	400	2	200	A	–	5D, 6B, 6C
NH_4Y[2]–37	100	4	100	A	–	7C
NaY–39	400	24	nq	A	–	7A
HY–40	400	1	nq	C	–	5D
HY–41	400	1½	nq	C	–	5D
HY–43	400	2	400	C	–	5D, 6B
NH_4Y[2]–45	200	4	200	A	–	7C
NaY–46	400	25	400	A	–	7A
NH_4Y[2]–47	250	4	250	A	–	7C
NaY–51	400	48	nq	A	–	7A
HY–52	400	8	400	C	–	6B
NH_4Y[2]–53	300	4	300	C	–	7C
HY–54	400	4	nq	AT	–	5D, 6B
NH_4Y[2]–55	250	4	250	AT	–	7C
NH_4Y[2]–56	300	4	300	CT	–	7C
NH_4Y[2]–57	300	4	300	CT	–	7C
HY–58	500	4	500	C	–	5D, 6B
HY–59	400	2	220	BT	–	6B
HY–60	400	4	nq	AT	–	6C
NH_4Y[2]–61	400	4	400	AT	–	7C
HY–62	400	4	400	AT	–	5C
HY–63	400	4	150	BT	–	6C
HY–66	400	4	250	AT	85%	5C
HY–67	400	4	250	AT	–	5C
AgY–ex–68	400	4	260	AT	–	5C
NaY–69	500	48	50	BT	–	7A
HY–71	60	18	60	NP	–	5C
HY–72	200	45	200	NP	–	5C

LIST OF LECTURES GIVEN BY INVITED SPEAKERS IN THE DEPARTMENT OF CHEMISTRY, UNIVERSITY OF DURHAM, DURING THE PERIOD OF STUDY

The lectures attended by the author are marked •.

Alder, Dr. B.J. (Lawrence Livermore Laboratories, California)
Hydrogen in All its Glory

•Aveyard, Dr. R. (University of Hull)
Surfactants at Your Surface

Aylett, Prof. B.J. (Queen Mary College, London)
Silicon–based Chips:– The Chemist's Contribution

•Badyal, Dr. J.P.S. (University of Durham)
Breakthroughs in Heterogeneous Catalysis

•Baldwin, Prof. J.E. (University of Oxford)
Recent Advances in the Bioorganic Chemistry of Penicillin Biosynthesis

Baldwin, Dr. R.R. & Walker, Dr. R.W. (University of Hull)
Combustion: Some Burning Problems

•Becher, Dr. J. (University of Odense)
Synthesis of New Macrocyclic Systems using Heterocyclic Building Blocks

•Bell, Prof. T. (State University of New York, Stony Brook, New York)
Functional Molecular Architecture and Molecular Recognition

•Bercaw, Prof. J.E. (California Institute of Technology)
Synthetic and Mechanistic Approaches to Zeigler–Natta Polymerization of Olefins

Bleasdale, Dr. C. (University of Newcastle–upon–Tyne)
The Mode of Action of some Anti–Tumour Agents

Bochmann, Dr. M. (University of East Anglia)
Synthesis, Reactions and Catalytic Activity of Cationic Titanium Alkyls

Bowman, Prof. J.M. (Emory University)
Fitting Experiment with Theory in Ar–OH

Brimble, Dr. M.A. (Massey University, New Zealand)
Synthetic Studies Towards the Antibiotic Griseusin–A

Brookhart, Prof. M.S. (University of North Carolina)
Olefin Polymerization, Oligomerizations and Dimerizations Using Electrophilic Late Transition Metal Catalysts

•Brown, Dr. J. (University of Oxford)
Can Chemistry Provide Catalysts Superior to Enzymes?

•Bushby, Dr. R. (University of Leeds)
Biradicals and Organic Magnets

•Butler, Dr. A.R. (University of St. Andrews)
The Discovery of Penicillin: Facts and Fancies

•Butler, Dr. A.R. (University of St. Andrews)
Cancer in Linxian: The Chemical Dimension

Cadogan, Prof. J.I.G. (BP)
From Pure Science to Profit

Casey, Dr. M. (University of Salford)
Sulphoxides in Stereoselective Synthesis

Cheetham, Dr. A.K. (University of Oxford)
Chemistry of Zeolite Cages

•Chowla, Dr. H.M. (Indian Institute of Technology, Delhi)
The Sensitized Photo–Oxygenation of Imidazoles in Organized Media

•Clark, Prof. D.T. (ICI Wilton)
Spatially Resolved Chemistry (Using Nature's Paradigm in the Advanced Materials Arena)

Cole–Hamilton, Prof. D.J. (University of St. Andrews)
New Polymers from Homogeneous Catalysis

Cowley, Prof. A.H. (University of Texas)
New Organometallic Routes to Electronic Materials

Crich, Dr. D. (University College, London)
Some Novel Uses of Free Radicals in Organic Synthesis

Crombie, Prof. L. (University of Nottingham)
The Chemistry of Cannabis and Khat

Crout, Prof. D. (University of Warwick)
Enzymes in Organic Synthesis

Dingwall, Dr. J. (Ciba–Geigy)
Phosphorus–Containing Amino Acids: Biologically Active Natural and Unnatural Products

•Dobson, Dr. C.M. (University of Oxford)
NMR Studies of Dynamics in Molecular Crystals

Dyer, Dr. U. (Glaxo)
Synthesis and Conformation of C–Glycosides

Errington, Dr. R.J. (University of Newcastle–upon–Tyne)
Polymetallate Assembly in Organic Solvents

Floriani, Prof. C. (University of Lausanne, Switzerland)
Molecular Aggregates – A Bridge Between Homogeneous and Heterogeneous Systems

•Frey, Dr. J. (University of Southampton)
Spectroscopy of the Reaction Path: Photodissociation Raman Spectra of NOCl

German, Prof. L.S. (USSR Academy of Sciences, Moscow)
New Syntheses in Fluoroaliphatic Chemistry: Recent Advances in the Chemistry of Fluorinated Oxiranes

•Gerrard, Dr. D. (BP)
Raman Spectroscopy for Industrial Analysis

•Graham, Dr. D. (BP Research Centre)
How Proteins Adsorb to Interfaces

Greenwood, Prof. N.N. (University of Leeds)
Novel Cluster Geometries in Metalloborane Chemistry

•Hall, Prof. L.D. (Addenbrooke's Hospital, Cambridge)
NMR – A Window to the Human Body

•Hardgrove, Dr. G.L. (St. Olaf College, USA)
Polymers in the Physical Chemistry Laboratory

Harwood, Dr. L. (University of Oxford)
Synthetic Approaches to Phorbols Via Intramolecular Furan Diels–Alder Reactions: Chemistry Under Pressure

•Hemer, Dr. I. & Paleta, Dr. O. (Technical University of Prague)
Chemistry of Fluorinated Alkanes and Alkenes

Holloway, Prof. J.H. (University of Leicester)
Noble Gas Chemistry

Hudlicky, Prof. T. (Virginia Polytechnic Institute)
Biocatalysis and Symmetry Based Approaches to the Efficient Synthesis of Complex Natural Products

•Hughes, Dr. M.N. (King's College, London)
A Bug's Eye View of the Periodic Table

Huisgen, Prof. R. (Universität München)
Recent Mechanistic Studies of [2+2] Additions

Jackson, Dr. R. (University of Newcastle–upon–Tyne)
New Synthetic Methods: α–Amino Acids and Small Rings

•Jäger, Dr. C. (Friedrich–Schiller University, Germany)
NMR Investigations of Fast Ion Conductors of the NASICON Type

•Jain, Dr. S.C. (Delhi)
Chemical Defence and Communication Among Insects

Jennings, Prof. R.R. (University of Warwick)
Chemistry of the Masses

•Johnson, Dr. B.F.G. (University of Cambridge)
The Binary Carbonyls

•Klinowski, Dr. J. (University of Cambridge)
Solid State NMR Studies of Zeolite Catalysts

Kocovsky, Dr. P. (University of Uppsala)
Stereo–Controlled Reactions Mediated by Transition and Non–Transition Metals

•Lacey, Dr. D. (University of Hull)
Liquid Crystals

Lancaster, Rev. R. (Kimbolton Fireworks)
Fireworks – Principles and Practice

Logan, Dr. N. (University of Nottingham)
Rocket Propellants

Lunazzi, Prof. L. (University of Bologna)
Application of Dynamic NMR to the Study of Conformational Enantiomerism

Ludman, Dr. C.J. (University of Durham)
The Energetics of Explosives

•MacDonald, Dr. E.A. (ICI Wilton)
Materials for the Space Age

•MacDougall, Dr. G. (University of Edinburgh)
Vibrational Spectroscopy of Model Catalytic Systems

•Markham, Dr. A. (ICI Pharmaceuticals)
DNA Fingerprinting

Marko, Dr. I. (University of Sheffield)
Catalytic Asymmetric Osmylation of Olefins

•McLaughlan, Dr. K.A. (University of Oxford)
The Effect of Magnetic Fields on Chemical Reactions

Moody, Dr. C.J. (Imperial College, London)
Reactive Intermediates in Heterocyclic Synthesis

Paetzold, Prof. P. (Aachen)
Iminoboranes XB≡NR: Inorganic Acetylenes?

Page, Dr. P.C.B. (University of Liverpool)
Stereocontrol of Organic Reactions Using 1,3–Dithiane–1–oxides

Palmer, Dr. F. (University of Nottingham)
Thunder and Lightning

•Parker, Dr. D. (University of Durham)
Macrocycles, Drugs and Rock 'n' Roll

Perutz, Dr. R.N. (University of York)
Plotting the Course of C–H Activations with Organometallics

•Petty, Dr. M.C. (University of Durham)
Molecular Electronics

Platonov, Prof. V.E. (USSR Academy of Sciences, Novosibirsk)
Polyfluoroindanes: Synthesis and Transformation

Pola, Prof. J. (Czechoslovak Academy of Sciences)
Carbon Dioxide Laser Induced Chemical Reactions – New Pathways in Gas–Phase Chemistry

Powell, Dr. R.L. (ICI)
The Development of CFC Replacements

•Powis, Dr. I. (University of Nottingham)
Spinning Off in a Huff: Photodissociation of Methyl Iodide

•Pringle, Dr. P.G. (University of Bristol)
Metal Complexes with Functionalized Phosphines

Pritchard, Prof. J. (Queen Mary & Westfield College, London)
Copper Surfaces and Catalysts

Rees, Prof. C.W. (Imperial College, London)
Some Very Heterocyclic Compounds

Rozhkov, Prof. I.N. (USSR Academy of Sciences, Moscow)
Reactivity of Perfluoroalkyl Bromides

Sadler, Dr. P.J. (Birkbeck College, London)
Design of Inorganic Drugs: Precious Metals, Hypertension + HIV

Sarre, Dr. P. (University of Nottingham)
Comet Chemistry

Schmutzler, Prof. R. (Technische Universität Braunschweig)
Fluorophosphines Revisited – New Contributions to an Old Theme

•Schrock, Prof. R.R. (MIT)
Recent Advances in Living Metathesis

•Schrock, Prof. R.R. (MIT)
Metal–Ligand Multiple Bonds and Metathesis Initiators

Scott, Dr. S.K. (University of Leeds)
Clocks, Oscillations and Chaos

Shaw, Prof. B.L. (University of Leeds)
Syntheses with Coordinated, Unsaturated Phosphine Ligands

Singh, Dr. G. (Teesside Polytechnic)
Towards Third Generation Anti–Leukæmics

•Sinn, Prof. E. (University of Hull)
Coupling of Little Electrons in Big Molecules. Implications for the Active Sites of (Metalloproteins and Other) Macromolecules

Snaith, Dr. R. (University of Cambridge)
Egyptian Mummies: What, Where, Why and How?

•Soulen, Prof. R. (South Western University, Texas)
Preparation and Reactions of Bicycloalkenes

•Stibr, Dr. R. (Czechoslovak Academy of Sciences)
Recent Developments in the Chemistry of Intermediate–Sited Carboranes

•Stoddart, Dr. J.F. (University of Sheffield)
Molecular Lego

Sutton, Prof. D. (Simon Fraser University, Vancouver, B.C., Canada)
Synthesis and Applications of Dinitrogen and Diazo Compounds of Rhenium and Iridium

•Symons, Prof. M.C.R. (University of Leicester)
Spectroscopic Studies of Solvation

Thomas, Dr. R.K. (University of Oxford)
Neutron Reflectometry from Surfaces

Thompson, Dr. D.P. (University of Newcastle–upon–Tyne)
The Role of Nitrogen in Extending Silicate Crystal Chemistry

Von Rague Schleyer, Prof. P. (Universität Erlangen Nürnberg)
The Fruitful Interplay Between Calculational and Experimental Chemistry

•Wells, Prof. P.B. (University of Hull)
Catalyst Characterization and Activity

•Whitaker, Dr. B.J. (University of Leeds)
Two–Dimensional Velocity Imaging of State–Selected Reaction Products

CONFERENCES ATTENDED DURING THE PERIOD OF STUDY

1. North–East Graduate Symposium, University of Durham, April 1989.
2. North–East Graduate Symposium, University of Newcastle–upon–Tyne, April 1990.
3. British Zeolite Association, 13th Annual Meeting, Chislehurst, Kent, July 1990. Poster presented by the Author.
4. British Zeolite Association, 14th Annual Meeting, University of Durham, March 1991.
5. North–East Graduate Symposium, University of Newcastle–upon–Tyne, April 1991. Paper read by the Author.
6. ICI Chemicals & Polymers, Runcorn, Private Colloquium, April 1991. Paper read by the Author.